REPORT DOCUMENTATION PAGE			Form Approved OMB No. 0704-0188

1. AGENCY USE ONLY *(Leave blank)*	2. REPORT DATE	3. REPORT TYPE AND DATES COVERED
	3.Nov.99	DISSERTATION

4. TITLE AND SUBTITLE
HUMAN FENI EXPRESSION AND SOLUBILITY PATTERSN IN D

5. FUNDING NUMBERS

6. AUTHOR(S)
MAJ CARRIER RICHARD J

7. PERFORMING ORGANIZATION NAME(S) AND ADDRESS(ES)
UNIVERSITY OF OXFORD AT GREEN COLLEGE

8. PERFORMING ORGANIZATION REPORT NUMBER

9. SPONSORING/MONITORING AGENCY NAME(S) AND ADDRESS(ES)
THE DEPARTMENT OF THE AIR FORCE
AFIT/CIA, BLDG 125
2950 P STREET
WPAFB OH 45433

10. SPONSORING/MONITORING AGENCY REPORT NUMBER
FY99-388

11. SUPPLEMENTARY NOTES

12a. DISTRIBUTION AVAILABILITY STATEMENT
Unlimited distribution
In Accordance With AFI 35-205/AFIT Sup 1

12b. DISTRIBUTION CODE

13. ABSTRACT *(Maximum 200 words)*

DISTRIBUTION STATEMENT A
Approved for Public Release
Distribution Unlimited

19991117 069

14. SUBJECT TERMS			15. NUMBER OF PAGES 254
			16. PRICE CODE
17. SECURITY CLASSIFICATION OF REPORT	18. SECURITY CLASSIFICATION OF THIS PAGE	19. SECURITY CLASSIFICATION OF ABSTRACT	20. LIMITATION OF ABSTRACT

DTIC QUALITY INSPECTED 4

Human FEN1 Expression and Protein Solubility Patterns during DNA Replication and Repair

A thesis submitted to the Board of the Faculty of Biological Sciences,
University of Oxford, in partial fulfilment of the requirements for
the degree of Doctor of Philosophy

Richard J. Carrier

Green College

May 1999

ABSTRACT

Human FEN1 Expression and Solubility Patterns in DNA Replication and Repair

Richard J. Carrier
Green College

Submitted for the Degree of Doctor of Philosophy

Trinity Term, 1999

Flap endo-/exonuclease (FEN1) is a highly conserved protein shown to be one of 10 essential human proteins required for the production of form I DNA following DNA replication from the simian virus 40 (SV40) origin of replication *in vitro*. Human FEN1, and FEN1 homologues from yeast to mammals, are also implicated in different forms of DNA repair. In this thesis, I provide additional evidence supporting human FEN1's role in nuclear DNA replication *in vivo*. I show that human FEN1 mRNA and protein levels increase in a cell cycle-dependent manner, with peak mRNA and protein levels attained coincident with S phase DNA replication in both primary and transformed cells. Using novel antibodies that recognize human FEN1, I further show that very little DNase I-extractable FEN1 protein is present in S phase cells, suggesting that FEN1 protein is not stably associated with DNA, or DNA-associated proteins such as PCNA. Furthermore, I demonstrate that substantial levels of insoluble (SDS-extracted) FEN1 protein are present in human cells throughout the cell cycle. Fluorescence microscopic analysis of HeLa cells transfected with Green Fluorescent Protein-human FEN1 (GFP-FEN1) plasmid cDNA also supports this observation, and further suggests that human FEN1 is a nuclear protein, supporting a role for human FEN1 protein during nuclear DNA replication *in vivo*. Human SV40-transformed MRC-5 (MRC5-SV) cells treated with UV irradiation or the alkylating agent MMS show no significant increase in either FEN1 mRNA or protein

levels, or any changes in FEN1 protein solubility. In light of those observations, a potential role for FEN1 protein in DNA repair is discussed in context of a proposed mechanism of FEN1 enzyme activity during DNA replication. Lastly, examination of the recently available human *FEN1* genomic DNA sequence, and computer analysis of the DNA sequence 5' to the *FEN1* open reading frame (ORF), suggest a putative transcriptional start site, as well as several putative transcriptional regulatory elements that may control the cell cycle-dependent or DNA repair-dependent expression of the human *FEN1* gene.

To Peggy, Jordan, and Jake

ACKNOWLEDGEMENTS

I would like to first thank Dr Lynne Cox for accepting me as her first student in Oxford, and for explaining to me the "world of research". Despite my grumblings and other acts of displeasure at seeing "so much red", I greatly appreciate the many hours she spent reading this manuscript and her many suggestions on how to improve it (not to mention English vs. American spelling!).

I would also like to thank and wish good luck to my lab colleagues: Dr Ji-Liang Li, Dr Ana Rodriguez-Lopez, Phil Howard, Anna Warren, and Gonilla Harbour. I'm sure that they're all looking forward to my freezer space and storage boxes.

Many heartfelt thanks also go to the many people who told me and showed me how to do the variety of tasks needed to complete my degree. I especially want to thank Dr Borek Vojtesek, Dr Matthew Whitby, Lindy Castell, Gabby, Dr Fran Platt, and all the members of the Newell, Pears, and Gross lab groups for their help along the way.

I also want to recognize and thank the USAF and USAF Academy for this opportunity and for the financial support they've provided.

Last, but certainly not least, I want to thank God, my wonderful wife Peggy, Jordan, Jake, and Jack for all their patience, encouragement, and support over the past 3 years. They shared my workload, and will hopefully share the fruits of our labor in the future.

ABBREVIATIONS

APS	ammonium persulphate
AP sites	apurinic/apyrimidinic sites
AT	ataxia telangiectasia
ATP	adenosine 5'-triphosphate
BER	base excision repair
bp	base pair
CAK	CDK activating kinase
CDDP	Cis-diamminedichloroplatinum II
CDK	cyclin-dependent kinase
CKI	cyclin-dependent kinase inhibitor
CMF	calcium/magnesium-free
CMV	cytomegalovirus
ConA	concanavilin A
DEPC	diethylpyrocarbonate
DMEM	Dulbecco's Modified Eagles Medium
DMSO	dimethylsulfoxide
DNA	deoxyribonucleic acid
dsDNA	double-stranded DNA
DTT	dithiothreotol
ECL	enhanced chemiluminescence
EDTA	ethylenediaminetetraacetic acid
ELISA	enzyme-linked immunosorbent assay
FACS	fluorescence-activated cell sorter

FCS	foetal calf serum
FEN1	flap endo-/exonuclease 1
FISH	fluorescent *in situ* hybridization
GAPDH	glyceraldehyde 3-phosphate dehydrogenase
GFP	Green Fluorescent Protein
HA	hypoxanthine-azaserine
HRP	horseradish peroxidase
Ig	immunoglobulin
IMAC	immobilized metal-affinity chromatography
IPTG	isopropylthio-β-D-galactoside
kb	kilobase
KLH	Keyhole Limpet Hemocyanin
LB	Luria Bertani media
MMR	mismatch repair
MMS	methylmethane sulfonate
MRC5-SV	SV40-transformed MRC-5 cells
mRNA	messenger RNA
NER	nucleotide excision repair
nt	nucleotide
NNPP	Promoter Prediction by Neural Network
ORF	open reading frame
PARP	poly-(ADP-ribose) polymerase
PBLs	peripheral blood lymphocytes
PBS	phosphate buffered saline
PCNA	proliferating cell nuclear antigen

PCR	polymerase chain reaction
PI	propidium iodide
PMSF	phenylmethyl-sulfonyl fluoride
rbs	ribosome binding site
RF-C	replication factor C
RNA	ribonucleic acid
RP-A	replication protein A
RSB	reducing sample buffer
RT-PCR	reverse transcription-PCR
SDS-PAGE	sodium dodecyl sulfate polyacrylamide gel electrophoresis
SSB	single-stranded binding protein
ssDNA	single-stranded DNA
SV40	simian virus 40
TRE	transcriptional regulatory elements
TSS	transcriptional start site
UTR	untranslated region
UV	ultraviolet
XP	xeroderma pigmentosum

CONTENTS

CHAPTER ONE: INTRODUCTION

1-1 The Cell Cycle

Two fundamental properties of all living organisms are their capacity to grow and reproduce. From single-cell yeast, to complex multi-cellular organisms such as mammals, cell division typically follows a period of growth and DNA synthesis. The mechanism by which eukaryotic cells coordinate the inseparable processes of growth and division is best described by the cell cycle (Figure 1-1).

Figure 1-1 typical eukaryotic cell cycle

Although simplistic in detail, the typical eukaryotic cell cycle depicted in Figure 1-1 graphically illustrates how cell division (mitosis and cytokinesis) is preceded by a period of growth (G_1 phase) and DNA synthesis (S phase). In an asynchronous cell population, most cells exist in the G_1 phase of the cell cycle (see Figure 1-2), performing housekeeping and metabolic processes necessary for growth and maintenance. It is also the most variable phase in terms of duration. During DNA synthesis (S phase), cells replicate their nuclear DNA in preparation for cell division; this phase also may vary in duration between different cell types. The G_2 phase is an intervening gap between S phase and mitosis (M) and allows for corrections of deficiencies arising from DNA replication, and further growth. Finally, during mitosis (M), newly replicated sister chromatids are equally segregated before the actual cellular division (cytokinesis) occurs at the end of the cell cycle. Unlike the other cell cycle phases, the length of mitosis and cytokinesis varies little within individual cell populations.

To study how cell cycle progression is controlled, it is essential to dissect the process and determine where cells are within the cycle. Determining cell cycle stage can be accomplished by measuring DNA content during flow cytometry. Specialized spectrophotometers can measure the amount of DNA in individual cells by detecting the fluorescence from DNA-binding dyes like propidium iodide. After numerous cells pass through the spectrophotometer (often called a FACS, fluorescence-activated cell sorter), the FACS software provides a readout of the distribution of cells with different fluorescence intensities (DNA content) within the population. Figure 1-2 shows that cells in G_2 and M (prior to cytokinesis) have twice the fluorescence intensity (DNA content) of cells in G_1, while cells in S phase have an intermediate amount. By using synchronized cell populations, as verified by FACS analysis, cellular changes in components such as RNA and protein levels can be examined as cell populations progress from one cell cycle phase to the next.

Figure 1-2 FACS analysis of asynchronous cell population

1-2 Cell Cycle Regulatory Mechanisms

Numerous proteins have been discovered that play key roles in regulating cell cycle progression (reviewed by Elledge, 1996; Nasmyth, 1996). These proteins participate in various processes such as transcriptional regulation, post-translational modification, proteolysis (reviewed by King *et al.*, 1996), and other positive and negative regulation of cellular replicative processes. Early studies, using the techniques of nuclear transplantation (Gurdon, 1967) and cell fusion (Rao and Johnson, 1970), discovered that entry into the various stages, especially the DNA

synthesis (S) and mitotic (M) phases of the cell cycle, were controlled by 'trans-acting' cytoplasmic inducers. Pioneering genetic analyses in the yeasts *S. pombe* (Nurse *et al.*, 1976) and *S. cerevisiae* (Hartwell *et al.*, 1970), along with studies of amphibian oocytes and eggs from *Rana pipiens* (Masui and Makert, 1971) and *Xenopus* (Harland and Laskey, 1980; Newport and Kirschner, 1984), led to the subsequent discovery of cyclins (Rosenthal *et al.*, 1980; Evans *et al.*, 1983) and cyclin-dependent kinases (CDKs, Nurse and Bissett, 1981; Gautier *et al.*, 1988), and helped demonstrate how CDKs and phosphatases account for the phosphorylation and dephosphorylation events that help drive cell cycle progression (reviewed by Nigg, 1995).

Figure 1-3 Major cyclin-CDK complexes during mammalian cell cycle progression

Figure 1-3 is a simplistic model (adapted from Hutchinson and Glover, 1995) demonstrating the periodicity of cyclin-CDK interactions that helps drive higher eukaryotic cell cycle progression. To effect an orderly cell cycle progression, activated CDKs function by phosphorylating target proteins in a cell cycle-dependent manner (reviewed by Lees, 1995). Monomeric CDKs have virtually no kinase activity. They require the binding of cyclin regulatory subunits as an initial step in their activation process (Koff *et al*, 1992, Lahue *et al.*, 1991). Additionally, the recently solved crystal structure of cyclin A-CDK2 demonstrated that cyclin A binding results in exposure and stabilization of the catalytic and CDK-activating kinase (CAK) phosphorylation (T160) sites on CDK2 by allosterically inducing displacement of the T loop of inactivated CDK2 (Jeffrey *et al.*, 1995; Russo *et al.*,

1996). It is thought that this step in the activation process may be applicable to all cyclin-CDK interactions. Figure 1-3 also shows that in higher eukaryotes, a number of different cyclins bind and activate different CDKs in a temporally-specific manner. The periodic synthesis and proteolytic degradation of cyclins modulates their CDK association and helps drive cell cycle progression (Irniger *et al.*, 1995; King *et al.*, 1995; reviewed by King *et al.*, 1996).

Cyclins are not the only components of the cell cycle machinery that are subject to regulation. CDKs, themselves, are regulated by phosphorylation and dephosphorylation events of key amino acid residues. For example, CAK phosphorylation of the conserved CDK T160 residue serves to activate cyclin-CDK complexes (Lee *et al.*, 1991), while inhibitory phosphorylation of T14 or Y15 residues by other kinases can be reversed by de-phosphorylation of those sites by the cdc25 protein phosphatase (reviewed by Pines, 1995).

CDKs and cyclin-CDK complexes can also be regulated by association with proteins known as cyclin-dependent kinase inhibitors (CKIs). These CKIs negatively regulate CDK activity through their association and binding to cyclins, CDKs, or cyclin-CDK complexes (reviewed by Sherr and Roberts, 1995). Two families of CDK inhibitors have been discovered. The Ink4 family includes $p15^{Ink4b}$ (Lee *et al.*, 1995), $p16^{Ink4a}$ (Serrano *et al.*, 1993), $p18^{Ink4c}$ (Guan *et al.*, 1994), and $p19^{Ink4d}$ (El-Deiry *et al.*, 1993) proteins which specifically inhibit the cyclin D-dependent kinases CDK4 and CDK6. The structurally unrelated Cip/Kip family of CKIs includes $p21^{CIP1/WAF1}$ (Harper *et al.*, 1993; El-Deiry *et al.*, 1993), $p27^{KIP1}$ (Polyak *et al.*, 1993), and $p57^{KIP2}$ (Lee *et al.*, 1995) which can interact and inhibit several different cyclin-CDK complexes; although different affinities for the various cyclin-CDK complexes

suggests that the inhibition predominantly targets G_1 cyclin-CDK complexes (Gu *et al.*, 1993; Harper *et al.*, 1995; reviewed by Sherr and Roberts, 1995). Additionally, the *CIP1/WAF1* gene has been shown to be transcriptionally-induced by the tumour suppressor protein p53 in response to some forms of DNA damage (El-Deiry *et al.*, 1993), linking DNA damage and p53-mediated cell cycle arrest. *CIP1/WAF1* induction in response to DNA damage is just one of many examples of cellular surveillance mechanisms involved in cell cycle regulation.

Coordination of the timing and order of cell cycle events is critical for high fidelity transmission of genetic information from one generation to the next. As a result, it is thought that numerous biochemical pathways and feedback mechanisms have evolved to ensure that the initiation of particular cell cycle events is dependent on successful completion of the previous event (Hartwell and Weinert, 1989). Failing to repair DNA damage or replication errors, entering mitosis with unreplicated DNA, or initiating chromatid segregation during anaphase before aligning chromosomes on the mitotic spindle may give rise to dead or mutant cells. The term 'cell cycle checkpoint' refers to the process of monitoring cell cycle events, such as DNA replication and mitotic spindle assembly, generating signals in response to completion or errors in these processes, and allowing progression, or arresting the cell cycle at particular points in time (Hartwell and Weinert, 1989; reviewed by Murray, 1994 and Elledge, 1996).

1-3 DNA Damage, Repair, and Cell Cycle Checkpoints

DNA damage can arise as a result of spontaneous mutational events or environmental mutagens (reviewed by Friedberg *et al.*, 1995). To maintain their

genomic integrity, cells must be able both to recognize and to repair DNA damage. Additionally, proliferating cells must also be able to delay cell cycle progression to allow any necessary DNA repair to avoid fixing mutated DNA sequences as a result of DNA replication and subsequent cell division.

Various types of DNA damage elicit different cellular responses. DNA helix-distorting lesions such as pyrimidine dimers and 6-4 photoproducts caused by UV irradiation appear to be repaired primarily by nucleotide excision repair (NER) pathways (reviewed by Lindahl *et al.*, 1997). Bulky DNA adducts and base modifications caused by alkylation damage and oxidative stress are repaired by cellular base excision repair (BER) processes (reviewed by Croteau and Bohr, 1997). Further damage caused by ionizing radiation and some chemotherapeutic agents such as etoposide and adriamycin result in double strand DNA breaks that appear to be corrected by both DNA end-joining and homologous recombination mechanisms (reviewed by Chu, 1997). Finally, DNA mismatches that result from replication errors or DNA damage are resolved primarily by mismatch repair pathways (reviewed by Modrich, 1997).

Many human diseases such as cancer, xeroderma pigmentosum (XP) and ataxia telangiectasia (AT) are characterized by genomic instability, and are linked to DNA repair deficiencies. Numerous genes associated with these human diseases have been discovered by genetic complementation and pedigree analyses, but discovering those genes' functional relevance in disease progression has been accelerated in recent years by comparative studies in other model systems.

Genetic and biochemical studies in organisms as diverse as yeast and humans show that many DNA repair processes are highly conserved. XP has been identified

as a human DNA repair disorder where patients exhibit hypersensitivity to sun light (UV) and are predisposed to skin cancer and other degenerative conditions (reviewed by Wang, 1998). Studies of yeast mutants that are also hypersensitive to UV irradiation and exhibit DNA repair defects have revealed that many yeast DNA repair mechanisms appear to be conserved in mammalian systems. For example, during mammalian NER of UV-induced damage *in vitro*, it has been shown that the structure-specific nucleases XPF-ERCC1 and XPG are responsible for cleaving the 5'- and 3'- sides of the lesion, respectively (Sijbers *et al.*, 1996; reviewed by Wood, 1997), whereas in the yeast *S. cerevisiae*, the XPF-ERCC1 and XPG homologues RAD1-RAD10 and RAD2 function in a similar manner (Bardwell *et al.*, 1992; O'Donovan *et al.*, 1994). With only a few exceptions, all known human genes involved in NER have identified homologous counterparts in yeast (reviewed by Hoeijmakers, 1993).

Cell cycle checkpoint mechanisms are perhaps best understood in the yeasts *S. pombe* and *S. cerevisiae*. Because it appears that yeast and mammals exhibit significant similarities in the actual temporal sequence and mechanics of DNA repair, it is thought that additional similarities may also exist in cellular responses to DNA damage, particularly with regard to checkpoint control of cell proliferation. Although the absence of yeast homologues to higher eukaryotic genes such as *p53* and $p21^{CIP1/WAF1}$ suggests some differences exist between yeast and mammalian systems, similarities in other DNA repair and cell cycle checkpoint mechanisms are being elucidated. Figure 1-4 illustrates how checkpoint activation functions in blocking cell cycle progression in response to DNA damage, incomplete replication, or improper spindle assembly (reviewed by Kitazono and Matsumoto, 1998).

Figure 1-4 Cell cycle checkpoints activation

The following examples illustrate the similarities between yeast and mammalian cell cycle checkpoint mechanisms. *S.pombe Rad3* and *S. cerevisiae MEC1* genes exhibit a high degree of homology with the *ATM* gene in mammals, which is mutated in the recessive childhood disease ataxia telangiectasia and manifested by radiation sensitivity and many other degenerative symptoms (Savitsky *et al.*, 1995). Defects observed in ATM null mice suggest that the AT phenotype is associated with signal-transduction defects (Lavin and Shiloh, 1997). Yeast Rad3 and MEC1 mutants are not only hypersensitive to UV radiation and defective in DNA repair, they are also unable to delay cell cycle progression in response to radiation-induced damage (Jimenez *et al.*, 1992; Weinert *et al.*, 1994). Similarly, it appears that ATM-deficient human and mouse cells are also unable to delay cell cycle progression upon exposure to ionizing radiation (Savitsky *et al.*, 1996; reviewed by Elledge, 1996). Although not fully elucidated, studies suggest that ATM protein kinase activity is an important upstream element in the p53 and $p21^{CIP1/WAF1}$ proteins signaling cascade, which functions to block G_1 to S phase cell cycle progression (Kastan *et al.*, 1992; Xu and Baltimore, 1996; Westphal *et al.*, 1997; reviewed by Westphal, 1997).

To further illustrate similarities between yeast and mammalian checkpoint mechanisms, additional studies show that another protein in the ATM/Rad3/MEC1 pathway, Chk1, also functions in response to DNA damage in both yeast and mammals by phosphorylating the Cdc25 phosphatase (Furnari *et al.*, 1997; Peng *et*

al., 1997; Sanchez *et al.*, 1997). Phosphorylation of Cdc25 appears to lead to its degradation and prevents Cdc25 activation of CDC28 (*S. cerevisiae*)/cdc2 (*S. pombe*)/CDK1 (mammals), thus blocking cells at the G_2/M transition until damage is repaired (Peng *et al.*, 1997).

Another possible similarity between yeast and mammalian checkpoint mechanisms is suggested by the proteins Rad9 in *S. cerevisiae* and BRCA1 in humans. *S. cerevisiae* Rad9p has been shown to be involved in cell cycle arrest at both the G_1/S and G_2/M transitions and a slowing of S phase in response to DNA damage (Weinert and Hartwell, 1988; Siede *et al.*, 1993; Paulovich and Hartwell, 1995). The human *BRCA1* gene is often found mutated in familial breast and ovarian cancers (Futreal *et al.*, 1994), and the BRCA1 protein contains BRCT repeat domains (Koonin *et al.*, 1996) that are also found in Rad9 (Bork *et al.*, 1997). Both Rad9 and BRCA1 proteins are putative transcription factors that are phosphorylated at the G1/S transition and become further phosphorylated when cells are exposed to UV or ionizing radiation (Vialard *et al.*, 1998). It is thought that they may have similar DNA damage checkpoint functions not yet determined (Vialard *et al.*, 1998).

1-4 Controlling the G1/S Transition

Cells must be capable not only of blocking cell cycle progression in response to DNA damage, but they must also be able to regulate responses to proliferative signals. Oncogenic processes exert their greatest effect by targeting particular regulators of G_1 phase progression (Hunter and Pines, 1994; reviewed by Hall and Peters, 1996). It is during the G_1 phase that cells are competent to respond to extracellular signals by either advancing towards another division or withdrawing

from the cycle into the resting G_0 state (reviewed by Pardee, 1989; Sherr, 1994). The decision to divide occurs as cells pass a restriction point late in G_1 (R_1 in Figure 1-3), after which they no longer respond to extracellular signals and instead commit to the autonomous program that carries them through to division, unless cell cycle checkpoints are activated (Pardee, 1989; Sherr, 1994). An understanding of the extracellular signals, downstream effectors, and inhibitors of those signals is crucial to understanding proliferative control and neoplastic progression.

Among the more important and well-characterized downstream effectors controlling cell cycle progression are the tumour suppressor proteins p53 (Lane and Crawford, 1979; Linzer and Levine, 1979) and pRb (Knudson, 1993). The p53 protein has been aptly called the "guardian of the genome" (Lane, 1992) because of its ability to protect genomic integrity by negatively regulating cell proliferation. In response to DNA damage, p53 may transcriptionally activate as many as 100 genes (Tokino *et al.*, 1994), including several key proteins such as $p21^{CIP11/WAF1}$ (El-Deiry *et al.*, 1993), which can inhibit cyclin-CDK complexes and block cell cycle progression (Xiong *et al.*, 1994), and GADD45 (Wang and Prives, 1995). pRb also serves as a negative regulator of cell proliferation. Hypophosphorylated pRb is able to bind and sequester members of the E2F family of transcription factors, preventing transcriptional activation of genes important for DNA replication (Buchkovich *et al.*, 1993). Cell cycle-dependent phosphorylation of pRb initially by D-type cyclin-CDK4/CDK6 complexes (Kato *et al.*, 1993; Meyerson and Harlow, 1994) releases E2F to induce transcription of genes necessary for S phase to occur.

Although tumour suppressor proteins such as p53 and pRb are essential negative regulators of cell growth, other proteins have been identified that also

control cell proliferation. The INK4 and CIP/KIP families of cyclin-dependent kinase inhibitors (CKIs) have all been shown to prevent CDK phosphorylation of target proteins, such as pRb, necessary for cell cycle progression (reviewed by Sherr and Roberts, 1995). More specifically, it appears that the primary targets of CKIs are the cyclin D-CDK4/6 and cyclin E-CDK2 complexes necessary for the G1/S transition (reviewed by Lees, 1995). Another layer of regulation exists in that CKIs, themselves, also appear to be regulated by transcriptional control and proteolytic degradation (Pagano *et al.*, 1995).

Regulating expression of the enzymes involved in DNA synthesis provides yet another way of controlling cell proliferation. Increased mRNA and protein expression during G_1 towards S phase cell cycle progression has been demonstrated for DNA polymerase α (Thömmes *et al.*, 1986), thymidine kinase (Schlosser *et al.*, 1981), topoisomerase I (Tricoli *et al.*, 1985), PCNA (Almendral *et al.*, 1987; Matsumoto *et al.*, 1987; Morris and Mathews, 1989), and other genes/gene products involved either directly or indirectly in nuclear DNA synthesis. In addition to regulated expression, replicative enzymes may also be controlled by post-translational modification or sub-cellular localization. For example, Replication factor C (RFC), which facilitates proliferating cell nuclear antigen (PCNA) loading at primer-template junctions during DNA replication, has recently been shown to be phosphorylated by calmodulin-dependent kinase II (CaMKII). Phosphorylation inhibits binding to the PCNA sliding clamp and prevents processive DNA synthesis (Maga *et al.*, 1997). Immunofluorescence studies have shown punctate nuclear staining of PCNA protein during S-phase and in response to DNA damage (Bravo and MacDonald-Bravo, 1985; Celis and Madsen, 1986; Li *et al.*, 1996). This staining pattern appears to be the

result of subcellular localization of PCNA protein to sites of DNA replication and repair. Additionally, the cyclin/CDK inhibitor $p21^{CIP1/WAF1}$ has also been shown to bind and inhibit PCNA, blocking processive DNA replication (Li *et al.*, 1994). Interestingly, $p21^{CIP1/WAF1}$ binds to the same region of PCNA as the flap endonuclease FEN1 (Warbrick *et al.*, 1995, 1997; Jönsson *et al.*, 1997), a protein shown to be required for SV40 DNA replication (Waga *et al.*, 1994). It is proposed that FEN1 and p21 may compete for binding of PCNA, providing a possible molecular switch from DNA replication to repair following damage-dependent induction by p53 (Warbrick *et al.*, 1997; reviewed by Cox, 1998).

1-5 Model Systems of DNA Replication

Insight into the mechanisms and regulation of eukaryotic DNA replication has been gained through *in vitro* studies of replication with simian virus 40 (SV40) (Weinberg *et al.*, 1990; Tsurimoto and Stillman, 1989; Wobbe *et al.*, 1987), *Xenopus* cell-free systems (Lohka and Masui, 1983; Blow and Laskey, 1986; reviewed by Romanowski and Madine, 1996), and biochemical and genetic studies in yeast (reviewed by Wuarin and Nurse, 1996). Recently, a human cell-free system was developed, showing a requirement for cyclin E or cyclin A and CDK2 in mammalian DNA replication (Krude *et al.*, 1997). However, this system has experienced problems with reproducibility and it will not be further discussed here.

The *Xenopus* system (Blow and Laskey, 1986) has been a valuable tool in identifying the mechanical and structural aspects of replication, as well as for studies into licensing and initiation of replication (Blow and Laskey, 1988). However, the *Xenopus* system is limited in that the activated egg extracts used exhibit very rapid

cell cycles of alternating S and M phases, and key regulatory steps (eg. G_1 and G_2 checkpoints) are formally absent. Additionally, although studies in the yeasts *S. pombe* and *S. cerevisiae* have also helped elucidate the mechanisms of DNA licensing, initiation of replication, and replication control, due to the scope of this investigation, they will not be further discussed here.

Similar to *Xenopus* cell-free systems, the SV40 system is also limited in studying regulation of DNA replication in that the viral trans-acting control protein (T antigen) is able to circumvent normal cellular controls of replication (Wold *et al.*, 1987). However, because the SV40 system has been invaluable in studying the actual mechanics of nuclear DNA replication, and in identifying proteins essential to the process, I will address the mechanics of DNA replication in the SV40 system.

1-5.1 SV40 DNA Replication

The SV40 circular, double-stranded DNA virus has a single origin of replication. The only viral protein required for replication is large T antigen (Wold *et al.*, 1987). The other enzymes necessary for DNA replication are derived from the host cell, and have been subsequently purified by fractionation of human cell extracts into individual components that reconstitute replication of plasmid DNA containing the SV40 origin of replication (Weinberg *et al.*, 1990; Tsurimoto and Stillman, 1989; Wobbe *et al.*, 1987). Such studies have demonstrated a requirement for 10 different mammalian proteins, in addition to the viral T antigen, to reconstitute replication of form I DNA.

The viral large T antigen binds as a double hexamer to the origin of replication in a sequence-specific, ATP-dependent manner (Tsurimoto and Stillman,

1989) and utilizes a 3' to 5' helicase activity to separate the strands, creating replication forks moving in both directions away from the origin. The single-stranded DNA-binding protein, replication protein A (RP-A), stimulates and stabilizes origin unwinding by binding newly exposed nucleotides at the replication fork, thus preventing re-annealing of separated strands (Wold and Kelly, 1987).

Figure 1-5 Leading stand DNA synthesis (Waga *et al.*, 1994)

At the leading strand, short oligoribonucleotide primers of approximately 6-14 bases are generated by the primase enzyme associated with DNA polymerase α (Tseng and Goulian, 1977). The 180 kDa catalytic subunit of DNA pol α then adds a stretch of deoxyribonucleotides to the RNA primer (Tsurimoto and Stillman, 1990). Next, replication factor C (RF-C), initiates a reaction called polymerase switching (Waga and Stillman, 1994) upon binding to the primer-template junction (Lee *et al.*, 1991). In this reaction, DNA polymerase α dissociates from DNA in an ATP-dependent manner and RF-C assembles trimeric proliferating cell nuclear antigen (PCNA) around DNA in the region of the primer terminus. The trimeric structure of eukaryotic PCNA may serve as a platform to load DNA polymerase δ at the primer terminus, and then serve to increase the processivity of DNA pol δ in leading strand synthesis (Prelich *et al.*, 1987; Bravo et al., 1987; Burgers and Yoder, 1993). It is possible that this complex of PCNA, RF-C, and DNA pol δ remain complexed during leading strand synthesis.

On the lagging strand, the RNA priming step and polymerase switching from DNA pol α to DNA pol δ in the SV40 model are virtually the same as in leading

strand synthesis (Tsurimoto and Stillman, 1990). However, it is still unclear whether DNA pol δ or ε is responsible for elongation after DNA primer synthesis. Major differences between leading and lagging strand synthesis are subsequent to the priming step and are due primarily to the frequency of priming reactions required for the generation of Okazaki fragments. The SV40 replication system has revealed that priming on the lagging strand is very frequent, with initial placement of primers approximately 50 nucleotides apart (Nethanel *et al.*, 1992). It appears that primase synthesizes ribonucleotide primers of approximately 10 nts and then DNA Pol α extends the primer by 10-20 additional deoxyribonucleotides before polymerase switching occurs (Nethanel *et al.*, 1992). After the polymerase switching occurs, another 10-20 deoxyribonucleotides are added by DNA pol δ/ε prior to arriving at the next downstream initiator RNA primer.

All RNA primers must be removed during Okazaki fragment processing. It appears that there are two essential nucleases to perform this task in higher eukaryotes (Turchi *et al.*, 1994). Figure 1-6 depicts the two current hypotheses for Okazaki fragment processing. One proposes that RNAase H1 endo-nucleolytically cleaves the initiator primer one nucleotide upstream of the RNA-DNA junction. Cleavage characteristically leaves one ribonucleotide regardless of RNA primer length or sequence, which is then removed by an enzyme known as FEN1 (see Section 1-6 below). The other hypothesis proposes that FEN1 may act independently of RNAase H1 (Turchi *et al.*, 1994; Waga *et al.*, 1994; Bambara *et al.*, 1997). Recent evidence by Murante *et al.* (1998) suggests that bovine FEN1 may also endonucleolytically removes additional nucleotides synthesized by DNA polymerase α. They suggest that this mechanism may compensate for lack of Pol α 3' to 5'

exonuclease proofreading capability by removing any mismatched pairs synthesized by Pol α.

Figure 1-6 FEN1 participation in Okazaki fragment processing

1-6 Discovery of FEN1

Flap endonuclease and 5' exonuclease (FEN1) was originally purified as a 5' to 3' exonuclease in rabbits by Lindahl in 1969 and called mammalian DNAase IV (Lindahl *et al.*, 1969). In the late 1980s and early 1990s, a similar enzyme activity was subsequently purified and characterized from different organisms in several different laboratories. Ishimi *et al.* (1988) discovered the requirement of a 5' to 3' endonuclease for completion of SV40 DNA synthesis using HeLa cell extracts. Later, FEN1's role in Okazaki fragment processing was revealed in DNA replication studies using purified proteins *in vitro* (Goulian *et al.*, 1990; Siegal *et al.*, 1992; Turchi and Bambara, 1993; Waga *et al.*, 1994). In addition to being referred to as DNAase IV, the enzyme was also called 5' to 3' exonuclease in the bovine and human systems (Turchi and Bambara, 1993; Ishimi *et al.*, 1988), respectively; and maturation factor-1 (MF1) by Waga *et al.* (1994) in a fully defined *in vitro* DNA replication system using purified proteins. Human FEN1 cDNA was initially cloned from a HeLa cDNA library during a screen for human homologues to the *S. pombe Rad2* gene (Murray *et al.*, 1994). Subsequently, the murine FEN1 gene was cloned and the endo-/exonucleolytic and biochemical properties of the encoded protein characterized (Harrington and Lieber, 1994a, 1995). Today, the murine and human genes are

generally designated as Fen-1 and FEN1, respectively, in genome maps (Harrington and Lieber, 1994b; Hiraoka *et al.*, 1995).

1-7 Characterization and Functional Studies of FEN1

The past decade has seen extensive characterization of the biochemical properties of FEN1 and its substrate specificity. To date, biochemical and enzymatic studies have been carried out on human FEN1 and its homologues in bovine, murine, rabbit, *Xenopus*, yeast, and prokaryotic systems. Complementation studies, and rescue experiments using human or *Xenopus* FEN1 cDNA, have also been performed in the yeasts *S. pombe* and *S. cerevisiae*, respectively, demonstrating FEN1's functional conservation throughout evolution (Murray *et al.*, 1994; Kim *et al.*, 1998).

Figure 1-7 shows the strict substrate specificity of mammalian FEN1 protein. As an endonuclease, FEN1 is capable of cleaving 5' (Figure 1-7A,C), but not 3' flap structures formed on either linear oligonucleotides or circular M13 DNA templates with short complementary DNA sequences (primers) annealed to the template strand (Harrington and Lieber, 1994b; Siegal *et al.*, 1992). FEN1 can also endonucleolytically cleave pseudo-Y structures (Figure 1-7B), but at a 20 to 100-fold lower efficiency than 5' flap structures containing primers annealed upstream (5') of the flap (Harrington and Lieber, 1994a). 5' to 3' exonuclease activity of FEN1 protein has also been observed at DNA gaps, nicks, and recessed 5' ends (Figures 1-7D, E, F, respectively) on linear synthetic DNA templates *in vitro* (Lindahl, 1971; Murante *et al.*, 1994; Harrington and Lieber, 1995). However, mammalian FEN1 protein appears to be unable to cleave single-stranded DNA or RNA, double-stranded DNA, mismatched bubble structures, Holliday junctions, heterologous loops, D-loops,

or 3' and 5' overhang structures by either exo- or endonucleolytic enzyme activity (Harrington and Lieber, 1994a; Murante *et al.*, 1994). It appears that FEN1 protein prefers branched DNA structures that have a single-stranded 5' flap (Lieber, 1997).

Figure 1-7 DNA structures cleaved by FEN1

The length and structure of complementary upstream primers annealed to DNA templates have an effect on FEN1 enzymatic activity *in vitro*. Primers or complementary DNA sequences annealed immediately upstream (5') of the 5' flap structure (see Figure 1-7) can increase endonuclease activity (Harrington and Lieber, 1995), but increasing gap length between upstream primers and 5' flap structures results in decreasing endonuclease activity (Murante *et al.*, 1994). Greatest enzyme activity is noted when primers are extended immediately adjacent to the flap structure (Murante *et al.*, 1994; Harrington and Lieber, 1995). It is possible that the presence of upstream primers may prevent any transient re-association of the flap with the DNA template, which would be inhibitory to FEN1 enzyme activity.

In contrast to their impact on endonucleolytic activity, the effects of upstream primers on exonucleolytic activity of FEN1 is currently unclear. Experiments with linear DNA templates and endogenous purified FEN1 protein from rabbit (Lindahl, 1971), calf (Murante *et al.*, 1994), and mouse (Harrington and Lieber, 1994a), found that the enzyme acts at a nick on double-stranded DNA (dsDNA), and less efficiently on gaps or recessed 5' ends on dsDNA (see Figure 1-7D-E). This suggested that dsDNA regions 5' and adjacent to the point of exonuclease activity stimulated enzymatic cleavage. Additionally, gel-shift assays by Harrington and Lieber (1994a)

showed that at gap structures, the efficiency of FEN1 binding to DNA decreases with increasing gap size, up to approximately 5 nucleotides, then stabilizes at a level of binding equivalent to that observed on a recessed 5' end on dsDNA. However, detailed FEN1 enzyme assays with various linear substrates by Huang *et al.* (1996) showed that exonucleolytic cleavage of either ribo- or deoxyribonucleotides may be partially inhibited by primers annealed upstream of the cleavage site. Previous conclusions that exonuclease activity is stimulated by upstream primers (Murante *et al.*, 1994; Harrington and Lieber, 1994a) may have been premature, in that the latter was actually measuring substrate binding. Additionally, although the substrates, enzymes, and assays used were similar, it is possible that conditions in earlier exonuclease assays were more conducive to FEN1 endonuclease, not exonuclease activity, which clearly shows increased enzyme activity where adjacent upstream primers are present. Finally, there may be subtle differences in enzymatic properties between species, but this is unlikely in that both Murante *et al.* (1994) and Huang *et al.* (1998) used FEN1 protein purified from calf thymus.

In addition to substrate specificity, FEN1 is also polarity-dependent, in that the enzyme must slide from the 5' end of the substrate to perform structure-specific cleavage (Murante *et al.*, 1994). Although FEN1 has been shown to be structure-specific, polarity-dependent, and strand-specific, its endonuclease activity is not dependent on the length or sequence of 5' flaps (Harrington and Lieber, 1994a; Murante *et al.*, 1994). However, as an exonuclease, recent data suggests that the 5' nucleotide of the downstream primer may affect exonucleolytic cleavage efficiency, with A, T, and U nucleotides being more susceptible to cleavage than G or C (Huang

et al., 1996). It is possible that the extra hydrogen bond between G and C bases may make those bases less susceptible to cleavage.

On linear synthetic templates, purified endogenous murine FEN1 protein exhibits optimum endonucleolytic activity pH 8 in the absence of monovalent ions (Harrington and Lieber, 1994a); although slight changes in pH do not appear to significantly effect enzyme activity. Divalent metal ions such as Mg^{2+} or Mn^{2+} are absolutely required for nuclease activity since enzyme activity is abolished in the presence of 5 mM EDTA (Harrington and Lieber, 1994a). It also appears that the type and concentration of divalent metal ion is of importance for two reasons. Firstly, endonuclease assays with purified murine FEN1 by Harrington and Lieber (1994a) showed that Mn^{2+} and Mg^{2+} ions stimulate, whereas Zn^{2+} and Ca^{2+} inhibited enzyme activity on linear templates. Secondly, the ionic concentration appears to affect the site of endonucleolytic cleavage. Increasing Mg^{2+} ion concentration above 0.1 mM results in increased cleavage one nucleotide 5' of the flap junction, whereas at 0.1 mM, the predominant cleavage site is 3' of the flap elbow (Harrington and Lieber, 1994a). Harrington and Lieber (1994a) speculate that divalent metal ionic concentrations may affect DNA base pairing at the junction, but ionic concentration effects on protein structure cannot be ruled out since the active site of prokaryotic homologues of FEN1 have been shown by X-ray crystallography to co-ordinate two Mg^{2+} ions (Shen *et al.*, 1997; Hosfield *et al.*, 1998; Hwang *et al.*, 1998).

1-8 Mechanism of FEN1 Enzyme Activity

The strict substrate specificity observed in the studies discussed in Section 1-7 above suggests a possible mechanism of FEN1 enzyme activity. Primers and adjuncts

annealed to the ssDNA flap, upstream of the point of cleavage, may affect FEN1's endonucleolytic cleavage efficiency. For example, regions of dsDNA along flap substrates can block FEN1 cleavage of 5' flap structures (Harrington and Lieber, 1994b; Murante *et al.*, 1995). Additionally, when bound to the 5' flap substrate, prokaryotic single-stranded binding protein (SSB), a functional homologue of eukaryotic RP-A, can inhibit cleavage with a degree of inhibition directly proportional to the flap length (Murante *et al.*, 1995), possibly because longer flaps allow greater RPA binding. However, yeast FEN1 (*S. cerevisiae* RAD27) endonucleolytic cleavage of flap substrates annealed to circular M13 templates was significantly stimulated by RP-A (Biswas *et al.*, 1997). It is possible that the FEN1 inhibition by RP-A noted previously (Murante *et al.*, 1995) was due to melting of the short duplex regions used in their assay, and also noted on similar templates tested by Biswas *et al.* (1997). FEN1 endonuclease activity *in vitro* is not inhibited by the presence of biotin covalently-linked to bases anywhere along the 5' flap structure. However, when streptavidin (60 kDa) was bound to these biotinylated substrates, cleavage was inhibited (Murante *et al.*, 1995). The conclusion from these data is that FEN1 binds to the free 5' end of the flap substrate and slides along the flap to the point of cleavage. This would place the single strand (ssDNA) to double strand (dsDNA) DNA transition point within the active site of the enzyme. Cis-diamminedichloroplatinum (II) (CDDP), a DNA-binding and crosslinking agent used in tumour therapy, also failed to inhibit FEN1 nuclease activity, unless it bound in the vicinity of the cleavage point, where it distorts the interaction of the FEN1 active site with its substrate (Barnes *et al.*, 1996). These results indicate that although adducts in the single-stranded flap DNA, larger than a base can be passed by FEN1, when the

adduct is large or dsDNA, the translocation of FEN1 down the flap is severely inhibited. Further *in vitro* experiments with synthetic templates have shown that the enzyme can be 'trapped' on the flap substrate by annealing complementary oligonucleotides to the flap DNA after incubation of FEN1 with labeled substrates (Murante *et al.*, 1995). This result indicates that movement of FEN1 on flap substrates is bi-directional, with nuclease molecules able to slide on and off the 5' end of the flap structure (Murante *et al.*, 1995). Finally, DNase I footprinting has revealed a 25-nucleotide region on the 5' flap DNA, adjacent to the point of annealing that is protected by FEN1 just prior to cleavage (Barnes *et al.*, 1996).

Figure 1-8 FEN1 and PCNA model for template loading

Accumulated evidence (see above) has led to the development of a model for FEN1 endonuclease activity (Figure 1-9). This model suggests that FEN1 binds and enters at the 5' termini of single-stranded flap structures. Movement of FEN1 on the DNA flap is bi-directional, and cleavage occurs when the enzyme slides down to the point at which the flap is annealed to a template DNA (eg. the ssDNA to dsDNA transition point) (Murante *et al.*, 1995). This endonucleolytic activity is compatible with the proposed model of exonuclease activity (Murante *et al.*, 1994; Harrington and Lieber, 1994a) in that a 5' terminal phosphate group at a nick may result in FEN1 nuclease activity due to the electrostatic repulsion of the negatively-charged group, resulting in "breathing" of the substrate and creating a pseudo-flap structure that can be cleaved more efficiently by FEN1 (Lieber, 1997).

1-9 FEN1 Structure and Functional Domains

The human FEN1 gene encodes a protein of 380 amino acids with an apparent molecular mass of 46 (+/- 4) kDa as measured by SDS-PAGE (Murray *et al.*, 1994; Hiraoka *et al.*, 1995). Homologous proteins include the 5' to 3' exonuclease domain of *E. coli* DNA Pol I (24% overall amino acid identity with 52% identity in specific domains; Robins *et al.*, 1994), archaebacterial FEN1 (up to 75% similarity in catalytic domains; Hwang *et al.*, 1998; Hosfield *et al.*, 1998; Shen *et al.*, 1998), *Xenopus* FEN1 (80% identity; Bibikova *et al.*, 1998; Kim *et al.*, 1998; Li *et al.*, manuscript in preparation), Rad2 in *S. pombe* (55% identity), RAD27/RTH-1 in *S. cerevisiae* (60% identity), and Fen1 in mouse (96% identity) (Murray *et al.*, 1994; Hiraoka *et al.*, 1995). The amino acid sequence of human FEN1, deduced from its cDNA sequence, exhibits blocks of homology with these homologues and with the vertebrate Xeroderma Pigmentosum complementation group G (XPG) protein (Harrington and Lieber, 1994b), designated N, I, and C regions. Prokaryotic DNA polymerases with 5' to 3' exonuclease activity also share homology blocks N and I, but not C (Robins *et al.*, 1994; Shen *et al.*, 1998; Hosfield *et al.*, 1998). Figure 1-9 shows a schematic comparison of conserved regions among 6 eukaryotic FEN1/XPG family members, 4 exo/endonuclease domains of prokaryotic DNA polymerases/nucleases, and 3 bacteriophage exonucleases (Robins *et al.*, 1994; Shen *et al.*, 1998).

Figure 1-9 FEN1 homologous proteins

Comparing the deduced human FEN1 amino acid sequence with other FEN1 homologues from Figure 1-10 reveals greater than 70% sequence similarity for

archaebacterial, and up to 92% sequence similarity for murine FEN1 in the two conserved N and I nuclease domains (Hosfield *et al.*, 1998). X-ray crystal structures of two different archaebacterial FEN1 proteins identified two clusters of acidic residues in the N and I domains that are absolutely conserved in all the known FEN1 enzymes (Hosfield *et al.*, 1998; Hwang *et al.*, 1998). Metal-soaking experiments revealed that both clusters form metal-binding (Mg^{2+}/Mn^{2+}) sites essential to enzyme activity (Shen *et al.*, 1997; Hosfield *et al.*, 1998; Hwang *et al.*, 1998). Additional studies with recombinant human FEN1 protein containing mutations in those same conserved regions shows that enzyme activity on model flap substrates is also abolished (Shen *et al.*, 1996; Shen *et al.*, 1997).

Crystal structures of FEN1 homologues T4 RNAase H and T5 exonuclease D15 have revealed an arch structure, below which is a hole through the enzyme (Mueser *et al.*, 1996; Ceska *et al.*, 1996). The arch is highly positively charged on the side closest to the catalytic region, which consists of a cluster of aspartic acid residues (conserved in human FEN1) that complex two magnesium ions important to enzyme activity (Mueser *et al.*, 1996). Additionally, the recently published crystal structure of the archaebacteria *Pyrococcus furiosus* FEN1 (Figure 1-10) exhibits the same arch structure, and they go on to suggest that DNA binding is accomplished by non-specific interactions between the DNA phosphodiester backbone and the active site (Hosfield *et al.*, 1998). In further studies using small angle-ray scattering, a magnesium-induced conformational change of wild-type human FEN1 has been discovered (Shen *et al.*, 1996). This implies that structural changes to the catalytic site caused by magnesium influxes may account for the ability of Mg^{2+} to stimulate FEN1 cleavage.

Figure 1-10 Pf FEN1 Crystal structure (Hosfield *et al.*, 1998)

1-10 FEN1 is Implicated in DNA Repair

Based on biochemical and genetic evidence, human FEN1 homologues in yeast (Rad2 in *S. pombe*, RAD27 in *S. cerevisiae*) have been implicated in DNA repair and recombination, suggesting that mammalian FEN1 might share this activity. In the budding yeast *S. cerevisiae*, yFEN1 mutants (RAD27Δ or RTH-1Δ) show instability of simple repetitive DNA sequences (Reagan *et al.*, 1995, Johnson *et al.*, 1995, Sommers *et al.*, 1995), with a 280-fold increase in repeat instability and a 30-fold increase in the spontaneous mutation rate compared to wild-type RAD27+ (Johnson *et al.*, 1995). Additional epistasis analysis with yeast mismatch repair (MMR) mutants is consistent with a role of *S. cerevisiae* yFEN1 (RAD27/RTH-1) in the MSH2-MLH1-PMS1 MMR pathway (Johnson *et al.*, 1995), which is highly conserved from bacteria to humans (Umar *et al.*, 1996). However, further evidence suggests that the majority of genetic alterations in yFEN1 (RAD27Δ) mutants are the result of a novel process, distinct from MMR, involving increased chromosomal double-strand breaks during faulty Okazaki fragment processing (Tishkoff et al., 1997). During lagging strand synthesis, DNA synthesis extending the 3' end of an Okazaki fragment runs into the next Okazaki fragment and displaces it. It is thought that if the resulting flap is not endonucleolytically removed by RNAse H and FEN1, extensive strand displacement caused by the on-coming polymerase makes the resulting single-stranded template highly susceptible to breakage (Tishkoff *et al.*,

1997). Inefficient or saturated double-strand break repair mechanisms may lead to the mutator phenotype observed in yFEN1 mutants. This result further suggests that FEN1 may have a role in DNA end-joining events seen in V(D)J recombination in immunoglobulin genes, and double-strand break repair during cellular responses to ionizing radiation (Lieber, 1997). Interestingly, Wu *et al.* (1999) recently demonstrated that targeted deletion of yFEN1 (*S. cerevisiae* RAD27) resulted in a significant (over 4-fold) reduction in nonhomologous DNA end joining events when 5' flaps are the expected intermediate DNA structures.

Rad2Δ and RAD27Δ (yFEN1) mutants also show sensitivity to both UV irradiation and alkylating agents (Murray *et al.*, 1994; Reagan *et al.*, 1995; Sommers *et al.*, 1995), but it is thought that this sensitivity is caused by inactivation of an alternate base excision pathway, involving FEN1, that removes modified AP sites and bulky UV lesions (Klungland and Lindahl, 1997; Kim *et al.*, 1998), rather than an activity in NER. Although a role for RAD27/RTH-1 in NER has not been detected to date, genetic studies in yeast RAD27/RTH-1 deletion mutants have shown that RAD27/RTH-1 is important for the repair of alkylation damage via BER and recombinational repair (Li *et al.*, 1995).

Further evidence supporting a potential role for human FEN1 in DNA repair comes from studies using purified human proteins *in vitro*. *In vitro* repair assays on synthetic templates by Klungland and Lindahl (1997) showed that FEN1 protein was absolutely required for long-patch BER of modified AP sites not susceptible to the predominant short-patch BER pathway. Additional studies using purified recombinant protein and synthetic linear templates in a reconstituted *Xenopus* system,

showed that *Xenopus* FEN1 was also required for long-patch BER (Kim *et al.*, 1998). These studies suggest a role for mammalian FEN1 during BER *in vivo*.

1-11 FEN1-Associated Proteins

Because of FEN1's role in DNA replication (see Section 1-5), it would seem logical that there would be some interactions and associations of FEN1 with other proteins of the DNA replication complex. PCNA, the homotrimeric sliding clamp that is a processivity factor for DNA polymerases δ/ε (Prelich *et al.*, 1987; Bravo *et al.*, 1987), has been shown to be associated with FEN1. This association was initially demonstrated in a yeast two-hybrid screen (Li *et al.*, 1995, Chen *et al.*, 1996; Warbrick *et al.*, 1997). Further biochemical and enzymatic studies using co-immunoprecipitation with purified proteins and synthetic peptides reaffirmed the association between PCNA and FEN1 in yeast (Li *et al.*, 1995) and humans (Chen *et al.*, 1996; Warbrick *et al.*, 1997; Jönsson et al., 1998). Furthermore, it was shown that PCNA stimulated the endonuclease activity of FEN1 (RTH-1) on model flap structures 10- to 50-fold (Li *et al.*, 1995; Wu *et al.*, 1996) in both human and yeast *in vitro* systems. A FEN1-PCNA interaction is further supported by a PCNA-binding domain that has been mapped on FEN1 (Warbrick *et al.*, 1997). Recently, homologous regions of FEN1 and the cyclin/CDK inhibitor, p21, have been found to compete for binding to the same site on PCNA (Chen *et al.*, 1996, Warbrick *et al.*, 1997). It is speculated that this could provide a mechanism for coordination between DNA replication and repair (Warbrick *et al.*, 1997; Cox, 1998).

Although DNA synthesis from upstream primers by bovine DNA Pol ε was found to stimulate removal of downstream primers by bovine FEN1 protein *in vitro*

(Siegal *et al.*, 1992), no protein-protein interaction has been observed. Similarly, although yFEN1 (*S. cerevisiae* RAD27) co-purifies with DNA Pol α (Zhu *et al.*, 1997), no other evidence for a direct protein-protein interaction has been reported.

Lastly, a yeast replicative helicase, Dna2 Helicase, was found to interact genetically and biochemically with yeast FEN1, as determined by rescue experiments and *in vitro* binding assays with recombinant proteins (Budd and Campbell, 1997). This finding may link a known DNA helicase to Okazaki fragment processing and DNA repair. This may be important because it may identify how helicases recruit replication proteins to the sites of DNA synthesis and repair.

1-12 The Aims of this Thesis

Although considerable evidence strongly supports a role for human FEN1 protein in DNA replication and DNA repair, it is largely based on *in vitro* studies. The next logical step in establishing a role for human FEN1 in DNA replication and repair is to examine FEN1 *ex vivo*.

In this thesis I purify human FEN1 protein and raise antibodies suitable for use in subsequent stages of this project (Chapter 3). I also determine the subcellular distribution of recombinant human FEN1 protein in cultured cells (Chapter 3). In subsequent chapters, I examine human FEN1 mRNA and protein levels during the cell cycle (Chapter 4) and in response to DNA damage (Chapter 5) in human cell cultures, to determine if human FEN1 mRNA or protein levels change as cells progress through the cell cycle or as part of a cellular response to DNA damage. In addition, human FEN1 protein solubility patterns are also examined to determine if FEN1 protein solubility changes in either a cell cycle-dependent or DNA damage-

dependent manner (Chapters 4 and 5). I also identify putative regulatory elements in the human *FEN1* gene promoter that may control its expression during the cell cycle or in response to DNA damage (Chapter 6).

These aims are intended to investigate the properties of human FEN1 in cultured cells, and determine if FEN1's putative role in DNA replication and repair *in vitro* is supported by observations *ex vivo*.

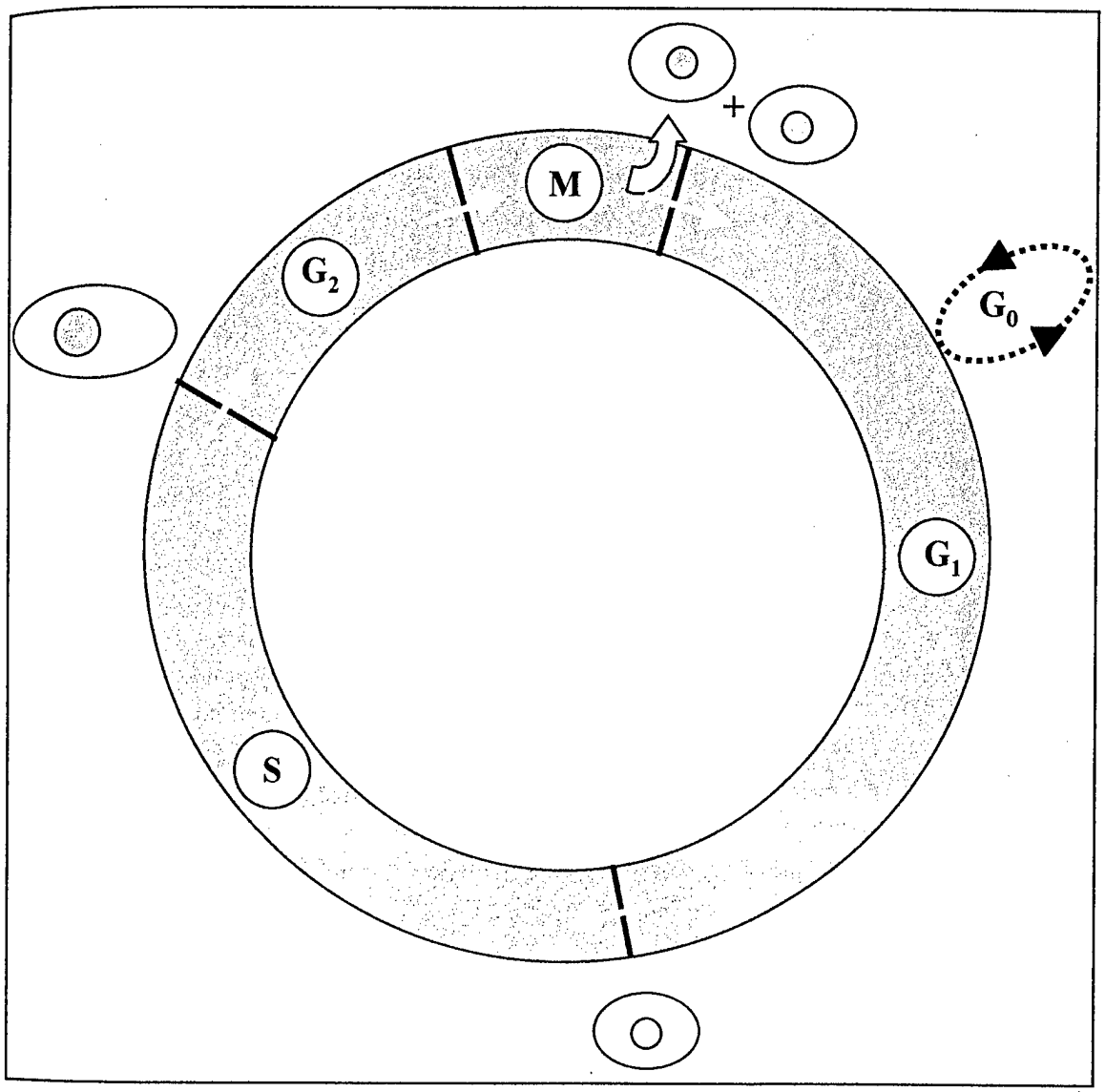

Figure 1-1. The eukaryotic cell cycle. During G_1, cells grow whilst performing essential metabolic processes. They are also responsive to growth stimuli that signal them to replicate their DNA (S phase) in preparation for mitosis (M) and cell division. Additionally, some quiescent (G_0) cells are also capable of responding to mitogenic stimuli and re-enter the cell cycle during G_1. During G_2, cells may correct replication errors that remain after S phase, thus preventing fixation of mutations in daughter cells. The cell cycle depicted above is only a representative sample, as the duration of each phase may vary relative to the other phases. The G_1 phase is generally the most variable in terms of duration, while M phase typically varies the least (adapted from Alberts *et al.*, 1994).

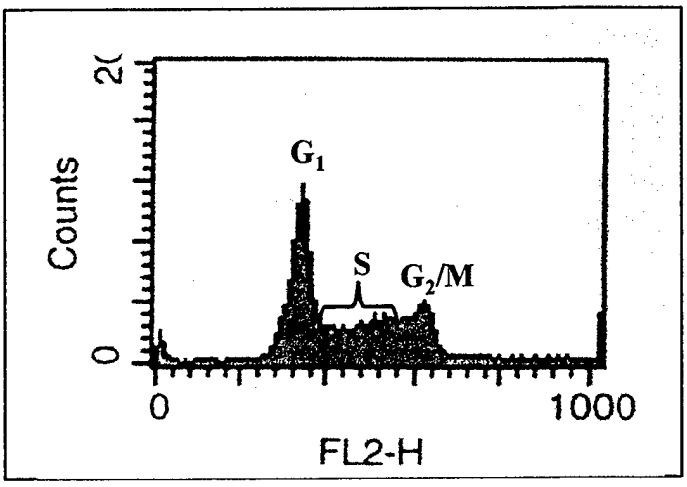

Figure 1-2. FACS analysis profile of a typical asynchronous cell population. The DNA content of cells within an asynchronous cell population was determined during FACS analysis by measuring the fluorescence intensity of individual cells stained with a DNA stain such as propidium iodide. The approximate cell cycle stages can then be determined as a function of fluorescence intensity (DNA content) and are depicted above. The X-axis (FL2-H) depicts the fluorescence intensity (arbitrary units) and the Y-axis (counts) indicates the cell number.

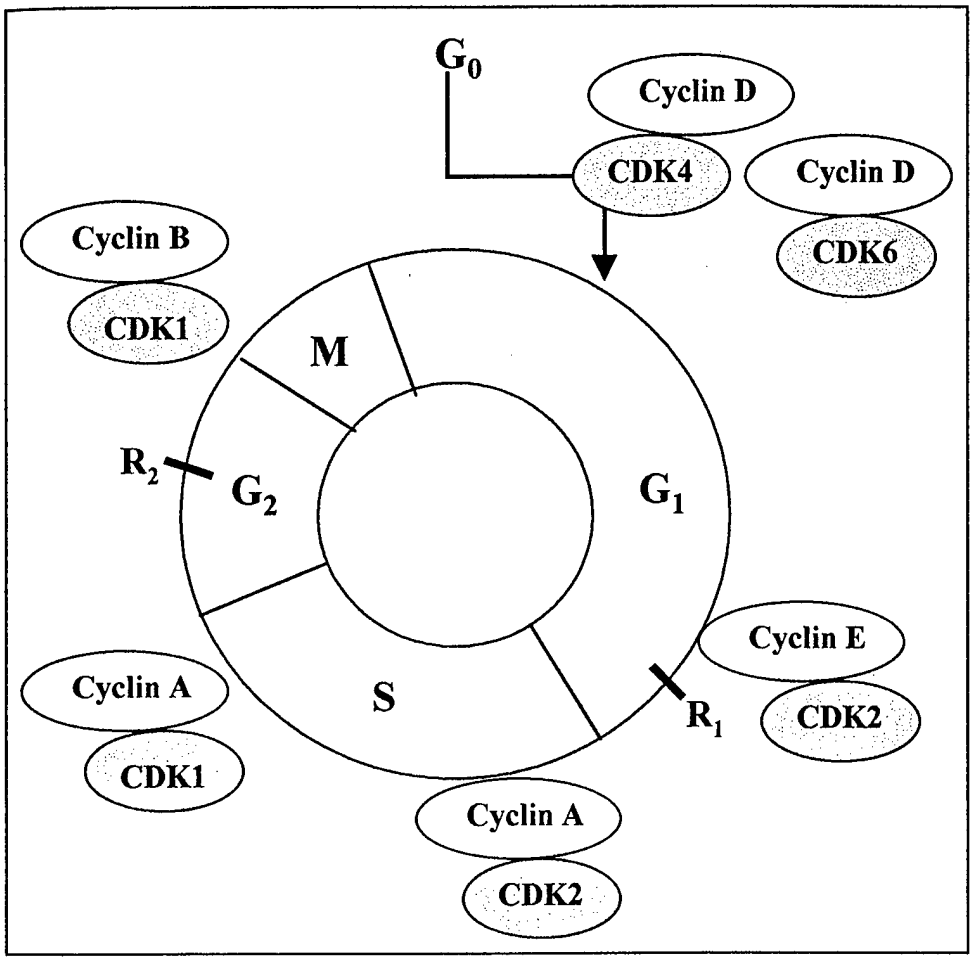

Figure 1-3. Major cyclin-CDK complexes responsible for transitions during the mammalian cell cycle. Cyclins accumulating during various points of the cell cycle bind and activate different cyclin-dependent kinases (CDKs) that drive cell cycle progression. Cyclin activity is partly controlled by periodic synthesis and proteolytic degradation at specific times during the cell cycle. R_1 refers to the restriction point, after which mitogenic signals are no longer required for cell cycle progression (adapted from Hutchison and Glover, 1995).

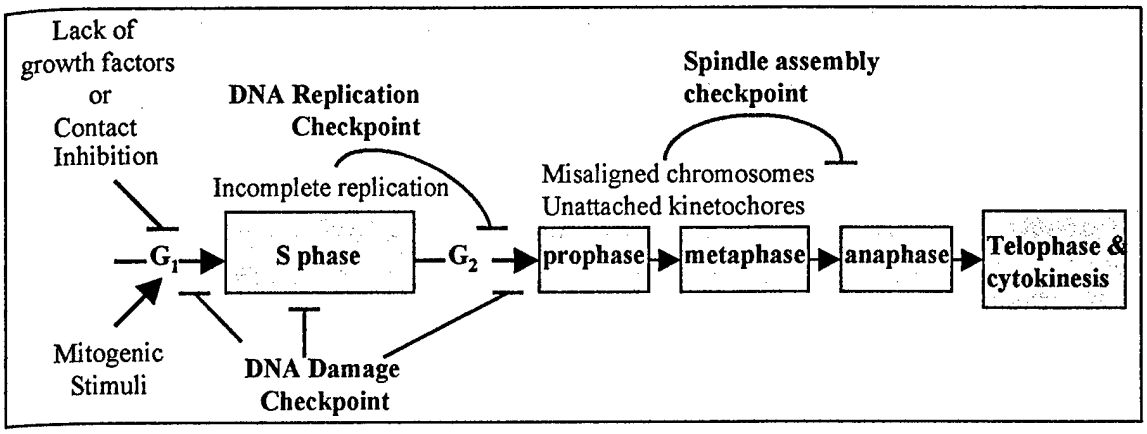

Figure 1-4. Checkpoint activation can block cell cycle progression. During mammalian cell cycle progression from G_1 to mitosis, numerous checkpoint mechanisms have been identified that can block progression (shown in red). While mitogenic signals can stimulate the G_1 to S phase transition, DNA damage, contact inhibition, and lack of growth factors can block that cell cycle progression. Additionally, DNA damage and incomplete replication can activate the DNA replication checkpoint, preventing cells from entering mitosis with damaged or incompletely replicated DNA. Further checkpoints in mitosis have been identified that can block the metaphase to anaphase transition (spindle assembly checkpoint) if chromosomes are misaligned or not attached to the mitotic spindle (adapted from Elledge, 1996).

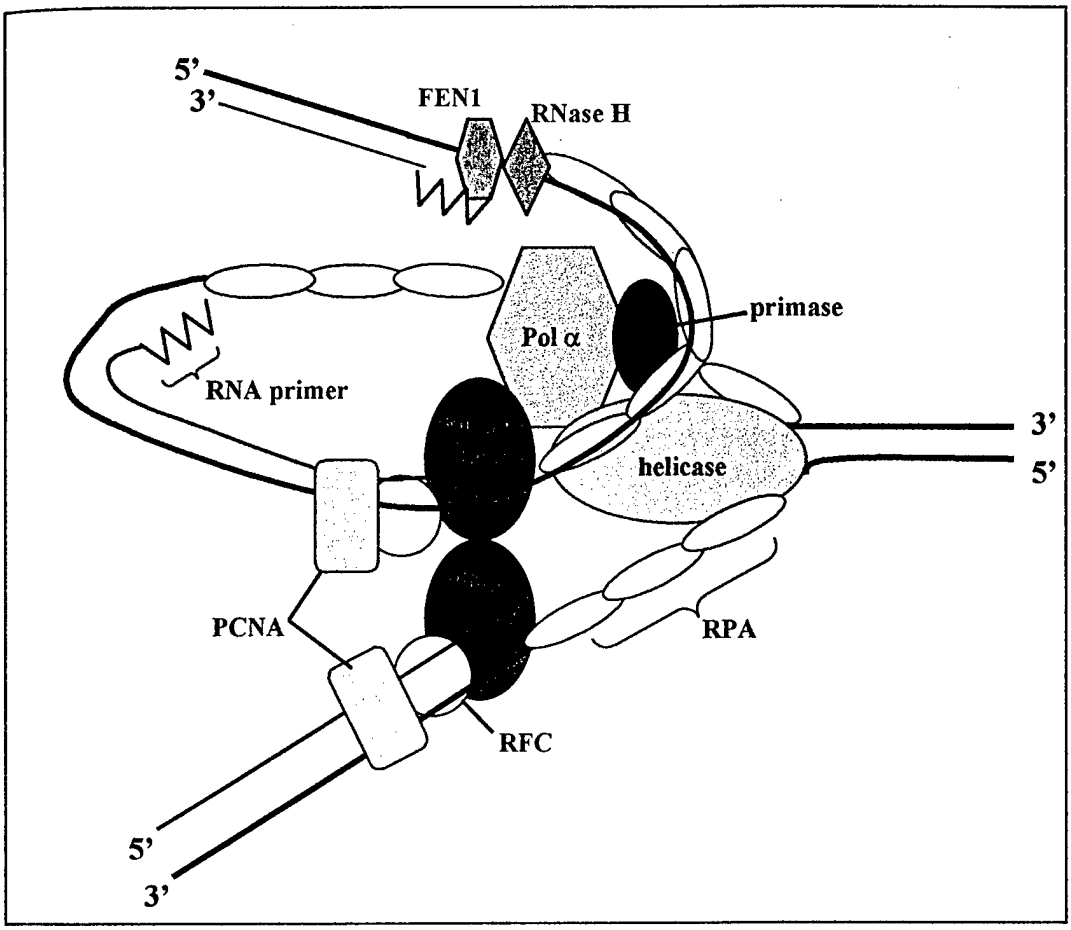

Figure 1-5. Model for the multi-protein complex acting at the eukaryotic DNA replication fork. As a DNA helicase unwinds the DNA duplex, RPA binds exposed bases to prevent re-annealing. Processive DNA synthesis on the leading strand is accomplished by DNA Pol δ, with PCNA and RFC. On the lagging strand, DNA synthesis is discontinuous, with numerous RNA primers synthesized by the primase enzyme associated with DNA Pol α. The catalytic subunit of DNA Pol α then adds a stretch of deoxyribonucleotides to the RNA primers before polymerase switching occurs. RFC loads PCNA at primer termini, and directs either DNA Pol δ or Pol ε to continue DNA synthesis on the lagging strand. As the polymerase complex approaches the downstream primer, RNase H1 cleaves the RNA primer, leaving one ribonucleotide at the RNA-DNA junction. That remaining ribonucleotide is removed by FEN1 before the in-coming polymerase complex finishes synthesis. DNA ligase seals the nick to ligate the processed Okazaki fragments (adapted from Waga and Stillman, 1994).

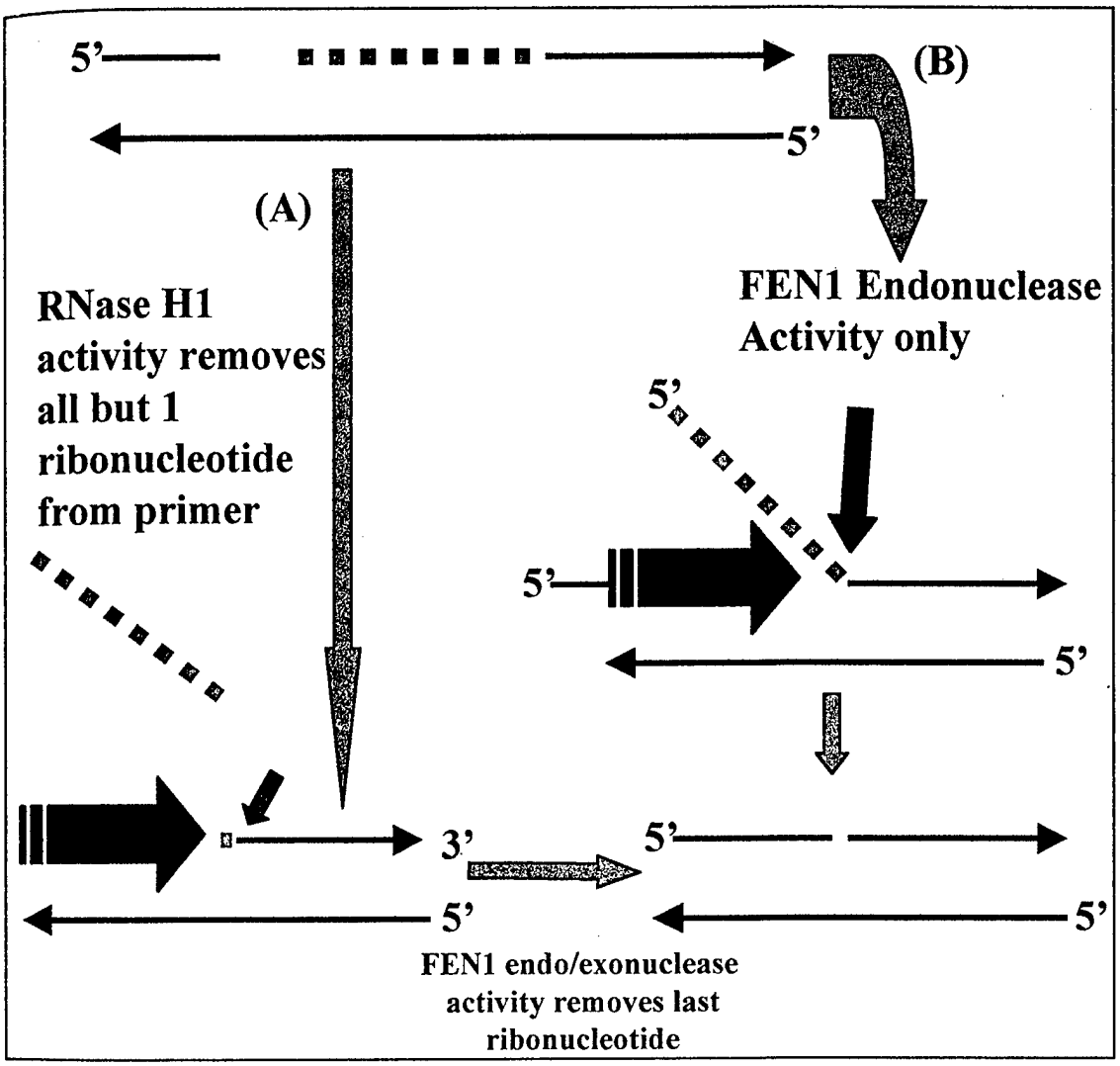

Figure 1-6. Two potential pathways for FEN1 function in removal of RNA primers during Okazaki fragment processing. Red squares represent the ribonucleotides of the RNA primer for each Okazaki fragment. The large blue arrow indicates recent extension of the upstream primer by the DNA polymerase complex (either DNA Pol δ or ε). In **(A)** RNase H1 endonucleolytically cleaves the RNA primer, leaving 1 ribonucleotide. FEN1 subsequently either endo- or exonucleolytically removes the remaining ribonucleotide (cleavage site is indicated by turquoise arrow). **(B)** Following 5' flap formation due to displacement by the in-coming replication complex, the RNA primer is removed in its entirety by the endonuclease activity of FEN1.

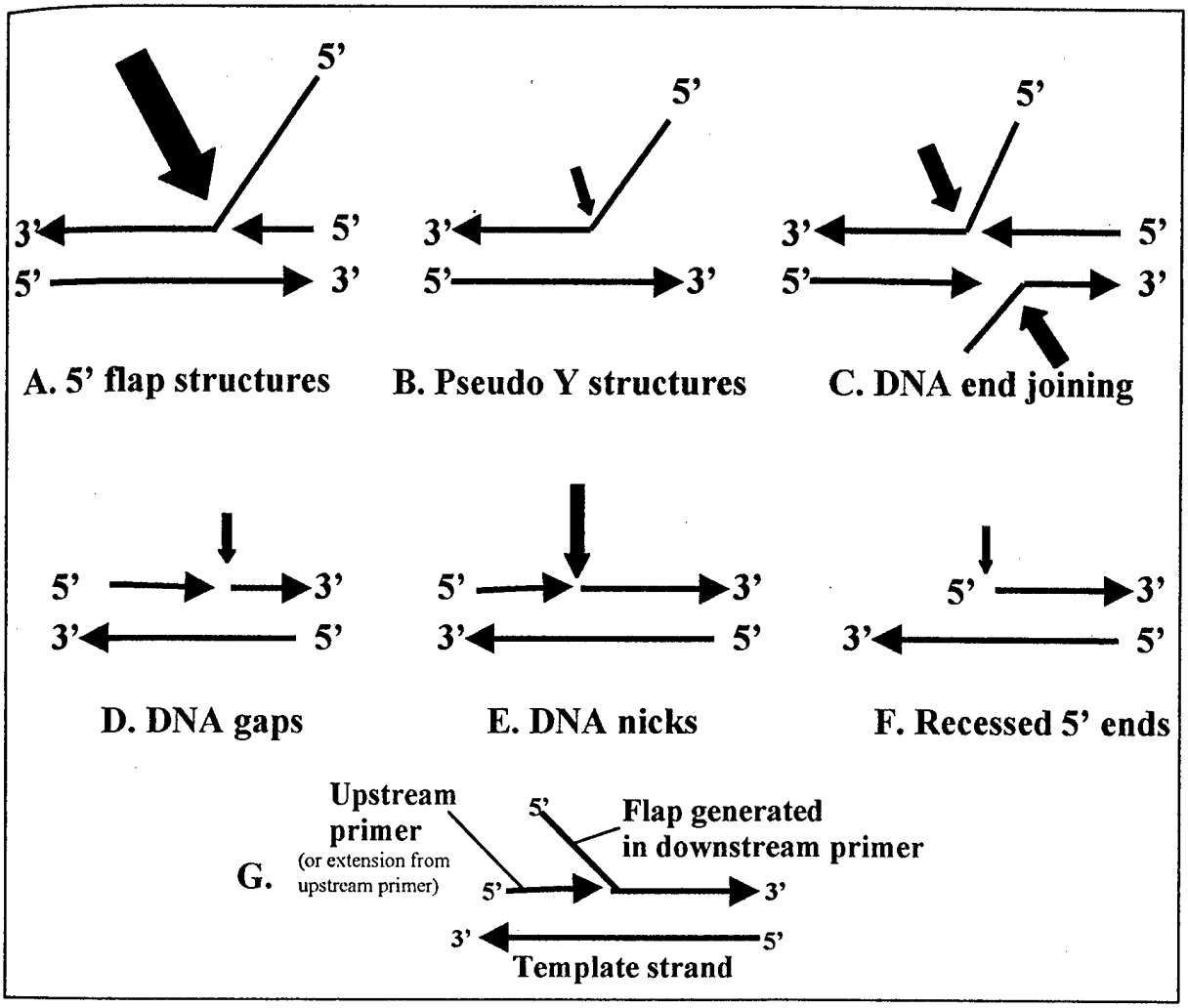

Figures 1-7. DNA intermediate structures thought to be cleaved by FEN1.
(A-F) Branched intermediate structures in DNA metabolism that are excised by FEN1 nuclease activity. Size of the arrow indicates efficiency of nuclease activity. **(G)** Describes the various structures of DNA templates discussed in the text. Arrowheads represent 3' ends of DNA (adapted from Lieber, 1997).

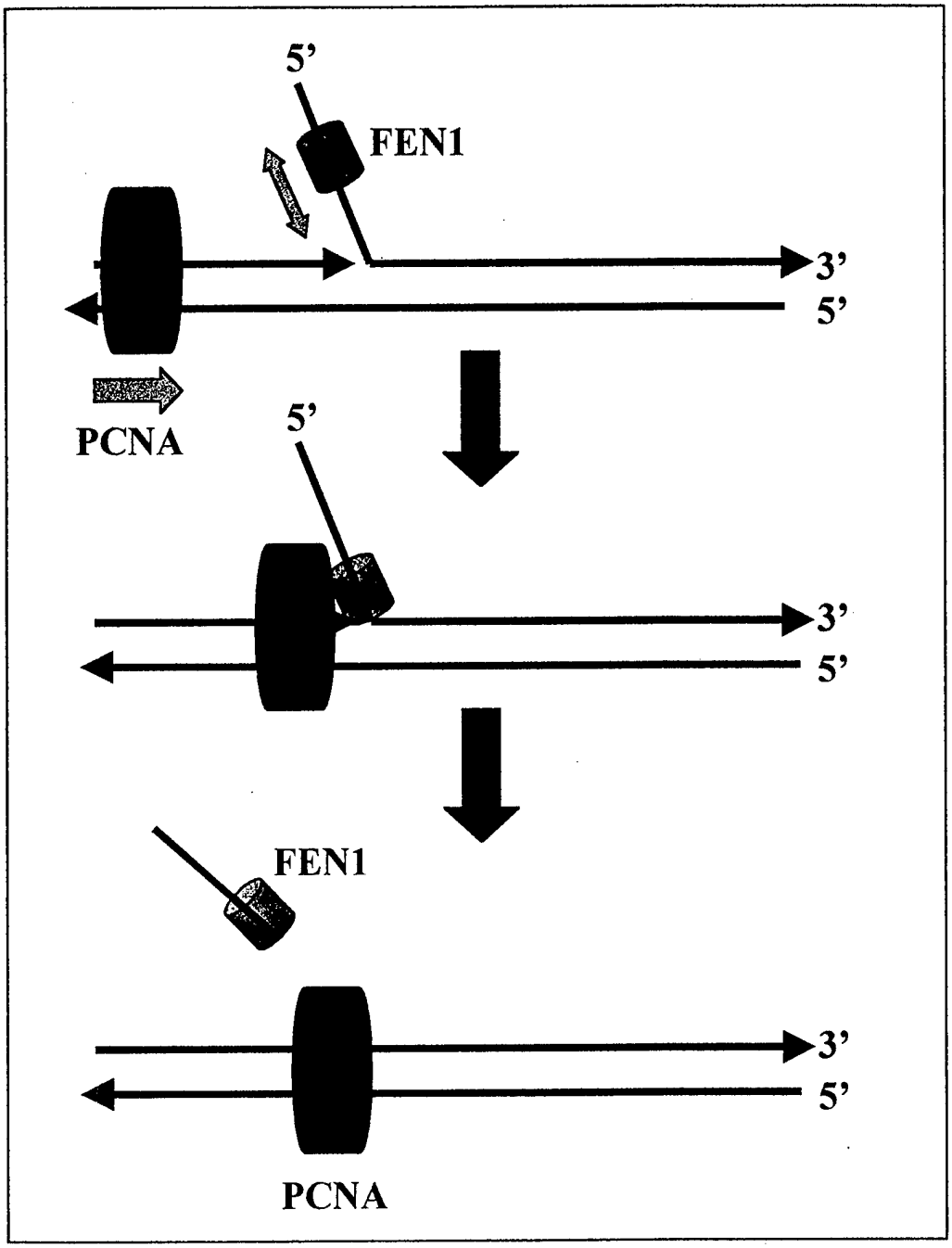

Figure 1-8. Model for FEN1 and PCNA loading onto flap substrates. FEN1 tracks along the single-stranded 5' flap of a branched DNA structure. Without this 5' single-stranded entry point, FEN1 is unable to localize to the DNA branch point. Double-stranded regions or large molecular interruptions of the single-stranded character at any point along the flap prevents FEN1 from reaching the branch point and cleavage is prevented (Murante *et al.*, 1995). PCNA loads onto ds-DNA termini by diffusion, or onto long linear DNAs and circular DNA by the action of RFC, which requires ATP hydrolysis. FEN1 and PCNA proteins have been shown to interact *in vitro* (Li *et al.*, 1995; Chen *et al.*, 1996; Warbrick *et al.*, 1997). It is proposed that PCNA may stimulate FEN1 nuclease activity by increasing the residence time at the branch point, or it may stabilize FEN1 activity at physiological salt concentrations. Arrowheads represent 3' ends of DNA.

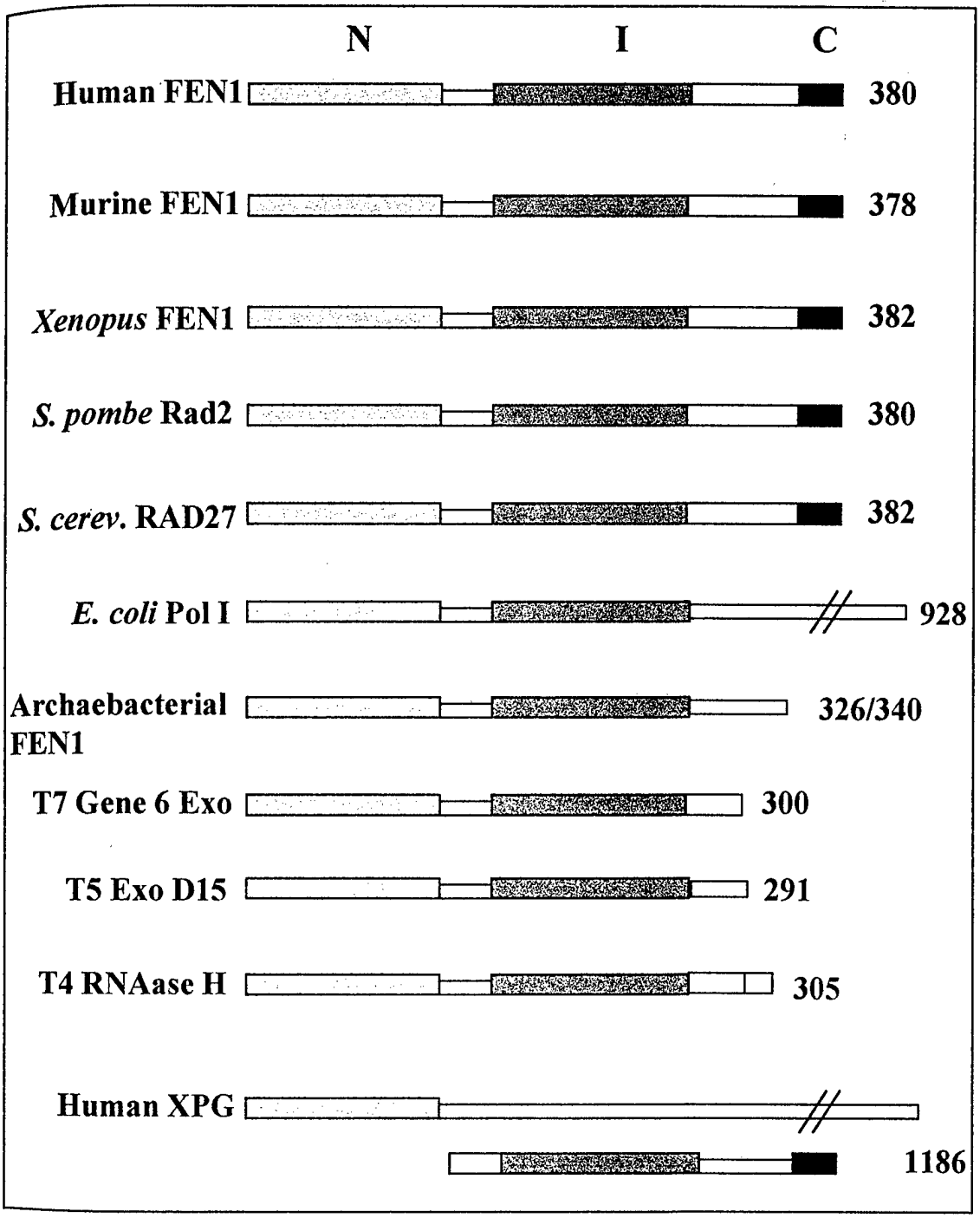

Figure 1-9. FEN1 homologues containing homologous N and I domains. The N (blue) and I (gray) domains appear to be important for DNA binding and FEN1 enzymatic activity. The N domain is typically the first 100 amino acids and is typically separated from the I domain by approximately 18 residues. XPG is the exception, in that the separation is over 640 amino acids. The C domain (black) consists of highly basic residues thought to be important for nuclear localization, and are not present in bacteriophage exonucleases or prokaryotic enzymes. The total number of amino acids of each protein is indicated on the right. The symbol // in E. coli Pol I and human XPG indicates that they are not to scale as amino acids in those domains are omitted in this diagram. The references for each are indicated in the text.

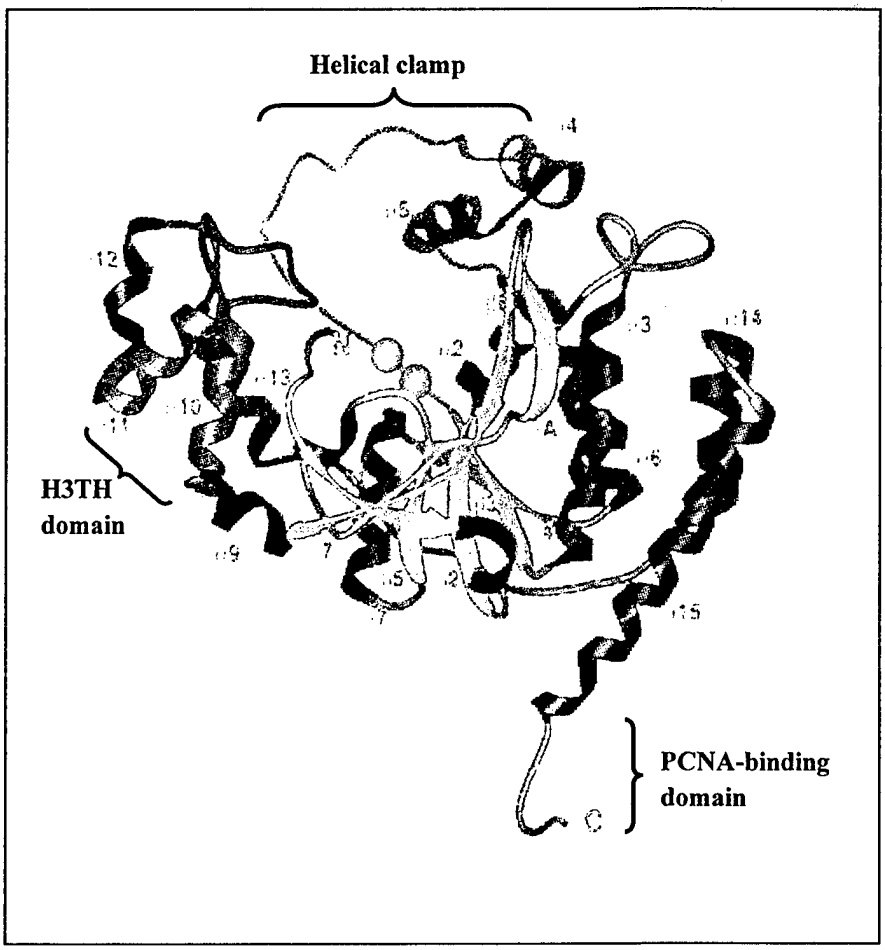

Figure 1-10. Structure of archaebacterial *P. furiosus* FEN1. N-terminal histidine-tagged recombinant *P. furiosus* FEN1 protein was purified, crystallised, and the structure determined (Hosfield *et al.*, 1998). Key structural features include a C-terminal PCNA-binding domain, a helical clamp, a H3TH duplex DNA binding domain, and an active site in complex with 2 metal (Mg^{2+}/Mn^{2+}) ions (shown as yellow spheres in centre of figure) that are all highly conserved in human FEN1 and its homologues. It is thought that FEN1 protein binds to the front face of PCNA by its C-terminal binding domain, and as flap structures are generated by displacement during lagging strand DNA synthesis, single-stranded flaps thread through the helical clamp. As FEN1 slides down the flap, the H3TH domain comes into contact with double-stranded DNA at the flap junction. H3TH-dsDNA binding induces a conformational change in the helical clamp as it closes around the flap and brings the ssDNA flap into the catalytic site, where it is cleaved (from Hosfield *et al.*, 1998).

CHAPTER TWO: METHODS AND MATERIALS

2-1 Materials

All biochemicals and reagents described were obtained from Sigma unless otherwise stated.

2-1.1 General Culture Media

All bacterial media solutions were autoclaved at 15 psi (1 bar) for 20 minutes at 121°C.

Luria-Bertani (LB) Medium, pH 7.0 (Sambrook *et al.*, 1989)

Bacto-Tryptone (DIFCO)	10 g (w/v)
Bacto-Yeast extract (DIFCO)	5 g (w/v)
NaCl (BDH)	170 mM
H_20	to 1 litre

LB-Agar, pH 7.0 (Sambrook *et al.*, 1989)

Bacto-Tryptone	10 g (w/v)
Bacto-Yeast extract	5 g (w/v)
NaCl	170 mM
H_20	to 1 litre

Tissue Culture Medium (10% FCS)

Dulbecco's modified Eagle's medium	500 ml
Foetal Calf Serum (FCS)	10% (v/v)
L-glutamine	2 mM
penicillin	100 U/ml
streptomycin	100 µg/ml

Trypsin-EDTA

trypsin in Ca^{2+}/Mg^{2+}-free tissue culture grade PBS	0.5 mg/ml(w/v)
EDTA	0.5 mM

2-1.2 General Buffers

All buffers were autoclaved at 15 psi (1 bar) for 20 minutes at 121°C, unless annotated (*) otherwise.

TE buffer (Sambrook *et al.*, 1989)

Tris-HCl, pH 8.0 (Boehringer Mannheim)	10 mM
EDTA	1 mM

TAE buffer (Sambrook *et al.*, 1989)

Tris base	40 mM
glacial acetic acid (BDH)	0.058 N
EDTA	1 mM

* SDS Running buffer (Harlow and Lane, 1988)

glycine (BDH)	0.192 M
Tris base	25 mM
sodium dodecyl sulphate (SDS)	2.88 mM

Western Blotting buffer (Harlow and Lane, 1988)

glycine	0.192 M
Tris base	25 mM
methanol (BDH)	20% (v/v)

* 2X SDS Gel Loading buffer (Harlow and Lane, 1988)

SDS	2% (w/v)
glycerol (BDH)	20% (v/v)
Tris-HCl, pH 6.8	125 mM
bromophenol blue	0.01% (w/v)
dithiothreotol (DTT)	200 mM

* 6X DNA Gel Loading buffer (Sambrook *et al.*, 1989)

bromophenol blue	0.025% (w/v)
sucrose (BDH)	40% (w/v)

Phosphate-buffered Saline solution (PBS)

$NaH_2PO_4.H_20$ (BDH)	7.4 mM
Na_2HPO_4 (BDH)	3.6 mM
NaCl	0.142 M

2-1.3 RNA Materials and Solutions

All glassware and spatulas were autoclaved, then baked at 180°C for 5 hours minimum and kept separate from all other laboratory glassware. Exclusive-use RNA electrophoresis tanks were washed with 10% SDS and rinsed extensively with DEPC-treated water prior to use. All RNA solutions were prepared with DEPC-treated water.

DEPC-treated water

diethylpyrocarbonate	0.1% (v/v)

The solution was agitated and incubated at room temperature overnight before autoclaving.

RNA gel buffer

MOPS	0.2 M
sodium acetate.NaOH, pH 7.0 (BDH)	50 mM
EDTA	10 mM

20x SSC

NaCl	1.5 M
sodium citrate-NaOH, pH 7.0	150 mM

6X RNA gel loading buffer (Sambrook *et al.*, 1989)

glycerol	0.5% (v/v)
EDTA	1 mM
bromophenol blue	0.4% (w/v)
xylene cyanol	0.4% (w/v)

Formamide

Formamide (BDH) was deionized by mixing with BioRad AG501-X8 (D) mixed bed resin for 1-2 hours and filtered through Whatman No. 1 paper. Treated formamide was aliquoted and stored at -20°C.

2-1.4 Protein Analysis Reagents

Stripping buffer

Tris-HCl, pH 6.9	62.5 mM
β-mercaptoethanol	100 mM
SDS	2% (w/v)

NP40 lysis buffer

NP40	1% (v/v)
Tris-HCl, pH 8.0	50 mM

NaCl	150 mM
EDTA	5 mM
Coomassie Stain	
methanol	50% (v/v)
acetic acid	10% (v/v)
Coomassie Blue R-250 (Sigma)	1 g (w/v)
H_2O	to 500 ml
Coomassie Destain solution	
methanol	7.5% (v/v)
acetic acid	10% (v/v)
10% SDS-PAGE gel (Harlow and Lane, 1988)	
Resolving gel (5 ml final volume):	
acrylamide-bis (30:0.8) (Protogel, National Diagnostics)	1.67 ml
3M Tris-HCl, pH 8.8	0.625 ml
10% SDS	50 µl
H_20	2.63 ml
10% APS	25 µl
TEMED (USB)	2.5 µl
Stacking gel (2.5 ml final volume):	
acrylamide-bis (30:0.8) (Protogel, National Diagnostics)	312.5 µl
1M Tris-HCl, pH 6.8	312.5 µl
10% SDS	25 µl

H_20	1.85 ml
10% APS	25 µl
TEMED	2.5 µl

2-2 Methods

2-2.1 Plasmid Construction

Bacterial plasmids were constructed to contain the human *FEN1* open-reading frame (ORF) in-frame with the translational start site of an inducible promoter, and in some instances, an in-frame protein expression epitope (tag) to facilitate subsequent purification.

The pDR2-FEN1 cDNA encoding the human FEN1 protein was a generous gift of J Murray (Univ. Of Sussex, UK). pET-FEN1 plasmids were constructed with the Nco I/Dra I fragment of shuttle vector pDR2-FEN1 cDNA (containing human *FEN1*) ligated into the C-terminal histidine-tagged vector, pET-21d (Novagen). The pET-21d vector was digested with Nco I/BamH1 and subsequently Klenow (NEB) filled-in to create a compatible blunt end. Briefly, approximately 10 µg of pET-21d plasmid DNA was digested with 10 units (U) of Bam H1 restriction enzyme (Boehringer Mannheim) in 40 µl reaction volumes at 37°C for 3 hours. Complete Bam H1 digestion was verified by separating 1 µl of the reaction mixture on a 1% agarose gel before heating to 75°C for 10 minutes to inactivate the restriction enzyme. The remaining Bam H1-digested pET-21d plasmid was mixed with all 4 dNTPs (all at 2.5 mM, Promega) and 3 U Klenow enzyme (Boehringer Mannheim) in a 50 µl reaction volume, and incubated at 37°C for 30 minutes

to create a blunt end by Klenow polymerization. The entire reaction mixture was subsequently separated on a 1% agarose gel and the linearized plasmid band was excised and isolated by Gene Clean (Amersham). The pET-21d (Bam H1-Klenow) plasmids were finally digested with 10 U of NcoI (Boehringer Mannheim) in 40 µl reaction volumes overnight at 37°C. The linearized pET21d plasmid (NcoI-blunt end) was isolated from a 1% agarose gel by Gene Clean. Approximately 20 µg of pDR2-FEN1 plasmid DNA was also double digested with 14 U of NcoI and DraI restriction enzymes in 40 µl reaction volumes overnight at 37°C. The presence of an approximately 1.2 kb human FEN1 cDNA band was verified on a 1% agarose gel before isolation of the FEN1 cDNA (NcoI-DraI) insert by Gene Clean. The prepared pET-21d vector and human FEN1 cDNA insert were ligated together in 20 µl reaction volumes containing 1 U T4 ligase (Boehringer Mannheim) and a 3:1 molar ratio of insert:vector DNA overnight at 16°C. The ligated pET21d-FEN1 plasmids resulted in deletion of the 4 C-terminal amino acids from full-length FEN1 in-frame with 6 histidine residues at the C-terminus of the protein (His_6-FEN1).

pT7.7-FEN1 plasmids were a gift of Dr J-L Li (University of Oxford) and were constructed by ligating PCR-amplified *FEN1* with engineered EcoRI/SalI sites into SmaI/SalI-digested pT7.7 (EcoRI and SmaI provide compatible blunt ends). Additionally, the *FEN1* sequence in pET-21d (pET21d-FEN1) and the PCR-amplified sequence in pT7.7 were subsequently verified by DNA sequencing of purified plasmid DNA by ABI automatic sequencing (University of Oxford, UK). The human FEN1

cDNA sequence, as well as the pET-21d and pT7.7 plasmid maps, are depicted in the Appendix.

All plasmid constructs were subsequently used to transform DH5α bacteria for DNA amplification and purification. Briefly, competent *E. coli* DH5α bacteria were prepared according to the method of Hanahan (1983), as described in Sambrook *et al.* (1989). DH5α were transformed by adding approximately 1 μg of plasmid DNA to 100 μl (approx. 1 X 10^6 cells) of competent bacteria, gently tap mixing, and incubating on ice for 30 minutes. The DH5α-plasmid DNA suspensions were then heat-shocked at 42°C for 1 minute and 0.5 ml of LB at 37°C was added. The suspension was gently tap mixed and incubated at 37°C for 1 hour to allow antibiotic gene expression from incorporated plasmid DNA. Approximately 25-50 μl of this preparation was plated out on LB agar petri dishes containing 100 μg/ml ampicillin to select for plasmid-containing bacteria and incubated overnight at 37°C. Individual transformed bacteria colonies were selected and grown in 10 ml volumes of LB containing 100 μg/ml ampicillin overnight at 37°C. Plasmid DNA was prepared as described in Sambrook *et al.* (1989) and DNA digests of plasmid DNA were performed to verify that proper size fragments were released following restriction digests.

2-2.2 Transformation and Protein Expression

Purified FEN1 plasmids were transformed as described in Section 2-2.1 into competent *E. coli* BL21 (DE3) for protein expression. Transformants were selected on ampicillin plates (100 μg/ml), then individual colonies were picked and grown at 37°C in 500 ml of Luria-

Bertani broth (LB) plus 0.5M sorbitol (Sigma) and 2.5mM betaine (Blackwell and Horgan, 1991) and recombinant protein expression was induced once bacteria had grown to an OD_{600} of 0.4 with 1mM isopropylthio-β-D-galactoside (IPTG) (Melford Labs) for 3 hours at 22°C. It was observed that the addition of betaine and sorbitol increased recombinant protein solubility upon promoter induction by IPTG.

2-2.3 Protein Purification

To isolate His_6-FEN1 protein, transformed, induced bacterial cells were collected by centrifugation in a Beckman J2-HS JLA rotor (3000*g* for 10 min) and lysing cells by sonication in 1X PBS with 10 mM imidazole plus protease inhibitors (1mM phenylmethyl-sulfonyl fluoride (PMSF), 1mM benzamidine, 1 μg/ml pepstatin). Lysates were cleared by centrifugation at 14,000 RPM in a Beckman GS-15R with S4180 rotor for 30 minutes at 4° C and the supernatant subsequently collected and passed through a 0.45 μm filter (Millipore) to remove any insoluble material. Following column equilibration, the recombinant protein was purified by immobilized metal affinity chromatography (IMAC) on a 1 ml Ni^{2+} His-Trap column (Pharmacia) following manufacturer's instructions, collecting 0.5 ml fractions at a flow rate of 0.5 ml/min. The purest eluted fractions containing His_6-FEN1, as determined by Coomassie staining and immunoprobing of western blots, were pooled and further purified on a Sephacryl 16/60 gel filtration column (Pharmacia) at a flow rate of 0.5 ml/min in PBS buffer. Eluted fractions were run on 10% SDS PAGE and briefly Coomassie-stained. The Fen1 protein

band was excised from the gel and FEN1 protein was eluted in a Model 422 Electro-Eluter (BioRad) in 1X SDS running buffer according to manufacturer's instructions.

Untagged pT7.7-FEN1 protein was partially purified by isolation of inclusion bodies. Briefly, *E. coli* BL21 (DE3) transformed with pT7.7-FEN1 were grown and protein expression induced as described above (Section 2-2), except sorbitol and betaine were omitted from the growth media. Cells were collected as described above (Section 2-2.3) and bacterial pellets were resuspended in 0.66 ml/g cell pellet in lysis buffer (50mM Tris-HCl, pH 8.0, 10% (w/v) sucrose) with 50 mM NaCl, and 150 µg/ml lysozyme (Sigma)(final concentrations). Resuspended bacterial cell pellets were incubated on ice for 45 minutes, warmed to 37° C for 1 min, and sonicated on ice to shear DNA. The suspension was centrifuged in a Beckman GS-15R with S4180 rotor at 10000 *g* for 10 minutes at 4° C and the pellet was washed in wash buffer (50 mM Tris.HCl, pH 8.0, 2 mM EDTA, 100 mM NaCl, 1 mM PMSF, 0.5% Triton X-100) and centrifuged again. The resulting pellet, containing inclusion bodies, was then solubilized with 1 ml/100 ml culture of solubilization buffer (5M guanidine hydrochloride, 0.005% (v/v) Tween 80, 50 mM Tris.HCl, pH 8.0) and gently mixed on a rotary wheel for 5 hours at 4° C. Re-solubilized FEN1 was centrifuged at 10000*g* for 10 minutes to remove insoluble debris, and the soluble fraction containing FEN1 protein was recovered. The FEN1 protein-containing solution was rapidly diluted to 1M guanidine hydrochloride with re-naturation buffer (50mM Tris.HCl, pH 8.0, 0.005% (v/v) Tween 80, 5mM reduced glutathione, 0.5mM DTT, 0.5mM oxidized glutathione) and gently mixed for 16 hours at 4° C to facilitate protein refolding. The protein lysate was subsequently dialyzed at 4° C in one

litre dialysis volumes, gradually reducing NaCl concentration to 150mM NaCl, with 0.005% (v/v) Tween 80 and 50mM Tris, pH 8.0.

2-2.4 mRNA Analysis

2-2.4a Probes

Using the published cDNA sequences for the human *FEN1* and glyceraldehyde 3-phosphate dehydrogenase (*GAPDH*) genes, primers (see below) were designed and synthesized (Genosys) to PCR amplify human cDNA probes from previously purified plasmids (pT7.7-FEN1) or human genomic DNA. Full-length human *FEN1* cDNA probes were either PCR-amplified or removed from purified plasmid (pT7.7-FEN1) using restriction enzyme digestion. Full-length products (approx. 1180 bp) from the reaction were separated on a 1% agarose gel and isolated by Gene Clean (Amersham) and resuspended in 20 µl TE (25 mM Tris.HCl, pH 8.0, 10 mM EDTA). A 396 bp control probe (encoding nucleotides 529-925 of *GAPDH* cDNA), from the coding region of the human glyceraldehyde 3-phosphate dehydrogenase gene (approximately 1.3 kb), was also PCR amplified from human genomic DNA using the primers (GAPDH1, GAPDH2) depicted below. Human β-*actin* cDNA probes were purchased from Ambion. *PCNA* cDNA probes were constructed by NdeI/BamHI double digests of purified plasmid DNA (PAS-PCNA).

FEN A: 5' GAAGATCTCATATGGGAATTCAAGGCCTGGC 3'

FEN B: 5' CCCAAGCTTATTTTCCCCTTTTAAACTTCCC 3'

GAPDH1: 5' CACAGTCCATGCCATCACTG 3'

GAPDH2: 5' GACAAAGTGGTCGTTGAGGG 3'

2-2.4b RNA Extraction

RNA samples were prepared by trypsin harvesting of human cell populations by a 3 minute incubation at 37°C with 1 ml of trypsin-EDTA (see Section 2-1.1 for concentrations) solution per 10 cm culture dish. After the 3 minute incubation, 5 ml of complete media was added to quench the trypsin before cell suspensions were recovered by centrifugation in a Beckman GS-15R with S4180 rotor (400*g* for 5 minutes at 21°C), followed by washing cells in 1X PBS. Cells were lysed by adding 1.5ml GITC (4M guanidium isothiocyanate, 25mM sodium citrate-NaOH, pH7, 0.5% Na-N-lauryl sarcosine, 0.1M 2-mercaptoethanol) solution per 10-centimetre (cm) culture dish (approx. 2.5 x 10^6 viable cells, as determined by Coulter counter analysis, and trypan blue exclusion using a haemocytometer). Lysates were homogenized by passage through a 23-gauge syringe, and 0.025 volumes of 1M glacial acetic acid and 0.75 volumes of 100% ethanol were added to precipitate nucleic acids. Following centrifugation at 1600*g* for 20 minutes, the supernatant was discarded and the pellet was resuspended in 2 ml GITC solution, carefully overlayered on a 2 ml CsCl gradient and centrifuged at 31000 RPM for 18 hours at 21° C in a Beckman L8-70 ultracentrifuge (Ti-70 rotor). The pellet was extracted twice with phenol:chloroform (1:1) and RNA precipitated from the aqueous phase with 2.5 volumes ethanol and 0.1 volume 3M sodium acetate (pH 4.8). The RNA pellet was washed with 70% ethanol and resuspended in 20 µl DEPC-dH_2O. Total RNA was also extracted by RNeasy mini kits (Qiagen) according to manufacturer's instructions

and RNA was subsequently concentrated by precipitation (as above) and resuspended in 20 µl DEPC-treated water.

2-2.4c Random Primer Labeling

cDNA probes for Northern hybridizations, prepared as described in Section 2-2.4a, were radiolabeled with [α-^{32}P] dATP using Prime-It II Random Primer Labeling kit (Stratagene) according to manufacturer's instructions and subsequently purified by centrifugation (400 *g* for 1 minute at room temperature) in a 1 ml syringe packed with Sephadex G50 (Pharmacia) resin to remove unincorporated nucleotides and radiolabel.

2-2.4d Gel Electrophoresis, Northern Blotting, and Hybridization

Denaturing gel electrophoresis of RNA in 1% agarose gels containing 1% formaldehyde was performed according to Sambrook *et al.* (1989). Capillary (Northern) blotting onto Hybond nylon membranes (Amersham) was also according to Sambrook *et al.* (1989) and was performed overnight at room temperature. RNA was cross-linked to solid support by UV-crosslinking at 1200 J/m^2 in UV Stratalinker 2400 (Stratagene). Blots were pre-hybridized (in the absence of salmon sperm DNA), hybridized, and washed according to the method and reagents described in Sambrook *et al.* (1989). Northern blots were autoradiographed by exposing the hybridized filter (in Saran wrap) to X-ray film (Kodak XAR-2) for 1-192 hours at –80°C.

2-2.5 Mammalian Cell Lines Used

All tissue culture reagents were purchased from Sigma unless noted otherwise. All cell lines used were previously verified as free of mycoplasm infection by the Dunn School of Pathology. All tissue culture plastics were obtained from Falcon.

Primary, non-transformed, mortal lines NCTC 2544 human keratinocytes, WI38, and MRC5 lung fibroblast human cell lines were obtained from the Dunn School of Pathology (Oxford, UK); passage number for primary lines is indicated in the Results section. Primary human MRC-5, mouse 3T3, HeLa, and SV40-transformed MRC-5 (MRC5-SV) human cell lines were cultured in Dulbecco's Modified Eagle Media (DMEM) with 10% foetal calf serum (FCS), 2mM L-glutamine, 5.6 μg/ml amphotericin B, 100 μg/ml penicillin-streptomycin (pen/strep) at 37° in a humidified atmosphere with 5% CO_2. NCTC 2544 human cell line was similarly cultured with NCTC 135 media (Gibco) in place of DMEM.

2-2.6 Cell Synchronizations

Sub-confluent HeLa cells were synchronized by addition of 2mM thymidine for 12 hours, washed twice at 37° with sterile (tissue culture grade) PBS, and fresh media containing 2mM deoxycytidine and 20 ng/ml nocodazole was added. 12 hours after addition of nocodazole, cells were released from mitotic block by washing twice in PBS at 37° and adding fresh media containing 10% FCS.

MRC-5 embryonic male lung fibroblast cells were synchronized by growing to confluence in 10 cm culture dishes, aspirating media, washing in PBS at 37°C, and

adding fresh media containing 0.5% FCS. Cells were incubated in low serum for 55 hours before they were trypsinized (as described in Section 2-2.4b) and transferred to 15 cm culture dishes with 15% FCS in DMEM to stimulate growth and proliferation.

2-2.7 Trypan Blue exclusion and Coulter Counting

Trypan Blue (Sigma) lipid-insoluble dye was diluted from stock solution to 0.2% (v/v) in calcium/magnesium-free (CMF) tissue culture grade PBS and added to aliquots of resuspended cell suspensions in complete medium at a 1:1 ratio. After thorough mixing of the cell and dye suspension, aliquots were loaded onto a haemocytometer for cell counting and viability analysis on a Leitz light microscope. Cell counts were also performed using a Coulter counter (Coulter) according to manufacturer's instructions. Briefly, small volumes of cell suspensions were mixed in an isotonic buffer (Isotone, Coulter) and passed through a Coulter counter in 500 µl volumes to count cells. Counts were accomplished at least twice to verify accuracy.

2-2.8 Flow Cytometry

Synchronized cells were trypsin harvested (as described in Section 2-2.4b), collected by centrifugation (400*g* for 5 minutes at 21°C), washed twice in tissue culture grade PBS, re-pelleted, resuspended in 1 ml PBS, and permeabilized and fixed by adding 3 volumes of 100% methanol whilst gently vortexing. Samples were stored at 4°C for a minimum of 24 hours prior to washing twice in PBS, and finally incubated in staining solution (25 µg/ml DNase-free RNase (Sigma), 25 µg/ml propidium iodide (Sigma) in PBS) at 37°C for 30

minutes. Flow cytometry was carried out using FACScan (Becton Dickenson) and fluorescence profiles were subsequently analyzed by Cell Quest software (Becton Dickenson).

2-2.9 Antibody Production

Immunizations and antibody production were carried out at the Musaryk Memorial Cancer Institute (Brno, Czech Republic) under the supervision of Dr Borek Vojtesek.

2-2.9a Immunization Schedule

New Zealand White rabbits used for polyclonal antibody production were first immunized by subcutaneous injections with 500 μg purified FEN1 protein (either His_6-FEN1 or untagged FEN1) mixed 1:1 with Freund's Complete adjuvant (Sigma). Second and subsequent injections were done at 2 and 4 weeks, respectively, with 500 μg protein in incomplete adjuvant. Pre-immune serum was collected prior to the first injection and a test bleed was taken 9 days after the third immunization with His_6-FEN1 antigen. No test bleed was accomplished on the rabbit immunized with untagged FEN1 protein. Serum tested here was from the final bleed out, 9 days after the fourth immunization.

Two Balb/C mice used for monoclonal antibody production were first immunized by subcutaneous injection with 50 μg of purified His_6-FEN1 or untagged FEN1 preparations mixed 1:1 with complete adjuvant. Second and third immunizations were done with similar protein concentrations in incomplete adjuvant at 14 and 35 days after the first immunization, respectively. In addition, mice were given 20 μg booster injections (antigen only, without adjuvant) 4 and 3 days prior to sacrifice.

2-2.9b Serum Preparation

Rabbit and mouse polyclonal sera were prepared for testing by incubation of animal blood from the test bleed or final bleed out at 37°C for 60 minutes to allow clotting. After overnight incubation at 4°C, serum was centrifuged at 10,000*g* for 10 minutes at 4°C to remove any insoluble material before adding 0.01% sodium azide to prevent microbial contamination. Finally, polyclonal antibody-containing sera were subsequently tested for recognition of antigen.

2-2.9c Hybridoma Production

The SP2 myeloma cell line used for hybridoma cell fusions is defective in the purine nucleotide biosynthesis salvage pathway, and harbors a mutation preventing production of functional antibodies (Harlow and Lane, 1988). Consequently, only cell fusions of SP2 myeloma cells (providing cell immortality) and immunized mouse splenocytes (possessing a functional nucleotide biosynthesis salvage pathway) are able to proliferate in selective culture (HA media) conditions.

Mice were harvested 5 days after the third immunization. The spleen was extracted under sterile conditions and homogenized as described in Harlow and Lane (1988). Splenocytes were isolated and fused with SP2 myeloma cells using PEG-1500 (Boehringer Mannheim) as described in Harlow and Lane (1988). Approximately 10^7 possible hybridoma cells were evenly seeded into ten (fusion 1) or eleven (fusion 2) 96-well plates in HA-DMEM media (10^{-4} M hypoxanthine; 1 μg/ml azaserine) with 20% FCS and 100 U/ml penicillin/streptomycin and incubated at 37°C with 5% CO_2 in a humidified atmosphere. Seven plates contained feeder cell populations derived from

peritoneal cavity while 3 contained no feeder cells in case of contamination of feeder cell population.

2-2.9d Anti-PCNA (PC10) Hybridoma Culture and Antibody Purification

The anti-PCNA hybridoma cell line, PC10, was a generous gift of Professor David Lane (University of Dundee, Scotland). PC10 hybridoma cells secrete high-affinity monoclonal antibodies that recognize the epitope SDYEMKLMDLD, comprising amino acids 111-125 of monomeric PCNA (Roos *et al.*, 1993). PC10 cells were cultured (as described in Section 2-2.5) to high density (>10^6 cells/ml) in T75 tissue culture flasks (Falcon) and collected by centrifugation at 1000 RPM (400*g*) for 10 minutes in a Beckman GS15R (S4180 rotor) at room temperature. The supernatant, containing soluble anti-PCNA antibody, was removed and the cell pellet was resuspended in complete medium for subsequent sub-culturing. After addition of 0.01% sodium azide to prevent microbial contamination, 50 ml aliquots of PC10 hybridoma supernatant were mixed with 200 µl of pre-washed Protein G Sepharose Fast Flow beads (Pharmacia) and placed on a rotating mixer overnight at 4° C. Four 50 ml aliquots were then poured onto 0.8 X 4 cm Poly-Prep Chromatography columns (BioRad) to allow the fast-flow beads to settle and the flow-through collected. The column was washed with 10 bed volumes (approximately 10 ml) of PBS and pooled. PC10 antibody was subsequently eluted with 10 ml of 100 mM glycine (pH 2.5-3.0) and 1 ml fractions were collected. After collection, each fraction was immediately neutralized with 2M Tris and the pH of each fraction was tested to ensure the pH was between 7.0-7.5. Aliquots of fractions were subsequently analyzed on 10% SDS-PAGE followed by Coomassie staining to determine peak IgG fractions (determined by the heavy and light chains at approximately 55 and 30

kDa, respectively). Western blots of human cell lysates (HeLa) were probed with the purified antibody at various dilutions up to 1:4000 and showed strong recognition of PCNA protein (data not shown).

2-2.10 Protein Analysis

Protein concentrations were determined by a modification of the Bradford method (1976) using protein reagent (BioRad) according to manufacturer's instructions. 8-12% SDS-PAGE was carried out using a modification of the method of Laemmli (1970). Briefly, Miniprotean II (BioRad) gels were run at 150-200V (constant voltage) for 40-60 minutes. Protein was electrophoretically transferred to nitrocellulose (Schleicher & Schuell) membranes as described by Sambrook *et al.* (1989) at 250 mA for one hour. To minimize non-specific antibody binding, blots were blocked for a minimum of 30 minutes in 5% non-fat milk (Marvel, Cadbury) in PBS containing 0.4% (v/v) Tween 20, washed twice with PBS, then subsequently probed with primary antibody diluted in 0.1-1% milk-PBS for 30 minutes at room temperature or overnight at 4°C. Horseradish peroxidase-conjugated (HRP) secondary antibodies (Dako) were diluted at 1:500 to 1:2000 in 1% milk-PBS, and were incubated with the blots for 30-60 minutes at room temperature. Blots were washed after primary antibody with 0.2% (v/v) Tween 20-PBS, and with 2% (v/v) milk-PBS-0.2% Tween 20 following incubation with secondary antibody. Enhanced chemiluminescent (ECL) reactions were carried out according to manufacturer's instructions (Amersham). Antibody complexes were stripped from western blots in stripping buffer (Section 2-1.4) in a sealed container for 30 minutes at 50° C, then blots were washed extensively in deionized water prior to blocking and re-

probing. Total protein was stained using either Indian ink and Ponceau Red (Sigma) at 1:1000 dilution in PBS with 0.2% (v/v) Tween 20 for 5-10 minutes at room temperature. Blots were subsequently washed extensively in PBS-0.2% Tween prior to blocking and immunoprobing.

2-2.11 Silver staining

Silver staining of polyacrylamide gels was performed using the Rapid-Ag-Stain kit (ICN Biomedicals) following the manufacturer's protocol. Following silver staining, gels were extensively washed and stored in double-deionized, sterile water to minimize background staining.

2-2.12 Native PAGE

5-25% native gradient PAGE was performed using BioRad Miniprotein II gel kits. Gradients were manually formed in a drop-wise fashion in 5-ml pipettes and carefully poured into glass plates for polymerization before the 4% stacking gel was polymerized on top. Gels were pre-run at 70V for 15 minutes in a Tris-glycine native gel electrophoresis buffer (25 mM Tris.HCl, 192 mM glycine, pH 8.8) to equilibrate. Samples were then loaded in 5X sample loading buffer (312.5 mM Tris.HCl, pH 6.8, 50% (v/v) glycerol, 0.05% bromophenol blue) and electrophoresis was conducted at 150V for 3 hours at 4° C. Gradients formed by this method were extensively tested to ensure gradient reproducibility and maintenance of native protein complexes.

2-2.13 Glycerol Gradients

All buffers and reagents were pre-chilled prior to use. NP40 lysis buffer (without 1% NP40 detergent, see Section 2-1.4) was freshly prepared with either 15% or 30% (v/v) glycerol and protease inhibitors (Complete Mini protease inhibitors, Boehringer Mannheim). 2.4 ml of 30% glycerol solution, 2.4 ml of 15% glycerol solution, and 200 µl of soluble protein (with approximately 100 µg total protein) from mammalian cell extracts supplemented with 5% glycerol, were carefully layered sequentially in pre-chilled 10 ml centrifuge tubes and spun at 55,000 RPM for 18 hours at 4° C in an L8-70 ultracentrifuge with Ti-70 rotor (Beckman). Following centrifugation, the gradient was carefully removed from bottom to top in 0.8 mm tubing at 0.6 ml/minute using a BioRad EconoPump. 100 µl fractions were collected and immediately suspended with 25 µl 4X-reducing sample buffer (RSB-DTT). Aliquots of collected fractions were run on 10% SDS-PAGE, western blotted, and probed with anti-FEN1 and anti-PCNA antibodies (see Section 2-2.10).

2-2.14 Densitometry Measurements

Densitometry measurements of RNA and protein bands on exposed films were performed using a BioRad GS-670 Imaging Densitometer with Molecular Analyst software, version 1.2 (BioRad).

2-2.15 DNA Damage Studies

Methyl methane-sulfonate (11.4 M MMS stock solution) in DMSO (Sigma-Aldrich) was used to cause alkylation damage of human cells during DNA damage studies. Cellular

damage by UVC-irradiation was performed with a Stratalinker 2400 (Stratagene) at various intensities and durations.

2-2.16 Immunofluorescence Microscopy

The GFP-FEN1 and GFP-ΔFEN1 plasmids used in fluorescence microscopy were a gift from Dr J-L Li (University of Oxford). GFP-FEN1 plasmids were constructed with the BglII-HindIII restriction digest fragment, encoding the entire human *FEN1* ORF, ligated into similarly digested pEGFP-C1 plasmids (CLONTECH) containing the GFP cDNA sequence. The GFP-ΔFEN1 plasmid was constructed similarly, but the *FEN1* ORF contains a 69 bp in-frame deletion that results in mutant FEN1 protein lacking amino acids 225-247 from the full-length sequence. All construct DNA sequences were subsequently verified by ABI automatic sequencing (University of Oxford, UK). Both GFP-FEN1 constructs, when expressed from the constitutive cytomegalovirus (CMV) promoter, will produce recombinant human FEN1 protein with an N-terminal GFP fluorescence tag.

GFP, GFP-ΔFEN1, and GFP-wtFEN1 plasmids were transformed into *E. coli* DH5α (as described in Section 2-2.1) and individual colonies were screened by diagnostic restriction enzyme digest to verify the presence of the human FEN1 cDNA insert. Bacteria containing GFP, GFP-ΔFEN1, and GFP-wtFEN1 plasmids were selectively amplified in 100 ml culture volumes [LB with 50 μg/ml kanamyosin (Sigma)], and plasmid DNA was column-purified (Plasmid Mini kits, Qiagen) according to manufacturer's instructions.

Reagents were prepared for transfection by mixing 3 μg of DOSPER cationic lipofectamine (Boehringer Mannheim) with 0.5 μg of either GFP, GFP-ΔFEN1, or GFP-wtFEN1 plasmid DNA according to manufacturer's instructions.

Approximately 3 X 10^4 asynchronous HeLa cells were seeded on sterile 13 mm coverslips at the bottom of 24-well culture vessels, and were incubated in DMEM supplemented with 10% FCS for 24 hours prior to treatment. Following the 24-hour incubation, the medium was aspirated and 0.5 ml of fresh DMEM (without FCS), containing transfection reagents with either GFP, GFP-ΔFEN1, or GFP-wtFEN1 plasmid DNA, were added to individual culture vessels. Some cells were treated with DOSPER only to serve as a control for autofluorescence.

HeLa cells were incubated in the presence of transfection reagents (with and without plasmid DNA) for 6 hours, and then the medium was aspirated, cells washed with 37°C PBS, and fresh DMEM supplemented with 10% FCS was added to all culture vessels. Following an 18-hour incubation to allow GFP and GFP-FEN1 protein expression, HeLa cells on coverslips were washed twice in PBS, then fixed *in situ* with either 3% (w/v) paraformaldehyde-PBS (Sigma) or ice-cold methanol-acetone (50:50 v/v) for 10 minutes at room temperature. After three washes in PBS, nuclei were stained with 0.25 μg/ml Hoescht 33258 (Sigma) in PBS for 5 minutes at room temperature. In some instances, coverslips were also probed with anti-PCNA monoclonal antibody PC10 (diluted to 1:1000 in PBS) and TRITC-conjugated anti-mouse IgG (diluted to 1:64 in PBS) secondary antibodies (Sigma) prior to nuclear staining with Hoescht 33258. Following staining, coverslips were washed three times in PBS, mounted on glass slides containing

VECTASHIELD® mounting medium (Vector Labs), and sealed with molten agarose. Slides were viewed immediately with a Zeiss Axioskop 2 fluorescence microscope using blue (Hoescht 33258), red (TRITC), and green (GFP) filters, and photographed with an MC 80 DX microscope camera (Zeiss) and Fujichrome 64T colour transparency film at various exposure times.

CHAPTER THREE: HUMAN FEN1 PROTEIN PURIFICATION AND ANTIBODY PRODUCTION

3-1: Introduction

A primary aim of this project is to examine FEN1 protein expression *in vivo*, and determine its sub-cellular localization during the cell cycle and in response to DNA damage. In order to analyze FEN1 temporal and spatial expression *in vivo*, high-affinity monoclonal and polyclonal antibodies are essential.

At the start of this investigation, we possessed an extremely limited stock of anti-human FEN1 polyclonal antibody, 3220 (Warbrick *et al.*, 1997). Additionally, there are no commercial antibodies to FEN1, and recent attempts to obtain additional polyclonal FEN1 antibodies from published sources (Chen *et al.*, 1996; Warbrick *et al.*, 1997) have been unsuccessful. Consequently, considerable efforts were made to produce both monoclonal and polyclonal antibodies to either purified recombinant FEN1 protein or synthetic peptides comprising a region from FEN1.

Both polyclonal and monoclonal antibodies to human FEN1 were desired for specific reasons. Firstly, although it is a limited resource, polyclonal serum is typically capable of recognizing more than one antigenic epitope. Multiple recognition and binding sites may increase the possibility of immunological detection in some assays, even when epitopes are masked or hidden due to tertiary or quaternary protein structures (Harlow and Lane, 1988). In contrast, monoclonal antibody production, stemming from the technique developed by Köhler and Milstein (1975), provides an unlimited supply of homogeneous antibodies that recognize and bind a singular epitope (Harlow and Lane, 1988). A battery of several different monoclonal antibodies to human FEN1 protein

would provide a powerful tool to study possible changes in FEN1 epitope recognition during immunoprecipitation of native protein from synchronized or DNA-damaged cell populations. Changes in FEN1 epitope recognition by monoclonal antibodies may identify changes in FEN1 protein structure resulting from post-translational modifications or protein-to-protein interactions. Secondly, high-affinity monoclonal and polyclonal antibodies were to be used for immunoprecipitation of FEN1 protein from synchronized mammalian cells harvested throughout the cell cycle or subjected to DNA damage. Immunoprecipitation of FEN1 protein during various stages of the cell cycle, or in response to DNA damage, would allow a detailed analysis of protein expression levels and possibly identify putative interacting proteins during the cell cycle or during DNA repair. Lastly, high-affinity FEN1 antibodies would also provide a means to study FEN1 protein sub-cellular localization during the cell cycle and in response to DNA damage by immunofluorescence microscopy of fixed cell culture populations.

In addition to immunological-based methods of detection, recent advances in Green Fusion Protein (GFP) technology provide an alternative method of protein detection in fixed or living cell populations (Chalfie *et al.*, 1994). GFP, derived from the bioluminescent jellyfish *Aequorea victoria*, emits a strong green fluorescence when irradiated with near UV or blue light (Morin and Hastings, 1971). Cells transfected with GFP-containing plasmids, and expressing GFP protein, can be viewed microscopically upon illumination with UV light (Chalfie *et al.*, 1994). Additionally, researchers have previously demonstrated that transfection of COS-7 (Pines, 1995), HeLa (Inouye & Tsuji, 1994; Pines, 1995), and NIH 3T3 (Pines, 1995) mammalian cell lines with various GFP-cDNA constructs show proper sub-cellular localization of recombinant protein;

suggesting that the GFP tag does not interfere with normal spatial expression of target proteins. Consequently, transient or stable transfection of cultured cells with purified plasmid DNA containing the GFP-FEN1 DNA sequence, and subsequent constitutive expression of recombinant GFP-FEN1 protein from the cytomegalovirus (CMV) early promoter, may provide an alternative method for studying human FEN1 protein spatial expression and sub-cellular localization during the cell cycle and in response to DNA damage.

This chapter will discuss two separate protein purifications of recombinant human FEN1 protein and two subsequent attempts at producing both monoclonal and polyclonal antibodies. In addition, I will discuss the production, testing, and usage of novel anti-Xenopus FEN1 polyclonal antibodies and a peptide-derived monospecific polyclonal antibody to human FEN1. Lastly, I will examine the sub-cellular localization of recombinant human FEN1 protein *in vivo* using a Green Fluorescent Protein construct (GFP-FEN1).

3-2: Purification of His-tagged Recombinant Human FEN1

In order to produce sufficient purified antigen for antibody production, the open reading frame of human FEN1 (Murray *et al.*, 1994) was initially sub-cloned into plasmid pET-21d in-frame with a six-histidine residue, C-terminal affinity tag, to facilitate the initial protein purification steps. A schematic of the pET-21d plasmid vector and cloning sites used is shown in Appendix 1. Details of subcloning, transformation, and induced protein expression were as described in the Methods section. Briefly, pET21d-FEN1 was constructed with the NcoI-DraI fragment (containing the human FEN1 ORF) of shuttle

vector pDR2-FEN1 cDNA (Murray *et al.*, 1994) ligated into the C-terminal histidine-tagged vector, pET-21d (Novagen) that had been digested with NcoI-BamHI and subsequently Klenow filled-in to create a compatible blunt end (data not shown). Following restriction enzyme screening for constructs containing the FEN1 cDNA sequence, *E. coli* strain BL21 (DE3) bacteria were transformed with pET-21d-FEN1 plasmids, and protein expression induced using IPTG. Additionally, it should be noted that extensive optimization experiments had revealed that the addition of 0.5 M sorbitol in bacterial culture media was essential to prevent excessive insolubility of recombinant protein, in the form of inclusion bodies, when cultures were induced to express recombinant FEN1 protein. Consequently, all bacterial cultures induced to express His_6-FEN1 recombinant protein contained 0.5 M sorbitol and 2.5 mM betaine (Blackwell and Horgan, 1991) to facilitate its cellular uptake.

Induced 500 ml bacterial cultures, containing recombinant human FEN1 protein, were harvested and soluble protein was extracted in 30 ml volumes, with 10 mM imidazole (see Methods and Materials). The presence of soluble FEN1 protein in extracts was verified by immunoprobing of western blots with anti-FEN1 polyclonal antibody, 3220 (Warbrick et al., 1997) (data not shown). All protein extracts were filtered at 0.45 μm to remove insoluble precipitate and passed through a pre-equilibrated 1 ml His-Trap column (Pharmacia) at a flow rate of 0.5 ml/minute using a Pharmacia P1 pump. After collecting the flow-through and washing with 10 column volumes of buffer, bound protein was eluted by a stepwise increase in imidazole concentration (from 100-500 mM), collecting 0.5 ml fractions. It should be noted that several optimization experiments had previously shown that no discrete imidazole concentration was most

efficient for His_6-FEN1 elution. Consequently, several stepwise and linear gradient elutions were performed and Figure 3-1 shows a typical elution profile observed during His_6-FEN1 purification.

Figure 3-1 showing His-trap purification

As can be seen in Figure 3-1, fractions enriched for His_6-FEN1 protein could be detected by the second 100 mM fraction. All subsequent fractions eluted with 100 mM imidazole (100 mM 2-10) were enriched for His_6-FEN1 protein, with maximum levels of His_6-FEN1 detected in the fifth 100 mM fraction (100 mM-5). High levels of recombinant FEN1 protein were also observed in fractions eluted with 200 mM imidizole, with maximal levels detected in the first fraction (200 mM-1), and then gradually decreasing in subsequent 200 mM fractions (200 mM-2 until 200 mM-5). In addition, high levels of His_6-FEN1 protein were also noted in the first fraction eluted with 500 mM imidazole (500 mM-1), but protein concentrations were significantly decreased in subsequent fractions (500 mM-2 to 500 mM-3).

Following partial purification of His_6-FEN1 protein by metal-affinity chromatography, the purest FEN1 fractions (200 mM-3, 4, 5, 500 mM-1 in Figure 3-1), as determined by Coomassie staining, were subsequently pooled and 2 ml aliquots were then passed through a pre-equilibrated Sephacryl HighLoad 16/60 S-100 gel filtration column (Pharmacia). Pre-calibration of the column was performed previously, using molecular weight calibration standards (BioRad) (see Methods & Materials), and 0.5 ml fractions were collected at a flow rate of 0.5 ml/min. Analysis by Coomassie staining of

10% SDS-PAGE gels of eluted fractions following gel filtration (Figure 3-2) showed relatively pure fractions, but silver staining (Figure 3-3), and Coomassie staining of gels (data not shown) with higher protein concentrations, revealed numerous contaminating bands.

Figures 3-2 & 3-3 Showing gel filtration profile and silver stained gel filtration fractions

Based on the silver staining results (Figure 3-3), it was determined that further purification was desired to produce recombinant human FEN1 protein for use as antigen in polyclonal antibody production. Therefore, I chose to electroelute recombinant human FEN1 protein from 10% SDS-PAGE gels of peak gel filtration fractions (Fractions 3-9 in Figure 3-2A). Large 10 X 20 cm gels were used to allow greater volumes to be loaded and higher resolution, in an attempt to separate human FEN1 protein from similar molecular weight contaminants. Coomassie staining, prior to excision of bands and electroelution of recombinant human FEN1 protein, was also minimized to prevent excessive protein fixation and amino acid cross-linking. Electroelution of His_6-FEN1 protein from numerous gel filtration fractions, followed by dialysis in $NaHCO_3$ overnight at 4° C, yielded approximately 1.2 mg of highly purified, though denatured, FEN1 protein, as determined by comparison with BSA standards (Figure 3-4).

Figure 3-4 of electroeluted FEN1

During continuous dialysis in $NaHCO_3$, with several buffer changes over a 24-hour period, an increasing amount of precipitate in dialysis tubing was noted. It is possible that despite extensive dialysis, SDS concentrations may have remained high, resulting in salt or denatured protein precipitate forming in dialysis tubing. Despite this, recognition of electroeluted recombinant His_6-FEN1 protein was verified by western blot/immunoprobing and ELISA colorimetric reactions on immobilized protein in 96-well plates using the anti-FEN1 polyclonal antibody 3220 (Warbrick *et al.*, 1997) (data not shown). The purified protein was subsequently lyophilized (24 hours at –50 degrees C) to concentrate, and used as immunogen for production of polyclonal and monoclonal antibodies.

3-3: Production and Screening of Antibodies to Anti-His_6-FEN1

3-3.1: Polyclonal Antibody Production

to obtain polyclonal antibodies against FEN1, New Zealand White rabbits were immunized by subcutaneous injections of 500 μg of purified recombinant human His_6-FEN1 protein at bi-weekly intervals (see Methods & Materials). Nine days after the third immunization with 500 μg of purified His-tagged FEN1 antigen, serum from the immunized rabbit was prepared (see Methods & Materials) for analysis of recognition of purified recombinant FEN1 (as was used as antigen), or soluble FEN1 protein from SV40-transformed human MRC5 (MRC5-SV) and SKBR cells on western blots. Pilot experiments of similar western blots with identical protein concentrations loaded showed recognition of endogenous human FEN1 in MRC5-SV by anti-FEN1 polyclonal antibody, 3220 at dilutions of up to 1:16,000 (data not shown). However, using the

polyclonal serum produced here, following three immunizations with His_6-FEN1 protein, no FEN1 protein band at the expected molecular weight (approximately 47 kDa) could be detected on identical western blots at serum dilutions ranging from 1:500 to 1:1000 (Figure 3-5A, 3-5C). Comparison of the pre-immune with post-immune serum (Figure 3-5B) also shows that the primary antigenic response appears to be against unknown proteins in the human MRC5-SV cell extracts with molecular weights of approximately 38, 32, and 30 kDa. The identity of these proteins was not investigated. Because it appeared that there was no immunogenic response to His_6-FEN1 antigen, immunizations were subsequently terminated.

Figure 3-5A/B of polyclonal antibody recognition of His_6-FEN1

3-3.2: Monoclonal Antibody Production

In an attempt to produce monoclonal antibodies against recombinant human FEN1 protein, two Balb/C mice were initially immunized with 50 μg of His_6-FEN1 antigen. Further immunizations with 50 μg of His_6-FEN1 were carried out at 14 and 35 days, respectively, following the first immunization (see Methods & Materials). In addition, both mice were given booster injections of 50 μg of His_6-FEN1 protein four and three days prior to sacrifice to improve immunogenic response. Creation and selection of hybridoma cells from fusions of SP2 myeloma cells and immunized mouse splenocytes in selective HA media was as described in the Methods chapter. It should be noted that the extremely limited quantity of positive control antibody, 3220, was unavailable during screening of hybridoma supernatants.

Table 3-1 showing screening percentages

Ten days after hybridoma seeding, the first colonies were ready for screening for recognition of human FEN1. Screening continued for several days, during which time, all wells that contained colonies were screened. The following describes the strategy employed for hybridoma screening:

Cell culture supernatants were first tested for IgG secretion by dot blot analysis and colorimetric reactions on immobilized anti-mouse IgG blots. Individual supernatants were scored as +, ++, or +++ (see Table 3-1), relative to the positive control, for IgG secretion. Hybridoma supernatants from all cell colonies that secreted IgG, as determined by anti-mouse IgG dot blots, were next tested by dot blot analysis for recognition of recombinant His_6-FEN1 protein (cognate antigen) immobilized on nitrocellulose.

Figure 3-6 showing monoclonal screening blots

Supernatants from colonies secreting antibodies that appeared to recognize recombinant His_6-FEN1 protein on dot blots were next tested on western strip blots of human MRC5-SV cell extracts that I had previously shown, using polyclonal antibody 3220, to contain significant concentrations of endogenous FEN1 protein (data not shown). Lastly, hybridoma supernatant from colonies that secreted IgG, recognized recombinant His_6-FEN1 protein by dot blot analysis, and recognized a putative FEN1

band (based solely on molecular weight analysis) from human cell extracts, were analyzed for recognition of His_6-FEN1 run on a 10% SDS-PAGE and western blotted onto nitrocellulose. Table 3-1 details the number and percentage of colonies screened, and the results of their testing during the monoclonal antibody screening process. In addition, Figure 3-6 shows representative examples of test results observed with tissue culture supernatants from hybridoma cells derived from mice immunized with His_6-FEN1 protein.

As can be seen in Table 3-1, nearly 50% of the hybridoma cells from the first fusion and 69% from the second fusion, grew in selective media, and were subsequently screened for production of antibody against recombinant human FEN1 protein. The representative dot blot in Figure 3-6A shows that about 20% of the colonies tested by dot blot analysis secreted IgG, but at varying levels, as determined by staining intensity. Further tests on IgG-secreting colonies (A6,10,12; B1,11; C4,5,8,11; D1,3,12; E12; F1,6,8; G9 in Figure 3-6A), revealed that approximately 15% of these appeared to recognize recombinant His_6-FEN1 protein in dot blot analyses (15,18,19,20 in Figure 3-6B), again at various degrees of intensity. When IgG-secreting colonies, that also appeared to recognize recombinant FEN1 protein by dot blot analysis, were next tested for recognition of endogenous FEN1 protein in MRC5-SV cell extracts (Figure 3-6C), it appeared that some colonies secreting antibody recognized a putative endogenous FEN1 band on western strip blots (lanes 2, 5, 6, 9 in Figure 3-6C). However, further testing of those colonies on western blots of purified His6-FEN1 protein and soluble protein extracts from other cell lines (representative test of MRC5 cell extracts in Figure 3-6D) revealed no recognition of FEN1 protein. In total, over 500 hybridoma colonies per

immunized mouse were screened, but no positive clones secreting antibody against FEN1 were identified (Table 3-1) that tested positive in all four assays described above.

3-4: Purification of Untagged FEN1 Protein

The lack of immune response to His6-FEN1 may indicate that the His-tag somehow may obscure an immunogenic region of FEN1. To avoid any such potential problems, the entire open reading frame of FEN1 was also subcloned into the plasmid vector pT7-7 which permits expression of protein from the insert without a tag. Subcloning, transformation, and induced expression (in media without sorbitol and betaine) were carried out as described in the Methods chapter. Briefly, pT7.7 plasmids, containing the entire human FEN1 ORF, under the control of the T7 promoter, were transformed in *E. coli* BL21 (DE3) and protein expression induced using IPTG.

Figure 3-7. 10% SDS-PAGE of partially purified recombinant human FEN1 protein.

Inclusion bodies, containing insoluble recombinant FEN1 protein, were isolated, extracted by guanidine HCl denaturation of inclusion body complexes, and subsequently renatured (see Methods & Materials). This method of extraction resulted in partial purification and significant enrichment of recombinant human FEN1 protein as detected by Coomassie staining of extracted protein separated by 10% SDS-PAGE (Figure 3-7). The identity of the major 47 kDa protein band on Coomassie (Figure 3-7, lane 5) as FEN1 was verified on western blots by probing with polyclonal antibody 3220 (data not shown).

Solubilization of recombinant protein isolated from inclusion bodies by this method of extraction with 5M guanidine hydrochloride probably results in large quantities of highly denatured protein. Successful renaturation of insoluble protein extracted by this method has been reported, using renaturation conditions conducive to proper refolding of denatured proteins (Midgley *et al.*, 1992). I therefore attempted to renature recombinant FEN1 protein (see Methods & Materials) by attempting to optimize conditions to allow significant renaturation of solubilized protein. In attempts to optimize protein renaturation conditions and prevent protein precipitation on dilution of NaCl from 1M to 150 mM (physiological salt concentration), various incubation and dialysis conditions were tested. However, despite efforts to prevent precipitation by dilution, adjustment of salt concentrations, addition of oxidizing or reducing agents, or addition of 10% glycerol, protein continually precipitated from solution during dialysis at salt concentrations as high as 500 mM. To determine the solubility status of recombinant FEN1 protein in these conditions, protein suspensions were centrifuged at 3000g for 1 hr at 4°C and the soluble and insoluble (pellet) fractions were analyzed by SDS-PAGE. Coomassie staining revealed that the vast majority of FEN1 was contained in the pellet, but very little was detected in the soluble fraction (data not shown). The precipitate, containing 0.3 mg/ml (9 mg in total) of partially purified FEN1, was most probably denatured protein. Consequently, the entire preparation, containing soluble and insoluble recombinant FEN1 protein, was lyophilized and used as immunogen for the production of monoclonal antibodies in mice. Because more highly purified protein was desired for use as antigen in polyclonal antibody immunizations, a fraction of the precipitate containing FEN1 was further purified by 10% SDS-PAGE. After brief Coomassie staining, the

FEN1 band was excised, homogenized, lyophilized, and used as immunize rabbits for polyclonal antibody production.

3-5: Production and Screening of Antibodies against Untagged FEN1

3-5.1: Polyclonal Antibody Production

To avoid problems using tagged FEN1 antigen, a rabbit was immunized with untagged FEN1 protein expressed from pT7.7-FEN1 plasmids in *E. coli* BL21 (DE3) and purified as described above (Section 3-4). Four immunizations using 500 μg of protein (see Section 3-4) were carried out at bi-weekly intervals in the Czech Republic by Dr Borek Vojtesek (see Methods & Materials). No test bleed was carried out to prevent weakening any subsequent immune response due to the test bleed. Nine days after the fourth immunization, the rabbit was bled out, serum was again prepared, and sent to me at the University of Oxford for analysis. Polyclonal serum was tested for recognition of purified untagged FEN1 protein (cognate antigen) and endogenous FEN1 protein in human HeLa cell extracts, previously determined to contain substantial amounts of endogenous FEN1 protein (data not shown).

Figure 3-8 showing test of polyclonal sera from untagged FEN

The results in Figure 3-8 show that anti-human FEN1 polyclonal sera detects a putative FEN1 band of approximately 49 kDa in HeLa cell extracts, at serum dilutions of either 1:500 (Lane 6) or 1:1000 (Lane 7). However, it is extremely doubtful that the 49 kDa band detected by anti-human FEN1 polyclonal serum band is FEN1 based on several

observations. Firstly, that same 49 kDa band was not recognized by the positive control, anti-Xenopus FEN1 (described in Section 3-6) polyclonal antibody (Lane 2). Secondly, although it appears that a similar 49 kDa protein was recognized by the other positive control, anti-peptide FEN1 polyclonal antibody (described in Section 3-7) at 1:1000 (Lane 4) and 1:2000 (Lane 5) serum dilutions, the same 49 kDa band was also detected by the anti-peptide pre-immune serum (Lane 3), and is probably not FEN1. Although it is difficult to see the 49 kDa band recognized by the pre-immune serum in Figure 3-8 (Lane 3), a similar probe shown in Figure 3-11A clearly illustrates that proposed non-specific band in pre-immune serum. Finally, this serum was also tested for recognition of recombinant His_6-FEN1 and endogenous FEN1 protein in other human cell lines (data not shown). Interestingly, very long exposure times of enhanced chemiluminescent (ECL) reactions of probed western blots did detect a faint putative 47 kDa FEN1 band (data not shown), suggesting either very low concentrations of antibody or extremely weak recognition of FEN1 protein. Further experiments in the future are needed to confirm the presence of FEN1-specific polyclonal antibodies in this serum preparation. Additionally, if anti-FEN1 antibodies are present, affinity purification of FEN1-specific antibodies will be necessary to increase antibody concentrations for use in future experiments. However, due to time constraints and the availability of another suitable FEN1 antibody (anti-Xenopus FEN1 polyclonal antibody, Section 3-6), this was not pursued further.

3-5.2: Monoclonal Antibody Production

In order to raise antibodies against untagged human FEN1 protein, two Balb/C mice were immunized with untagged FEN1 protein partially purified during inclusion body preparations from *E. coli* BL21 transformed with the pT7.7-FEN1 vector (section 3-4 above). The immunizations, hybridoma cell fusions, selections, and initial screening for IgG secretion, and recognition of a putative FEN1 band on western blots of protein used as immunogen were conducted in the Czech Republic by Dr. Borek Vojtesek. Four potential hybridoma colonies that were positive for IgG secretion and recognition of a putative FEN1 band on western blots of inclusion body preparations (same preparation as antigen), were sent to me at the University of Oxford for further analysis. Figure 3-9A shows recognition of a putative FEN1 band on western blots of recombinant untagged FEN1 protein preparations that were also used as immunogen (conducted by Dr. Vojtesek). Figures 3-9B and 3-9C show further tests I conducted of hybridoma supernatants on human HeLa cell extracts and on recombinant His_6-FEN1 protein. All four supernatants failed to recognize FEN1, either recombinant or endogenous protein, while FEN1 protein was clearly recognized by the positive control, anti-Xenopus FEN1 (J-L. Li *et al.*, manuscript in preparation). Attempts to increase antibody titre by overgrowth of hybridoma cells or longer exposure times during ECL reactions also failed to show any antigen recognition (data not shown).

Figure 3-9A and B of monoclonal antibody tests from pT7.7-FEN1.

It is currently unclear as to why there appeared to be such a strong response by all 4 clones to a putative FEN1 band on western blots of FEN1 protein isolated from

inclusion bodies (Figure 3-9A, lane 4), compared to protein extracted from SVK17 (Lane 1) or MCF7 (Lanes 2,3) cells. Additionally, there was no recognition of FEN1 protein in HeLa cell extracts (Figure 3-9B, lanes 1-4) or recombinant His-tagged FEN1 extracts (Figure 3-9C, lanes 1-4) that were easily recognized by the positive control anti-Xenopus FEN1 (Figures 3-9B and 3-9C, Lane 5). It is quite possible that the inclusion body preparation used as immunogen contained bacterial proteins with molecular weights approximately the same as FEN1. As a result, murine immune responses may have been directed against bacterial antigens contained in the preparation and not FEN1 protein. Alternatively, because of the apparent strength of the immune response detected against approximately 47 kDa proteins in the antigen preparations, weaker responses against actual FEN1 protein may have been missed during subsequent screening and testing.

3-6: A Polyclonal Antibody raised against *Xenopus* FEN1 Cross-Reacts with Human FEN1 Protein

Recently, Xenopus *FEN1* was cloned in our laboratory (J-L Li *et al.*, manuscript in preparation) and polyclonal antibodies to denatured FEN1 protein isolated from polyacrylamide gels were raised in collaboration with Dr. Vojtesek in the Czech Republic. I conducted several tests to check for cross-reactivity of these anti-Xenopus FEN1 antibodies with recombinant and endogenous human FEN1 protein.

Figure 3-10 of Anti-Xenopus FEN1 cross-reactivity tests.

Figure 3-10A shows that anti-Xenopus FEN1 polyclonal serum recognizes a putative 47 kDa FEN1 band (Figure 3-10A, lane 2) in human MRC5-SV protein extracts, that the pre-immune serum (lane 1) does not recognize. Additionally, Figure 3-10B shows that this antibody also detects a similar 47 kDa band in recombinant His_6-FEN1 lysate after partial purification on Ni^{2+}-agarose (lane 3), and following electroelution (lane 4) of His_6-FEN1 protein. This 47 kDa band is the same size as that detected in MRC5-SV cell extracts by the positive control antibody, 3220. These findings suggest recognition of human FEN1 protein by anti-Xenopus FEN1 polyclonal antibodies. However, attempts to immunoprecipitate soluble human FEN1 protein from whole cell protein extracts, or detect endogenous FEN1 protein during immunofluorescence microscopy, using the anti-Xenopus FEN1 antibody have been unsuccessful (data not shown), suggesting possible recognition only of epitopes exposed on denatured protein.

3-7: Design and Testing of an Anti-Peptide FEN1 Polyclonal Antibody

In further attempts to generate an antibody against human FEN1 that may be useful in various immunological detection applications, a domain of the human FEN1 protein was selected based on homologous protein crystal structures (Mueser et al., 1996; Ceska et al., 1996), hydrophobicity plots, and known catalytic (Harrington and Lieber, 1994) and interactive domains (Warbrick et al., 1997) by Dr Lynne Cox (University of Oxford, UK). A peptide of this region was used as immunogen in the commercial production of monospecific, polyclonal antibodies (Genosys, UK). The amino acid sequence of the synthetic peptide is C-K-R-K-E-P-E-P-K-G-S-T-K-K-K-A-K (N- to C-terminus), representing amino acids 353-369 of human FEN1 protein. The amino acid,

alanine, at amino acid position 353 (N-terminus of the synthetic peptide) of the human FEN1 protein sequence was substituted with the amino acid cysteine to facilitate binding to the carrier molecule, Keyhole Limpet Hemocyanin; previously shown to increase the antigenicity and stability of peptides used as immunogen (Harlow and Lane, 1993).

The anti-peptide serum was tested first for recognition of endogenous FEN1 protein in human cell lysates. MRC5-SV extracts were separated on SDS-PAGE, transferred to nitrocellulose, and probed with the anti-peptide serum (Figure 3-11A, Lane 3), pre-immune serum (Figure 3-11A, Lane 2), and the positive control anti-Xenopus FEN1 (Figure 3-11A, Lane 1) polyclonal antibody. The results show that anti-peptide FEN1 polyclonal serum detects a putative FEN1 band (lane 3) in MRC5-SV protein extracts that was also recognized by the positive control anti-Xenopus FEN1 (lane 1), but not detected with pre-immune serum (lane 2). The anti-peptide serum was next tested for recognition of both endogenous and recombinant FEN1 protein. Protein extracted from MRC5-SV cells (Figure 3-11B, Lanes 1,4,7,10), *E. coli* BL21 (DE3) transformed with pT7.7-FEN1 plasmids (Figure 3-11B, Lanes 2,5,8,11) and induced with IPTG, or *E. coli* BL21 (DE3) transformed with pT7.7-only plasmids (Figure 3-11B, Lanes 3,6,9) and induced with IPTG were separated by SDS-PAGE and transferred to nitrocellulose. The membrane was then probed with anti-peptide FEN1 serum diluted to 1:1000 (Lanes 1-3) or 1:2000 (Lanes 7-9), anti-peptide FEN1 serum that was pre-incubated with the synthetic peptide used as antigen (Lanes 4-6), and the positive control anti-Xenopus FEN1 (Lanes 10-11) polyclonal antibody. The results show that a putative FEN1 band was again recognized by anti-peptide FEN1 antibody in MRC5-SV protein extracts (Lanes 1, 7), at serum dilutions of 1:1000 and 1:2000, respectively. This band was the

same size as that detected by the positive control, anti-Xenopus FEN1 polyclonal antibody (Lane 10). Anti-peptide FEN1 antibody also recognized a putative FEN1 band, resulting from induced expression of the pT7.7-FEN1 vector in BL21 *E. coli* bacteria (lanes 2, 8), that was similarly recognized by the positive control, anti-Xenopus FEN1 (lane 11) polyclonal antibody. Additionally, Figure 3-11B shows that anti-peptide FEN1 antibody does not detect a putative FEN1 band (lanes 3, 9) in the negative control, *E. coli* BL21 (DE3) transformed with pT7.7 vector, without insert, induced with IPTG. Lastly, Figure 3-11A shows that when the anti-peptide FEN1 serum is pre-incubated with the synthetic peptide used as antigen, recognition of a putative FEN1 band in MRC5-SV lysates (lane 4) or recombinant FEN1 protein in bacteria (lane 5) is greatly diminished. These results demonstrate that the anti-peptide FEN1 antibody specifically recognizes endogenous and recombinant human FEN1 protein, and that the epitope of this polyclonal antibody is the peptide region of human FEN1 against which the antibody was raised.

Figure 3-11A and B showing anti-peptide FEN1 tests on western blots.

It should be noted that attempts at reducing background during ECL detection and increasing antibody titres by purifying anti-peptide FEN1 serum on Protein G Sepharose beads (see Methods & Materials) were unsuccessful (data not shown). Additionally, attempts to immunoprecipitate soluble human FEN1 protein from HeLa cell extracts, and detect endogenous human FEN1 protein during immunofluorescence microscopy using the anti-peptide FEN1 antibody, have been unsuccessful (data not shown). This suggests

that anti-peptide FEN1 antibodies may only recognize human FEN1 protein epitopes exposed on denatured protein.

3-8: Sub-cellular Localization of Recombinant GFP-FEN1 Protein in HeLa Cells

One of the aims of this thesis is to determine the spatial distribution and sub-cellular localization of human FEN1 protein. Because I was unable to produce or obtain FEN1 antibodies suitable to study the spatial expression of human FEN1 protein, I next attempted to transiently transfect human HeLa cells with a DNA vector containing the Green Fluorescent Protein (GFP) gene, 5'- to, and in frame with the entire ORF of the human *FEN1* gene. It was thought that transient expression of recombinant GFP-FEN1 protein in asynchronous cell populations may provide insight into the spatial expression and sub-cellular localization of human FEN1 protein.

The GFP-FEN1 plasmid was constructed as described in the Methods chapter. Briefly, a BglII-HindIII fragment encoding the entire human FEN1 ORF was ligated into similarly digested pEGFP-C1 plasmids, containing the GFP cDNA sequence. pEGFP-C1-FEN1 plasmid constructs were transformed into *E. coli* DH5α and bacteria colonies were screened by diagnostic restriction enzyme digestion to verify the presence of the human FEN1 DNA insert (data not shown). Plasmid DNA, from colonies testing positive for release of the correct size FEN1 DNA insert (approximately 1.2 kb), were amplified and plasmid DNA purified. Additionally, plasmid DNA containing either GFP alone or a GFP-FEN1 mutant construct with a 69 bp in-frame deletion near the FEN1 C-terminus, therefore lacking amino acids 225-247, were also amplified and purified. The GFP-

FEN1 plasmid DNA sequence was subsequently verified by sequencing prior to transfections.

Asynchronous HeLa cell populations were transfected with either GFP plasmid DNA alone (GFP), mutant GFP-FEN1 plasmids containing a 69 base pair deletion in the FEN1 cDNA (GFP-ΔFEN1), or GFP-FEN1 plasmids containing the full-length human FEN1 cDNA (GFP-wtFEN1). Sterile 13 mm coverslips were seeded with 3 X 10^4 asynchronous HeLa cells, which were allowed to adhere and proliferate for 24 hours. Cells were transfected with 3 μg DOSPER cationic lipofectamine reagents (Boehringer Mannheim) containing either 0.5 μg GFP, GFP-ΔFEN1, or GFP-wtFEN1 plasmid DNA. Control cells were treated with DOSPER only, without plasmid DNA. Following a 6 hour incubation with transfection reagents containing various GFP-plasmid DNA constructs, cells were washed in PBS and fresh media was added, prior to a further 18 hour incubation to allow GFP protein expression. Following the 18 hour incubation, HeLa cells on coverslips were washed then fixed *in situ* with either 3% paraformaldehyde or ice-cold methanol-acetone (50:50) and nuclei were stained with 0.25 μg/ml Hoescht 33258. Coverslips were then mounted on glass slides and viewed with a Zeiss Axioskop 2 fluorescence microscope (see Methods & Materials).

Figure 3-12 showing GFP/GFP-FEN1 fluorescence microscopy

Figure 3-12A shows the nuclei in HeLa cells transiently transfected with GFP, fixed with 3% paraformaldehyde, and stained with Hoescht 33258. Analysis of those same cells (Figure 3-12B) viewed with an FITC filter to show GFP fluorescence, shows

that GFP-transfected cells exhibit predominantly cytoplasmic localization of GFP protein. This result is similar to that reported previously in HeLa cells transfected with GFP alone (Inouge and Tsuji, 1994; Pines, 1995). In contrast, HeLa cells transiently transfected with either GFP-ΔFEN1 (Figure 3-12D) or GFP-wtFEN1 (Figure 3-12F) exhibited predominantly nuclear localization of recombinant GFP-FEN1 protein. The same nuclei stained with Hoescht 33258 are shown in Figures 3-12C and 3-12E, respectively. This result strongly suggests that human FEN1 protein is localized to the nucleus, as suggested by its putative nuclear localization signal (Murray *et al.*, 1994) and its proposed role in DNA replication (Ishimi *et al.*, 1988; Goulian *et al.*, 1990; Turchi and Bambara, 1993; Waga *et al.*, 1994) and other forms of DNA metabolism (Matsumoto *et al.*, 1994; Frosina *et al.*, 1996; Klungland and Lindahl, 1997).

Figure 3-13 showing GFP-FEN1 and PCNA staining

Because FEN1-PCNA protein interactions have been implicated in Okazaki fragment processing during DNA replication (Li et al., 1995; Chen et al., 1996; Warbrick et al., 1997), I next wanted to examine if there are similar localization patterns of FEN1 and PCNA protein in asynchronous HeLa cell populations. To address this question, HeLa cells were treated as described above, except coverslips were fixed with methanol-acetone only and cells were also stained with the anti-PCNA monoclonal antibody PC10 (see Methods & Materials), prior to DNA staining with Hoescht 33258. The organic solvent, methanol-acetone, was used because previous studies (Celis and Celis, 1985; Bravo and MacDonald-Bravo, 1987) had demonstrated that PCNA protein exhibits an S

phase-specific punctate staining pattern in cells fixed with organic solvents like methanol. As can be seen in Figure 3-13B, many cells exhibited nuclear PCNA staining (compare to Hoescht staining in Figure 3-13A). It is highly probable that those cells staining positively with PC10 represent the fraction of the HeLa cell population undergoing DNA replication in S phase of the cell cycle (Madsen and Celis, 1985; Bravo and MacDonald-Bravo, 1985, 1987; Hozak et al., 1993). Interestingly, although GFP-FEN1 protein expression was detected in those nuclei where PCNA staining was evident (presumptive S phase cells), GFP-FEN1 protein was also detected in nuclei where no PCNA staining was detected (Figure 3-13C). This result suggests that, unlike PCNA, a significant proportion of FEN1 protein remains in the nucleus in non-S phase cells.

3-9: Discussion

One of the primary aims of this project is to examine FEN1 protein expression *in vivo*, and determine its sub-cellular localization during the cell cycle and in response to DNA damage. To effectively determine FEN1's temporal and spatial expression, antibodies to human FEN1 protein were deemed essential. Consequently, significant time and effort were expended in trying to produce high-affinity antibodies to human FEN1, as well as develop alternative methods of examining FEN1 spatial expression *in vivo*. During this work I have extensively tested and verified that novel polyclonal antibodies to FEN1 protein (anti-Xenopus FEN1 and anti-peptide FEN1) recognize endogenous and recombinant denatured human FEN1 protein on western blots. Additionally, HeLa cell transfections with GFP-FEN1 cDNA constructs strongly suggest that human FEN1 protein is localized in the nucleus in cells throughout the cell cycle.

Although not entirely necessary for monoclonal antibody production, highly purified antigen was desired for the production of polyclonal antibodies. It was thought that this would minimize, or possibly eliminate the need for subsequent affinity purification steps that would probably be necessary following immunizations with less pure protein preparations. The pET21d-FEN1 plasmid construct, despite resulting in the deletion of the four C-terminal amino acids from full-length human FEN1 protein, was initially chosen to produce recombinant His_6-FEN1 protein in order to facilitate the initial protein purification steps. Although metal-affinity chromatography (Ni^{2+}) resulted in partial purification and significant enrichment of His_6-FEN1 protein in peak fractions (Figure 3-1), it was still deemed to be insufficiently pure for use as antigen in the production of polyclonal antibodies. Consequently, I elected to perform gel filtration of the purest Ni^{2+}-column fractions to remove the majority of higher and lower molecular weight contaminants. Although Coomassie staining of gel filtration fractions showed relatively pure His_6-FEN1 protein in peak fractions (Figure 3-2), silver staining of similar fractions (Figure 3-3) revealed numerous contaminating proteins. Because purity of antigen was essential, I decided to further purify His_6-FEN1 protein by electroelution of His_6-FEN1 bands carefully excised from SDS-PAGE gels. Although protein solubility was sacrificed in the process, antigen at greater than 98% purity was obtained (Figure 3-4).

Despite greater than 98% purity of His6-FEN1 antigen, no polyclonal antibodies to FEN1 protein were produced in this effort. It is possible that the primary immune response was to either the 15 amino acid linker (created during sub-cloning) between the coding region and the histidine tag, or to the histidine tag, itself. The latter possibility

could have easily been tested by serum probes of western blots containing another His-tagged protein. However, because an alternative His-tagged protein was unavailable during initial polyclonal serum screening, and because an anti-His antibody was not the aim here, that possibility was not further investigated. If either the 15 amino acid linker or His_6 epitopes were responsible for generating a specific immune response, it is possible that either domain may share homology with epitopes of the unknown human proteins in MRC5-SV cells that were recognized by test bleed serum (Figure 3-5A). Additionally, although Coomassie staining of SDS gels prior to electroelution was minimized to prevent excessive fixation and residue cross-linking, its effect may have contributed to either lack of immunogenicity or problems with antigen presentation during an immune response. However, this is unlikely in that the both anti-Xenopus FEN1 (J-L Li *et al.*, manuscript in preparation) and anti-human FEN1 (Warbrick *et al.*, 1997) polyclonal antibodies were produced from FEN1 protein contained in Coomassie-stained acrylamide gel slices. Other possibilities as to why no polyclonal antibodies to human FEN1 were produced against His_6-FEN1 antigen include that only one rabbit was immunized during this collaboration, and that immunizations were given on a bi-weekly schedule. It is possible that if more than one rabbit were immunized, or antigen injections were separated by more than 14 day minimum (Harlow and Lane, 1988), antibodies to FEN1 may have been produced. However, many high-affinity antibodies have previously been produced using this type of immunization schedule (Borek publications). Finally, the rabbit immunized may have had a weakened immune response due to exposure to other antigens as the result of disease or infection, but this is unlikey if rabbits are kept under standard lab conditions.

Hybridoma cell fusions from mice immunized with His_6-FEN1 exhibited colony formation in nearly 50% of seeded culture wells (Table 3-1). Despite successful hybridoma cell fusions, nearly 20% of colonies testing positive for IgG secretion, 6% testing positive for recognition of His_6-FEN1 antigen on dot blots, and supernatants from 5 colonies recognizing a putative FEN1 band on western blots of MRC5-SV cell extracts (Table 3-1); no monoclonal antibodies to His_6-FEN1 protein were produced. In addition to the possibilities cited above, it is also possible that clones recognizing FEN1 protein may have been missed or inadvertantly discarded during screening. The latter possibility is highly improbable because during every screen (Figure 3-6), even the weakest signals detected from tested supernatants were classified as positive and subjected to further tests. However, because only IgG-secreting clones were selected for, it is possible that other immunoglobulin classes may have been present that recognized FEN1, but were not identified. Because of the wider availability and variability of anti-IgG secondary antibodies necessary for many immunological detection methods, only IgG-secreting clones were desired and tested for. An additional problem in hybridoma clone detection may have been the result of insufficient antibody titres in hybridoma culture supernatants used during the screening process. Colony screening was performed before high levels of hybridoma cell confluency were attained in an effort to maintain maximum cell viability and minimize cellular stresses posed by high density cell culture. Consequently, secreted IgG levels from clones recognizing FEN1 epitopes may have been insufficient to detect FEN1 protein immobilized on western blots. Lastly, the extremely high level of homology (96%) of FEN1 protein between mouse and human (Lieber, 1997) may also have had an effect, although this is highly unlikely as PCNA is also well-conserved and

several excellent monoclonal antibodies to PCNA have been produced (Waseem and Lane, 1990).

Following the initial unsuccessful attempt at producing antibodies to His-tagged human FEN1 protein, it was decided to attempt to partially purify FEN1 protein by isolating and solubilizing recombinant untagged FEN1 protein present in insoluble inclusion bodies after induced expression in *E. coli* BL21 (DE3). Because similar methods of purifying recombinant human FEN1, and using homogenized acrylamide gel slices as antigen had previously been successful in producing polyclonal antibodies to FEN1 (3220 to human FEN1, Warbrick et al., 1997; anti-Xenopus FEN1, J-L Li *et al.*, manuscript in preparation), it was thought that there may be some aspect of antigen preparation, and subsequent antigen presentation inherent in this method that may improve FEN1 immunogenicity.

During the purification process of untagged FEN1, approximately 9 mg of partially purified protein (Figure 3-7) was recovered following solubilization of inclusion bodies, however, difficulties were encountered trying to renature the protein. Several attempts were made to optimize conditions for renaturation, as well as the subsequent dialysis to remove excessive salt concentrations. It is unclear as to why partially purified protein continued to precipitate during dialysis, but it is suspected that the majority of protein remained denatured because optimal renaturation conditions were not achieved. Rather than spending additional time and effort trying to optimize renaturation conditions, I elected to lyophilize the entire preparation, both soluble and precipitated protein, and use that as immunogen for monoclonal antibody production. It was thought that the combination of denatured and native recombinant FEN1 protein would serve as

excellent antigen by presenting a higher number of epitopes from which to elicit an immune response. A proportion of this preparation was also separated by SDS-PAGE, and the FEN1 band carefully excised to remove the majority of non-specific protein contaminants, homogenized, and used as antigen for polyclonal antibody production

With the exception of immunogenic responses to epitope tags and linker sequences in His_6-FEN1, the possible problems cited above also may have contributed to this unsuccessful attempt at polyclonal antibody production in rabbits using untagged FEN1 protein. Although the possibility exists that there may have been a very weak response to untagged FEN1, the time required to investigate that possibility and affinity purify anti-FEN1 antibody was deemed unsatisfactory due to the recent availability of another suitable antibody (anti-Xenopus FEN1) to continue this project.

During monoclonal antibody production from mice immunized with untagged FEN1, there appeared to be a strong response to a putative FEN1 band with protein used as antigen on western blots (Figure 3-9A), but no subsequent recognition of FEN1 protein in human cell extracts (Figures 3-9B) or other recombinant human FEN1 lysates (Figure 3-9C). It is quite possible that the primary immune response, in mice immunized with partially purified untagged FEN1, was to bacterial proteins contained in the partially purified preparation, that have a molecular weight similar to FEN1. However, because of the apparant strength of that possible non-specific response, it is also possible that weaker signals, due to recognition of actual FEN1 protein on western blots, may have been overlooked during screening of hybridoma clones produced from mice immunized with untagged FEN1.

During the four unsuccessful attempts at antibody production, a suitable antibody that recognized human FEN1 protein on western blots was produced (J-L Li *et al.*, manuscript in preparation). Extensive testing of anti-Xenopus FEN1 (Figures 3-10A & B) polyclonal antibodies showed that it recognized denatured recombinant and endogenous human FEN1 protein on western blots. In comparison with the commercially-produced anti-peptide monospecific polyclonal antibody, it appears that the anti-Xenopus FEN1 antibody provides a stronger detection signal during immunoprobing of western blots (Figure 3-11B). In addition, the anti-peptide FEN1 serum also contains an antibody species that detects a protein with a molecular weight slightly higher than FEN1. This protein band was also detected with pre-immune serum from the same rabbit prior to immunization with the FEN1-peptide antigen, suggesting that the higher molecular weight band represents a non-specific protein. Consequently, although both anti-peptide and anti-Xenopus FEN1 polyclonal antibodies recognize both recombinant and endogenous human FEN1 protein on western blots, I decided to use anti-Xenopus FEN1 for the remainder of my research project. It should also be noted that both anti-Xenopus and anti-peptide FEN1 antibodies were tested to see if they could be used for immunofluorescence microscopy of fixed cells or for immunoprecipitation of soluble human FEN1 protein from human cell lysates. No differences were noted between either antibody and pre-immune sera (data not shown). It is possible that both antibodies only recognize FEN1 protein in a denatured state. Because it appeared that both antibodies were unsuitable for immunoprecipitation or immunofluorescence, and unpurified anti-Xenopus FEN1 serum was found to be suitable for ECL detection on

western blots, time was not expended trying to affinity-purify either antibody from serum.

Because a major aim of this project is to examine the spatial expression and sub-cellular localization of human FEN1 protein, and because attempts at obtaining or producing antibodies suitable for immunofluorescence have been unsuccessful, a practical alternative to an immunological-based method of analysis was necessary. Consequently, I elected to try transient transfections of GFP-FEN1 DNA into human cells and examine the sub-cellular localization of GFP-FEN1 protein.

It appears that GFP-FEN1 protein is localized in the nucleus, based on the results in Figures 3-12 E and 3-12 F. By inference, endogenous FEN1 protein in human cells may also be expressed as a nuclear protein. This result is in agreement with FEN1's putative role in DNA replication (Ishimi et al., 1988; Goulian et al., 1990; Turchi and Bambara, 1993; Waga et al., 1994) and its consensus nuclear localization signal (Murray et al., 1994). Additionally, the GFP-ΔFEN1 mutant also shows nuclear localization (Figure 3-12C & D). Since this mutant lacks a 23 amino acid domain (amino acids 225-247) near the FEN1 C-terminus, it is probable that amino acids 225-247 of the FEN1 protein sequence are not essential for nuclear localization of FEN1.

Because FEN1 protein has been shown to interact with PCNA protein *in vitro* (Li et al., 1995; Chen et al., 1996; Warbrick et al., 1997), and is suspected to interact with PCNA in an S phase-specific manner *in vivo* (Warbrick et al., 1997; Lieber, 1997), I wanted to determine if spatial expression patterns of GFP-FEN1 and PCNA were similar. It has been demonstrated that significant amounts of methanol-insoluble PCNA protein remain in cell nuclei in an S phase-specific manner (Celis and Celis, 1985; Bravo and

MacDonald-Bravo, 1987). By fixing transfected cells *in situ* with methanol-acetone, it was thought that S phase cells could be distinguished from non-S phase cells, and GFP-FEN1 and PCNA protein spatial expression patterns could be compared in cells in S phase as well as other cell cycle stages. After methanol-acetone fixation of asynchronous HeLa cells, nuclear PCNA staining could be detected in only approximately 50% of the cells examined (data not shown). Although HeLa cells are highly proliferative and a large percentage of cells in an asynchronous HeLa cell population can be found in S phase (see Chapter 4, Figure 4-1), this percentage appears to be abnormally high. This may indicate nuclear PCNA staining of non-S phase cells, possibly caused by cross-linking of soluble nuclear PCNA protein not involved in DNA replication. Despite this result, it was still observed that GFP-FEN1 protein was expressed in many nuclei where little or no PCNA staining was detected (Figures 3-13 C & D). This suggests that FEN1 protein may be a nuclear insoluble protein in non-S phase, as well as S phase cells. Future experiments with stable expression of GFP-FEN1 protein in synchronized cell populations will be necessary to verify this observation.

To summarize, I now possess two polyclonal antibodies (anti-Xenopus FEN1 and anti-peptide FEN1) capable of detecting endogenous and recombinant human FEN1 protein on western blots. The anti-Xenopus FEN1 antibody will be used in future experiments to examine FEN1 protein expression in synchronized and DNA damaged cell populations. I have also shown that GFP-FEN1 recombinant protein appears to be a nuclear protein in HeLa cells transiently transfected with GFP-FEN1 cDNA. Additionally, other results (Figure 3-13) also show that this nuclear localization is observed in methanol-acetone fixed cells where nuclear PCNA staining is not observed.

This suggests that some human FEN1 protein may remain nuclear-insoluble in non-S phase cells.

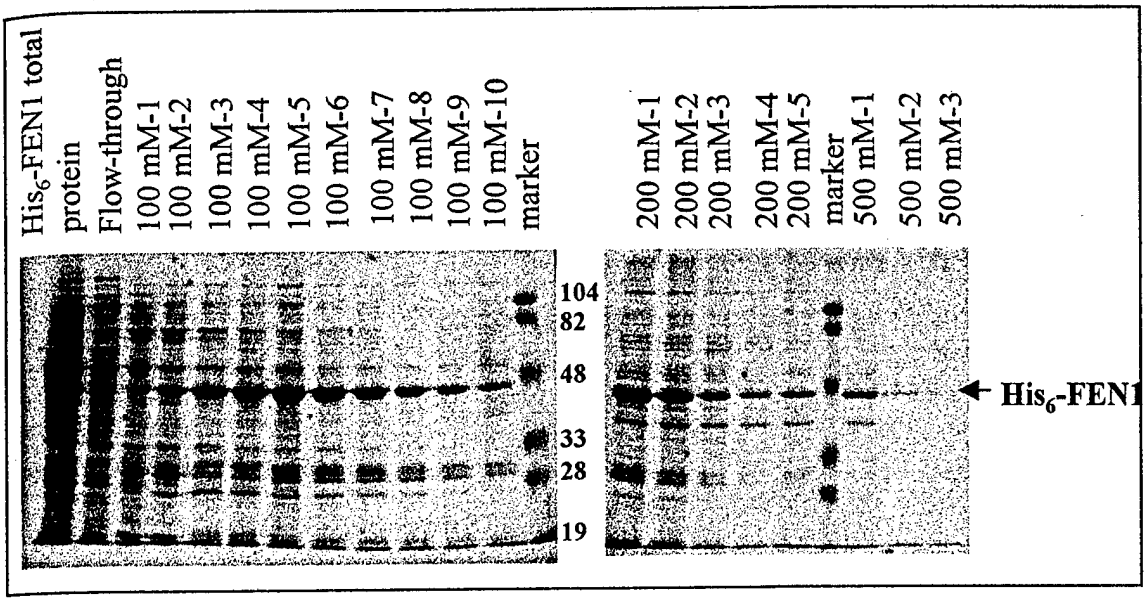

Figure 3-1. 10% SDS-PAGE of column fractions eluted from a Ni^{2+} column loaded with recombinant human His_6-FEN1 protein. 30 ml of soluble protein extracted from a 500 ml culture of *E. coli* BL21 induced to express recombinant human His_6-FEN1 protein were loaded on a 1 ml Ni^{2+} column and eluted in a stepwise manner with increasing concentrations of imidazole (from 100 mM-500 mM) in a phosphate buffer. 0.5 ml fractions were collected, aliquots from each were diluted in 4 X SDS loading buffer, and separated by 10% SDS-PAGE. The predominant enriched band at approximately 47 kDa is His_6-FEN1 protein. Molecular weight marker sizes are shown in the centre of the figure.

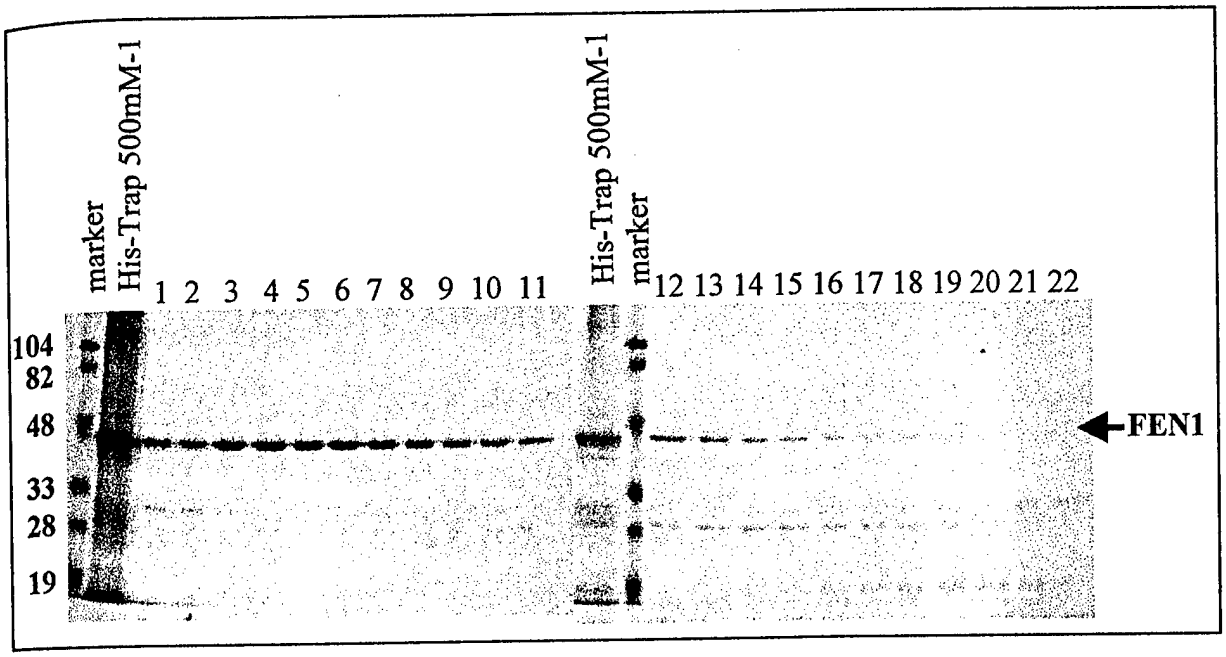

Figure 3-2. 10% SDS-PAGE of column fractions eluted from a Sephacryl 16/60 gel filtration column. 2 ml aliquots of Ni^{2+}column purified His_6-FEN1 protein were separated on a Sephacryl 16/60 gel filtration column, collecting 0.5 ml fractions. Fractions were collected during the estimated V_e (elution volume) determined during column calibration (only peak fractions are shown). Fractions collected were diluted 3:4 in 4 X SDS loading buffer and aliquots from each were separated by 10% SDS-PAGE and Coomassie-stained. The His-Trap 500 mM-1 fractions indicated show the pooled protein that was loaded onto the gel filtration column. Marker sizes are indicated on the left.

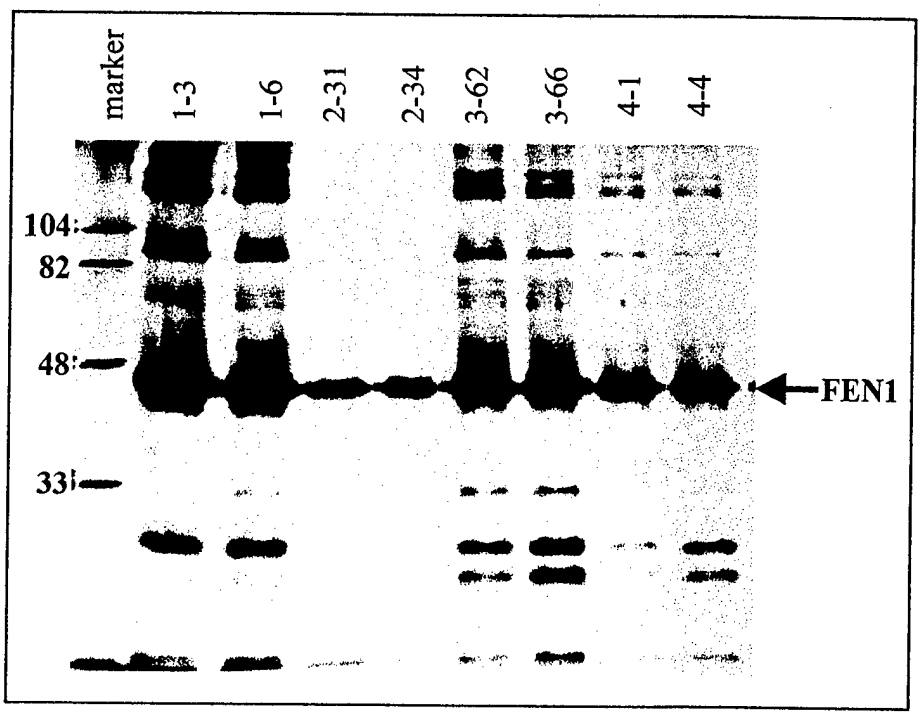

Figure 3-3. Silver stained 10% SDS-PAGE of various gel filtration fractions. Equal volumes from various representative fractions collected during several gel filtration runs were separated by 10% SDS-PAGE and silver stained. The first number above each lane refers to the gel filtration run and the second refers to the fraction number. The fractions 2-31 and 2-34 appear relatively pure, but protein concentrations in these fractions were very low and undetectable by Coomassie-staining. The molecular weight marker sizes are indicated on the left.

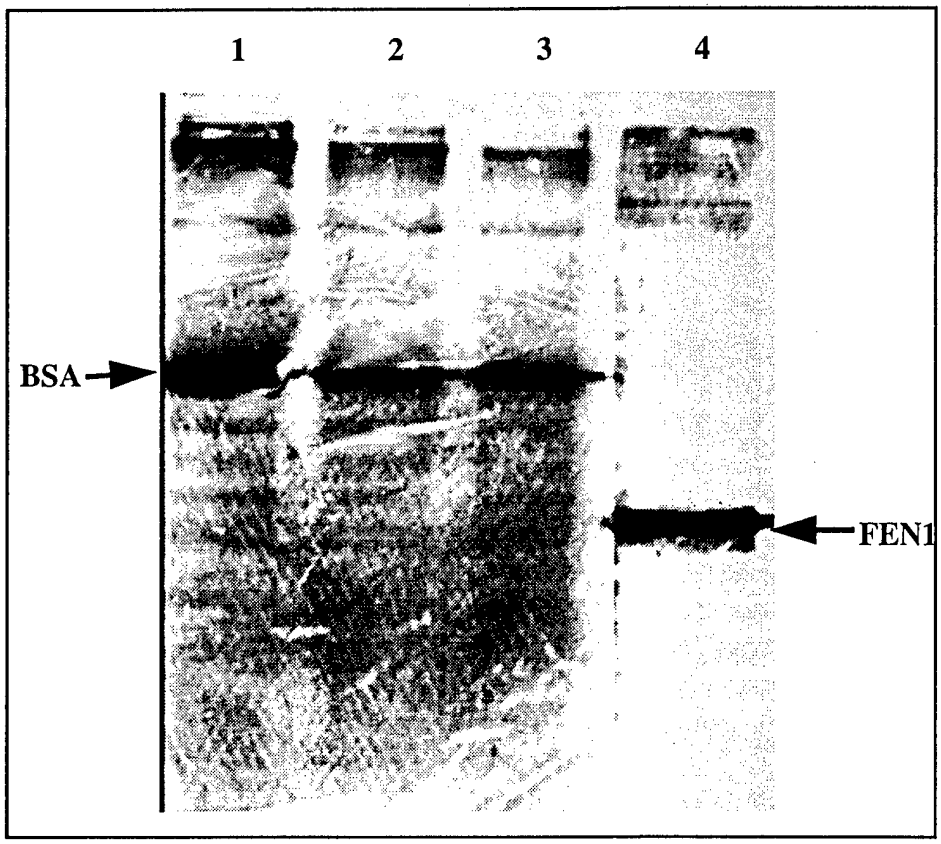

Figure 3-4: 10% SDS-PAGE of electroeluted His_6-FEN1 protein. Electroeluted His_6-FEN1 protein was separated on 10% SDS-PAGE and silver-stained (lane 4). Purified BSA (USB Biochemicals) serves as a purity and concentration control. Lane 1: 2 μg BSA, Lane 2: 1 μg BSA, Lane 3: 0.5 μg BSA.

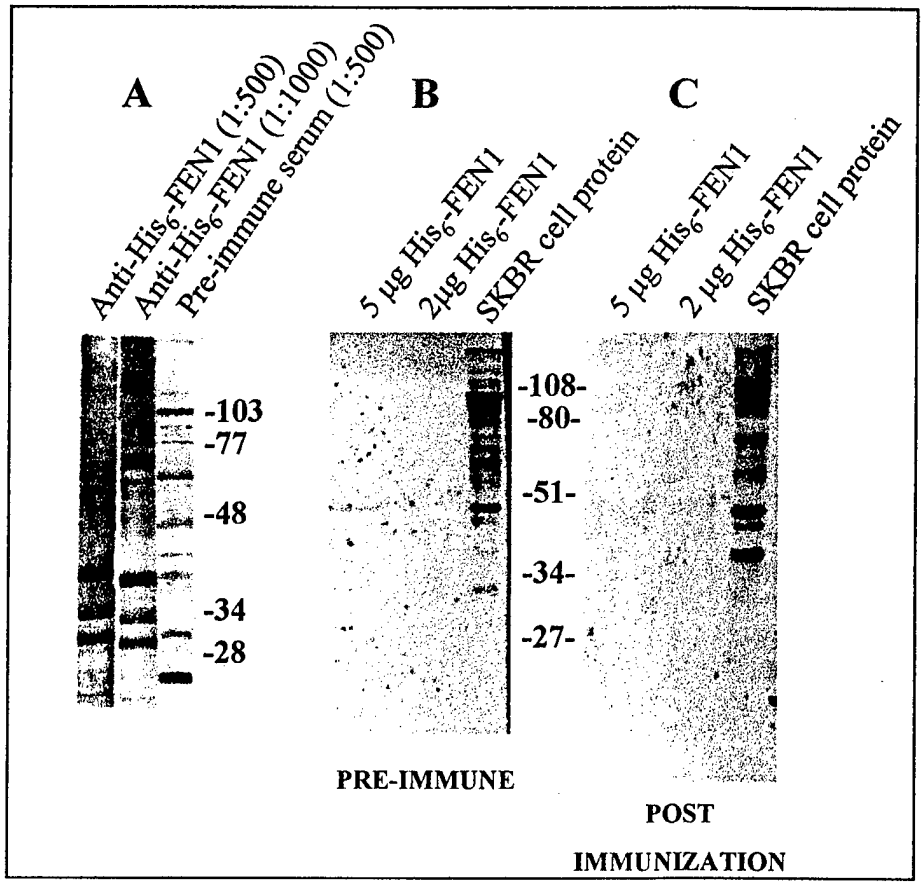

Figure 3-5. Immunoprobes of western blots by polyclonal antibody serum from rabbits immunized with His_6-FEN1. (A) Western strip blots from a 10% SDS-PAGE gel of human MRC5-SV protein extract (200 μg total protein) that was transferred to nitrocellulose and probed with either pre-immune serum (1:500) or serum (1:500, 1:1000) from a rabbit immunized with His_6-FEN1. There appears to be no immunogenic response to FEN1 (approximately 47 kDa) when comparing pre-immune (on right) to serum prepared after the third immunization (on left). **(B,C)** Western blots of a 10% SDS-PAGE gel containing either recombinant electroeluted His_6-FEN1 (2 & 5 μg) or total protein (20 μg) extracted from a human mammary carcinoma cell line, SKBR, and subsequently probed with either **(B)** pre-immune serum or **(C)** serum prepared after the third immunization from a rabbit immunized with His_6-FEN1 protein. The putative 47 kDa protein detected in SKBR cells is recognized by both pre-immune and post-immune serum, and is therefore probably not FEN1. Molecular weight marker sizes are indicated.

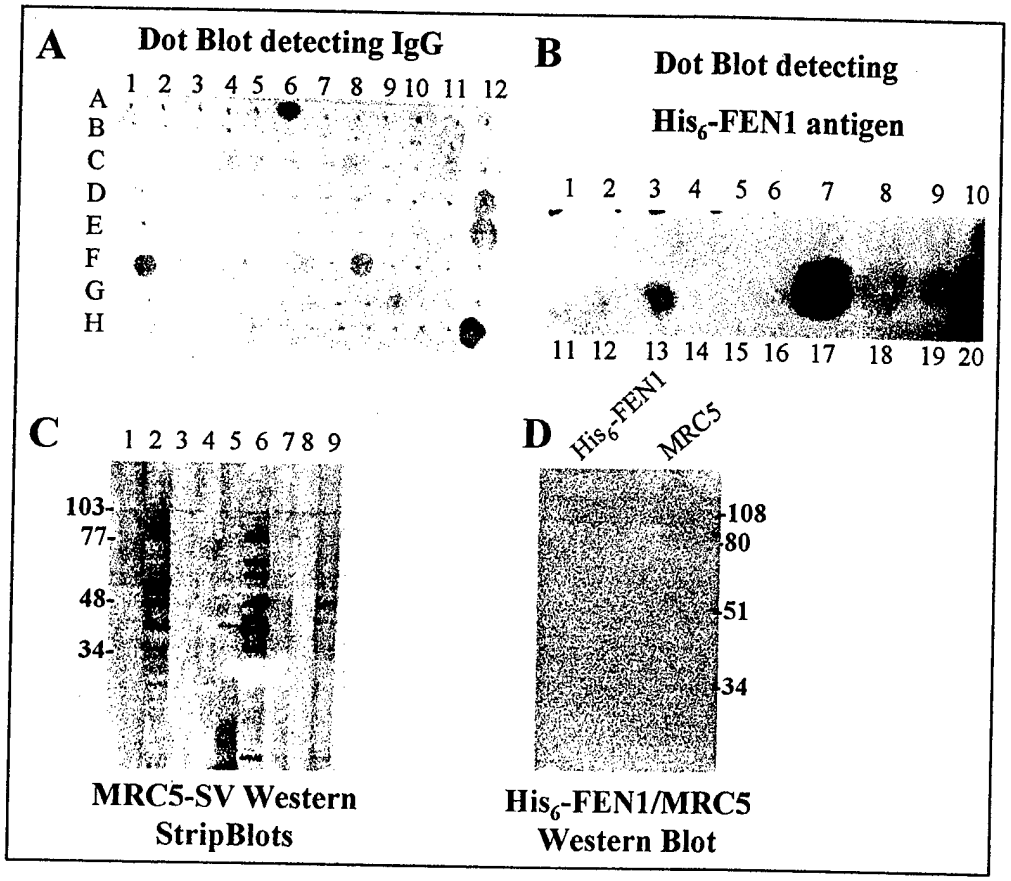

Figure 3-6. Testing of various hybridoma supernatants for recognition of human FEN1 protein. (A) Representative dot blot with rabbit anti-mouse IgG immobilized on nitrocellulose and probed with various supernatants from hybridoma colonies derived from mice immunized with His_6-FEN1protein. Following the primary antibody, membranes were probed with HRP-conjugated anti-mouse IgG (diluted to 1:1000) and subjected to colorimetric reactions to detect IgG-secreting colonies. The positive control for IgG secretion is at position H-12. **(B)** Representative dot blot with recombinant purified His_6-FEN1protein (used as antigen) immobilized on nitrocellulose and probed with hybridoma supernatants from colonies testing positive for IgG secretion. Following probing with the secondary antibody, HRP-conjugated anti-mouse IgG (diluted to 1:1000), blots were subjected to ECL detection. **(C)** Representative western strip blots of 100 μg soluble protein from human MRC5-SV cells probed with hybridoma supernatants that secreted IgG and recognized His_6-FEN1 antigen on dot blot analysis. Any hybridoma supernnatant that recognized a putative 46-47 kDa protein here was finally tested for recognition of His_6-FEN1 antigen or FEN1 in western blots of primary human MRC5 cell lysates. **(D)**.Western blot of MRC5 cell lysate and purified recombinant His_6-FEN1 protein that was probed with hybridoma supernatant from clone 2 in (C). Supernatants from other clones (5, 6, 9) that recognized a putative 46-47 kDa band in (C) were also tested similarly, but no clones were identified that were positive for all tests of human FEN1 protein recognition.

	A	B	C	D	E	F
	Number of culture wells seeded	(+) for colony formation	(+) for IgG secretion	(+) for recognition of His_6-FEN1 antigen on dot blot	(+) for recognition of putative FEN1 band on MRC5-SV western blot	(+) for recognition of recombinant His_6-FEN1on western blot
Immunized **Mouse 1**	960	473 (49%)	92 (19%) *	27 (6%) *	5 (1%) *	0 (0%) *
Immunized **Mouse 2**	1056	730 (69%)	106 (15%) *	28 (4%) *	1 (0.1%)*	0 (0%) *

* Indicates that percentage (in parentheses) is calculated as a percentage of the total number of positives for colony formation in B.

Table 3-1: Screen of hybridoma culture supernatants derived from mice immunized with His_6-FEN1 antigen. Hybridoma cells, from fusions of SP2 myeloma cells and mouse splenocytes following immunization of two mice with His_6-FEN1 antigen, were seeded in 96-well culture dishes and screened for production of monoclonal antibodies to human FEN1 protein. All hybridoma supernatants that tested positive for IgG secretion (either +, ++, or +++) were simply classified as (+). The first column (A) refers to the total number of wells that were initially seeded with hybridoma fusions and the second (B) shows the number (and percentage of total seeded) of wells that grew hybridoma colonies. The third (C), fourth (D), and fifth (E) columns show the number of hybridoma supernatants (from hybridoma colonies) that tested positive for IgG secretion on dot blot analysis, recognition of protein in His_6-FEN1 antigen preparations on dot blots, and recognition of a putative FEN1 band on western blots of MRC5-SV lysates, respectively. Supernatants from hybridoma colonies that tested positive in all 4 screens above were subsequently tested for recognition of purified His_6-FEN1 protein on western blots (F). No supernatants tested positive for recognition of His_6-FEN1 protein on western blots.

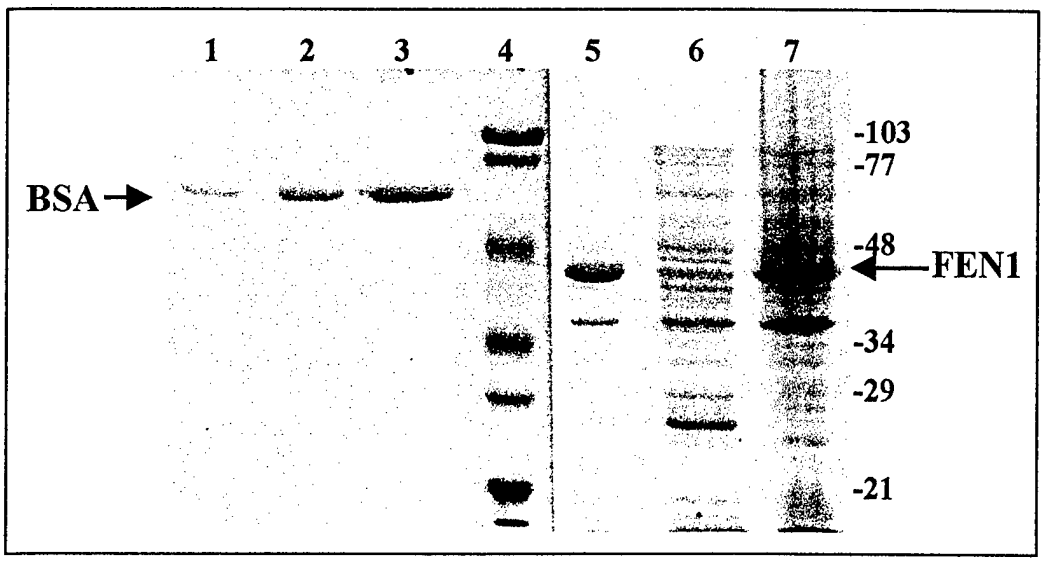

Figure 3-7. 10% SDS-PAGE of partially purified recombinant human FEN1 protein. Untagged pT7.7-FEN1 plasmids were transformed into *E. coli* BL21 and protein expression induced with IPTG. Inclusion bodies were isolated and solubilized, with 9 mg of untagged FEN1 protein extracted from a 500 ml culture volume. Protein from solubilized inclusion bodies was separated by 10% SDS-PAGE and Coomassie-stained. BSA serves as a concentration and purity control. Lane 1: 0.5 μg BSA, Lane 2: 1μg BSA, Lane 3: 2 μg BSA, Lane 4: molecular weight markers, Lane 5: 2.5 μl aliquot of untagged human FEN1 extracted from partially purified inclusion bodies, Lane 6: lysate from *E. coli* BL21 transformed with pT7.7 plasmid without insert, induced with IPTG, Lane 7: total protein extracted from *E. coli* BL21 transformed with pT7.7-FEN1 and induced with IPTG. Molecular weight marker sizes are indicated on the right.

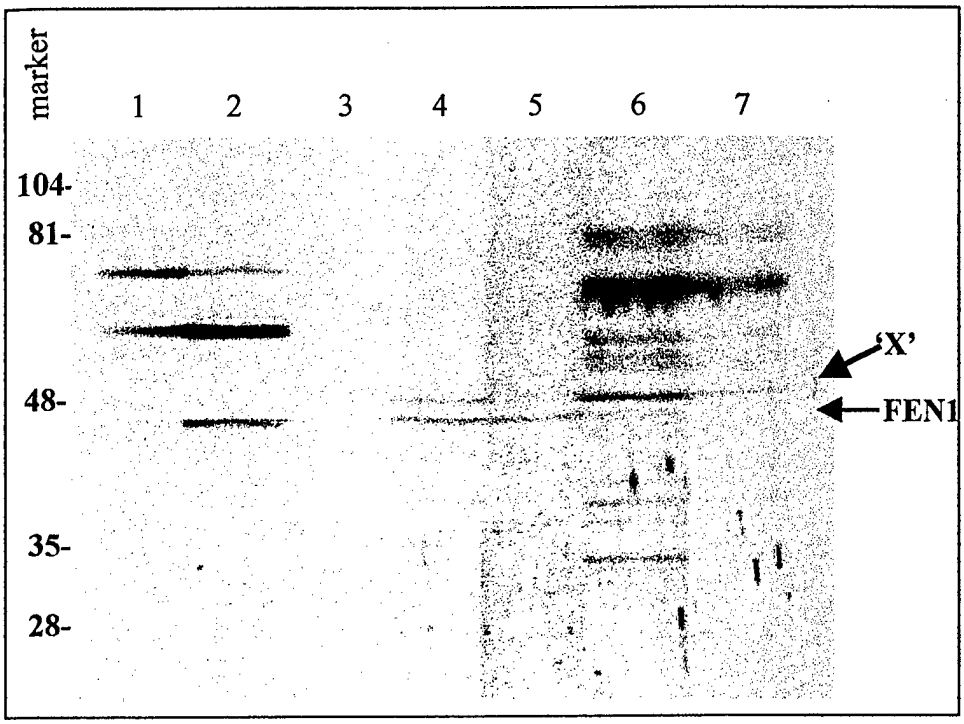

Figure 3-8. Test for recognition of human FEN1 by western blots of HeLa cell extracts using polyclonal antibody serum from rabbits immunized with recombinant human FEN1 protein. Western strip blots of HeLa cell lysates were probed with various antibodies derived from rabbits immunized with FEN1 protein. Lane 1: anti-Xenopus FEN1 pre-immune serum (1:500), Lane 2: anti-Xenopus FEN1 (J-L Li *et al.*, manuscript submitted) (1:1000), Lane 3: anti-peptide FEN1 pre-immune serum (1:500), Lane 4,5: anti-peptide FEN1 (1:500, 1:1000), Lane 6,7: polyclonal sera from rabbit immunized with untagged FEN1 (1:500, 1:1000, respectively). Following the primary antibody , membranes were probed with HRP-conjugated anti-rabbit IgG (diluted 1:1000) and subjected to ECL detection. Although not clear in this figure, the upper band at approximately 49 kDa in Lanes 4,5 (marked 'X') is also recognized by the anti-peptide FEN1 pre-immune serum and is probably not FEN1.

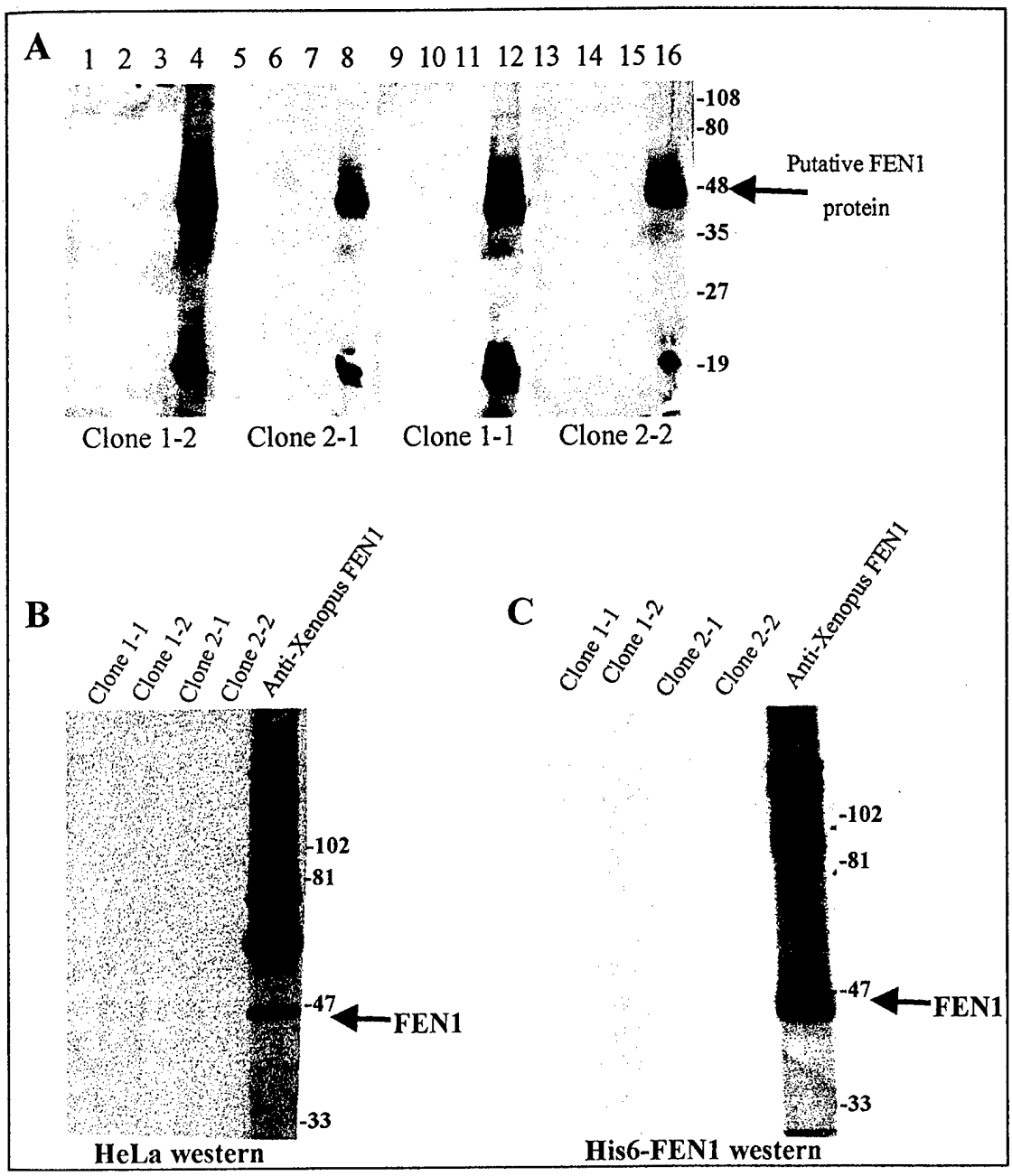

Figure 3-9. Tests of hybridoma supernatants derived from mice immunized with recombinant untagged human FEN1 protein. (A) Western blots of protein lysates from 2 different human cancer cell lines (Lanes 1,5,9,13: SVK17, Lanes 2,3,6,7,10,11,14,15: MCF7) and recombinant untagged human FEN1 protein (Lanes 4,8,12,16) (same as antigen) that were probed with 4 different hybridoma supernatants (Clones 1-1, 1-2, 2-1, 2-2) during screening for FEN1 recognition. **(B)** and **(C)** Those same hybridoma supernatants were used to probe western blots with either HeLa protein (B) or partially purified His_6-FEN1 protein (C). Compared to the positive control (anti-Xenopus FEN1), no recognition of either endogenous or recombinant FEN1 was detected using any of the 4 hybridoma colony supernatants, 1-1, 1-2, 2-1, 2-2.

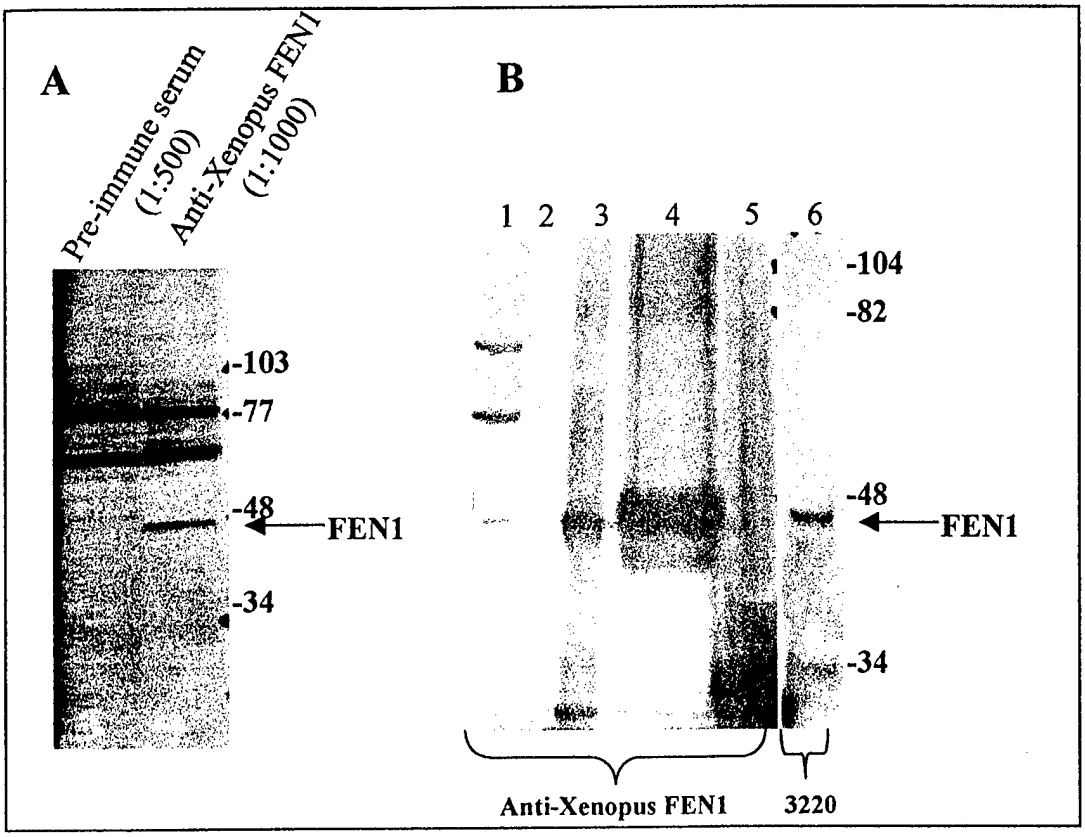

Figure 3-10. Test for recognition of human FEN1 protein by anti-Xenopus FEN1 polyclonal antibody. (A) Western blot containing 100 μg MRC5-SV protein was cut into strips and probed with either pre-immune serum (1:500) or serum (1:1000) from a rabbit immunized with GST-tagged Xenopus FEN1 protein. **(B)** Western blot of various cell lysates probed with anti-Xenopus FEN1 polyclonal serum (1:1000). Lane 1: human MRC5-SV, Lane 2: blank, Lane 3: His_6-FEN1 (partially purified on a Ni^{2+}-agarose column), Lane 4: electroeluted purified His_6-FEN1 protein, Lane 5: lysate from *E. coli* BL21 (DE3) transformed with pET21d vector only and induced with IPTG (negative control), Lane 6: human MRC5-SV lysate probed with the positive control, polyclonal antibody 3220 (Warbrick *et al.*, 1997). These examples clearly show that anti-Xenopus FEN1 recognizes both endogenous and recombinant human FEN1 protein.

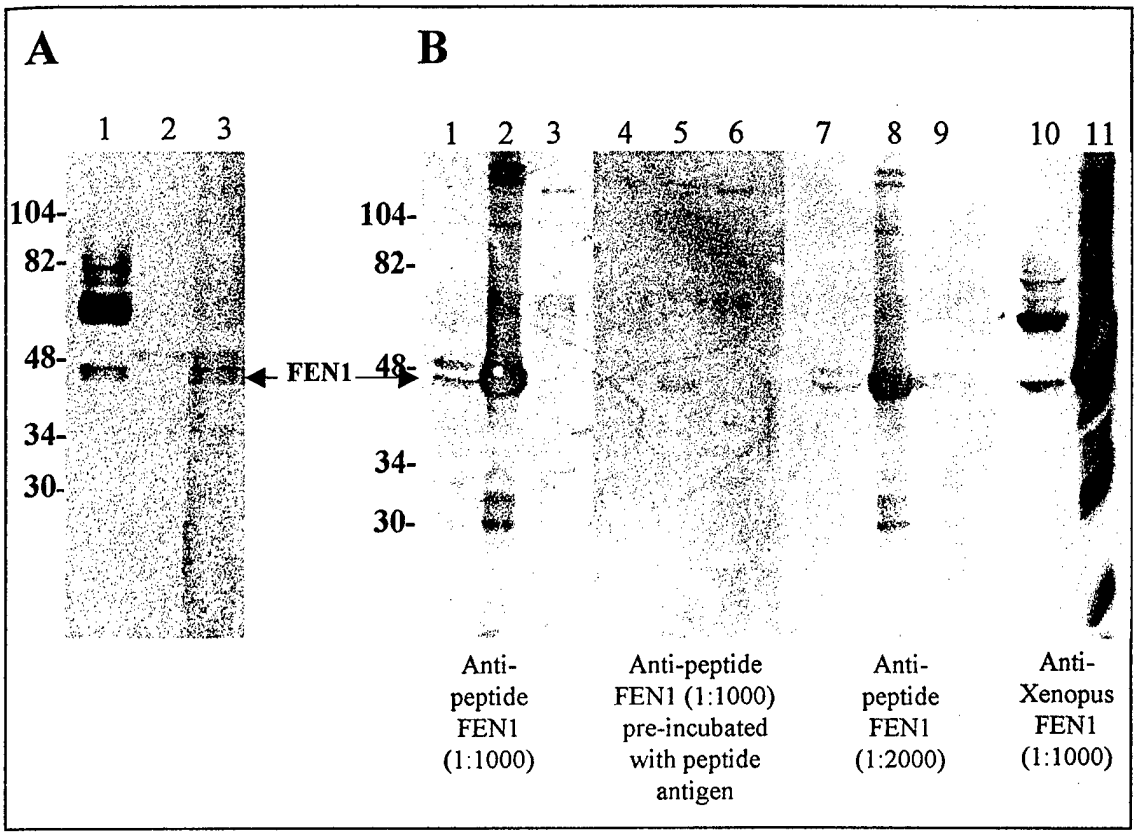

Figure 3-11. Testing for recognition of recombinant and endogenous human FEN1 protein by anti-peptide FEN1 polyclonal antibodies. (A) Western strip blots of human MRC5-SV lysate separated by 10% SDS-PAGE, transferred to nitrocellulose, and probed with (Lane 1) positive control anti-Xenopus (1:1000) FEN1, (Lane 2) pre-immune serum (diluted to 1:500), or (Lane 3) test bleed serum (diluted to 1:1000) from a rabbit immunized with a synthetic peptide antigen comprising a C-terminal region of human FEN1. **(B)** Four identical western blots of various protein lysates (Lanes 1,4,7,10: human MRC5-SV lysate, Lanes 2,5,8,11: lysate from *E. coli* BL21 transformed with pT7.7-FEN1and induced with IPTG, Lanes 3,6,9: lysate from *E.* coli BL21 transformed with pT7.7 vector only and induced with IPTG) that were probed with either anti-peptide FEN1, anti-peptide FEN1 pre-incubated with the cognate FEN1 peptide used as antigen, or anti-Xenopus FEN1 (positive control). These results show that anti-peptide FEN1 polyclonal antibody recognizes recombinant and endogenous human FEN1 from MRC5-SV cells, and that recognition is specific for the peptide sequence used as antigen.

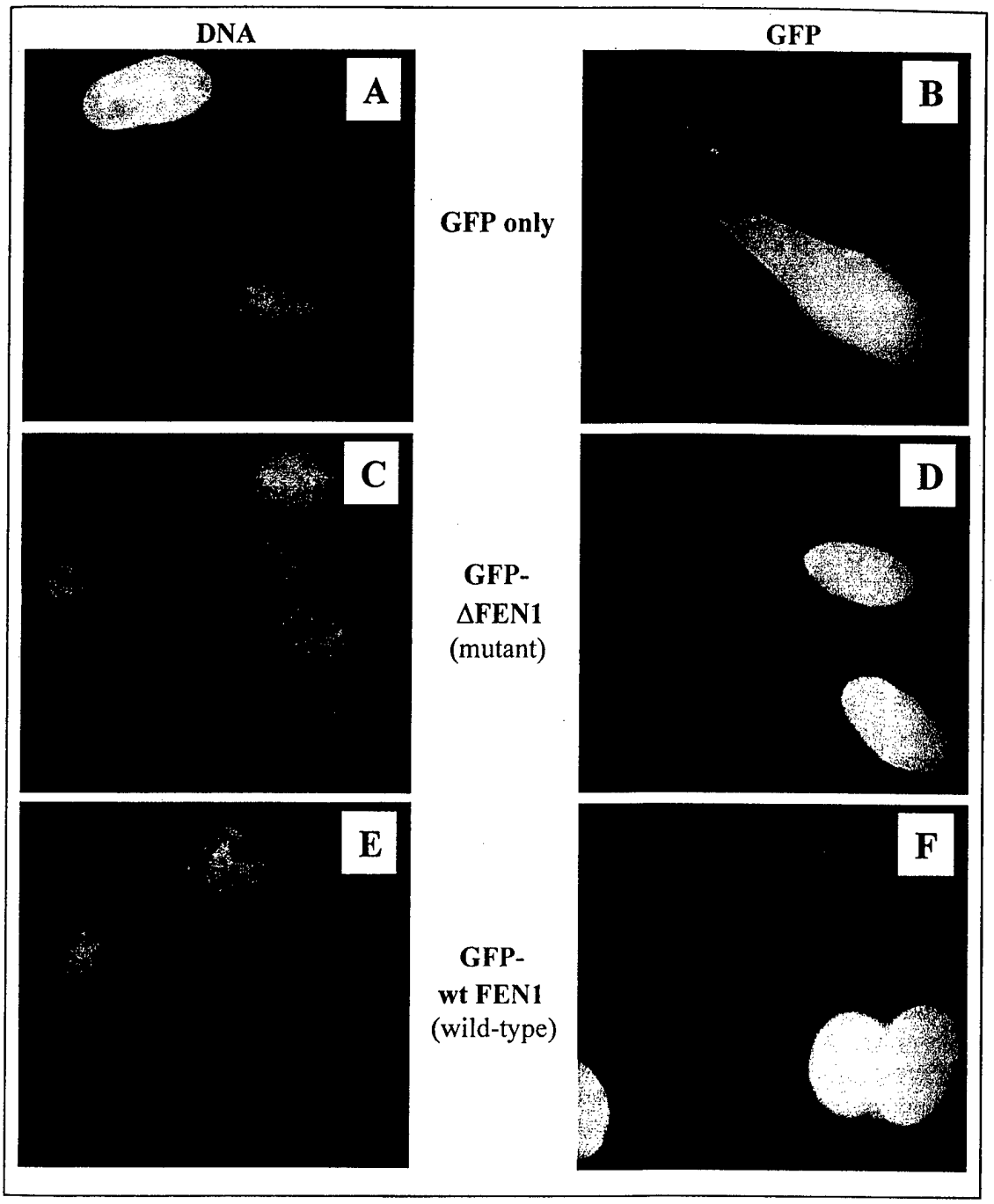

Figure 3-12. Fluorescence microscopy of GFP, GFP-ΔFEN1, and GFP-wt FEN1 transfected HeLa cells. Asynchronous HeLa cells growing on glass coverslips were transiently transfected with 0.5 μg of purified plasmid DNA mixed with 3 μg of DOSPER cationic lipofectamine in DMEM. Following an 18 hour incubation to allow expression of the various GFP constructs from the CMV promoter, cells were fixed *in situ* with 3% paraformaldehyde and stained with the DNA stain Hoescht 33258 at 0.25 μg/ml in PBS. Coverslips were mounted on glass slides and viewed with a Zeiss Axioskop 2 fluorescence microscope. **(A)** Hoescht nuclear DNA staining of cells transfected with GFP-only plasmid cDNA, and **(B)** those same nuclei viewed with the FITC (green) filter showing GFP protein. **(C)** DNA and **(D)** GFP-ΔFEN1 protein in cells transfected with GFP-ΔFEN1 plasmid cDNA; **(E)** DNA and **(F)** GFP-wt FEN1 protein in cells transfected with GFP-wt FEN1 plasmid cDNA. Although GFP protein is found throughout the cell, both mutant (GFP- ΔFEN1) and wild-type (GFP-wt FEN1) GFP-FEN1 proteins appear to be localized to the nucleus.

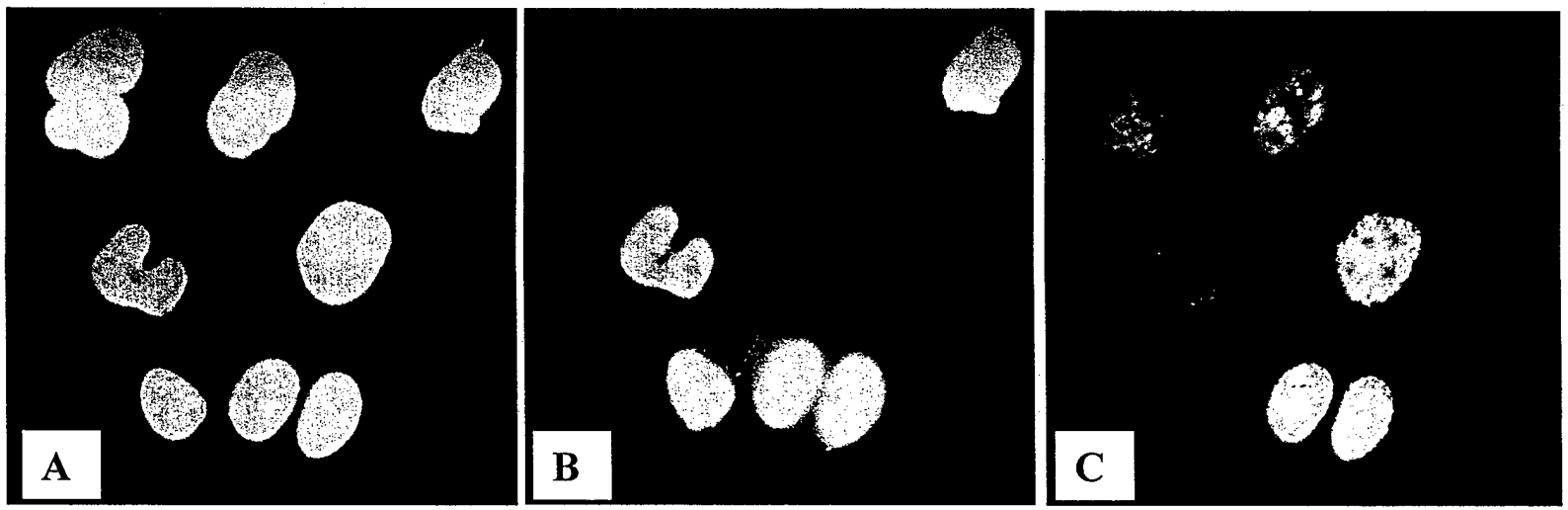

Figure 3-13. Fluorescence microscopy of GFP-FEN1 transfected HeLa cells. Asynchronous HeLa cells growing on glass coverslips were transiently transfected using 3 μg of DOSPER cationic lipofectamine and 0.5 μg of GFP-wt FEN1 plasmid DNA. Following an 18 hour incubation to allow expression of GFP-FEN1 from the CMV promoter, cells were fixed *in situ* with ice-cold methanol-acetone, and stained with the anti-PCNA monoclonal antibody PC10 (diluted to 1:1000 in PBS), followed by TRITC-conjugated anti-mouse IgG (diluted 1:128 in PBS), and the DNA stain Hoescht 33258 (0.25 μg/ml). Coverslips were mounted on glass coverslips and viewed with a Zeiss Axioskop 2 fluorescence microscope. **(A)** Nuclei stained with Hoescht and viewed with the blue filter, **(B)** GFP-wt FEN1 protein detected with the FITC (green) filter, and **(C)** PCNA protein detected by PC10, viewed with the TRITC (red) filter. The results show that GFP-wt FEN1 protein is localized to the nucleus and can be seen in cell nuclei where PCNA protein was present and in nuclei where no PCNA was detected.

CHAPTER FOUR: ANALYSIS OF HUMAN FEN1 mRNA/PROTEIN EXPRESSION AND PROTEIN SOLUBILITY PATTERNS DURING THE CELL CYCLE

4-1: Introduction

A role for FEN1 protein during DNA replication *in vitro* has been demonstrated by several laboratories using purified proteins (Goulian *et al.*, 1990; Turchi and Bambara, 1993) and SV40 cell-free extracts (Ishimi *et al.*, 1988). SV40 DNA replication in cell-free extracts (Li and Kelly, 1984, 1985; Stillman and Gluzman, 1985; Wobbe *et al.*, 1985) has served to identify cellular proteins required for DNA replication from the SV40 origin of replication. It is thought that these same proteins, identified in the SV40 system, also function during nuclear DNA replication in non-SV40-infected mammalian cells (Waga *et al.*, 1994). When complete reconstitution of SV40 DNA replication and production of form I DNA was finally accomplished, FEN1 was found to be an essential protein in the process (Waga *et al.*, 1994). Because the SV40 system only serves as a model for the mechanisms of mammalian DNA replication, a detailed analysis of human FEN1 in non-SV40-infected cells is necessary to verify its putative role in human nuclear DNA replication.

Several proteins essential for DNA replication, identified by SV40 studies and other DNA replication assays, show increased mRNA and protein expression as cells progress from early G_1 through S phase of the cell cycle. Increased mRNA and protein expression during cell cycle progression from early G_1 towards S phase has been demonstrated for DNA polymerase α (Thömmes *et al.*, 1986), thymidine kinase

(Schlosser *et al.*, 1981), topoisomerase I (Tricoli *et al.*, 1985), PCNA (Almendral *et al.*, 1987; Matsumoto *et al.*, 1987; Morris and Mathews, 1989), and other genes/gene products involved either directly or indirectly to nuclear DNA synthesis. If FEN1 is required for nuclear DNA synthesis, it is possible that its mRNA and protein expression levels may also be regulated in a cell cycle-dependent manner.

In addition to cell cycle-dependent mRNA and protein expression, some proteins required for nuclear DNA synthesis also exhibit cell cycle-dependent changes in protein solubility and sub-cellular localization. DNA ligase I (Montecucco *et al.*, 1995), DNA polymerase α (Hozak *et al.*, 1993), RP-A (Cardoso *et al.*, 1993), and PCNA (Madsen and Celis, 1985; Bravo and MacDonald-Bravo, 1985, 1987; Hozak *et al.*, 1993) are some of the replication proteins that have been shown to localize to discrete sites of DNA replication (replication foci) during S phase of the cell cycle. In addition, PCNA localization to replication foci during S phase (Celis and Celis, 1985; Bravo and MacDonald-Bravo, 1987; Hozak *et al.*, 1993) directly correlates to its cell cycle-dependent decrease in protein solubility (Bravo and MacDonald-Bravo, 1987). Because FEN1 has been shown to interact with PCNA *in vitro* (Li *et al.*, 1995; Chen *et al.*, 1996) and is suspected to interact with PCNA in an S phase-specific manner *in vivo* (Warbrick *et al.*, 1997; Lieber, 1997), it is possible that FEN1 protein may also exhibit solubility changes in a cell cycle-dependent manner, similar to PCNA.

To determine if human FEN1 mRNA and protein levels and protein solubility change in a cell cycle-dependent manner, primary and transformed human cell populations were synchronized by blocking cell cycle progression at various stages of the cell cycle. Cell populations were then released from their cell cycle block, and harvested

over the cell cycle. FACS, mRNA, and protein analysis of harvested cell populations was then carried out to analyze human FEN1 mRNA/protein expression and protein solubility patterns during the cell cycle.

4-2: Results

4-2.1: Cell Synchronizations during the Cell Cycle

Because of FEN1's putative role in DNA replication (Ishimi *et al.*, 1988; Goulian *et al.*, 1990; Turchi and Bambara, 1993; Waga *et al.*, 1994), it is important to study synchronous cell populations through G_1 and S phases of the cell cycle to evaluate possible cell cycle-dependent changes in expression of FEN1 mRNA and protein and analyze FEN1 protein solubility patterns.

Several cell lines and methods of synchronization were initially used during this work in an effort to obtain cell populations capable of synchronous re-entry and passage through the cell cycle. The following briefly describes the different cell lines and synchronization methods attempted: serum starvation and contact inhibition of non-transformed lines (murine 3T3, hamster BHK, human keratinocyte NCTC 2544); use of cell cycle progression-inhibiting drugs including aphidicolin, hydroxyurea, excess thymidine, mevastatin, and nocodazole at varying concentrations, times, and combinations on immortalized and transformed cell lines (SV40-transformed MRC5, HeLa); use of peripheral blood lymphocytes (PBLs) isolated from whole blood and stimulated to proliferate with the mitogen, Concanavilin A (ConA); and the use of a temperature-sensitive murine mammary carcinoma cell line (FT210) that arrests in late G_2 at the restrictive temperature of 40° C due to thermolability of Cdk1 (Th'ng *et al.*, 1990). Various difficulties were encountered during these tests, but could be summarized

by two recurrent factors: insufficient synchrony and lack of reproducibility (data not shown).

Obtaining sufficient synchrony and reproducibility was finally obtained by extensive testing using a double block of excess thymidine and the microtubule polymerization inhibitor, nocodazole, on HeLa cells at varying times and concentrations. This method of cell synchronization (See Methods & Materials) provides greater than 75% synchrony, allows re-entry into cycle following drug removal, minimizes loss of cell viability, and is readily reproducible.

4-2.2: Mitotic Synchronization of HeLa Cells

In order to synchronize HeLa cells in M phase of the cell cycle, a double block with 2 mM thymidine (12 hours) and 20 ng/ml nocodazole (12 hours) was utilized. In addition to being an effective way of synchronizing HeLa cell populations with minimal loss of cell viability, removal of the mitotic block (nocodazole) allowed rapid cell cycle progression into G_1 and synchronous progression throughout G_1 and S phase of the cell cycle.

Suspensions of asynchronous HeLa cells were used to carefully establish 0.5 X 10^6 and 1.5 X 10^6 initial seeding densities (as determined by Coulter counter analysis) in 10 cm and 15 cm culture dishes, respectively. Cells were allowed to adhere for 24 hours prior to synchronization treatment, and cell loss (as determined by presence of non-adherent cells) was insignificant and similar for all seeded culture vessels. To further minimize any potential differences in cell densities, several culture dishes were harvested at each time-point and cells pooled. Harvest times, after release from mitotic block (T0),

were determined as to provide representative cell populations from early G_1 (T2 or T3), mid-G_1 (T6), early S (T10 or T11), mid-S (T13 or T14), and late S (T16).

FIGURE 4-1: FACS Analysis figure of a typical HeLa synchronization

Following sequential 12 hour incubations with excess thymidine and nocodazole, arrested cell populations were released from their mitotic block by aspirating nocodazole-containing media, washing in 37° PBS, and then re-incubating culture vessels in fresh media supplemented with 10% FCS. Efficacy of nocodazole-mediated G_2/M arrest, and progression throughout the cell cycle on release from the mitotic block was analyzed by flow cytometry following cell fixation and DNA staining with propidium iodide. Figure 4-1 shows a typical flow cytometric (FACS) analysis of HeLa cell cycle progression after this synchronization regime. At the time of release from nocodazole treatment (T0), over 75% of the HeLa cell population had a 4N DNA complement, typical of G_2/M cells. Based on the known activity of nocodazole as a microtubule polymerization inhibitor, these data suggest that a mitotic block had been imposed. By two hours post-treatment (T2), the major fluorescence peak shifts to an intensity approximately 50% (2N DNA complement) of that seen at T0, suggesting completion of mitosis and progression of those cell populations into early G_1 of the cell cycle. At six hours (T6) post-release, the percentage of cells in G_1 increases further, probably as those cells slow to recover from nocodazole treatment, complete mitosis and progress to G_1 of the cell cycle. Analysis of fluorescence at 10 hours (T10) indicates a broadening of the major G1 peak and increase (shift to the right) in intensity, presumably the result of DNA synthesis as S phase

commences. At 13 hours (T13) the number of G_1 cells decreases significantly, coincident with a dramatic increase in the number of cells with intermediate DNA fluorescence intensities, which represent cells in S phase. By 16 hours (T16), analysis of cellular fluorescence intensity indicates that the majority of cells are well into S phase, although the minor peak of lower fluorescence intensity (far left peak in T16) indicates that approximately 25% of cells are still in G_1. At 19 hours (T19) post-release, the two major fluorescence peaks indicate that approximately half of the cells are in late S or G_2/M (4N DNA) and the other half have completed mitosis and have progressed back into G_1 (2N DNA). By 21 hours (T21), the majority (approximately 65%) of cells has the fluorescence intensity of G_1 cell populations (2N DNA), indicating that most cells have now completed mitosis and progressed to G_1 of the cell cycle.

This analysis of FACS data strongly implies an efficient mitotic block (T0), rapid progression into G1 by two hours (T2) following drug removal, and synchronous progression of the majority of cells from early G_1 through S phase (T6, T10, T13, T16) of the cell cycle.

4-2.3: Expression of FEN1 mRNA throughout the HeLa Cell Cycle

To examine FEN1 mRNA expression levels during the cell cycle, synchronized HeLa cell populations were harvested at the times indicated (Figure 4-1), frozen until ready for analysis, then lysed, and total RNA extracted. RNA extraction, electrophoresis, and probing of Northern blots from three individual HeLa synchronizations were simultaneously carried out to eliminate any inherent differences arising from separate procedures performed on different days. Total RNA from equal aliquots, representing equivalent cell numbers within three separate synchronizations, was extracted using

RNEasy spin columns (Qiagen). Following elution, RNA samples were concentrated by ethanol precipitation and re-suspended in small volumes of DEPC-treated water (See Methods & Materials).

Following RNA extraction and precipitation, RNA sample concentrations and purity were determined by A_{260}/A_{280} spectrophotometer readings (See Methods & Materials). Equal amounts of RNA, as determined by A_{260} measurements, were loaded on a 0.8% TAE-agarose, non-denaturing gel to verify concentrations (data not shown). Approximately 15 μg of total RNA from each time-point were electrophoresed on a 1% formaldehyde-agarose denaturing gel containing 0.3 μg/ml ethidium bromide. Following electrophoresis, the gel was photographed and the location of 28S and 18S rRNA bands (6.33 and 2.37 kb, respectively, Patel, 1994) were measured for subsequent use as relative size markers (data not shown). The RNA gel was then capillary blotted onto nylon membrane, photographed again (data not shown) to determine transfer efficiency, and finally RNA was cross-linked to the membrane by 1200 J/m^2 UV-exposure (See Methods & Materials).

Figure 4-2A/B/C showing RNA expression of FEN1, PCNA, and GAPDH

The Northern blot was first pre-hybridized and probed with α-[^{32}P] dATP-labeled human FEN1 cDNA (Figure 4-2A). Although FEN1 mRNA bands vary slightly in intensity from one experiment to another due to the amount of total RNA loaded, a pattern of FEN1 mRNA expression is evident. In all three synchronizations, the FEN1 mRNA band gradually increases in intensity from release of the mitotic block (T0) up to

10-13 hours (T10/T13) post-release, with peak intensity occurring at either T10 or T13. FEN1 mRNA band intensities then gradually decrease at 16 (T16), 19 (T19), and 21 (T21) hours, eventually attaining levels similar to those noted at the time of release (T0) from the mitotic block. In addition to the three HeLa synchronizations, total RNA from three separate asynchronous HeLa cell populations (Figure 4-2) were also simultaneously separated, Northern blotted, and probed on the same membrane. Analysis of those bands show minor variations in band intensity, with possibly higher levels of FEN1 mRNA detected in the asynchronous HeLa cell population in the third experiment (A/S3).

Following the FEN1 cDNA probe, the same blot was subsequently stripped of probe, pre-hybridized, and re-probed with α-[^{32}P] dATP-labeled PCNA cDNA. Analysis of PCNA mRNA band intensities in Figure 4-2B shows that, like FEN1 mRNA, PCNA mRNA band intensities exhibit a distinct pattern. In all three experiments, PCNA mRNA bands increase in intensity from release of the mitotic block (T0) until 10 (T10) to 13 (T13) hours post-release, with peak intensity occurring at either T10 or T13. After peaking at T10/T13, PCNA mRNA band intensities also decrease gradually 16 (T16), 19 (T19), and 21 (T21) hours following release from the mitotic block (T0). Also similar to FEN1 mRNA, PCNA mRNA levels 21 hours (T21) post-release approach T0 levels. In addition, PCNA mRNA band intensities in the three asynchronous populations show little variation, with the exception of slightly higher band intensity again noted in the asynchronous population from experiment 3 (A/S3).

Immediately following the FEN1 and PCNA cDNA probes, the same membrane was again stripped, pre-hybridized, and re-probed with the GAPDH control probe to check for RNA loading variations. GAPDH mRNA levels show little variation during

the cell cycle (Dani *et al.*, 1984) and variations in GAPDH band intensities noted here should be the result of RNA loading variations and not cell cycle-dependent changes in expression. Similar to FEN1 and PCNA mRNA levels, GAPDH mRNA levels vary slightly between experiments. However, as can be seen in Figure 4-2C, GAPDH mRNA levels show only minor variations for all time-points examined within all three experiments. Notable exceptions are the bands from 2 (T2) and 6 (T6) hours post-treatment in experiment 2. Very low band intensities noted here are most likely the result of RNA degradation (evidenced by RNA band smearing in the gel) that was also noted previously during analysis of 28S and 18S rRNA bands. To account for such variations in the amount of RNA loaded, films from all Northern blots were subjected to densitometry analysis (see Methods & Materials) and all FEN1 and PCNA expression levels were normalized against loading differences detected by the GAPDH probe.

Figure 4-2C/D Showing Excel graphs of FEN1 and PCNA expression

Figure 4-2D shows the graph depicting FEN1 mRNA expression during the cell cycle in synchronized HeLa cell populations. In all three experiments, the results show a definitive increase in FEN1 mRNA expression after release from the mitotic block (T0) that continues until 10 hours (T10) post-release. FEN1 mRNA expression levels appears to reach a maximum 10 hours (T10) after release and then FEN1 mRNA levels show a gradually decline (T13, T16, T19, T21) to levels similar to those seen at the time of release (T0). Although the rate and magnitude of FEN1 mRNA expression level changes

do vary between the three synchronizations, the overall pattern and timing of FEN1 mRNA expression remains the same.

Analysis of normalized PCNA expression in Figure 4-2E shows a pattern similar to FEN1's mRNA expression, with PCNA mRNA levels increasing after release from the mitotic block (T0) until 10 hours (T10) post-release. Also similar to FEN1, PCNA mRNA expression peaks at 10 hours (T10) and then decreases gradually 13 (T13), 16 (T16), 19 (T19), and 21 (T21) hours after release. However, it is interesting to note that PCNA peak expression levels may be sustained longer than what was observed for FEN1. Again, although the rate and magnitude of PCNA mRNA expression level changes do vary between the three experiments, the same pattern is observed in each experiment and the pattern shows similarities to the FEN1 mRNA expression pattern (Figure 4-2D).

Finally, it should also be noted that both FEN1 and PCNA mRNA expression levels appear to remain relatively constant in cycling, asynchronous HeLa cell populations (Figures 4-2A & B).

Analysis of FEN1 and PCNA mRNA expression suggests that both genes are expressed in a cell cycle-dependent manner. The results also suggest a maximal two- to three-fold increase in both FEN1 and PCNA mRNA expression during the HeLa cell cycle, with peak expression occurring 10-13 (T10/T13) hours following release from the mitotic block. In addition, peak expression appears to occur coincident with the onset of DNA replication as determined by FACS analysis (Figure 4-1). Lastly, it appears that both FEN1 and PCNA mRNA expression levels in asynchronous, cycling HeLa cell populations remain virtually unchanged from one generation to the next.

4-2.4: Analysis of Soluble FEN1 Protein Levels

Because FEN1 mRNA levels appear to increase in a cell cycle-dependent manner, I wanted to investigate if FEN1 protein levels also change in a similar manner. To address this question, cell pellets containing equivalent cell numbers from the various cell cycle time-points described above (Figure 4-1) were lysed, and cellular protein was extracted. It should be noted that care was taken at all times to ensure that equal volumes were used and recovered during protein extraction from equivalent cell numbers. The following briefly describes the protein extraction strategy.

Initially, HeLa cells were harvested at the same times as described in Figure 4-1, and protein was extracted by sufficient NP40 lysis buffer (600-800 μl) to recover most soluble protein (NP40 fractions). DNA-associated protein was subsequently extracted from the remaining cell pellets by re-suspension in small volumes (200-300 μl) of buffered DNAase I lysate (DNAase I fractions), and finally the remaining pellet was extracted with NP40 buffer containing 1% SDS (or 1%-SDS loading buffer) to recover relatively insoluble protein (SDS fractions). 8% to 12% SDS-PAGE gels of the various fractions were western blotted and probed with antibodies against FEN1 and PCNA. Bradford assays, Coomassie-stained gels, and Ponceau Red staining of western blots ensured equal total protein concentrations were loaded (where indicated); alternatively, protein from equivalent cell numbers was loaded. Because equal cell numbers, extraction, and loading volumes were used during experiments, any differences in relative protein concentrations during cell cycle progression are thought to reflect protein synthesis on cell growth or increased protein stability.

Interestingly, multiple experiments using this strategy have shown that although the amount of total protein in NP40 and DNAase I fractions appears to increase, as determined by Bradford assays and Coomassie-stained gels, total insoluble (SDS fractions) protein concentrations did not appear to alter significantly (data not shown) during cell cycle progression from early G_1 through late S phase.

Figure 4-3 showing soluble FEN1 and PCNA

Initial experiments using lysis volumes of 600-800 µl suggested that NP40-soluble FEN1 (Figure 4-3B) and PCNA (Figure 4-3C) protein levels remained relatively constant throughout the cell cycle. For PCNA protein expression, this result differed from previous reports (Morris and Mathews, 1989). However, it was possible that slight variations in protein levels could be masked by insufficient lysis of soluble protein or by an excessively strong signal on the immunoblot during ECL detection. Further experiments were conducted to address this issue and to ensure that most, if not all, soluble protein was being extracted during NP40 lysis.

Firstly, equal cell numbers from various times during the cell cycle were subjected to NP40 lysis in 600 µl volumes. Following centrifugation, the soluble protein-containing supernatant was carefully removed, and the remaining pellet was re-suspended in 200 µl of NP40 lysis buffer, incubated on ice for 30 minutes, centrifuged again, and the supernatant removed (wash 1). This wash was repeated a second time (wash 2) and aliquots of the original lysis and washes were subsequently separated by 10% SDS-PAGE and Coomassie-stained (Figure 4-4A). Two additional SDS-PAGE gels were run

in parallel, western blotted, and probed with anti-Xenopus FEN1 (1:2000) polyclonal (Figure 4-4B) and anti-PCNA (PC10) monoclonal (1:1000) antibodies (Figure 4-4C).

Figure 4-4A/B/C showing HeLa gels and western blots

As can be seen, the proportion of soluble FEN1 (Figure 4-4B) to total protein extracted (Figure 4-4A) by the initial NP40 lysis remained relatively constant throughout the cell cycle, but it appears that soluble FEN1 protein was still remaining because soluble FEN1 protein was still detected in subsequent wash lysates. Interestingly, even though care was taken to ensure equal cell numbers and extraction volumes were used for all time-points analyzed, the amounts of soluble FEN1 protein extracted during the first wash increased as cell populations progressed from early G1 (T3) to late S phase (T16). Most notably, FEN1 protein was only detected in S phase extracts (T13 and T16) in the second wash (Figure 4-4B). This pattern is similar to that noted for soluble PCNA protein extraction (Figure 4-4C).

To determine if the increases witnessed in wash fractions of soluble FEN1 and PCNA protein were due solely to increases in total cellular protein, densitometry measurements of the FEN1 (Figure 4-4B) and PCNA (Figure 4-4C) bands were compared with total protein concentrations estimated by Bradford assays. Because total protein concentrations of wash fractions were below Bradford detection limits, initial NP40 extraction lysates were used to determine total protein concentrations. It is assumed that, although the amount of total soluble protein extracted increases from T3 to T16, the ratio of soluble protein extracted during subsequent wash 1 and 2 remains the

same. Total soluble protein was found to be similar (0.75 mg/ml) in T3, T6, and T10, but it increased approximately 50% (1.05 mg/ml) by T13, and 67% (1.15 mg/ml) by T16, as determined by Bradford assay. However, densitometry measurements show that the level of FEN1 protein detected in wash 1 fractions increased by up to 100% (T13) and 200% (T16) over T3 levels. PCNA protein levels detected in wash 1 fractions also similarly increased. This result, combined with FEN1 and PCNA protein being detected only in T13 and T16 fractions in wash 2, suggests that soluble FEN1 protein levels may increase in a cell cycle-dependent manner.

In the previous experiment described above, cell pellets were subjected to vigorous pipetting to re-suspend during washes and it was possible that this may have resulted in normally NP40-insoluble protein being solubilized. Additionally, it appeared that initial soluble protein extraction volumes may have been insufficient to recover all soluble protein. To test these possibilities, equivalent cell numbers from the same cell cycle time-points (T3 to T16) used previously, were again subjected to NP40 lysis, using 3 ml extraction volumes to ensure complete extraction of all soluble protein. Following extraction, protein samples were separated on 10% SDS-PAGE and Coomassie-stained to analyze total soluble protein (Figure 4-5A). Additionally, western blots of the same samples were probed to analyze FEN1 (Figure 4-5B) and PCNA (Figure 4-5C) protein levels.

FIGURE 4-5 showing HeLa 3ml protein extraction

Although the detected FEN1 protein signal is weak (Figure 4-5B), and it appears that the level of FEN1 protein detected at T10 is slightly less than T6, it is still possible to discern an increase in soluble FEN1 protein as cells progress from early G_1 (T3) towards late S phase (T16). Because total protein concentrations loaded on the gels were five times lower compared to previous experiments (eg. Figure 4-4A), it was possible to note a subtle increase in FEN1 expression that was not masked by excessive ECL detection signals seen previously (Figure 4-4B, NP40 fractions). This increase in soluble FEN1 protein levels as cells approach S phase is similar to the increase in soluble FEN1 protein observed in wash steps when smaller original lysis volumes were used (Figure 4-4B, Wash 1 & 2).

An increase in soluble PCNA protein during the cell cycle was also noted when this same blot was re-probed with the anti-PCNA antibody, PC10 (Figure 4-5C). Interestingly, it appears that soluble PCNA protein levels vary little from early G_1 (T3) through mid-S phase (T13), but significantly increases by late S phase (T16). Despite that observation, it still appears that soluble PCNA protein levels are increased as cells progress towards late S phase of the cell cycle.

To determine if the increases witnessed in soluble FEN1 and PCNA protein were due solely to increases in total cellular protein, densitometry measurements of the FEN1 (Figure 4-5B) and PCNA (Figure 4-5C) bands were compared with total protein concentrations estimated by Bradford assays. Total soluble protein concentrations increased approximately 18% (0.47 mg/ml) by T6 and T10, 33% (0.53 mg/ml) by T13, and 40% (0.56 mg/ml) by T16 over T3 (0.4 mg/ml) levels. In contrast, detected FEN1 protein levels increased nearly 100% (T13) and 200% (T16) over FEN1 levels detected in

T3 extracts. This suggests that soluble FEN1 protein levels increase significantly more (2-3 times) than relative increases in total cellular protein levels as cells progress from early G_1 towards S phase of the cell cycle. This result, together with the results shown in Figures 4-4B and 4-5B, strongly suggest that NP40-soluble FEN1 protein levels increase in a cell cycle-dependent manner, as cells approach S phase (approximately 13-16 hours) after release from mitotic block.

4-2.5: Analysis of DNAase I-soluble FEN1 Protein during the HeLa Cell Cycle

Because of FEN1's putative role in DNA replication (Ishimi *et al*,., 1988; Goulian *et al.*, 1990; Turchi and Bambara, 1993; Waga *et al.*, 1994), it was logical to examine if any FEN1 was bound to DNA and whether this could be released by DNAase I treatment of cell pellets following extraction of soluble proteins with NP40. The current model for FEN1 activity (Wu *et al.*, 1996; Huang *et al.*, 1997) suggests that FEN1 protein may be bound to DNA flap structures in an S phase-specific manner (Warbrick *et al.*, 1997; Lieber, 1997). To address this question, cell pellets from various cell cycle stages, remaining after NP40 lysis, were subjected to DNAase I digestion (200 μg/ml) at 37° C for 30 minutes. Samples from the various time-points were separated on 10% SDS-PAGE, and either Coomassie-stained for total protein (Figure 4-6A), or western blotted and probed with anti-Xenopus FEN1 antibody (Figure 4-6B) or anti-PCNA monoclonal antibody PC10 (Figure 4-6C).

FIGURE 4-6 showing DNAase gel

Although high levels of PCNA were detected (Figure 4-6C), especially in S phase fractions (T10, T13, T16), no FEN1 protein was detected in any cell cycle stage (T3 to T16, Figure 4-6B) in extracts following DNAase I treatment.

To confirm the effects of DNAase I digestion, this same blot was re-probed with anti-PCNA antibody, PC10. Previous studies (Celis and Madsen, 1985) have shown that non-detergent-soluble PCNA protein can be found in complex with DNA in an S-phase-specific manner. As seen in Figure 4-6C, DNA digestion was efficient as high levels of non-NP40-soluble PCNA protein was released by DNAase I treatment. The substantially higher levels of PCNA protein detected in T10, T13, and T16 DNAase I fractions (compared to T3 and T6 fractions), in combination with the FACS data in Figure 4-1, strongly suggest that those cell populations were in S phase. To determine if any FEN1 protein was released by DNAase I treatment, but not visualized because FEN1 protein concentrations were below the detection limits of this antibody-ECL system (approximately 25-50 pg for high-affinity antibodies; Bers and Garfin, 1985), an 8% SDS-PAGE gel was loaded with approximately 10 μg of DNAase-extracted material per lane.

FIGURE 4-7 showing FEN1/PCNA western blots

Figure 4-7A shows that FEN1 protein could only be detected in S phase populations (T10, 13, 16), but levels are at or near the limits of ECL detection. PCNA protein levels from those same fractions, as seen in Figure 4-7B, are much higher and easily detected in ECL reactions, even at very short exposure times. It is currently uncertain as to whether

FEN1 detected in DNAase I-treated S phase fractions represents minute concentrations of soluble protein remaining after NP40 lysis or FEN1 protein that was released from DNA on DNAase treatment. However, it is clear from these experiments that FEN1 and PCNA are not present in the same stoichiometric amounts in DNAase I-extractable material, suggesting that they may exist in different sub-nuclear compartments.

4-2.6: Analysis of SDS-Soluble FEN1 During the HeLa Cell Cycle

Following NP40 and DNAase I extraction, any remaining cellular proteins were finally extracted from resulting cell pellets with 1% SDS. Samples were separated by 10% SDS-PAGE and Coomassie-stained (Figure 4-8A), or western blotted and probed with antibodies against FEN1 (Figure 4-8B) or PCNA (Figure 4-8C).

Figure 4-8 showing SDS gels/western blots

Figure 4-8A shows that levels of total cellular protein extracted by SDS treatment vary little during the cell cycle. Interestingly, it was also discovered that a proportion of FEN1 protein remained even after NP40 and DNAase treatment (Figure 4-8B). In addition, Figure 4-8B also shows that levels of NP40-insoluble FEN1 protein may actually decrease as cells progress from early G_1 towards S phase of the cell cycle. In contrast, very little PCNA protein remained after DNAase I treatment, with only small amounts of protein detected in S phase (T13 and T16) fractions (Figure 4-8C). Because prior DNAase treatment appeared to release the vast majority of DNA-associated PCNA protein (compare Figures 4-7B & 4-8C), and very little, if any, FEN1 protein, it is

unlikely that relatively insoluble (SDS-extractable) FEN1 is bound to PCNA. It is currently unclear as to what FEN1 is bound to in its SDS-extractable form. Although it cannot be entirely ruled out that the insoluble pool of FEN1 may be sequestered to cytoskeletal components, it is much more likely that FEN1 protein is immobilized within the nucleus, based on three major characteristics. Firstly, FEN1 possesses a putative nuclear localization signal (Murray *et al.*, 1994) suggesting that it may be transported into the nucleus. Secondly, FEN1 must be nuclear if it is to carry out its proposed role in DNA replication (Ishimi *et al.*, 1988; Goulian *et al.*, 1990; Turchi and Bambara, 1993; Waga *et al.*, 1994) or DNA repair (Frosina *et al.*, 1996; Klungland and Lindahl, 1997). Finally, the data presented in Chapter 3 (Figure 3-13) of this thesis shows that GFP-FEN1 protein localizes predominantly within the cell nucleus.

4-2.7: Synchronization of Human MRC-5 Cells by Serum Starvation

Following analysis of a transformed cell line (HeLa), I wanted to investigate if the observed pattern of FEN1 mRNA levels, protein levels, and protein solubility would be similar in non-transformed, primary cell lines. Using a primary human MRC-5 fibroblast cell line (Jacobs, 1966), one synchronization was performed at passage number 34, and protein and total RNA were extracted for analysis. A second synchronization was performed at passage number 39, but FACS data revealed that relatively few (fewer than 5%) cells were stimulated to proliferate, even 48 hours after the addition of fresh media supplemented with 15% FCS (data not shown). In addition, these cells showed considerable staining for SA-β-gal (A. Rodrigues-Lopez, personal communication), indicative of replicative senescence (Dimri *et al.*, 1995). Additional synchronizations

were attempted with frozen stocks of cells at passage numbers 30-32, but they were similarly hampered by the high percentage of senescent, non-proliferating cells within the population.

Figure 4-9 showing GOOD MRC-5 synchronization

The strategy behind the method of MRC-5 synchronization and harvest was to obtain equivalent numbers of cells at various defined stages of the cell cycle. The various time-points used were determined in pilot test synchronizations (Figure 4-9), using conditions similar to those used to obtain the data discussed below. In addition, several culture dishes were harvested and pooled at each time-point, then cell numbers were determined by Coulter counter analysis. All time-points harvested had similar cell numbers, with the exception of T 37, which had approximately 20% more cells than the other time-points examined (data not shown). The reason for this difference was that by 37 hours after re-feeding, a proportion of the cell population had divided and now resembled an asynchronous cell population (see Figure 4-10A).

To synchronize primary MRC-5 fibroblasts, asynchronously growing cells at passage 34 were used to seed evenly 10 cm culture dishes with 5 X 10^5 cells per dish (as determined by Coulter counter analysis) in DMEM supplemented with 10% FCS. Cells were allowed to grow for 2.5 days and reached near confluence. At that time, the cells were subjected to serum starvation, when the medium was replaced with fresh DMEM containing 0.5% FCS. Following a 55 hour incubation in low serum medium, cells were trypsinized, pooled, and seeded at 1.2 X10^6 cells per 15 cm culture dish in fresh DMEM, supplemented with 15% FCS to stimulate proliferation. Loss of cell viability during re-

plating was estimated to be less than 5% as determined by trypan blue exclusion, although it is possible that a slight additional loss of cell viability may have occurred after re-plating, as suggested by the presence of non-adherent cells at time of harvest.

Figure 4-10A & B FACS Figure from MRC-5 synchronization

Figure 4-10A shows the flow cytometric analysis (FACS) of passage 34 MRC-5 fibroblasts after release from serum starvation. Analysis of the major peak in cell populations, at the time of re-feeding (T0), shows that greater than 77% of the cells had a diploid DNA complement characteristic of G_0/G_1 cells. To distinguish between G_0 and G_1 cells, soluble protein was extracted from cells of the various time-points, separated by 10% SDS-PAGE, blotted onto nitrocellulose, and probed with a monoclonal antibody against c-JUN. Previous studies (Kaczmarek, 1986) have demonstrated that this immediate early response transcription factor is absent in quiescent (G_0) cells, but is rapidly expressed as cells come into cycle. The results of the immunoprobe seen in Figure 4-10B show that no JUN protein was detected at the time of re-feeding (T0), suggesting that serum starvation had resulted in withdrawal from the cell cycle to a quiescent state (G_0). By 10 hours after re-feeding (T10), JUN protein was detectable and remained so throughout the time course of the experiment. It should be noted that the levels of JUN protein detected at 18 (T18) and 21 (T21) hours after re-feeding appear lower than other time-points examined. The reason for this is not clear since Coomassie staining of another gel run in parallel (Figure 4-12A), shows no significant loading variations from T0 through T24. Regardless, JUN protein levels were still detectable at all time-points subsequent to T0 and the FACS data (Figure 4-10A) indicate that those

cell populations were not quiescent. Overall, these results suggest that the MRC-5 cells were arrested in a quiescent (G_0) state following the 55 hour serum starvation, and re-entered G_1 of the cell cycle by 10 hours (T10) after re-feeding. Additionally, the FACS data also suggest that S phase commences between 18 (T18) and 21 (T21) hours, with the number of cells in S phase increasing by 24 hours (T24).

4-2.9: Analysis of FEN1 mRNA Expression in Synchronized MRC-5 Cells

Total RNA was extracted from MRC-5 cells at various cell cycle stages, electrophoresed on a 1% formaldehyde-agarose denaturing gel, and the location of 28S and 18S rRNA bands were measured for subsequent use as relative size markers (data not shown). The RNA gel was then Northern blotted, fixed onto nylon membrane (see Methods & Materials), pre-hybridized, and probed with α-[^{32}P] dATP-labeled human FEN1 cDNA.

Figure 4-11A/B/C/D/E showing FEN1, PCNA, GAPDH Northerns and Excel graphs

Figure 4-11A shows that no FEN1 mRNA was detected at T0 (cells in G_0), but low levels of FEN1 transcripts were detected by 10 hours (T10) following re-feeding. FEN1 expression increased throughout G_1 and early S phase and peaked between T 21 and T 24, which coincides with early/mid-S phase (based on FACS data in Figure 4-10A) for those cells that had re-entered the cell cycle and were stimulated to proliferate.

To eliminate any differences arising from unequal loading, the blot was re-probed with α-[^{32}P] dATP-labeled GAPDH cDNA (Figure 4-11C). GAPDH mRNA levels show

little variation during the cell cycle (Dani *et al.*, 1984) and variations in GAPDH band intensities noted here should be the result of total RNA loading variations and not cell cycle-dependent changes in expression. As can be seen (Figure 4-11C), only minor variations in GAPDH mRNA were witnessed, with slightly less mRNA detected at T0, and slightly more GAPDH mRNA detected at T18 and in asynchronous cell samples.

When FEN1 band intensities (as determined by densitometry measurements) were normalized against the GAPDH control (Figure 4-11C), it confirmed that FEN1 mRNA levels were higher at T 21 and T 24 than in either T 37 or asynchronous, cycling cell populations (Figure 4-11D). This strongly suggests that FEN1 mRNA levels are controlled in a cell cycle-dependent manner in primary cells, with peak expression coincident with DNA replication.

Because FEN1 mRNA levels appeared to mirror PCNA mRNA levels during the HeLa cell cycle, I next examined PCNA mRNA levels in synchronized MRC-5 cells by stripping the blot and re-probing with α-[^{32}P] dATP-labeled human PCNA cDNA (Figures 4-11B). In addition, PCNA mRNA levels were also normalized (Figure 4-11E) against loading differences detected by the GAPDH control probe (Figure 4-11C). Unlike FEN1, PCNA mRNA is detected at low levels, even in quiescent cells (T0). However, similar to FEN1 (compare Figures 4-11A and 4-11B), PCNA expression does appear to increase in a cell cycle-dependent manner, with peak mRNA levels coincident with DNA replication, between T 21 and T 24 (Figure 4-11E). Additionally, it also appears that PCNA mRNA levels in asynchronous populations (Figure 4-11B) may be higher than peak PCNA mRNA levels (T24) detected in the MRC-5 synchronization by serum starvation. The reason for this is currently unclear.

Comparing Figures 4-11D and 4-11E, it appears that both FEN1 and PCNA mRNA levels increase approximately two-fold as synchronized MRC-5 cell populations progress from early G_1 (T10) towards S phase (T21/T24). Peak FEN1 and PCNA mRNA levels occur between T21 and T24, which again corresponds to mid-S phase based on FACS data (Figure 4-10A). It should also be noted that peak expression of FEN1 mRNA in this primary line appeared to occur in mid-S phase (Figure 4-10A), which is slightly later than the peak expression at the G_1/S transition observed for the transformed (HeLa) line (Figure 4-2). It is currently unknown whether this reflects a real difference between primary and transformed lines, or a difference that occurred as a result of the synchronization methods employed.

4-2.10: Analysis of NP40-soluble FEN1 Protein from Synchronized MRC5 Cells

I have shown that in HeLa cells, FEN1 mRNA levels increase as cells approach S phase (Figure 4-2D), and that soluble FEN1 protein levels subsequently reflect this observed increase (Figures 4-4B & 4-5). Having now demonstrated that FEN1 mRNA levels similarly increase in primary cells (MRC-5) as they reach S phase of the cell cycle, it was important to determine levels of FEN1 protein and its relative solubility throughout the cell cycle.

To ensure complete extraction of all soluble protein, cell pellets, containing 1.2 X 10^6 cells, were initially lysed in 2 mls of NP40 lysis buffer. A 2 ml extraction volume was used here due to lower cell counts in MRC-5 synchronizations compared to HeLa cell synchronization experiments described earlier (Section 4-2.2). Following centrifugation, supernatants containing NP40-soluble protein were collected for analysis

and remaining pellets were resuspended in small volumes of NP40 lysis buffer containing 200 μg/ml DNAase I, to release any DNA-bound protein. Cell pellets after DNAase I extraction were finally solubilized in SDS loading buffer to extract any remaining insoluble protein.

Samples of NP40-soluble protein from cells at different cell cycle stages (Figure 4-10A) were separated by 10% SDS-PAGE and Coomassie-stained (Figure 4-12A) or western blotted and probed with anti-FEN1 antibody, 3220 (1:4000) (Figure 4-12B). It should be noted that the membrane was originally probed with anti-Xenopus FEN1 antibody, but the exact FEN1 band was unclear and difficult to analyze (data not shown).

Figure 4-12A/B/C showing MRC5 NP40 Coomassie and western probes

Although detected levels of protein were low, possibly due to the large extraction volumes used, a subtle increase in NP40-soluble FEN1 protein was still noted as cells progressed from quiescence (T0) until mid-S phase (T24). It is interesting to note that FEN1 levels were still detectable after a 55 hour serum starvation (T0), but appeared much higher by 37 hours (T37) after re-feeding, as well as in the asynchronous population fractions (A/S). However, after accounting for loading variations, FEN1 protein in the T 37 fraction approaches asynchronous fraction levels (data not shown).

Following the FEN1 antibody probe, the western blots were re-probed with the anti-PCNA antibody, PC10 (1:1000). Figure 4-12C shows detectable levels of PCNA protein, even at T0, with a gradual increase as cells progressed toward mid-S phase (T24). It should also be noted that the observed higher levels of PCNA protein detected

at T0, compared to FEN1 protein levels in Figure 4-12B, may, at least in part, be due to basal levels of PCNA gene transcription in quiescent cells (T0, Figure 4-11B) not observed with the FEN1 mRNA probe (T0, Figure 4-11A).

4-2.11: Analysis of DNAase I and SDS-Soluble FEN1 Protein in MRC-5 Cells

I wanted to determine if the pattern of NP40-insoluble FEN1 and PCNA protein observed in synchronized HeLa cells would be similar in synchronized MRC-5 cells. To examine this, following extraction of soluble protein, remaining MRC5 cell pellets were extracted with small volumes of NP40 lysis buffer containing 200 μg/ml DNAase I to remove DNA-bound proteins, and remaining cell pellets were finally re-suspended in SDS loading buffer to release any remaining protein. Following protein extraction, 20 μl aliquots from each time-point, representing distinct cell cycle phases (Figure 4-10A), were separated by 10% SDS-PAGE and Coomassie-stained (Figure 4-13A) or western blotted, and probed with anti-Xenopus FEN1 (Figure 4-13B, 4-13D) then anti-PCNA (Figure 4-13C, 4-13E) antibodies.

Figure 4-13A/B/C/D of DNAase & SDS Coomassies and western probes

No FEN1 was detected in DNAase I fractions (Figure 4-13B). Interestingly, analysis of SDS-soluble FEN1 (Figure 4-13D) shows that low levels of insoluble FEN1 could be detected following the 55 hour serum starvation (T0). Additionally, SDS-soluble FEN1 levels were higher by 10 hours after re-feeding (T10), and then appeared to remain relatively constant in all subsequent time-points analyzed. This observation of

relatively stable levels of insoluble FEN1 protein over the cell cycle parallels similar results observed in synchronized HeLa cells (Figure 4-8B). It is currently not known whether the low levels of SDS-soluble FEN1 at T0, following serum starvation, are the result of proteolysis, nuclear export, or lower FEN1 protein levels relative to total cellular protein. Additionally, the low level of SDS-soluble FEN1 observed at T0 may also be influenced by the lack of detectable FEN1 mRNA following the 55 hour serum starvation (T0) (Figure 4-11A).

An analysis of PCNA protein levels show that significant levels of DNAase I-soluble (Figures 4-13C) and SDS-soluble (Figures 4-13E) PCNA protein were detected initially at T18, which from FACS data (Figure 4-10A), represents the start of S phase. Additionally, the levels of DNAase I-soluble and SDS-soluble PCNA protein increased as cells progressed from early (T18) to mid-S phase (T24). The higher levels of SDS-soluble PCNA observed here (Figure 4-13E) probably represents less efficient DNAase I digestion of MRC-5 cell pellets than was previously observed in synchronized HeLa cell pellets (Figures 4-6C, 4-7B, 4-8C).

4-2.12: NP40-soluble FEN1 Protein Sedimentation in Glycerol Gradients

I have demonstrated that FEN1 mRNA and protein levels increase in primary (MRC-5) and transformed (HeLa) cells as they progress from early G_1 towards S phase of the cell cycle. In addition, because FEN1 has been shown to interact with PCNA *in vitro* (Li *et al.*, 1995; Chen *et al.*, 1996) and is suspected to interact with PCNA in an S phase-specific manner *in vivo* (Warbrick *et al.*, 1997; Lieber, 1997), I expected to see both proteins extracted in synchronized cells under similar conditions (ie. DNAase I

treatment). However, this was not observed as FEN1 protein was detected in SDS-soluble fractions (Figure 4-8B), where PCNA was barely detectable (Figure 4-8C) because it had been released previously by DNAase I treatment. Because it appears that FEN1 protein does not exhibit significant cell cycle-dependent solubility changes, indicative of sequestration to less soluble cellular components, it is logical to next examine if FEN1 protein interacts with other soluble proteins that may regulate its function.

In the absence of antibodies that can immunoprecipitate FEN1 protein (see Chapter 3), possible changes in FEN1 association with other proteins may be assessed by glycerol gradient centrifugation. Significant changes in the sedimentation velocity of soluble FEN1 protein during glycerol gradient centrifugation may indicate changes in the quarternary structure of FEN1 protein; specifically, it may indicate if FEN1 binds other soluble cell components in a cell cycle-dependent manner.

Soluble native proteins are expected to separate during density-gradient centrifugation according to their molecular weight and shape (Rickwood, 1978). If soluble FEN1 binds other soluble proteins, significantly altering its molecular weight or shape, it is possible that those changes may be observed as a change in sedimentation velocity during glycerol gradient centrifugation.

To examine soluble FEN1 protein sedimentation velocities during the various cell cycle phases, approximately 150 μg of NP40-soluble protein (in 200 μl volumes) from mitotic (T0), mid-G_1 (T6), G_1/S (T10), and mid-S (T13) HeLa cell populations (Figure 4-1) were separated on a 5 ml 15-30% glycerol gradient (See Methods & Materials).

Aliquots from alternate fractions were separated by 10% SDS-PAGE, western blotted, and probed with anti-Xenopus FEN1 polyclonal antibodies (Figure 4-14A).

Figure 4-14A shows that soluble FEN1 protein can be detected in numerous fractions from all time-points investigated, with mitotic (T0) HeLa cells appearing to exhibit two peak FEN1 fractions (fractions 9 & 23). The mid-G_1 gradient (T6) shows maximal levels of FEN1 detected in fraction 11, but a second peak fraction is unclear. The G_1/S (T10) and mid-S gradients also appear to exhibit two peak fractions, both at fractions 13 and 25. It appears that as HeLa cells exit mitosis and progress from early G_1 towards S phase of the cell cycle, the FEN1 sedimentation velocity appears to decrease slightly. This result suggests that soluble FEN1 protein may witness post-translational modifications or disassociate from other soluble proteins as synchronized HeLa cells progress from early G_1 towards S phase of the cell cycle.

The same blots were subsequently re-probed with anti-PCNA monoclonal antibody, PC10 (Figure 4-14B). As can be seen, soluble PCNA protein was also detected in numerous fractions from all time-points examined, with mitotic (T0) HeLa cell populations appearing to exhibit three separate peak PCNA protein fractions (9, 17, 25). The mid-G_1 gradient (T6) shows maximal levels of soluble PCNA protein detected in fractions 11, 15, and 21. The G_1/S transition (T10) and mid-S (T13) phase gradients also appear to exhibit three separate peak PCNA fractions at 13, 17, 21 and 15, 19, 23, respectively. Similar to what was observed with soluble FEN1 protein, it appears that as HeLa cell populations exit mitosis and progress from early G_1 towards S phase of the cell cycle, the soluble PCNA protein sedimentation velocity appears to decrease slightly. Although not conclusive, this result may suggest that soluble PCNA protein may witness

post-translational modifications or possibly dissociate and re-associate with other soluble proteins as synchronized HeLa cell populations progress from early G_1 towards S phase of the cell cycle.

4-3: Discussion

There is strong *in vitro* evidence suggesting an essential role for FEN1 protein in nuclear DNA replication. Studies using purified proteins (Goulian *et al.*, 1990; Turchi and Bambara, 1993) and SV40 DNA replication assays (Ishimi *et al.*, 1988; Waga *et al.*, 1994) have demonstrated that FEN1 protein can excise DNA and RNA intermediate structures formed during Okazaki fragment processing (Li *et al.*, 1995; Wu *et al.*, 1996; Huang *et al.*, 1996), and that FEN1 protein is absolutely required for the production of form I DNA during SV40 DNA replication (Waga *et al.*, 1994). In addition, studies of human FEN1 homologues in yeast (RAD27 in *S. cerevisiae* and rad2 in *S. pombe*) have shown that FEN1 mutants exhibit high levels of genomic instability (Johnson *et al.*, 1995; Schweitzer *et al.*, 1998) and a temperature-sensitive lethality whose terminal arrest phenotype suggests a defect in DNA replication (Reagan *et al.*, 1995; Kokoska *et al.*, 1998).

Given the putative role of FEN1 in mammalian DNA replication, a detailed analysis of human FEN1 mRNA and protein levels in primary and transformed human cell lines was carried out to determine if FEN1 levels exhibit a pattern of cell cycle-dependent expression that has been witnessed with other proteins known to be required for nuclear DNA replication such as thymidine kinase (Schlosser *et al.*, 1981),

topoisomerase I (Tricoli *et al.*, 1985), DNA Pol α (Thömmes *et al.*, 1986), and PCNA (Morris and Mathews, 1989).

In this chapter, the synchronization and analysis of both a primary (MRC-5) and transformed (HeLa) cell line revealed that human FEN1 mRNA expression is controlled in a cell cycle-dependent manner, with peak mRNA levels occurring coincident with the onset of DNA replication (Figures 4-2A/D & 4-11A/D). In this respect, FEN1 mRNA levels appear to follow the same pattern as another well-characterized DNA replication protein, PCNA (Bravo and Bravo-MacDonald, 1985; Morris and Mathews, 1989; Figures 4-2B/E & 4-11B/E).

Further studies reported here also show that NP40-soluble FEN1 protein levels measurably increase in a cell cycle-dependent manner (Figures 4-5B & 4-12B), with peak soluble protein levels detected shortly after maximum mRNA levels were attained during S phase. Again, this cell cycle-dependent increase in soluble FEN1 protein was similar to that of soluble PCNA protein (Figures 4-5C & 4-12C; Almendral *et al.*, 1987; Matsumoto *et al.*, 1987; Morris and Mathews, 1989). Additionally, although FEN1 mRNA and soluble protein levels increase as mitotically-arrested or quiescent cells are released from cell cycle arrest and progress from early G_1 towards S phase of the cell cycle, they appear to stabilize at steady-state levels in continuously cycling populations (Figures 4-2A & 4-11A). This steady-state level of soluble FEN1 protein in cycling cell populations is similar to that observed with PCNA (Figures 4-2B & 4-11B; Morris and Mathews, 1989).

Previous *in vitro* studies suggest that FEN1 activity is stimulated by interaction with PCNA protein during Okazaki fragment processing in DNA replication. This interaction has been demonstrated by *in vitro* experiments with purified recombinant

proteins (Li *et al.*, 1995; Wu *et al.*, 1996), Far-Western blotting (Warbrick *et al.*, 1997), and co-immunoprecipitations (Chen *et al.*, 1996; Warbrick *et al.*, 1997). In addition, a PCNA binding domain has been mapped on FEN1 (Warbrick *et al.*, 1997) and subsequent mutagenesis studies with purified recombinant proteins (Jónnson *et al.*, 1998) have supported that result.

Based on these findings, I expected FEN1 protein to mirror PCNA protein solubility patterns in synchronized cell populations. After extraction of soluble cellular protein, large amounts of PCNA protein were found to be associated with DNA and could be extracted from remaining cell pellets by DNAase I digestion (Figures 4-6C & 4-13C). DNA-associated PCNA could be detected preferentially in S phase populations, supporting its role in DNA synthesis (Madsen and Celis, 1985; Bravo and MacDonald-Bravo, 1985, 1987; Figures 4-1, 4-6C, 4-10A, 4-13C). Surprisingly, very little FEN1 was detected by western blotting DNAase I extracts of S phase cells (Figure 4-6A), despite observing high levels of DNAase I-extracted PCNA (Figure 4-6B) on the same blot. It has been previously speculated (Warbrick *et al.*, 1997; Lieber, 1997) that the FEN1-PCNA association may be a very transient association and that PCNA may serve only to either stimulate FEN1 enzymatic activity (Li *et al.*, 1995) or stabilize FEN1 protein on DNA structures in physiological salt conditions (Wu *et al.*, 1996). The latter proposal is supported by evidence showing dramatic inhibition of FEN1 nuclease activity in physiological salt conditions in the absence of PCNA (Harrington and Lieber, 1994), and efficient processing of DNA flap structures under the same conditions in the presence of PCNA protein (Wu *et al.*, 1996). The extremely low levels of DNAase I-extracted FEN1 protein detected in S phase HeLa cell populations (Figure 4-6A), and the total lack of

DNAase I-extracted FEN1 protein detected in S phase MRC-5 cells (Figure 4-13B), suggests either that the FEN1-PCNA association may be very transient and difficult to detect at physiological protein levels, or that the association does not take place between DNA-bound PCNA and FEN1 protein.

Another surprising result was the presence of a population of insoluble FEN1 protein that remained in cell pellets even after NP40 extraction of soluble protein, multiple washes of remaining cell pellets, and DNA digestion with DNAase I (Figures 4-8B, 4-13C). Unlike insoluble PCNA protein that was associated with S phase populations and could be extracted with DNAase I treatment (Figures 4-6C, 4-13C), insoluble FEN1 protein was detected in all phases of the cell cycle and could not be extracted with DNAase I treatment. This result, combined with the putative FEN1 C-terminal nuclear localization signal (Murray *et al.*, 1994) and the finding that GFP-tagged FEN1 is a predominantly nuclear protein (Chapter 3, Figures 3-12, 3-13), suggest that basal levels of insoluble FEN1 protein may be maintained in the nucleus throughout the cell cycle. In addition, SDS-soluble FEN1 protein levels may actually decrease during S phase (Figure 4-8B). If confirmed, this may suggest that after translation, a proportion of soluble FEN1 protein is imported to the nucleus to maintain a certain level of insoluble nuclear protein. During DNA replication, it is possible that previously insoluble FEN1 protein becomes soluble and subsequently functions during Okazaki fragment processing. This hypothesis needs to be investigated in the future. If supported, the sub-nuclear localization of insoluble FEN1 protein, its protein partners, and signals that release it to function during DNA replication (eg. phosphorylation, ADP-ribosylation, etc.) would need to be investigated.

Lastly, the results of the glycerol gradients suggest that soluble FEN1 may experience either cell cycle-dependent association with other soluble proteins or post-translational modifications that effect its sedimentation during glycerol gradient centrifugation. The significance of this observation is still unclear, but the development of high-affinity antibodies in the future may allow co-immunoprecipitation of FEN1 protein complexes from synchronized cell extracts, and the possible identification of cell cycle-dependent FEN1-binding partners. Interestingly, soluble PCNA protein in complex with various cyclins/CDKs and P21 protein has been previously co-immunoprecipitated from [^{35}S]-labeled WI-38 cell lysates, and specific complex proteins subsequently identified (Zhang et al., 1993). In addition, phosphatase treatment or poly-ADP-ribosylation (PARP) studies, similar to investigations done previously with other DNA replication proteins (Simbulan-Rosenthal, 1996), may elucidate possible cell cycle-dependent post-translational modifications of either soluble or nuclear-insoluble FEN1 protein that may serve to regulate its sub-cellular localisation and/or enzymatic function.

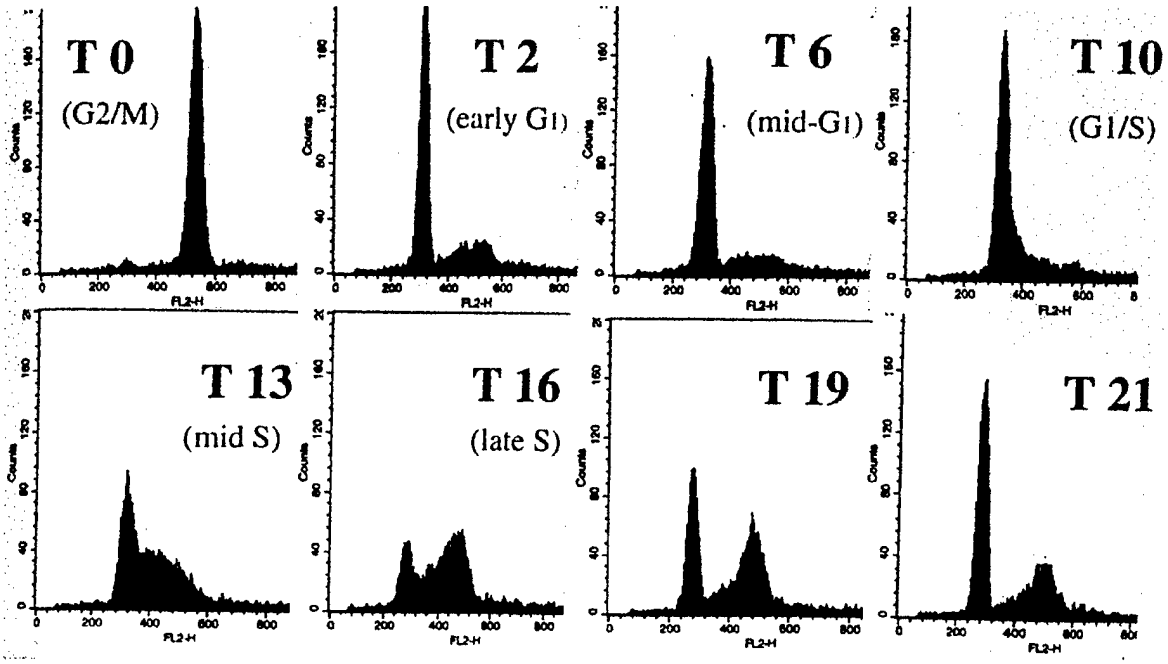

Figure 4-1. FACS analysis of HeLa synchronization. Cells were arrested in mitosis using a 24 hour double block with 2 mM thymidine and 20 ng/ml nocodazole, and released from mitotic arrest by resuspending cells in fresh media supplemented with 10% FCS. Cells were harvested at various times, methanol-fixed, and stained with propidium iodide (PI) (25 μg/ml). Times indicated are measured from release from the mitotic block (T0). The X-axis indicates fluorescence intensity measuring DNA content (PI staining intensity) and the Y-axis indicates relative cell numbers. Non-gated analysis of this method of synchronization reveals that greater than 75% of the cells were arrested at G_2/M (T0). The approximate cell cycle stage of cell populations analyzed, as determined by DNA content, is also indicated (in parentheses).

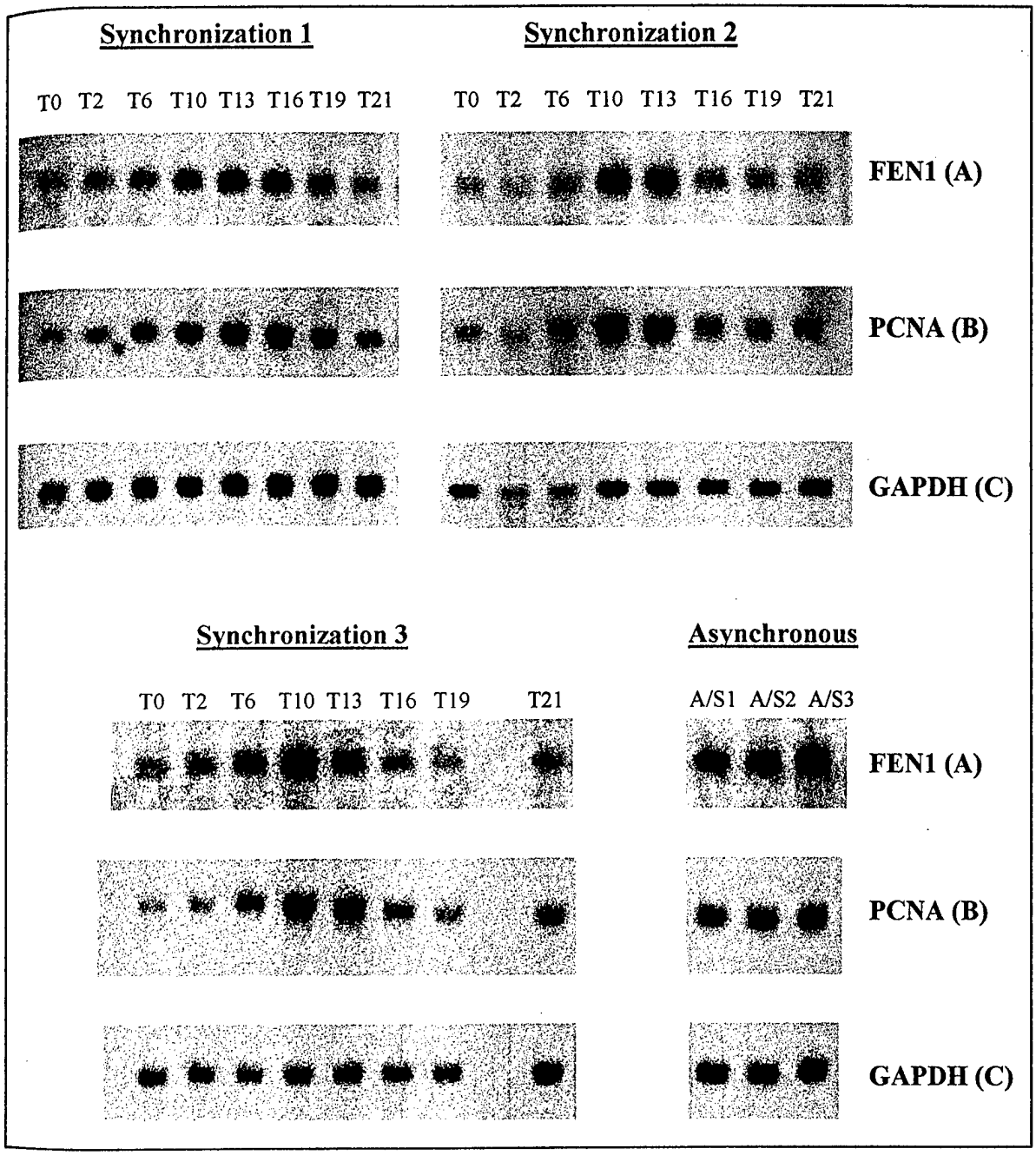

Figure 4-2. FEN1 and PCNA mRNA levels throughout the HeLa cell cycle. Total RNA was extracted from cells at various time-points during three separate HeLa synchronizations and 15 μg from each was electrophoresed on the same 1% formaldehyde- agarose gel. The gel was Northern blotted and probed with [α-^{32}P] dATP-labelled **(A)** FEN1 cDNA, **(B)** PCNA cDNA, or **(C)** GAPDH cDNA control probe. The results show a definitive cell cycle-associated expression of both FEN1 and PCNA, with peak levels occurring coincident with early S phase (T10/T13). A/S 1-3 are RNA samples from asynchronous HeLa populations harvested prior to the start of each synchronization. 28S and 18S rRNA bands were used to verify expected RNA sizes during probing (not shown). Approximate transcript sizes detected: FEN1 2.2 kb; PCNA 1.7 kb; GAPDH 1.4 kb.

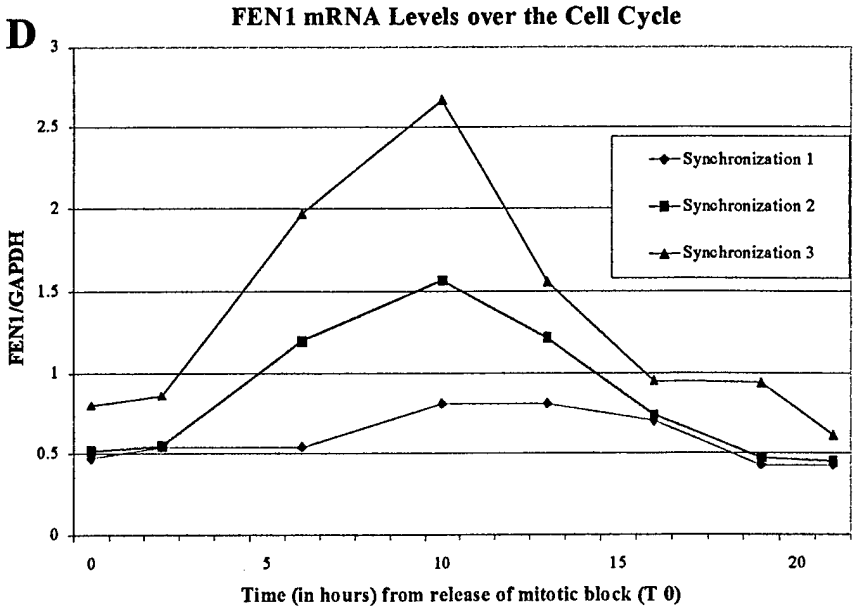

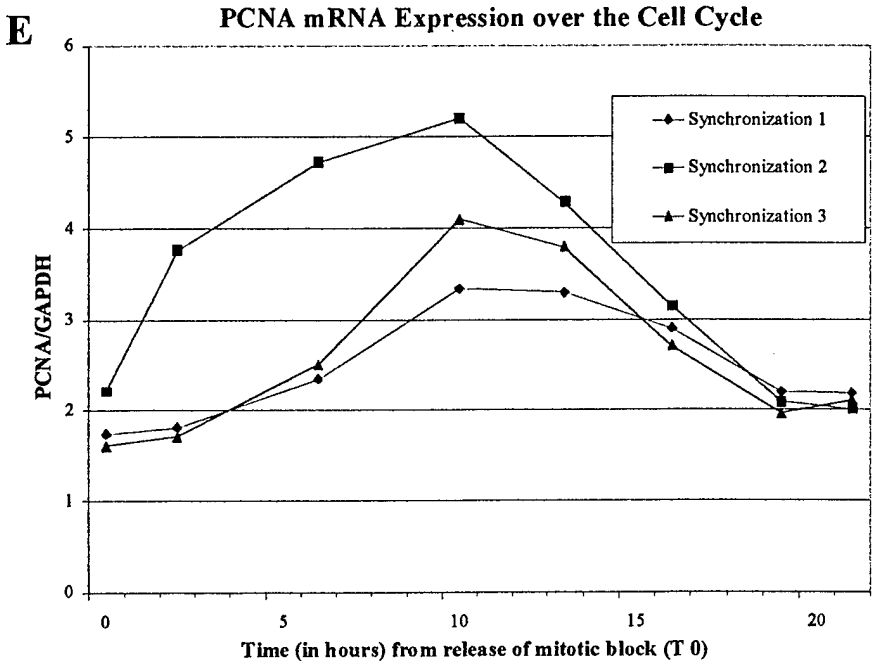

Figure 4-2 (cont.). Normalized levels of FEN1 and PCNA mRNA throughout the HeLa cell cycle. Following probing of Northern blots with [α-^{32}P] dATP-labeled FEN1, PCNA, and GAPDH cDNA probes, mRNA levels of both FEN1 and PCNA were normalized for loading variations by comparison with levels of the control probe, GAPDH, using a BioRad GS-670 Imaging Densitometer. **(D)** normalized FEN1 mRNA and **(E)** PCNA mRNA levels from 0-21 hours after release of HeLa cell populations from mitotic arrest. The results from three independent synchronization experiments are shown. The Y-axis indicates normalized mRNA levels (in arbitrary units) and the X-axis indicates the time (in hours) cell populations were harvested following release from mitotic block (T0).

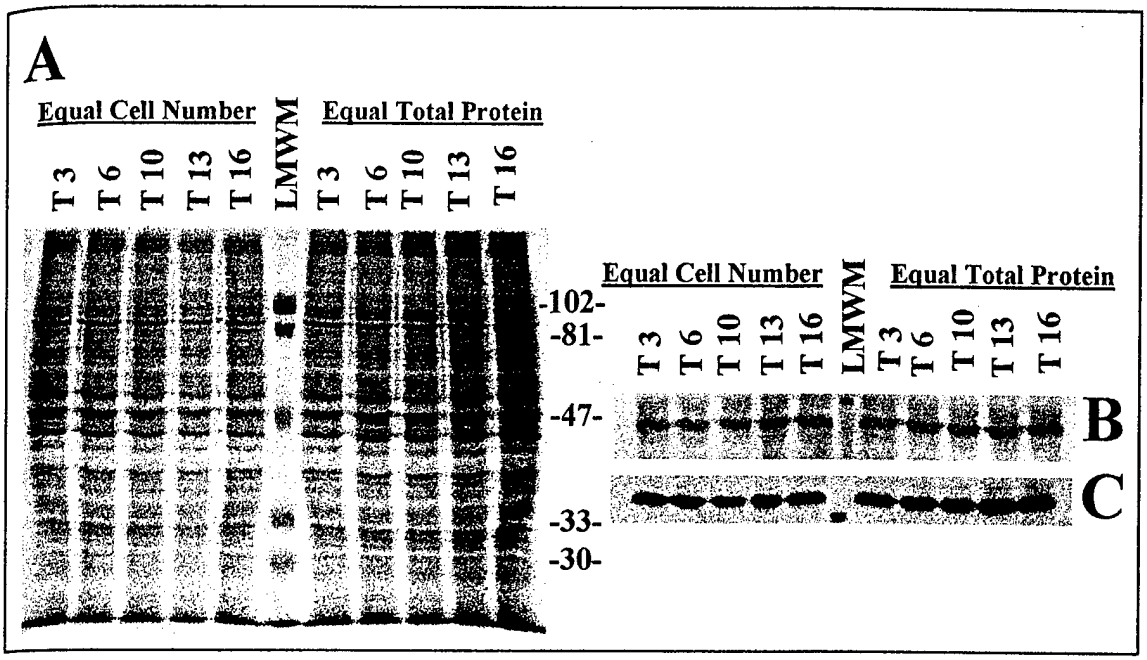

Figure 4-3. NP40-soluble FEN1 and PCNA protein levels over the HeLa cell cycle. HeLa cells were synchronized, released and harvested from early G_1 (T3) through to late S phase (T16) of the cell cycle. Soluble protein was extracted using 600 µl NP40 lysis buffer and aliquots of the various time-points were run on 10% SDS-PAGE and Coomassie-stained **(A)**, or western blotted, and probed with either **(B)** anti-Xenopus FEN1 polyclonal antibody (1:2000) or **(C)** anti-PCNA monoclonal antibody, PC10 (1:1000). Soluble protein from equal cell numbers are loaded to the left of the marker (M) and to the right of the marker, fractions were loaded to equalize total protein from the various time-points. In both instances, it appears that soluble FEN1 and PCNA protein levels remain constant over the cell cycle. Times indicated are from release from the nocodazole block (T0). Molecular weight marker sizes are depicted in the centre.

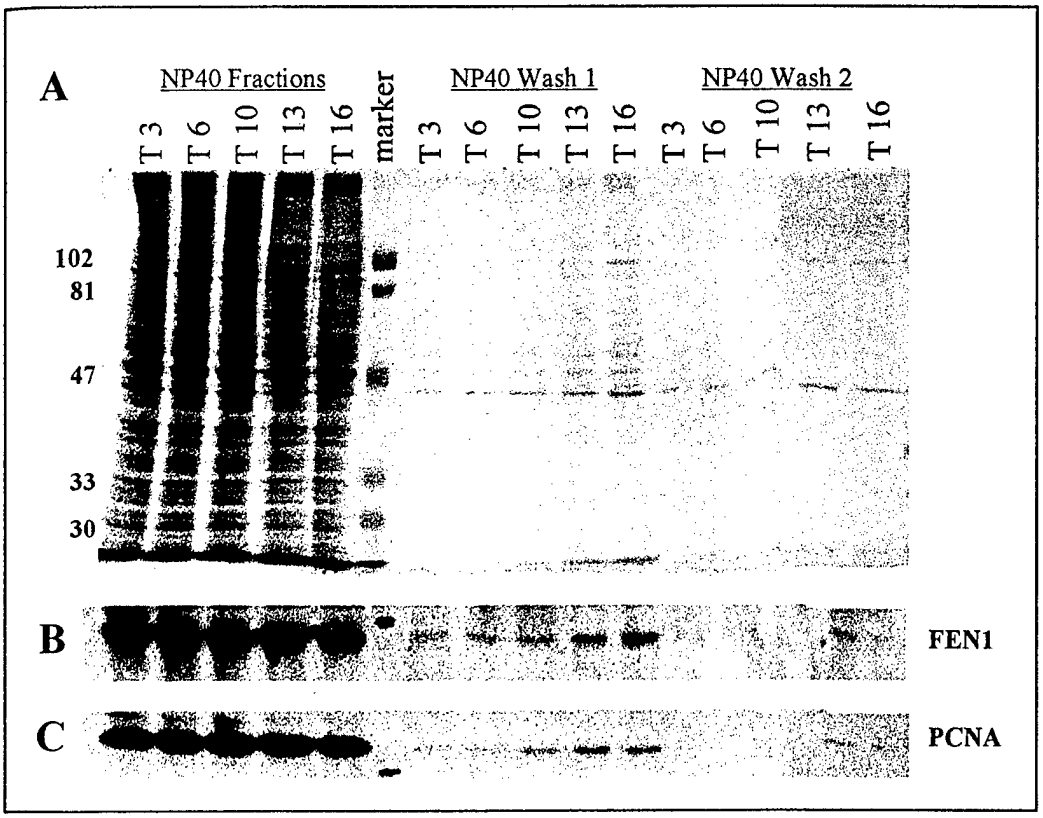

Figure 4-4. Sequential extraction of NP40-soluble FEN1 and PCNA protein from synchronized HeLa cell populations. HeLa cells were synchronized with excess thymidine and nocodazole and harvested at various points during the cell cycle. Cell pellets were initially extracted in 600 µl NP40 lysis buffer (NP40 fractions), centrifuged, and remaining pellets were washed twice (NP40 wash 1 & 2) in 200 µl of NP40 buffer. Protein from equivalent cell numbers was separated by 10% SDS-PAGE and Coomassie stained **(A)** , or western blotted, and probed with **(B)** anti-Xenopus FEN1 antibody (1:2000) or **(C)** anti-PCNA (PC10) monoclonal antibody (1:1000). Note that soluble FEN1 and PCNA protein were detected in increasing amounts over the cell cycle in wash 1 and only detected in T13 and T16 of the second NP40 wash. The molecular weight marker sizes are depicted on the left.

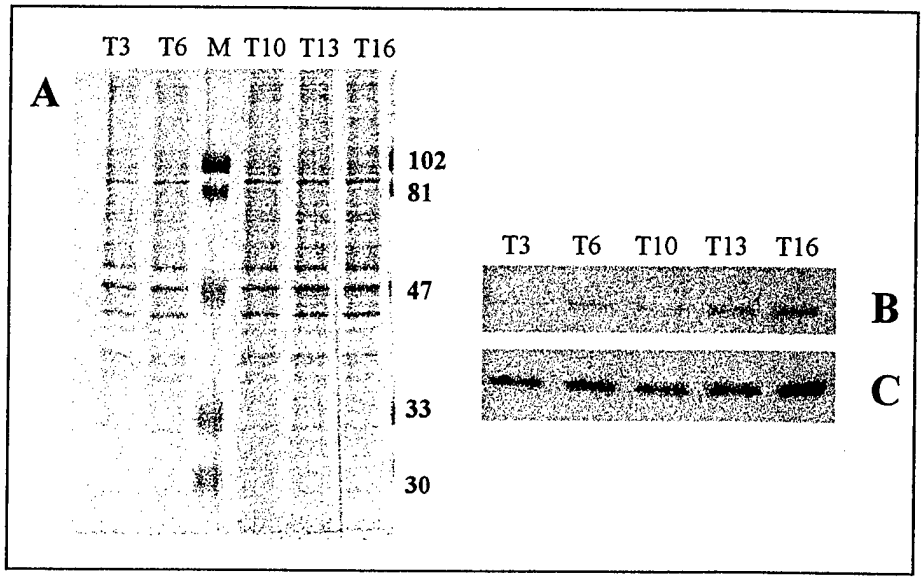

Figure 4-5. Analysis of soluble FEN1 and PCNA protein levels as HeLa cell populations progress from G_1 towards S phase of the cell cycle. HeLa cells were synchronized and NP40-soluble protein from equivalent cell numbers was extracted at various times during the cell cycle. Equal volumes from each time-point were separated by 10% SDS-PAGE and Coomassie-stained **(A)**. The same samples were also analyzed in parallel by western blotting, and probing with **(B)** anti-Xenopus FEN1 polyclonal antibody (1:2000), then **(C)** anti-PCNA monoclonal antibody, PC10 (1:1000), followed by ECL detection. Molecular weight marker (Lane M) sizes are indicated to the right-hand-side of the gel **(A)**.

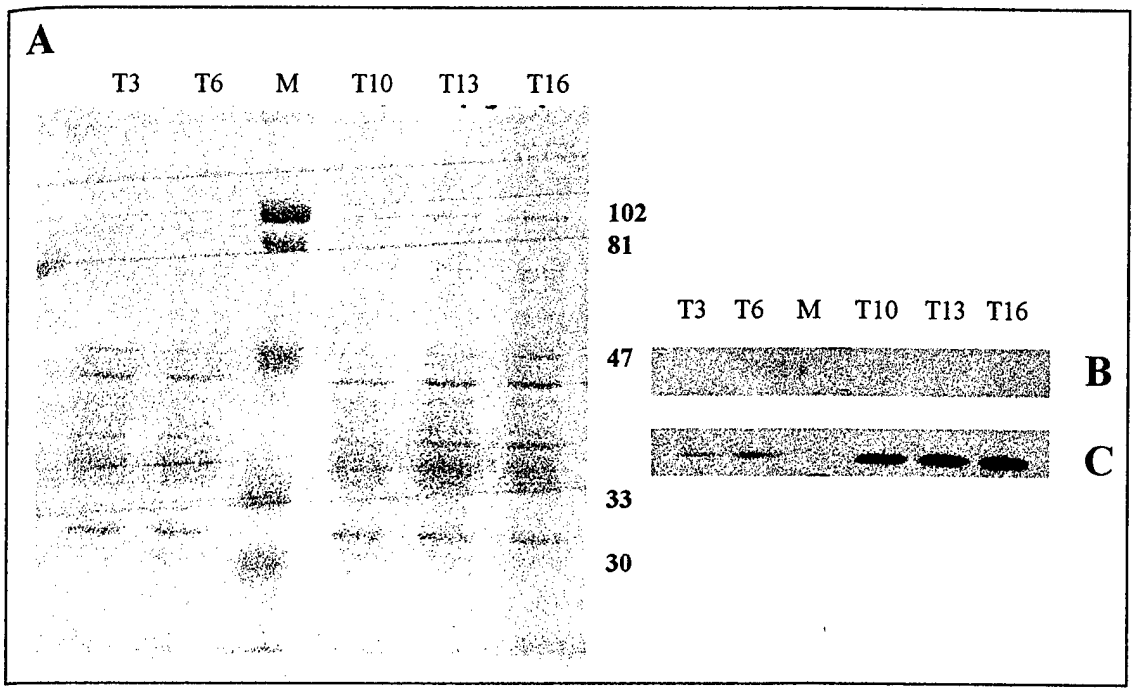

Figure 4-6. DNase I-extracted protein from synchronized HeLa cells. Following NP40 extraction of soluble protein from synchronized HeLa cell populations, remaining cell pellets were subjected to DNase I treatment (200 μg/ml) to remove DNA-bound proteins, and equal volumes, representing equivalent cell numbers, were separated by 10% SDS-PAGE and Coomassie-stained **(A)** or western blotted, and probed with **(B)** anti-Xenopus FEN1 (1:2000) polyclonal antibody, then **(C)** anti-PCNA monoclonal antibody, PC10 (1:1000), followed by ECL detection. Molecular weight marker (Lane M) sizes are indicated to the right-hand-side of the gel **(A)**. Although significant levels of DNase I-extractable PCNA protein were detected, primarily in S phase (T10, T13, T16), no DNase I-extractable FEN1 protein was detected at any time during the cell cycle (T3-T16).

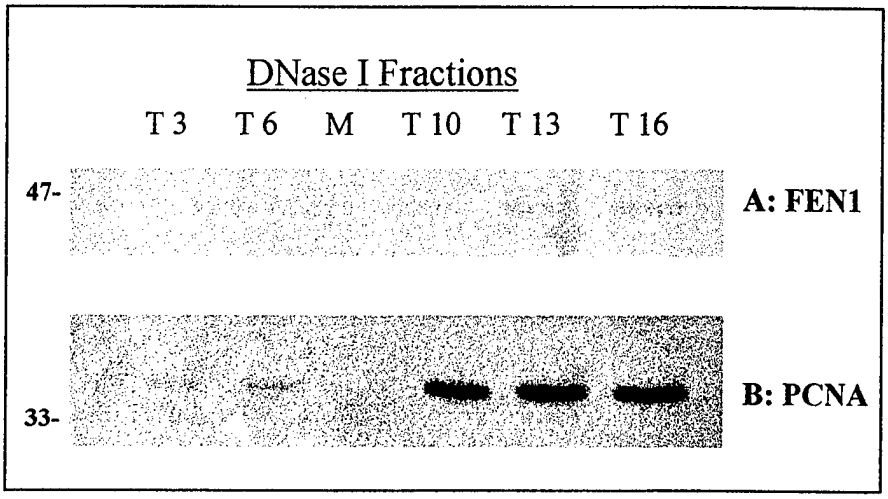

Figure 4-7. Extraction of DNA-bound protein from synchronized HeLa cell populations. HeLa cell populations were synchronized in mitosis, released, and harvested throughout the cell cycle (T3-T16). Following extraction of soluble protein with NP40 lysis buffer, DNase I-soluble protein was extracted from remaining cell pellets with 200 μg/ml DNase I. 25 μl aliquots from each time-point (approximately 2X the amount loaded in Figure 4-6) were separated by 8% SDS-PAGE, western blotted, and probed with **(A)** anti-Xenopus FEN1 (1:2000), then **(B)** anti-PCNA antibody, PC10 (1:1000), followed by ECL detection. Time-points are from release of the mitotic block (T0). Molecular weight marker sizes are indicated on the left. It should be noted that the image in (A) has been significantly enhanced on scanning to show the FEN1 protein that was detected during the antibody probing and does not reflect relative protein levels compared to the non-enhanced PCNA image. Significant levels of PCNA protein were detected, preferentially in S phase (T10, 13, 16) populations.

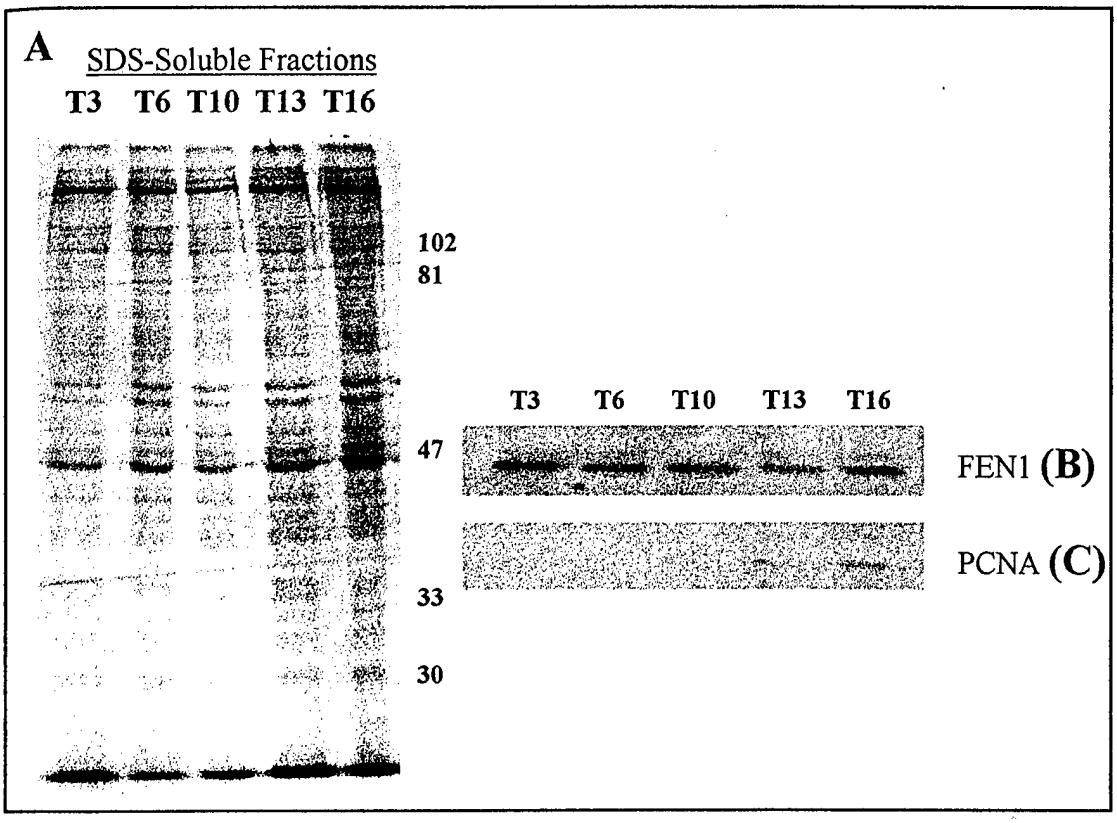

Figure 4-8. Analysis of SDS-soluble FEN1 protein detected throughout the HeLa cell cycle. Following NP40 and DNase I-extraction of protein from synchronized HeLa cell populations, remaining cell pellets were solubilized in SDS-loading buffer. Equal volumes, representing equivalent cell numbers, from various time-points throughout the cell cycle (T3-T16), were separated by 10% SDS-PAGE and Coomassie-stained **(A)**. The same samples were also analyzed in parallel by western blotting and probing with **(B)** anti-Xenopus FEN1 (1:2000) polyclonal antibody, then **(C)** anti-PCNA monoclonal antibody, PC10 (1:1000), followed by ECL detection. The molecular weight marker sizes are depicted to the right of the gel (in kDa). Significant levels of SDS-soluble FEN1 protein was detected throughout the cell cycle (T3-T16) in synchronized HeLa cells after protein extraction with NP40 and DNase I, while PCNA protein was only detected in S phase (T13, T16) populations. Times indicated are from release of mitotic arrest (T0).

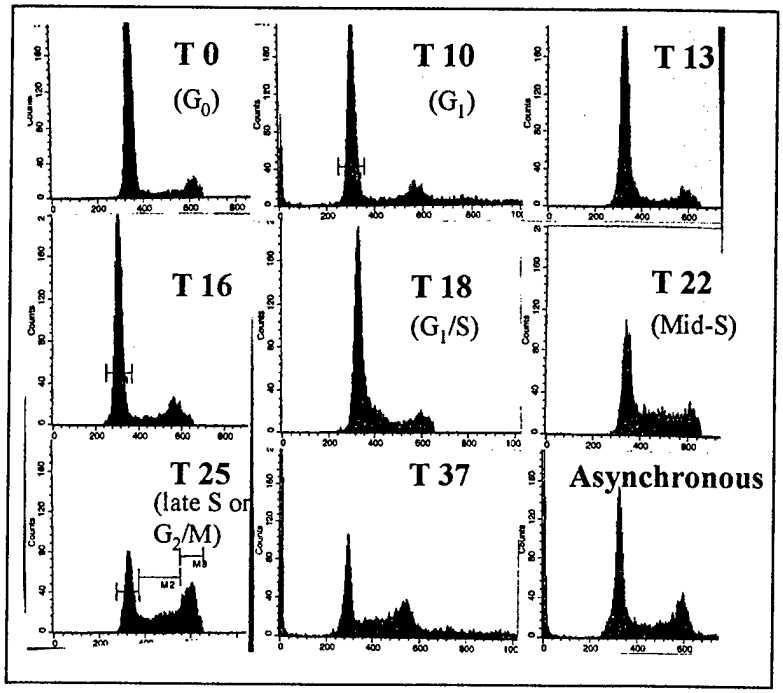

Figure 4-9. FACS analysis of a pilot study on MRC-5 primary cell line synchronized by serum starvation for 55 hours. MRC-5 cells in passage 31 were synchronized by a 55 hour incubation in DMEM supplemented with 0.5% FCS. Times indicated above are from time of re-feeding in DMEM supplemented with 15% FCS (T0). Cells were fixed in 75% methanol and stained with 25 μg/ml propidium iodide. 10,000 events were counted at each time-point and populations were gated to remove background fluorescence.The X-axis indicates fluorescence intensity measuring DNA content and the Y-axis indicates relative cell numbers. The approximate cell cycle stage of cell populations analyzed is also indicated above (in parentheses). The ⊢⊣ in some figures was used during analysis to measure population percentages at various cell cycle times. At T0, over 75% of MRC-5 cells have the DNA complement (fluorescence intensity) of G_0/G_1 cells, suggesting efficient synchrony.

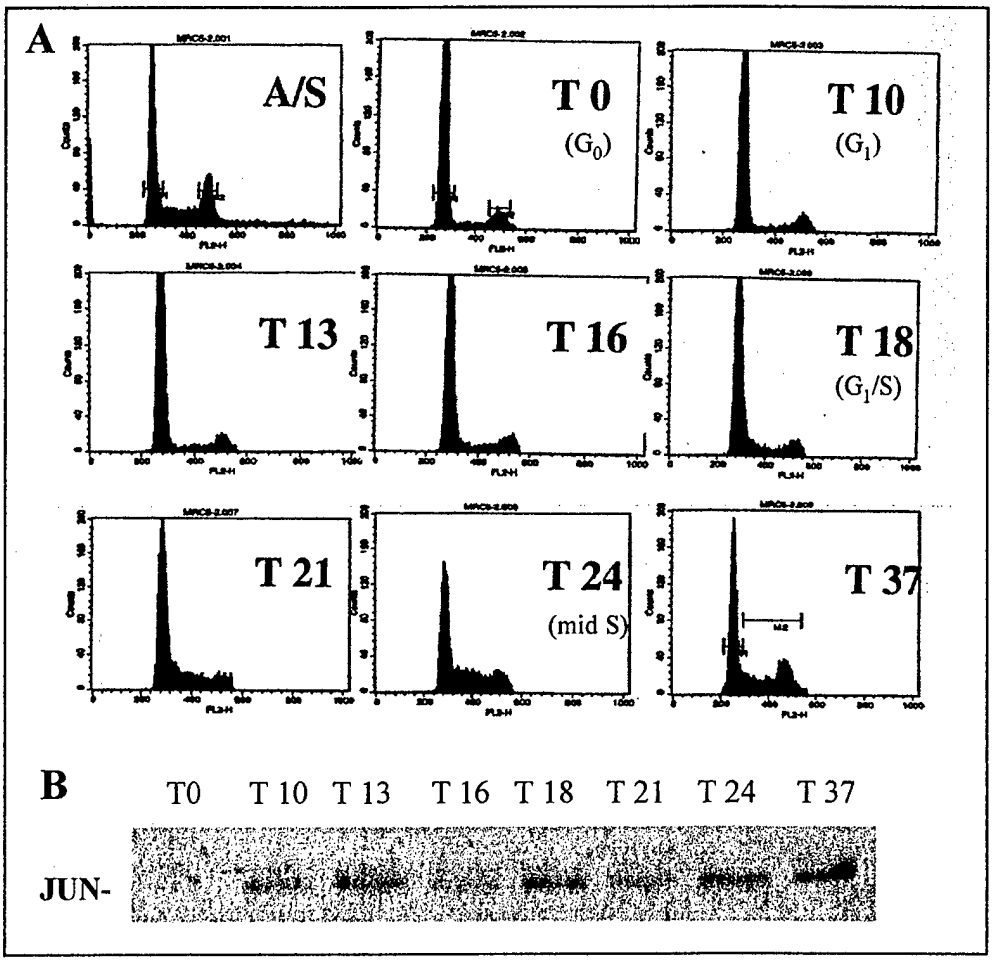

Figure 4-10. FACS analysis of MRC-5 cell synchronization. Passage 34 MRC5 cells were synchronized by incubation in DMEM supplemented with 0.5% FCS. Following re-feeding in DMEM supplemented with 15% FCS (T0), cells were subsequently harvested at various times during the cell cycle, methanol-fixed, and stained with propidium iodide (25 μg/ml). **(A)** FACS analysis of the MRC5 synchronization, indicating time following re-feeding. The X-axis indicates fluorescence intensity measuring DNA content (PI staining) and the Y-axis indicates relative cell numbers. The approximate cell cycle stage of cell populations analyzed is also indicated (in parentheses). **(B)** Soluble protein was extracted from equivalent numbers of cells at each time-point and equal volumes from each time-point were separated by 10% SDS-PAGE, western blotted, and probed with anti-JUN polyclonal antibody (1:1000). ECL detection shows that no JUN protein was detected at T0, suggesting that cells were quiescent (G_0) following serum starvation.

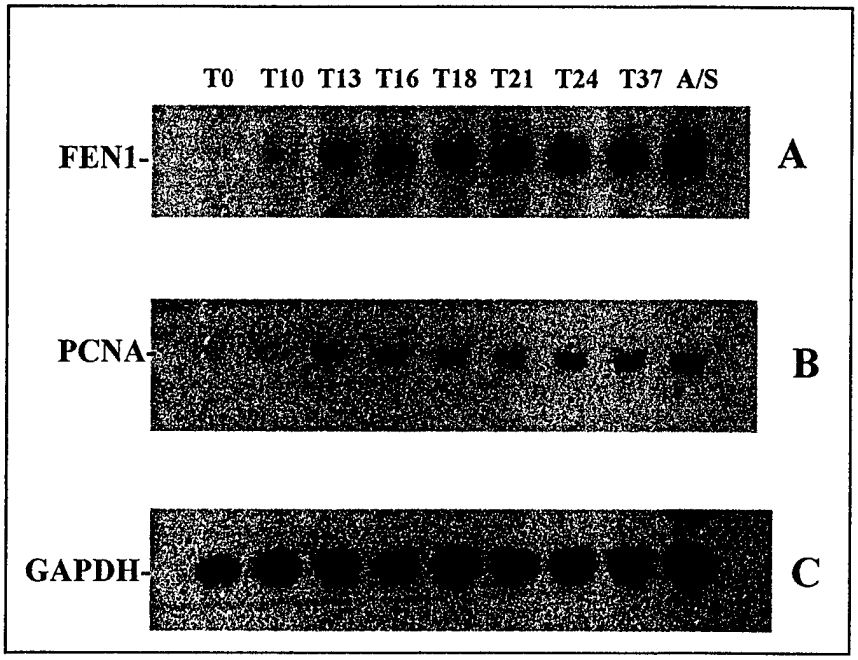

Figure 4-11. FEN1 and PCNA mRNA levels in synchronized MRC-5 cells from G_0 through to S phase of the cell cycle. MRC5 cells were synchronized by serum starvation and stimulated to proliferate by the addition of DMEM supplemented with 15% FCS (T0). Total RNA, at various time-points (T0-T37) over the cell cycle and from asynchronously growing cells (A/S), were extracted and 15 µg from each was separated on a 1% formaldehyde-agarose gel. The gel was Northern blotted and probed with [α-^{32}P] dATP-labeled FEN1 cDNA **(A)** , PCNA cDNA **(B)** , and the control probe, GAPDH cDNA **(C)** . The results show a definitive cell cycle-dependent increase in expression of both PCNA and FEN1 as cells exit G_0 (T0) and progress through S phase (T24).

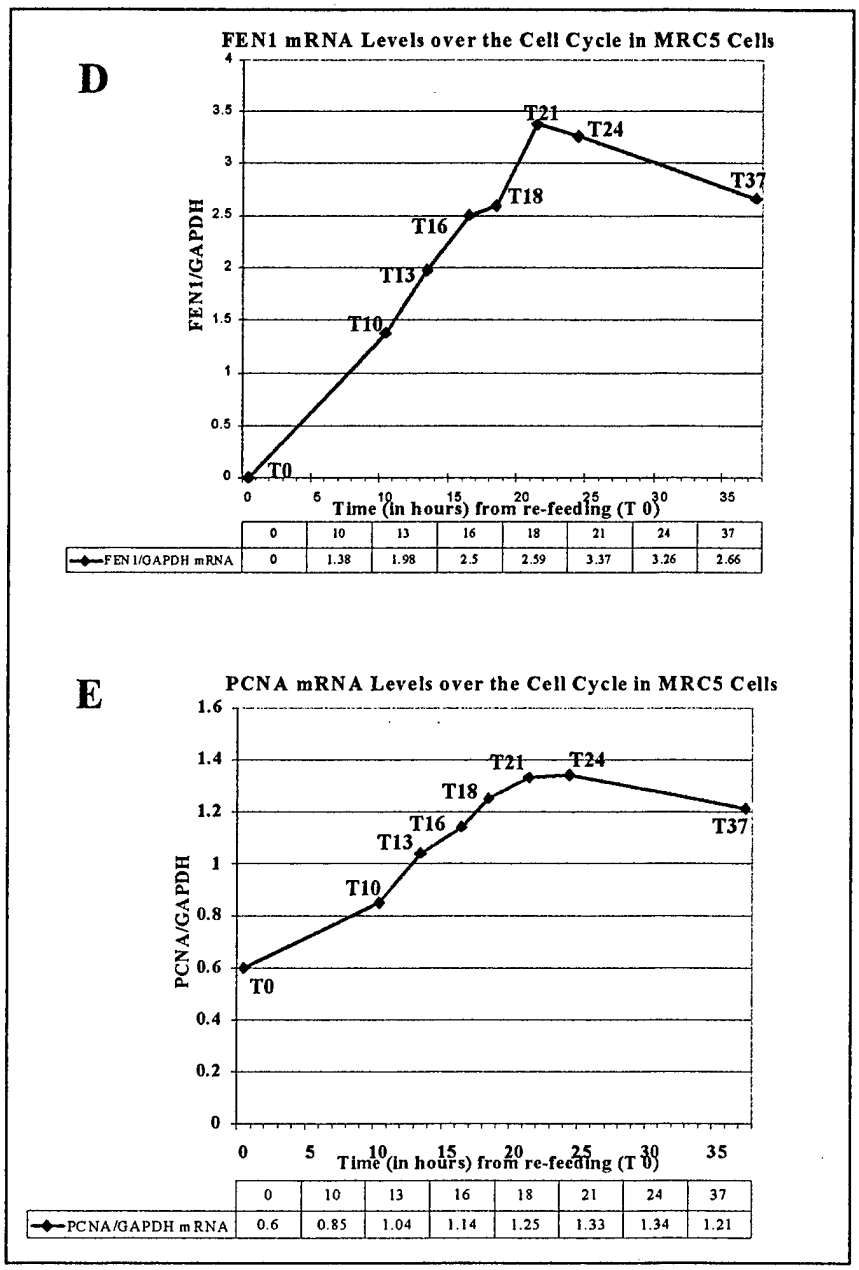

Figure 4-11 (cont.). FEN1 and PCNA mRNA levels during the MRC5 cell cycle. Following probing of Northern blots (Figure 4-11A-C) with [α-^{32}P] dATP-labeled FEN1, PCNA, and GAPDH cDNA, levels of both FEN1 and PCNA mRNA were normalized by comparison with levels of the control probe, GAPDH, using a BioRad GS-670 Imaging Densitometer. **(D)** normalized FEN1 mRNA levels and **(E)** normalized PCNA mRNA levels over the MRC-5 cell cycle after release from serum starvation (T0). The Y-axis indicates normalized mRNA levels (in arbitrary units) and the X-axis indicates the time-points (in hours) at which cell populations were harvested following release from serum starvation (T0). The tables below each graph provide the normalized values for both FEN1 and PCNA mRNA expression at each time-point.

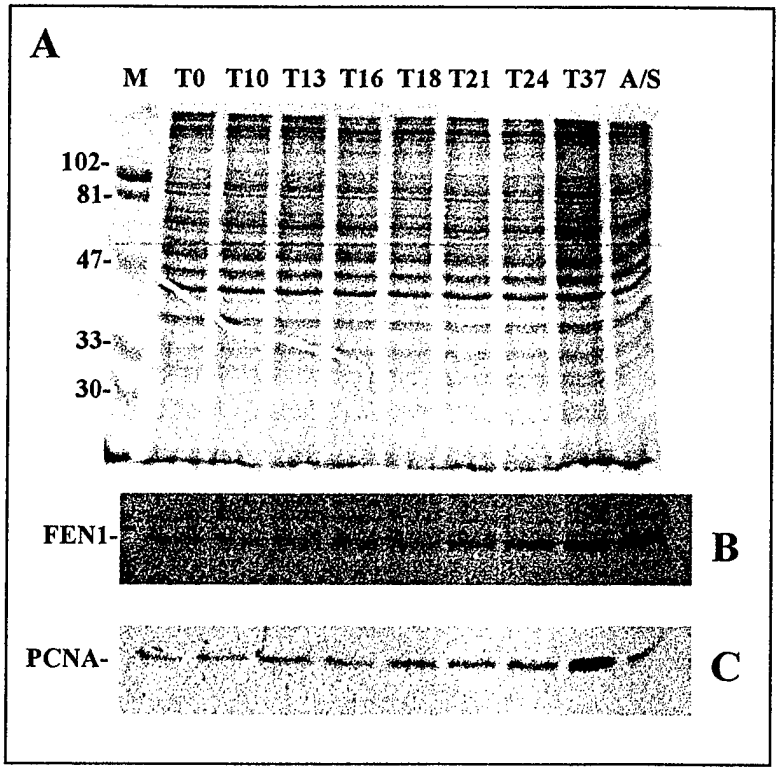

Figure 4-12. Soluble FEN1 and PCNA protein levels in MRC-5 cells as they progress from G_0 towards S phase of the cell cycle. Soluble protein was extracted from synchronized passage 34 MRC5 cells with NP40 lysis buffer. Samples containing equivalent cell numbers (with the exception of T37) were separated by 10% SDS-PAGE and Coomassie-stained **(A)** or western blotted, and probed with **(B)** anti-FEN1 antibody 3220 (1:4000) or **(C)** anti-PCNA monoclonal antibody PC10 (1:1000). ECL detection of protein bands shows a subtle cell cycle increase in FEN1 and PCNA soluble protein. Coomassie staining and immunoprobing of western blots reveal significantly more protein in the T37 fraction. This is the result of increased cell numbers at this time-point due to some cells dividing and resulting in an overall increase in cell numbers. Molecular weight marker (Lane M) sizes (in kDa) are indicated to the left of **(A)**.

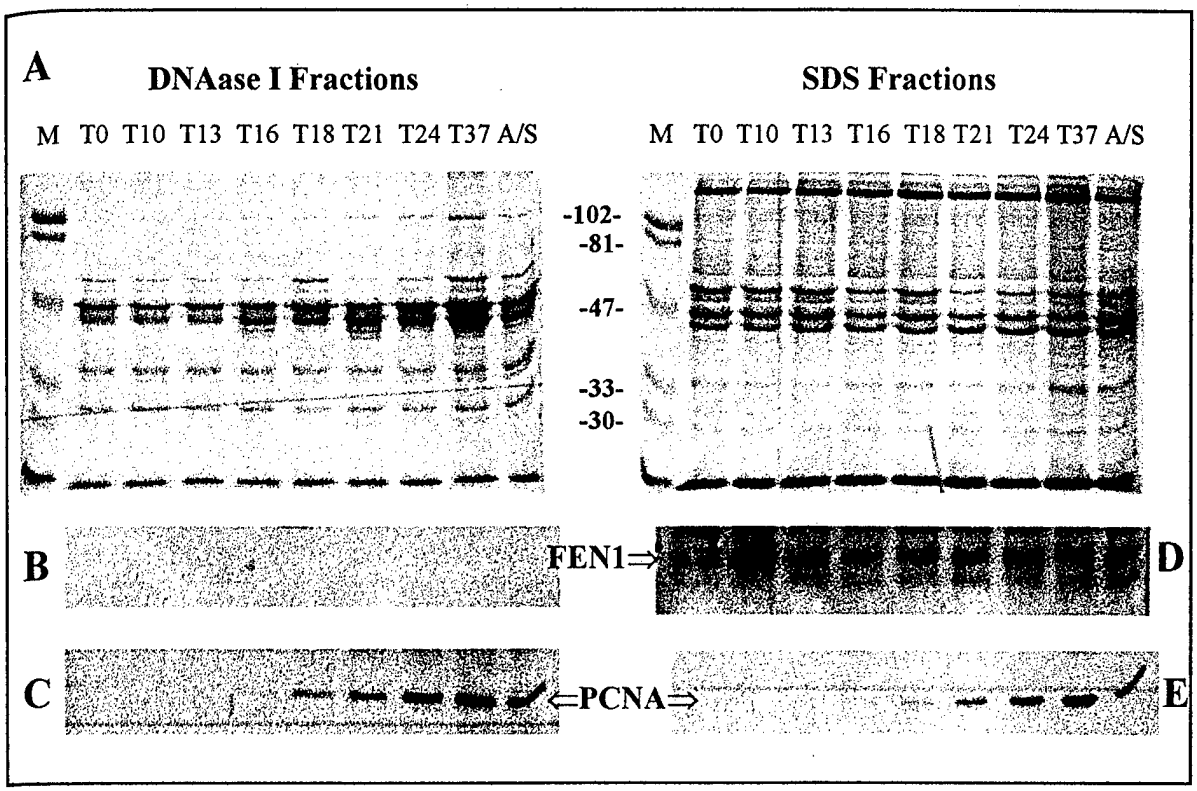

Figure 4-13. Analysis of DNase I and SDS-extracted protein from synchronized MRC-5 cells. Passage 34 MRC5 cells were synchronized, released, and cells harvested throughout the cell cycle. After extraction of soluble protein with NP40, remaining cell pellets were re-extracted with buffered DNase I (200 µg/ml) and finally, SDS loading buffer. Fractions, representing equivalent cell numbers (except for T37) were separated by 10% SDS-PAGE and Coomassie-stained **(A)**. The same samples were separated in parallel, western blotted, and probed with **(B)** and **(D)** anti-Xenopus FEN1 polyclonal (1:2000) then **(C)** and **(E)** anti-PCNA monoclonal antibody, PC10 (1:2000). No FEN1 protein was detected in DNAase I-extracted fractions, but analysis of SDS-soluble fractions reveals that FEN1 protein is still detected after a 55 hour serum starvation (T0), increases by 10 hours after re-feeding (T10), and remains relatively constant over the remainder of cell cycle (T13-T24). PCNA protein is detected preferentially in S phase populations (T18-T24) in increasing amounts in both DNase I and SDS-extracted fractions.

CHAPTER FIVE: ANALYSIS OF HUMAN FEN1 AND PCNA mRNA EXPRESSION, PROTEIN EXPRESSION, AND PROTEIN SOLUBILITY CHANGES IN RESPONSE TO DNA DAMAGE IN CULTURED CELLS

5-1 Introduction

To maintain genomic integrity and cell viability, cells must be capable of countering various types of DNA damage caused by environmental mutagens, spontaneous mutations, and even by-products of endogenous metabolic processes. To effectively deal with the continual assault on genomic integrity, cells possess multiple mechanisms to identify and correct a wide variety of DNA lesions such as intra-strand and inter-strand cross-linking, strand breaks, and base modifications induced by chemical and physical mutagens (reviewed by Wang, 1998). In addition, proliferating cells must also be able to delay cell cycle progression to allow DNA repair; avoiding fixation of mutations during replication and subsequent segregation of mutated DNA sequences (Hartwell and Weinert, 1989). Although numerous DNA repair mechanisms have been elucidated, the primary focus of this investigation will be the processes of base excision repair (BER) and nucleotide excision repair (NER).

DNA repair often involves excision and subsequent re-synthesis of damaged DNA sequences; from single nucleotide replacement in short-patch BER (Dianov *et al.*, 1992; Kubota *et al.*, 1996), to synthesis of longer repair patches (2-14 and 24-32 nucleotides, respectively) during long-patch BER (Frosina *et al.*, 1996; Klungland and Lindahl, 1997; Fortini *et al.*, 1998) and NER (Wood, 1996). Because of the need to excise and then re-synthesize DNA repair patches during many DNA repair processes, it is not surprising to find that many proteins involved in nuclear DNA replication function similarly during DNA repair. During NER in mammalian cells *in vitro*, the single-stranded binding protein RPA (Coverley *et al.*, 1991; Wood, 1996) has been

shown to be required for the initial excision reactions, while PCNA, DNA polymerase δ (DNA Pol δ) or ε (DNA Pol ε), and possibly RFC (Shivji *et al.*, 1992; Nichols and Sancar, 1992) appear to be necessary for the subsequent DNA re-synthesis step. Although short-patch BER may occur without the assistance of any typical DNA replication proteins, except a DNA ligase (Dianov et al., 1992; Kubota et al., 1996); long-patch BER *in vitro* appears to require FEN1 (Klungland and Lindahl, 1997; Kim et al., 1998), PCNA, DNA Pol δ or DNA Pol ε (Frosina et al., 1996; Klungland and Lindahl, 1997; Fortini et al., 1998), and possibly RPA (DeMott et al., 1998) and RFC (Stucki et al., 1998). These examples demonstrate that the processes of DNA replication and repair are closely related.

In contrast to many genes involved in DNA replication that are cell cycle-regulated (reviewed in Chapter 4, Section 4-1), many DNA repair genes appear to be constitutively expressed (Hoeijmakers, 1993). This may reflect the intrinsic need to regulate proliferation, whilst maintaining a DNA repair capability. Despite this, several genes implicated in DNA repair have been shown to be transcriptionally-induced upon DNA damage. In a BER response to oxidative stress, DNA polymerase β (DNA Pol β) and AP endonuclease (Ref-1, APE-1) mRNA levels are increased 2-fold within 3-9 hours of DNA base damage caused by reactive oxygen species (ROS) (Ramana et al., 1998; Grosch et al., 1998). Additionally, DNA Pol δ and PCNA mRNA levels in asynchronous WI-38 human fibroblast cells were shown to increase approximately 2-fold within one hour of exposure to 3 J/m2 UV-irradiation (Zeng et al., 1994). These results suggest that expression of other DNA repair proteins may also be induced upon DNA damage.

In addition to the apparent transcriptional induction of *PCNA* in response to UV treatment (Zeng *et al.*, 1994), PCNA protein has also been shown to witness a

change in solubility in response to UV irradiation. In non-S phase cells, PCNA protein is readily extracted by detergent lysis, however, upon UV-induced damage, PCNA protein becomes resistant to detergent extraction Toschi and Bravo, 1988, Li *et al.*, 1996) and is seen localized to sites of DNA repair (Celis and Madsen, 1986; Prosperi *et al.*, 1993; Aboussekhra and Wood, 1995; Miura *et al.*, 1996; Li *et al.*, 1996). Recently, PCNA protein was also shown to become detergent-insoluble in quiescent human lung fibroblasts subjected to the alkylating agent MMS (Savio *et al.*, 1998). This suggests that PCNA protein may become localised to BER sites *in vivo*.

I have previously examined FEN1 and PCNA expression and solubility patterns in synchronised human primary and transformed cell lines (Chapter 4). The results suggested that PCNA and FEN1 mRNA and soluble protein expression patterns were similar in both asynchronous and synchronised cell populations. Based on those results, PCNA and FEN1's purported interaction during Okazaki fragment processing during DNA replication *in vitro* (Li *et al.*, 1995; Chen *et al.*, 1996; Wu *et al.*, 1996; Warbrick *et al.*, 1997), and additional evidence of a PCNA-FEN1 interaction during BER *in vitro* (Klungland and Lindahl, 1997; Kim *et al.*, 1998); I ask two separate questions. Firstly, are PCNA and FEN1 mRNA/protein levels or protein solubility patterns altered in cellular responses to alkylation damage? Secondly, although not previously implicated in mammalian NER, does FEN1 mRNA and protein levels/solubility change in UV damaged cells in a manner similar to that reported previously for PCNA (Celis and Madsen, 1986; Toschi and Bravo, 1988; Zeng et al., 1994; Li et al., 1996)? To address these questions I decided to examine human FEN1 and PCNA expression and protein solubility patterns in cultured cell populations responding to DNA damage by both alkylating agents and UV irradiation.

5-2 Analysis of Human *FEN1* and *PCNA* mRNA Expression, Protein Expression, and Protein Solubility during BER

5-2.1 Introduction

Base excision repair (BER) is a process whereby cells can repair a wide variety of minor DNA lesions such as covalent DNA base adducts, deaminated cytosine residues (C→T conversion), spontaneous hydrolytic depurinated DNA, and other DNA alterations caused by normal metabolic pathway by-products and environmental mutagens (Lindahl, 1997). The main pathway for repair of these types of DNA damage involves recognition and excision of the altered base by specific DNA glycosylases, and excision and re-synthesis of the resulting apurinic/apyrimidinic (AP) site by the actions of an AP endonuclease, a DNA polymerase (Pol β), and a DNA ligase (Dianov *et al.*, 1992; Kubota *et al.*, 1996).

The predominant pathway for BER briefly described above is well-conserved from bacteria to higher eukaryotes and has been well characterised (reviewed by Lindahl, 1997). However, studies with reconstituted repair systems from *Xenopus laevis* oocytes suggested that repair of AP sites can also be accomplished by a PCNA-dependent mechanism (Matsumoto *et al.*, 1994; Kim *et al.*, 1998). Additional evidence for this alternative BER pathway in mammalian cells came from hamster and human cell-free repair assays using circular DNA duplex molecules with single AP sites (Frosina *et al.*, 1996). This study observed BER repair patches of 6-14 nucleotides long that could be inhibited by polyclonal antibodies to PCNA. Finally, using purified proteins in an *in vitro* system, Klungland and Lindahl (1997) demonstrated both pathways for BER: short-patch BER, involving replacement of a single nucleotide by a Pol β-dependent mechanism; and a long-patch BER pathway that generates repair patches several nucleotides in length. Their results suggest that

some types of DNA damage (eg. reduced AP sites) are resistant to short-patch BER and require the second, PCNA-dependent pathway (Klungland and Lindahl, 1997). However, it appears that the short-patch BER is predominant. This is based on the observation that antibodies to Pol β provide significantly greater inhibition of overall BER repair synthesis *in vitro* compared to anti-PCNA antibodies in the same assay (Nealon *et al.*, 1996). Additional kinetics studies using circular DNA templates *in vitro* further suggest that the short-patch BER pathway may account for as much as 80% of BER processes (Fortini et al., 1998).

Recently, changes in PCNA solubility were witnessed in quiescent human lung fibroblasts in response to the alkylating agent methyl methane sulfonate (MMS) (Savio *et al.*, 1998). MMS is known to cause alkylation damage in cells; predominantly non-bulky base damage in DNA which is subsequently repaired by BER mechanisms (Ey *et al.*, 1972). This result strongly suggests that PCNA participates in BER repair mechanisms triggered by DNA damage caused by alkylating agents *in vivo*.

Like PCNA, FEN1 is also implicated in long-patch BER. *In vitro* experiments with purified proteins (Klungland and Lindahl, 1997; DeMott *et al.*, 1998) and in reconstituted repair systems using proteins derived from *Xenopus laevis* (Kim *et al.*, 1998), three independent groups have demonstrated the requirement for FEN1 in PCNA-dependent long-patch BER *in vitro*. As a result, I chose to investigate human FEN1 and PCNA expression and protein solubility patterns in human cells subjected to the alkylating agent, MMS.

5-2.2 Experimental Design

To study FEN1 expression and protein solubility in response to alkylating agents, human MRC5-SV cells were subjected to treatment with MMS. Transformed

MRC5-SV cells were chosen so future experiments with parental MRC5 cells could be directly compared to assay similarities and differences in cellular responses between primary and transformed cell lines of similar lineage.

To determine the appropriate MMS concentration, MRC5-SV cells were seeded in 10 cm culture dishes at a density of 2 X 10^5 cells per dish and allowed to proliferate for 48 hours. At that time, cells were subjected to varying concentrations (from 0.5 mM to 5 mM) and exposure times (1 to 5 hours) of MMS to assay the effects on cell viability. It was noted that concentrations above 2 mM and exposure times in excess of two hours resulted in over 50% loss of cell viability (as determined by trypan blue exclusion). It was also observed that a one hour exposure to 1 mM MMS did not significantly affect cell viability when compared to non-treated controls (data not shown); consequently, that exposure time (1 hour) and MMS concentration (1 mM) was chosen to assay MRC5-SV cellular response to alkylating agents.

Two DNA damage experiments with MMS were performed and similar results were obtained. In each experiment, MRC5-SV cells were seeded similarly to the pilot study described above. Cells were allowed to proliferate for 48 hours and then MMS (in DMSO) was added to culture dishes at a final concentration of 1 mM. Control dishes were treated similarly with DMSO only. Following a one hour incubation, the medium was aspirated, cells washed twice with 37° C PBS, and fresh medium supplemented with 10% FCS was added to both treated and untreated culture vessels. Cells were harvested at 0, 0.5, 1, 2, 4, 8, and 24 hours following treatment (both treated and untreated controls). In addition, other treated cell populations were maintained in culture conditions for an additional 24 hours to assay long-term changes in cell viability. No differences in cell viability were noted between untreated and MMS-treated cells 48 hours following treatment (data not shown). Finally, several

culture vessels were harvested at each time-point to minimize any variability in cell treatment before subjecting all harvested cells to FACS, RNA, and protein analysis.

5-2.3 FACS Analysis following MMS Treatment of Human MRC5-SV Cells

To study the effects of alkylation damage on MRC5-SV cells, untreated and MMS-treated cell populations were analyzed by flow cytometry after methanol-fixation and DNA staining with 25 μg/ml propidium iodide (see Methods & Materials).

Figure 5-1 showing MMS FACS analysis

FACS analysis of MRC5-SV cells revealed a distinct effect on cell cycle progression by 1 mM MMS treatment (compared to untreated controls). Figure 5-1 shows that differences between treated and control populations can be witnessed starting at 2 hours (T2-NT) after treatment, with a slightly larger percentage of treated cells (T2-MMS) in G_1. By 8 hours (T8) post-treatment, a substantial proportion of treated cells (T8-MMS) appears to be in early S phase, in comparison to the control population (T8-NT). This could be indicative of a G_1 cell cycle checkpoint having been activated and delaying cell cycle progression in treated cell populations. Additionally, analysis at 24 hours following treatment reveals that the majority of treated cells have the DNA complement of G2/M cells (T24-MMS), implying that those cells that were previously at the G1/S boundary had progressed through DNA replication (S phase). This result suggests that, despite being a transformed cell line, MRC5-SV cells may have some intact cell cycle checkpoint mechanisms and alkylation damage by MMS serves to activate those checkpoint mechanisms and alter

cell cycle progression in treated cell populations. Additionally, because previous experiments had demonstrated that S phase in MRC5-SV cells was approximately four hours long (data not shown), these results also suggest that either an abnormally long S phase had occurred or an additional S or G_2/M checkpoint had been activated in response to MMS treatment.

Lastly, it should be noted that gated analysis was used here due to high fluorescence background levels, presumably due to the presence of RNA not effectively removed during cell preparations for FACS analysis. This high background was not due to either cell death and DNA fragmentation associated with cell death, nor due to the effects of MMS because the same background was present in both treated and untreated control populations.

5-2.4 *FEN1* and *PCNA* mRNA Expression in Response to MMS Treatment

To examine FEN1 and PCNA mRNA levels in response to alkylation damage in MRC5-SV cells, both untreated and 1 mM MMS-treated cell populations were harvested at the times indicated (Figure 5-1), frozen until ready for analysis, lysed, and total RNA extracted. RNA extraction, electrophoresis, and Northern blotting onto nylon membranes of total RNA from untreated and MMS-treated MRC5-SV cells was the same as described for other cell lines examined (see Chapter 4, Sections 4-2.3, 4-2.9). In addition, 28S and 18S rRNA bands were also photographed and used as relative size markers (data not shown) to validate expected transcript sizes during probe hybridizations. Lastly, total RNA from both MMS treatment experiments were separated on the same gel and probed simultaneously to prevent any variations due to transfer or probe hybridization efficiencies.

Figure 5-2 showing Northern probes with FEN1, PCNA, actin cDNA

The Northern blot was first pre-hybridized and probed with α-[^{32}P] dATP-labeled human FEN1 cDNA (Figure 5-2A). Figure 5-2A shows that FEN1 mRNA levels appear slightly higher in MMS-treated cells at 4 (T4-MMS), 8 (T8-MMS), and 24 (T24-MMS) hours post-treatment, compared to untreated controls at the same time-points (T4-NT, T8-NT, T24-NT). Additionally, although FEN1 mRNA levels appear elevated at 30 minutes post-treatment (T0.5-MMS) in the first experiment, a similar increase was not observed in the second experiment (T0.5-MMS).

Because FEN1 and PCNA have both been shown to participate in long-patch BER *in vitro* (Klungland and Lindahl, 1997; Kim *et al.*, 1998; DeMott *et al.*, 1998), I also wanted to examine PCNA mRNA levels in response to MMS treatment in parallel. Consequently, following the FEN1 cDNA probe, the blot was stripped and re-probed with α-[^{32}P] dATP-labeled PCNA cDNA. Analysis of PCNA mRNA levels in Figure 5-2B suggests that PCNA mRNA levels may also be elevated at 4 (T4-MMS) and 8 (T8-MMS) hours, as well as 2 hours (T2-MMS) following treatment, in comparison to untreated controls at the same time-points (T2-NT, T4-NT, T8-NT).

To eliminate any differences arising from unequal loading, the blot was stripped and re-probed with α-[^{32}P] dATP-labeled β-actin cDNA (Figure 5-2C). β-actin mRNA levels have been previously shown to be an accurate control of mRNA loading in DNA-damaged mammalian cells (Xu and Morris, 1999). Figure 5-2C shows that slightly higher amounts of β-actin were detected in the T0.5, T1, T2, and T4 MMS-treated fractions from the first experiment, and in the T2-MMS and T4-MMS fractions from the second experiment.

Following the β-actin probe, the intensity of the FEN1, PCNA, and β-actin mRNA bands were subjected to densitometry analysis on a BioRad GS-670 Imaging Densitometer and FEN1 and PCNA mRNA levels were subsequently normalized against loading differences detected by the β-actin contol (Figure 5-3A, 5-3B).

Figure 5-3 showing Excel graph of FEN1 and PCNA mRNA expression

As can be seen, FEN1 (Figure 5-3A) and PCNA (Figure 5-3B) mRNA levels in MRC5-SV cells are dramatically altered in response to MMS treatment. Surprisingly, a significant decrease in FEN1 and PCNA mRNA was observed, starting at 0.5 hours (red and light blue bars) following treatment. PCNA and FEN1 mRNA levels steadily decreased until 4 and 2 hours, respectively, (T1-MMS, T2-MMS, red and light blue bars in Figure 5-3A/B), however, a substantial increase in PCNA and FEN1 mRNA levels was noted by 4 (T4-MMS) hours and 8 (T8-MMS) hours, respectively, following MMS treatment. The reason for the slightly earlier increase in PCNA mRNA levels, relative to FEN1, is unclear. In contrast, FEN1 and PCNA mRNA levels in untreated control populations (purple and yellow bars, Figure 5-3A/B) remained relatively constant throughout the course of both experiments (T0-NT to T24-NT). This result is similar to previous observations of steady FEN1 and PCNA mRNA levels that were witnessed in asynchronous, cycling HeLa cell populations (Chapter 4, Section 4-2.3). It is thought that the increase observed in FEN1 and PCNA mRNA expression in MMS-treated cells, is most probably the result of cell cycle arrest and subsequent synchronous cell cycle progression into S phase around 8 hours post-treatment, as suggested by FACS analysis (Figure 5-1). If correct, this would support my previous observations of increased FEN1 and PCNA

mRNA levels during cell cycle progression from G_1 through S phase (Chapter 4). Additionally, it is unlikely that genetic expression of proteins involved in BER would increase 8 hours following alkylation damage, as BER is a fairly rapid process with most repair completed within one hour following DNA damage (Fortini *et al.*, 1998).

These results suggest that *FEN1* and *PCNA* genes may not be transcriptionally activated as part of a cellular response to DNA alkylation damage. They also suggest that cellular feedback mechanisms may exist to actually down-regulate the transcription of DNA replication genes like *PCNA* and *FEN1* as the result of G_1 cell cycle checkpoint activation caused by alkylation damage.

5-2.5 FEN1 and PCNA Protein Expression and Solubility Changes in Response to MMS Treatment

Because it appeared that FEN1 and PCNA were not transcriptionally activated as a result of alkylation damage to DNA, I decided to investigate if there were any changes in protein expression or protein solubility that may occur as a consequence of alkylation damage caused by MMS treatment. To examine this, soluble protein was extracted with NP40 lysis buffer from untreated and MMS-treated cells at the times indicated in Figure 5-1, and remaining insoluble protein was subsequently extracted with 1% SDS (see Methods & Materials). Approximately 20 μg of total soluble protein, as well as equivalent total protein concentrations from SDS-soluble fractions, from both treated and untreated cell populations, were separated by 12% SDS-PAGE gels and Coomassie-stained (Figure 5-4A). Two other 12% SDS-PAGE gels were run in parallel, western blotted, and probed with anti-Xenopus FEN1 polyclonal antibody (Figure 5-4B, D) then anti-PCNA monoclonal antibody PC10 (Figure 5-4C, E).

Figure 5-4 showing Coomassie and soluble/SDS-soluble FEN1 and PCNA probes

Analysis of soluble FEN1 (Figure 5-4B) and PCNA (Figure 5-4C) protein levels, indicates no significant differences between untreated and MMS-treated MRC5-SV cells at any of the time-points examined (T0-MMS to T24-MMS). Additionally, analysis of SDS-soluble FEN1 protein levels (Figure 5-4D) does not suggest any change in insoluble FEN1 protein levels (when compared to untreated controls) at any time-point analysed. This apparent lack of FEN1 solubility change, seen previously in synchronized HeLa cell populations (Chapter 4) and again here, may reflect that either subtle changes may occur that are below current detection limits, or simply that SDS-soluble FEN1 protein levels do not change in response to alkylation damage caused by MMS treatment.

Further analysis of SDS-soluble protein shows that a significantly higher amount of SDS-soluble PCNA was detected at 0.5 hours (SDS-T0.5-MMS) following MMS treatment, in comparison to the untreated control (SDS-T0.5-NT). In addition, SDS-soluble PCNA levels appear to remain elevated (compared to controls) in all subsequent time-points analysed (SDS-T1-T24). It is possible that elevated levels of insoluble PCNA may reflect residual BER taking place one (SDS-T1-MMS), two (SDS-T2-MMS), and four hours (SDS-T4-MMS) following treatment. Additionally, based on FACS (Figure 5-1) and mRNA (Figure 5-3) analysis suggesting G_1 arrest and subsequent entry into S phase around 8 hours (SDS-T8-MMS) following MMS treatment; it would not be surprising to witness decreased PCNA solubility (higher SDS-soluble PCNA protein levels) at 8 or 24 hours post treatment. It is also possible that the apparent increase in SDS-soluble PCNA observed at 24 hours (SDS-T24-

MMS), may reflect the slightly higher amount of total protein loaded on the gel. Total protein loaded from each fraction was relatively equal, with the exception of a slightly higher amounts loaded in T8-MMS, T24-MMS soluble and T24-MMS SDS-soluble protein samples (Figure 5-4A).

5-3 Analysis of Human *FEN1* and *PCNA* mRNA Expression and Protein Expression and Solubility during NER

Nucleotide excision repair (NER) acts on a wide variety of DNA lesions; particularly bulky, helix-distorting alterations like pyrimidine/purine dimers and 6-4 photoproducts that are caused by the mutagenic effects of ultraviolet (UV) light from the sun (Wood, 1997). Many details of NER have been elucidated (Aboussekhra *et al.*, 1995; Moggs *et al.*, 1996; Mu *et al.*, 1996) and PCNA is known to play a crucial role in the DNA synthesis step of NER (Shivji *et al.*, 1992). Although the nuclease XPG has been shown to be the 5' to 3' endonuclease (Mu *et al.*, 1996) involved in NER, and despite the fact that the DNA intermediate (bubble structure) formed during NER (Evans *et al.*, 1997) is not susceptible to human FEN1 cleavage (Harrington and Lieber, 1994); I still elected to analyze FEN1 expression and solubility patterns in UV-damaged cell populations because of PCNA's well-characterised role in NER, and to form a baseline for subsequent studies. In addition, FEN1 homologues in yeast (*S. pombe* rad2 and *S. cerevisiae* RAD27) have been implicated in repair of UV-induced damage (Murray *et al.*, 1994; Reagan *et al.*, 1995) and an alternate NER pathway (as has recently been elucidated in BER) that involves FEN1 activity, although not previously suspected, has not been ruled out.

5-3.1 Experimental Design of UV Treatment Pilot Study

To study FEN1 expression and solubility patterns in response to UV-induced damage, a pilot experiment was conducted. SV40-transformed MRC5 (MRC5-SV) cells were evenly seeded at a density of 2 X 10^5 cells per 10 cm dish and were allowed to proliferate for 48 hours prior to treatment. At the time of treatment, all dishes were aspirated, washed with 37° C PBS, treated with varying doses (5, 10, 20, 30, 50 J/m^2) of UV-irradiation (control dishes were not UV-treated), re-suspended in fresh media, and placed back in standard culture conditions (37° C/ 5% CO_2). Both treated and untreated cells were harvested at 0, 5, and 10 hours following treatment, and subjected to RNA and protein expression analysis. In addition, several culture dishes were left in culture conditions up to 48 hours post-treatment to assay any changes in cell viability.

It should be noted that UV treatment at 20, 30 and 50 J/m^2 resulted in increasing loss (> 10, 25 and 50%, respectively) of cell viability by 24 hours as determined by trypan blue exclusion and presence of non-adherent cells (data not shown). However, changes in cell viability at the other dosages tested (5 and 10 J/m^2) were not significantly different from untreated control cells at 24 and 48 hours following treatment (data not shown).

5-3.2 Human *FEN1* and *PCNA* mRNA Expression in Response to UV Treatment (Pilot Study)

To examine FEN1 and PCNA mRNA levels in response to various doses of UV irradiation, both untreated and UV-treated MRC5-SV cells were harvested at 0, 5, and 10 hours post-treatment, frozen until ready for analysis, lysed, and total RNA extracted. Total RNA extraction, electrophoresis, and Northern blotting of total RNA

from untreated and UV-treated MRC5-SV cells was the same as described previously for other cell lines (See Chapter 4). In addition, 28S and 18S rRNA bands were also photographed and used as relative size markers (data not shown) to validate expected transcript sizes during cDNA probe hybridizations. It should also be noted that the T10-NT and T10-10 fractions may be difficult to interpret due to a possible bubble in the RNA gel that affected RNA migration in those samples, and was noted during detection of 28S and 18S rRNA bands.

Figure 5-5A/B/C of Northern probes with FEN1, PCNA, and GAPDH

The Northern blot was first pre-hybridized and then probed with α-[^{32}P] dATP-labeled human FEN1 (Figure 5-5A) cDNA. The results in Figure 5-5A suggest that FEN1 mRNA levels are slightly increased by 5 hours following treatment with 5 (T5-5) and 10 (T5-10) J/m^2 UV-irradiation. In contrast, FEN1 mRNA levels are significantly decreased at 5 hours following higher dosage treatment with 20 (T5-20), 30 (T5-30), and 50 (T5-50) J/m^2, in comparison to the untreated control (T5-NT). FEN1 mRNA levels at 10 hours post-treatment were difficult to analyse due to unclear mRNA bands (T10-NT, T10-10) on the gel, however it appears that the FEN1 mRNA levels remain significantly decreased in cells treated with 50 J/m^2 UV.

Because I wanted to examine PCNA mRNA expression in parallel, the membrane was subsequently stripped and re-probed with α-[^{32}P] dATP-labeled PCNA (Figure 5-5B). Similar to FEN1, PCNA mRNA levels also appear slightly elevated by 5 hours following treatment with 5 (T5-5) and 10 (T5-10) J/m^2 UV-irradiation. Although the PCNA mRNA levels appear unchanged after 5 hours in cells treated with 20 (T5-20) J/m^2 UV, the PCNA mRNA levels in cells treated with

30 (T5-30) and 50 (T5-50) J/m^2 are decreased, in comparison to the untreated control (T5-NT).

To eliminate any differences arising from unequal loading, the blot was stripped and re-probed with α-[^{32}P] dATP-labeled GAPDH (Figure 5-5C) cDNA. Figure 5-5C shows that GAPDH mRNA levels are relatively the same in all samples, except slightly less GAPDH mRNA was detected in T0-NT. Also note that the RNA bands for T10-NT and T10-10 J/m^2 are slightly unclear due to most probably, a bubble in the denaturing gel. Despite this, the results of the three probes were subjected to densitometry analysis.

Figure 5-6 shows graph of normalized FEN1 and PCNA expression in UV pilot

All FEN1 and PCNA mRNA levels were normalized against total RNA loading differences detected by the GAPDH control probe (Figure 5-5C). The results suggest a possible increase in both FEN1 (red and yellow bars in Figure 5-6A) and PCNA (red and yellow bars in Figure 5-6B) mRNA levels (compared to untreated control cells, blue bars) by 5 hours at 5 (T5-5) and 10 (T5-10) J/m^2 UV, but analysis at 10 hours post-treatment was inconclusive due to the two aberrant samples noted earlier. In addition, expression of both FEN1 and PCNA in cells treated by higher doses (30 and 50 J/m^2) of UV was significantly decreased by 5 hours (T5-30 and T5-50) following treatment. This was most likely due to the significant cellular damage and loss of viability noted at the higher UV doses.

5-3.3 Analysis of FEN1 and PCNA Protein Expression and Solubility in Response to UV Treatment (Pilot Study)

To examine the effects of UV treatment on FEN1 and PCNA protein expression and solubility, soluble protein was extracted from non-treated and UV-treated cells with NP40 lysis buffer and remaining insoluble protein was extracted from residual cell pellets with 1% SDS (see Methods & Materials). Following Bradford assays to determine soluble protein concentrations (data not shown), 20 μg of soluble protein or equivalent total protein concentrations from SDS-soluble fractions were separated by 10% SDS-PAGE and Coomassie-stained (Figure 5-7A), or western blotted and probed with anti-Xenopus FEN1 (1:2000) polyclonal antibodies (Figures 5-7B & D) and anti-PCNA monoclonal antibody, PC10 (1:1000) (Figures 5-7C & E).

Figure 5-7A/B/C/D/E showing Coomassie and western probes of UV Pilot study

Figure 5-7 shows that soluble FEN1 and PCNA protein levels may actually decrease as the UV dose is increased. Analysis of FEN1 (Figure 5-7B) and PCNA (Figure 5-7C) protein levels 5 hours following treatment show a possible decrease in soluble protein at 20 (T5-20), 30 (T5-30), and 50 (T5-50) J/m^2, in comparison to the untreated control (T5-NT). Again, this may reflect greater damage and loss of cell viability at the higher UV doses. Interestingly, soluble FEN1 and PCNA protein levels appear unchanged at 5 hours (T5-10), but then subsequently increase by 10 hours (T10-10) at 10 J/m^2 UV-irradiation. Although not certain, it is unlikely that these differences represent slight variations in total protein loaded on the gels. As can be seen in Figure 5-7A, equal concentrations of NP40-soluble protein were loaded, with the exception of T0-NT (untreated sample harvested at beginning (T0) of UV-treatment), which appears to be slightly under-loaded. It is also noteworthy that

analysis of FEN1 and PCNA mRNA expression levels noted a slight increase in transcript levels 5 hours following treatment with 10 J/m^2. This may correlate with the slightly higher protein levels observed at 10 hours post-treatment.

Further analysis of SDS-soluble PCNA protein levels (Figure 5-7E) shows a possible increase above untreated control levels (T5-NT) by 5 hours at 20 (T5-20), 30 T5-30), and 50 (T5-50) J/m^2, but decrease below control levels (T5-NT) at the non-lethal doses 5 (T5-5) and 10 (T5-10) J/m^2 UV. In contrast, SDS-soluble FEN1 protein levels (Figure 5-7D) do not appear to vary significantly between treated and untreated cells at the time-points examined. Although it is unlikely, these detected differences mentioned above may reflect minor protein loading variations. Slightly less total SDS-soluble protein appears to be loaded in SDS-soluble fractions, T0-NT and T5-30 (Figure 5-7A), but these slight variations in total protein are thought to be inconsequential to the analysis.

Based on the results of the UV pilot study, 10 J/m2 was chosen as the UV dose to be used in subsequent studies. It is a non-lethal dose and similar to UV levels used previously to study PCNA (Miura *et al.*, 1996; Savio *et al.*, 1996; Li *et al.*, 1996). In addition, some differences at 10 J/m^2 noted in the pilot study above, need to be further investigated.

5-4 Analysis of Human *FEN1* and *PCNA* mRNA Expression, Protein Expression, and Protein Solubility Changes during NER

5-4.1 Experimental Design

Two experiments were conducted to study the effects of UV irradiation on FEN1 and PCNA mRNA/protein expression and solubility patterns in human MRC5-SV cells in culture. MRC5-SV cells were seeded at a density of 2 X 10^5 cells per 10

cm culture dish and were allowed to proliferate for 48 hours prior to treatment. Following the 48-hour incubation, cell preparations and UV treatment at 10 J/m^2 were similar to those described in the UV pilot study (see Section 5-3.1). Control dishes were treated similarly to UV-treated culture vessels, except they were not subjected to 10 J/m^2 UV irradiation. Both treated and untreated cell populations were harvested at 0, 3, 7, 10, 12, and 24 hours following UV treatment and subjected to FACS, mRNA expression, and protein analysis.

5-4.2 FACS Analysis of MRC5-SV cells following 10 J/m^2 UV Irradiation

To study the effects of 10 J/m^2 UV irradiation on MRC5-SV cell populations, untreated and UV-treated cells were methanol-fixed, stained with 25 μg/ml PI, and subjected to FACS analysis the same as described previously (see Section 5-2.3).

Figure 5-8 showing UV FACS data

Figure 5-8 depicts the FACS analyses comparing untreated (top rows) and 10 J/m^2 UV-treated (bottom rows) MRC5-SV cells harvested over a 24-hour period following UV irradiation. As can be seen, UV-treated cell populations exhibit distinct differences in FACS profiles, compared to the controls (T0-NT to T24-NT), beginning at three hours (T3-UV) following 10 J/m^2 UV treatment. At three hours, treated cell populations (T3-UV) show a higher percentage of G_1 cells and fewer S and G_2/M than the control (T3-NT). By 7 hours (T7-UV), cells appear to be accumulating at the G_1/S boundary, and by 10 hours (T10-UV), cells previously accumulating at the G_1/S boundary appear to be commencing S phase. At 12 hours (T12-UV), a significant percentage of the cell population appear to be well into S

phase, and by 24 hours (T24-UV), two distinct (G_1 & G_2/M) peaks are evident, indicating passage of a large number of cells through mitosis, back into G_1 of the cell cycle. In comparison, untreated cell populations maintain a DNA fluorescence profile typical of asynchronous, cycling cell populations for all time-points analysed (T0-NT to T24-NT). From the FACS data, it appears that treated cells observed a substantially longer period of DNA synthesis (10-12 hour S phase) than had been previously witnessed (approximately 4 hours). It is currently unclear whether DNA damage caused an excessively long S phase or whether cells that have the DNA complement of G_2/M cells at 24 hours (2^{nd} major peak in T24-UV) are those cells that were delayed in G_1 longer. However, despite this uncertainty, 10 J/m2 UV treatment appeared to alter cell cycle progression, possibly through activation of a G_1 DNA damage cell cycle checkpoint, as determined by FACS analysis.

5-4.3 FEN1 and PCNA mRNA Levels in MRC5-SV Cells Subjected to 10 J/m^2 UV Treatment

To examine FEN1 and PCNA mRNA levels in human MRC5-SV cells following 10 J/m^2 UV irradiation, total RNA was extracted, electrophoresed on a 1% formaldehyde-agarose denaturing gel, and Northern blotted onto nylon membrane (See Section 5-3.2). Total RNA from two UV irradiation experiments were run on the same gel and probed simultaneously to prevent any variation due to transfer or probe hybridisation efficiencies. In addition, prior to RNA transfer, the gel was photographed and the location of the 28S and 18S rRNA bands were noted for subsequent use as relative size markers (data not shown).

Figure 5-9A/B/C of Northern probes for FEN1, PCNA, GAPDH

The Northern blot was first pre-hybridized and then probed with α-[^{32}P] dATP-labeled human FEN1 cDNA (Figure 5-9A). Higher levels of FEN1 mRNA were detected in UV-treated cells at 3 (T3-UV), 7 (T7-UV), 12 (T12-UV), and possibly 24 (T24-UV) hours following treatment in both experiments, compared to non-irradiated controls at the same time-points (T3-NT, T7-NT, T12-NT, T24-NT). No other significant differences were noted.

To analyse PCNA mRNA levels in parallel, the membrane was subsequently stripped and re-probed with α-[^{32}P] dATP-labeled human PCNA (Figure 5-9B). Similar to FEN1, slightly higher levels of PCNA mRNA were detected in UV-treated cells at 3 (T3-UV), 7 (T7-UV), 12 (T12-UV), and possibly 24 (T24-UV) hours following treatment in both experiments, compared to non-irradiated controls at the same time-points (T3-NT, T7-NT, T12-NT, T24-NT).

To eliminate any differences arising from unequal loading, the blot was stripped and re-probed with α-[^{32}P] dATP-labeled GAPDH (Figure 5-9C) cDNA. No significant loading differences were noted in either experiment. However, it should be noted that the absence of any mRNA detected in sample T10-NT from UV experiment #2 was the result of RNA degradation. Despite this, the results of these three probes were subjected to densitometry analysis (see Methods & Materials).

Figure 5-10 Excel graph depicting normalized FEN1 and PCNA expression levels

Following densitometry measurements, FEN1 (Figure 5-10A) and PCNA (Figure 5-10B) mRNA levels were normalised to account for loading variations detected by the GAPDH control probe (Figure 5-9C). As can be seen, FEN1 (Figure

5-10A) and PCNA (Figure 5-10B) mRNA levels in MRC5-SV cells appear to be responsive to 10 J/m^2 UV treatment. FEN1 and PCNA mRNA expression levels appear highest in 10 J/m^2 UV-treated cells harvested 3, 7, and 10 hours (depicted by red and light blue bars) following treatment, in comparison to untreated control (purple and yellow bars). Figures 5-10A and 5-10B suggest that FEN1 and PCNA mRNA levels increase by 3 hours (T3-UV), peak at 7 hours (T7-UV), and then stabilize at untreated control levels (purple and yellow). In contrast, FEN1 and PCNA mRNA levels appear to remain relatively constant in asynchronous, untreated control populations (purple and yellow). This result is similar to previous observations of stable FEN1 and PCNA mRNA levels witnessed in asynchronous HeLa cell populations (Chapter 4). Because expression levels were analyzed at specified times after treatment, it is currently uncertain whether FEN1 and PCNA mRNA levels actually peak slightly before or after the 7 hour (T7-UV) time-point analysed here. However, assuming a gradual increase in expression, it would appear that FEN1 and PCNA mRNA levels probably peak between 7 and 10 hours post-treatment. Additionally, and similar to that witnessed in synchronized HeLa cell populations (Chapter Four), human FEN1 and PCNA mRNA levels follow a similar expression pattern in response to 10 J/m^2 UV treatment.

It should be noted that it is quite possible that the increases in FEN1 and PCNA expression levels witnessed here in response to 10 J/m^2 UV irradiation, may be in response to the putative G_1 cell cycle arrest suggested by FACS data (Figure 5-8). This possibility would be in line with what was reported previously (Chapter Four) about increasing FEN1 and PCNA mRNA levels during progression from G1 through S phase of the cell cycle.

5-4.4 Analysis of FEN1 and PCNA Protein Expression and Solubility Patterns in Response to 10 J/m^2 UV Treatment

To examine FEN1 and PCNA protein expression and solubility patterns in MRC5-SV cells in response to UV treatment, soluble protein was extracted from non-treated and UV-treated cells with NP40 lysis buffer and remaining insoluble protein was extracted from residual cell pellets with 1% SDS (see Methods & Materials). Following Bradford assays to determine soluble protein concentrations (data not shown), 20 μg of soluble protein or equivalent total protein concentrations from SDS-soluble fractions, were separated by 10% SDS-PAGE and Coomassie-stained (Figure 5-11A), or western blotted and probed with anti-Xenopus FEN1 (1:2000) polyclonal antibodies (Figures 5-11B & D) and anti-PCNA monoclonal antibody, PC10 (1:1000) (Figures 5-11C & E).

Figure 5-11A/B/C shows Coomassie and western probes from UV experiment

As can be seen, it appears that soluble FEN1 (Figure 5-11B) and PCNA (Figure 5-11C) protein levels remain relatively constant in both treated and untreated cell populations. However, analysis of SDS-soluble PCNA protein (Figure 5-11E) shows significantly higher levels of SDS-soluble PCNA protein at 3 (T3-UV), 7 (T7-UV), 10 (T10-UV), and 12 (T12-UV) hours following UV treatment, compared to non-treated controls harvested at the same time (T3-NT, T7-NT, T10-NT, T12-NT). Elevated levels of non-detergent-soluble PCNA protein, immediately following UV-irradiation, has been reported previously (Prosperi *et al.*, 1993; Li *et al.*, 1996; Savio *et al.*, 1998) and its decreased solubility is strongly linked to its proposed role in NER (Shivji *et al.*, 1992; Miura *et al.*, 1996). In contrast, it is interesting to note that SDS-

soluble FEN1 protein levels (Figure 5-11D) appear to remain relatively unchanged in all treated and untreated fractions analysed. This constant level of SDS-soluble FEN1 protein is similar to what I witnessed with SDS-soluble FEN1 protein extracted from synchronised HeLa cell populations (Chapter 4) as they progressed from early G_1 through S phase of the cell cycle.

It appeared that approximately equal quantities of total protein (Figure 5-11A) were loaded from all analysed fractions, with the exception of slightly higher total protein loaded in both the untreated (T24-NT) and UV-treated (T24-UV) fractions harvested at 24 hours. However, because it appears that both treated and untreated fractions at 24 hours contain similar total protein levels, they can still be used for comparison.

Finally, it should be noted that the increased levels of SDS-soluble PCNA protein detected at 3 (T3-UV) and 7 (T7-UV) hours following UV treatment are probably indicative of PCNA's reported (Shivji *et al.*, 1992; Miura *et al.*, 1996) involvement in NER repair mechanisms. However, based on FACS data (Figure 5-8), it is unclear as to whether the elevated levels of SDS-soluble PCNA protein detected at 10 (T10-UV) and 12 (T12-UV) hours post-treatment are associated with NER, S phase DNA replication following a putative G_1 arrest and subsequent cell cycle progression into S phase, or a combination of both.

5-5 Discussion

PCNA has been previously shown to be required for NER (Shivji *et al.*, 1992; Nichols and Sancar, 1992) and long-patch BER (Frosina *et al.*, 1996; Klungland and Lindahl, 1997; Kim *et al.*, 1998; Fortini *et al.*, 1998) *in vitro*. Further evidence for a PCNA role in DNA repair has been shown by the existence of a detergent-insoluble

population of PCNA protein found in non-S phase cells treated with UV irradiation (Toschi and Bravo, 1988; Prosperi *et al.*, 1993; Li *et al.*, 1996; Miura *et al.*, 1996) or MMS (Savio *et al.*, 1998). Because FEN1 has also been shown to be required for long-patch BER *in vitro* (Klungland and Lindahl, 1997; Kim *et al.*, 1998; DeMott *et al.*, 1998) and reportedly interacts with PCNA during DNA replication (Li *et al.*, 1995; Chen *et al.*, 1996; Warbrick *et al.*, 1997) *in vitro*, I wanted to examine FEN1 and PCNA mRNA/protein expression and protein solubility patterns in cells subjected to DNA damage by the alkylating agent MMS or UV irradiation.

When human MRC5-SV cells were subjected to alkylation damage by MMS, an effect on cell cycle progression was observed. FACS data (Figure 5-1) suggested that treated cell populations may have experienced activation of a G_1 cell cycle checkpoint that led to near synchronous entry and progression throughout S phase (Figure 5-1, T8-MMS and T24-MMS). Additionally, by 24 hours following MMS treatment, the majority of MMS-treated cells appeared to have the DNA complement of G_2/M cells (T24-MMS), suggesting that either an additional S or G_2/M checkpoint had been activated or alternatively, an unusually long (14-16 hour) S phase had occurred. Although most short-patch and long-patch BER processes are completed within 20 and 60 minutes (Fortini *et al.*, 1998), respectively, it is possible that further DNA damage occurred after MMS removal. The presence of new DNA lesions or former lesions not identified and corrected by repair mechanisms may have persisted in S phase, and that could lead to stalling or disassembly of replication complexes during S phase. This could possibly explain the putative abnormally long S phase observed in treated cell populations.

Previous studies with chinese hamster ovary (CHO) cells have demonstrated an increase in DNA Pol β and AP endonuclease (Ref-1) mRNA levels 3-9 hours

following DNA damage caused by the presence of either hydrogen peroxide (Grosch *et al.*, 1998) or MMS (Fornace *et al.*, 1989) in the medium. Although DNA Pol β and Ref-1 are involved in the predominant short-patch BER pathway (Dianov *et al.*, 1992; Fortini *et al.*, 1998); it was logical to examine if proteins required for long-patch BER could also be transcriptionally activated in response to DNA damage caused by MMS treatment. Results (Figure 5-2A/B, 5-3A/B) suggest that FEN1 and PCNA mRNA levels actually decrease for up to 4 hours following MMS treatment, but then subsequently increase by 8 hours to levels approaching untreated cells' mRNA levels. Additionally, both FEN1 and PCNA mRNA levels increased even further by 24 hours post-treatment. Although it is possible that the increase in FEN1 and PCNA mRNA levels observed between 4 and 8 hours was the result of transcriptional activation of those genes in a DNA damage response, it is more likely that the observed increase in mRNA levels was due to up-regulation of those genes in preparation for S phase DNA replication that appeared to occur between 8 and 24 hours post-treatment (Figure 5-1). Additionally, even though *DNA Pol β* and *Ref-1* were transcriptionally activated in response to oxidative stress (Grosch *et al.*, 1998) or alkylation damage (Fornace *et al.*, 1989), they are not implicated in S phase DNA replication (Waga *et al.*, 1994). This implies that their induction is most probably DNA repair-related, whereas the induction of *FEN1* and *PCNA* can also be attributed to cell cycle progression towards S phase. Because of their non-proliferative status, future experiments with quiescent MRC-5 cells may be necessary to determine if *PCNA* and *FEN1* are transcriptionally activated by DNA damage caused by MMS treatment.

Although DNA Pol β and Ref-1 protein levels also increase by 9 hours following oxidative stress (Grosch *et al.*, 1998) or MMS treatment (Fornace *et al.*, 1989), a similar increase in soluble FEN1 or PCNA protein was not observed here

following alkylation damage by MMS (Figures 5-4B, 5-4C). Several possibilities exist as to why no increase in FEN1 or PCNA protein was witnessed here. Firstly, a combination of FACS (Figure 5-1) and mRNA (Figures 5-2, 5-3) data suggests that FEN1 and PCNA expression may not have been induced by MMS treatment. Secondly, any increase that may have occurred between 8 and 24 hours post-treatment went undetected because of the time-points selected. Finally, an increase in FEN1 and PCNA soluble protein levels may have occurred prior to 8 hours, but was below the limits of detection. Based on my results, I propose that FEN1 and PCNA protein levels probably do not increase as a result of alkylation damage by MMS treatment.

It should also be noted that if the observed increase in FEN1 and PCNA mRNA levels was due to cell cycle progression towards S phase and not due to a DNA damage response, previous results (Chapter 4; Morris and Mathews, 1989) imply that soluble protein levels should also increase accordingly. However, because of the 16 hour interval between the last two time-points analysed (T8 and T24), an increase in FEN1 and PCNA protein would probably not have been detected. Similar experiments in the future with additional time-points between 8 and 24 hours will be necessary to address that possibility.

Although it appears that FEN1 and PCNA total protein levels may not be increased as a result of alkylation damage, an increase in insoluble (SDS-soluble) PCNA protein was witnessed as early as 30 minutes following MMS treatment (Figure 5-4E). Additionally, increased levels of insoluble PCNA were observed in all subsequent time-points examined (Figure 5-4E, T1-MMS to T24-MMS). These results suggest that the increased levels of insoluble PCNA protein were the direct result of PCNA participation in BER mechanisms. Lastly, it supports previous observations of decreased PCNA protein solubility in quiescent human fibroblasts

subjected to MMS treatment (Savio *et al.*, 1998). Because FACS data (Figure 5-1) suggest that S phase DNA replication occurred between 8 and 24 hours post-treatment, it is possible that the increased levels of insoluble PCNA protein witnessed at 8 and 24 hours were also the result of PCNA's participation in nuclear DNA replication (Celis and Celis, 1995; Bravo and MacDonald-Bravo, 1985). In contrast to PCNA, no change in FEN1 protein solubility was observed at any time-point examined (Figure 5-4D). This result suggests that either FEN1 protein may not participate in MMS-induced BER mechanisms *in vivo*, or that FEN1 function during BER is not contingent on a decrease in protein solubility. The latter possibility cannot be ruled out since changes in FEN1 protein solubility were not witnessed during S phase in synchronised HeLa or MRC-5 cells (Chapter4), despite that FEN1 protein participation in DNA replication is strongly suggested (Ishimi *et al.*, 1988; Goulian *et al.*, 1990; Turchi and Bambara, 1993; Waga *et al.*, 1994).

The effects of UV treatment show numerous similarities to the effects of MMS treatment in MRC5-SV cells. FACS analysis of MRC5-SV cells treated with 10 J/m^2 UV irradiation (Figure 5-8) suggested that UV treatment may also have triggered a G_1 cell cycle checkpoint in some cells. This suggestion is based on the increase in G_1 cells witnessed at 3 and 7 hours, and their near synchronous entry (T10-UV) and progression (T12-UV) through S phase following UV treatment. Interestingly, FACS analysis of cells at 24 hours following UV treatment shows two distinct cell populations, one population apparently in G_1 and the other with the DNA complement of cells in G_2/M (Figure 5-8, T24-UV). This implies that cells that appeared to enter S phase around 10 hours post-treatment (T10-UV) had either completed the cell cycle and progressed back to G_1 by 24 hours, or that they experienced an abnormally long S phase or subsequent additional G_2/M checkpoint. The former appears more likely in

that the number of cells in G_1 is greater at 24 hours than at 12 hours after UV treatment. This suggests that at least some cells had progressed through mitosis to G_1 of the cell cycle.

Following FACS analysis, examination of mRNA shows that FEN1 and PCNA mRNA levels appear to increase above untreated control levels within 3 hours, and peak between 7 and 10 hours in MRC5-SV cells subjected to 10 J/m^2 UV irradiation (Figures 5-9, 5-10). Those results and previous observations of elevated PCNA mRNA levels in asynchronous WI-38 human lung fibroblasts following 3 J/m^2 UV treatment (Zeng *et al.*, 1994) suggest that the increased PCNA and FEN1 mRNA levels observed here are the direct result of transcriptional activation of those genes by DNA repair processes. However, FACS data (Figure 5-8) and previous observations (Chapter 4; Morris and Mathews, 1989) of increasing PCNA and FEN1 mRNA levels during cell cycle progression from early G_1 to S phase, suggest otherwise. It is likely that the increased FEN1 and PCNA mRNA levels witnessed here were, at least in part, due to cell cycle progression following a putative G_1 arrest, and not due solely to transcriptional induction as part of a DNA damage response. Additionally, Zeng *et al.* (1994) suggest that the increase they observed in PCNA mRNA within one to two hours following 3 J/m^2 UV treatment was due solely to DNA repair mechanisms because asynchronous cells were used in their study. The FACS data here (Figure 5-8) show that some cell synchrony from UV treatment may result from possible activation of a G_1 cell cycle checkpoint, and that this may subsequently cause activation of genes in a cell cycle-dependent, and not repair-dependent manner. The absence of FACS data in the study by Zeng *et al.* (1994) may have led to a premature conclusion regarding *PCNA* inducibility following DNA damage. Although subsequent studies suggest a p53-dependent induction of *PCNA* in

response to UV irradiation (Shivakumar *et al.*, 1995; Morris *et al.*, 1996), a cell cycle effect on that observed transcriptional activation cannot be ruled out. Lastly, the lower (3 J/m^2) dosage used in their study, compared to the 10 J/m^2 used here may have also contributed to the differences in our results and subsequent data interpretation.

Analysis of FEN1 and PCNA protein levels suggests that no significant changes occurred in either FEN1 (Figure 5-11B) or PCNA (Figure 5-11C) soluble protein levels in MRC5-SV cells subjected to 10 J/m^2 UV irradiation. Although it appeared that there was some *FEN1* and *PCNA* transcriptional induction by either cell cycle-dependent or DNA repair mechanisms, the magnitude of the induction was probably insufficient to be detected during subsequent analysis of protein levels.

In addition to no apparent changes in protein levels, it also appeared that FEN1 protein solubility patterns are unaffected by UV treatment (Figure 5-11D). Similar to what I have observed previously in other studies of FEN1 protein solubility during the cell cycle (Chapter 4) and during repair of alkylation damage by MMS treatment (Chapter 5, Section 5-2), it appears that the levels of insoluble (SDS-soluble) FEN1 protein change little or not at all during the processes of DNA replication or repair. This suggests that either FEN1 protein is not involved in NER, or that its function during NER is not dependent on a change in its solubility. Because FEN1 is not implicated in mammalian NER (Shivji *et al.*, 1992; Nichols and Sancar, 1992; Mu *et al.*, 1996), the former possibility is most probable.

In contrast to FEN1, PCNA protein exhibited dramatic changes in its solubility (Figure 5-11E) in response to 10 J/m2 UV treatment of MRC5-SV cells. Elevated levels of insoluble PCNA were witnessed at 3, 7, 10, and 12 hours post-treatment, and previous observations (Toschi and Bravo, 1988; Prosperi *et al.*, 1993; Li *et al.*, 1996;

Miura *et al.*, 1996) suggest that this increase was a direct consequence of its role in NER pathways. It is also possible that the increased levels of insoluble PCNA protein observed at 7, 10, and 12 hours following UV treatment may also have been the result of higher levels of S phase DNA replication occurring in those cells, as suggested by FACS data (Figure 5-8).

In summary, both UV and MMS treatment of MRC5-SV cells dramatically altered cell cycle progression. It is thought that one or more cell cycle checkpoints may have been activated by DNA damage that resulted in the pronounced cell cycle effect. Although both FEN1 and PCNA mRNA levels were increased in treated cell populations, some, if not all observed mRNA increases may be accounted for by cell cycle-dependent mechanisms, and not DNA repair-related pathways. In addition, there appeared to be no change in either FEN1 total protein or protein solubility patterns caused by UV or MMS treatment. In contrast, PCNA protein becomes less soluble immediately following either UV or MMS treatment. This strongly supports a role for PCNA in NER and BER pathways.

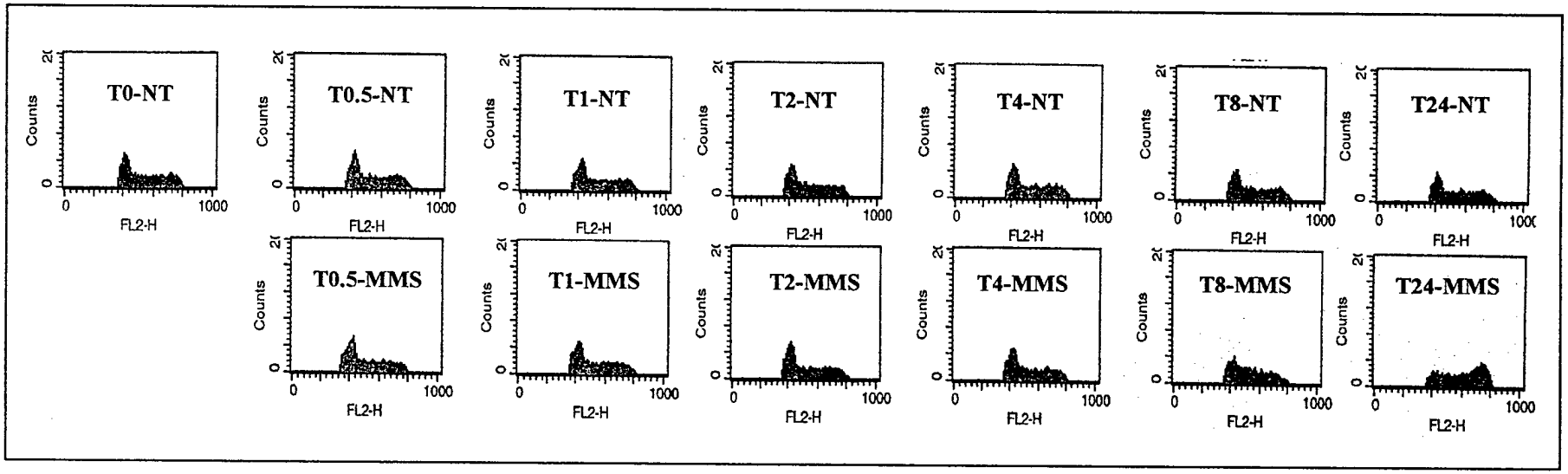

Figure 5-1. FACS analysis of human MRC5-SV cells treated with 1 mM MMS. Human MRC5-SV cells were treated for one hour with 1 mM MMS (in DMSO) and harvested at 0, 0.5, 1, 2, 4, 8, and 24 hours following treatment, along with controls treated with DMSO only. Cells were methanol-fixed, stained with 25 μg/ml propidium iodide (PI), and analyzed by Cell Quest software (Becton-Dickenson). Labels on the individual FACS profiles above indicate time of harvest following MMS treatment (T0-NT), and whether the cells graphically depicted were MMS-treated (MMS) or untreated (NT). The X-axis depicts relative fluorescence, measuring PI staining (DNA content), and the Y-axis indicates cell numbers.

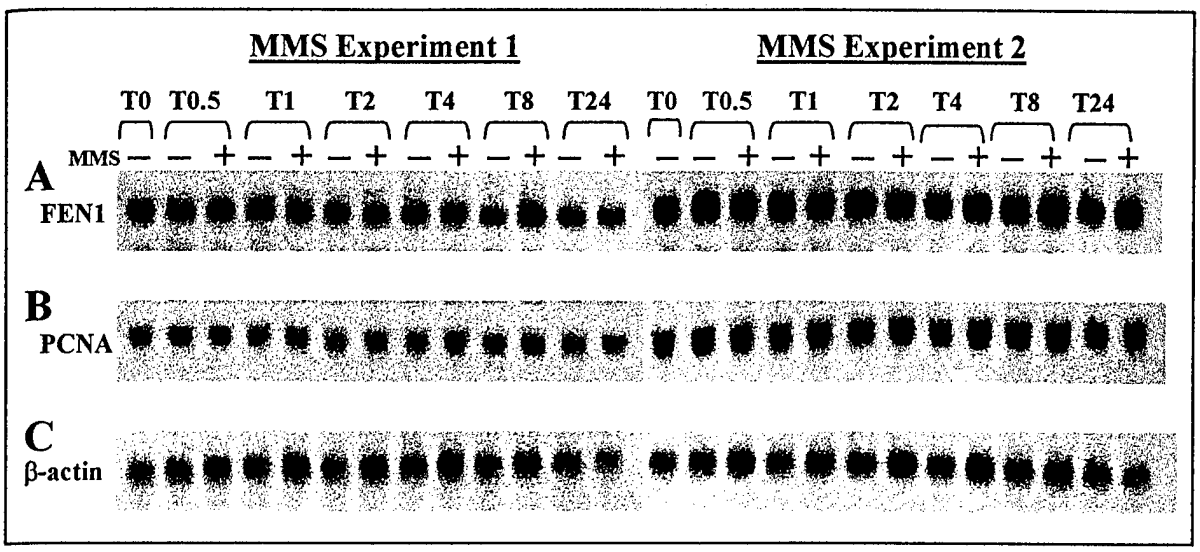

Figure 5-2. Northern blots of human MRC5-SV cells treated with 1 mM MMS detect FEN1, PCNA, and β-actin mRNA. Both 1 mM MMS-treated and non-treated MRC5-SV cells from two independent experiments were harvested at the times indicated, total RNA was extracted, separated on a 1% denaturing gel, and transferred to a nylon membrane. Membranes were subsequently probed with α-[^{32}P] dATP-labeled human FEN1 **(A)**, PCNA **(B)**, and the control β-actin **(C)** cDNA. Individual lanes are labeled to indicate the time of harvest following MMS treatment (T0), and whether cells were treated with 1 mM MMS (+) or control (DMSO only) (-).

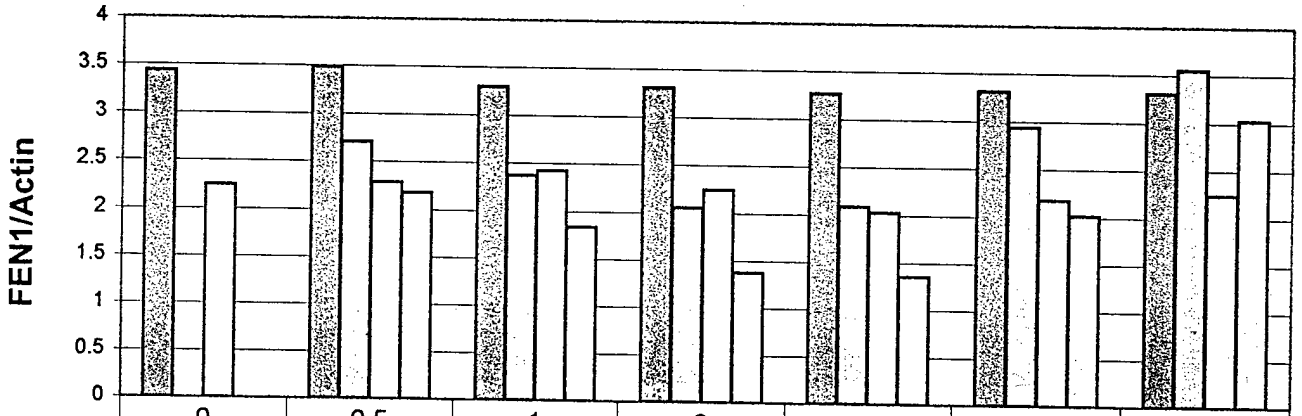

	0	0.5	1	2	4	8	24
Exp 1-untreated	3.44	3.49	3.3	3.31	3.27	3.32	3.31
Exp 1-MMS treated		2.71	2.38	2.06	2.09	2.94	3.56
Exp 2-untreated	2.25	2.29	2.43	2.25	2.03	2.18	2.25
Exp 2-MMS treated		2.18	1.84	1.38	1.36	2.02	3.03

Harvest Times (in hours) following MMS Treatment

Figure 5-3A. Normalized human FEN1 mRNA expression levels in MRC5-SV cells in response to 1 mM MMS treatment. The autoradiograph films from Northern probes depicted in Figure 5-2A & C were subjected to densitometry measurements on a BioRad GS-670 Imaging Densitometer and FEN1 mRNA levels were normalized to account for loading variations detected by the actin cDNA probe. **(A)** The results from two experiments show that FEN1 mRNA levels (in red and light blue) decrease within 30 minutes and continue decreasing up to 4 hours following MMS treatment. FEN1 mRNA levels then increase back to (or above) untreated control levels within 24 hours post-treatment. Asynchronous, non-treated controls (in purple and yellow) show little variation in FEN1 mRNA levels over the 24 hours analysed here. The numbers in the table below the graph are the normalized values of FEN1 mRNA levels obtained from densitometry measurements. The X-axis shows harvest times (in hours) following MMS treatment and the Y-axis depicts relative FEN1 mRNA expression levels (in arbitrary units).

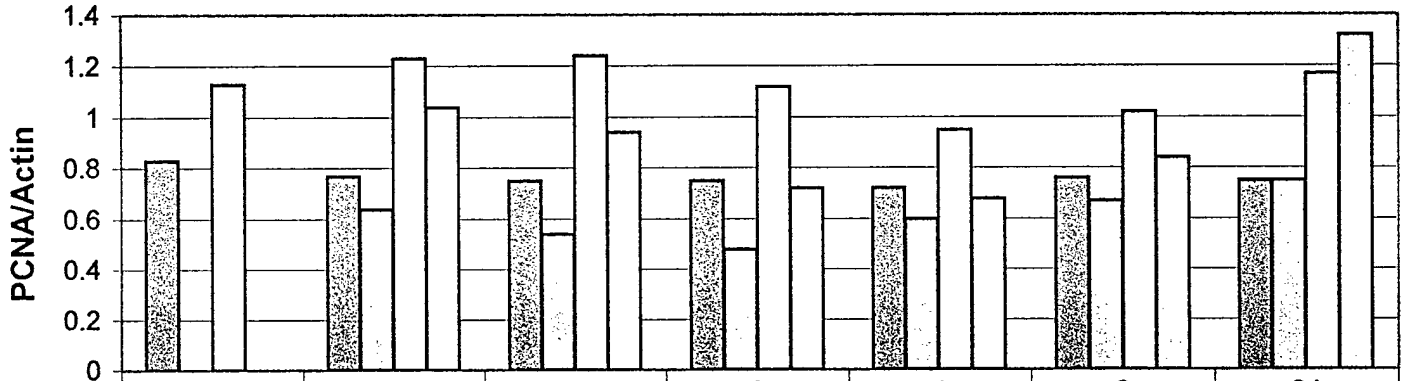

	0	0.5	1	2	4	8	24
Exp 1-untreated	0.83	0.77	0.75	0.75	0.72	0.76	0.75
Exp 1-MMS treated		0.64	0.54	0.48	0.6	0.67	0.75
Exp 2-untreated	1.13	1.23	1.24	1.12	0.95	1.02	1.17
Exp 2-MMS treated		1.04	0.94	0.72	0.68	0.84	1.32

Harvest Times (in hours) following MMS Treatment

Figure 5-3B. Normalized human PCNA mRNA expression levels in MRC5-SV cells in response to 1 mM MMS treatment. The autoradiograph films from Northern probes depicted in Figure 5-2B & C were subjected to densitometry measurements on a BioRad GS-670 Imaging Densitometer and PCNA mRNA levels were normalized to account for loading variations detected by the actin cDNA probe. **(B)** The results from two experiments show that, similar to FEN1 mRNA levels depicted in Figure 5-3A, PCNA mRNA levels (in red and light blue) decrease within 30 minutes and continue decreasing up to between 2-4 hours following MMS treatment. PCNA mRNA levels also subsequently increase back to (or above) untreated control levels within 24 hours post-treatment. Asynchronous, non-treated controls (in purple and yellow) show minor variations in PCNA mRNA levels over the 24 hours analysed here. The numbers in the table below the graph are the normalized values of PCNA mRNA levels obtained from densitometry measurements. The X-axis shows harvest times (in hours) following MMS treatment and the Y-axis depicts relative PCNA mRNA expression levels (in arbitrary units).

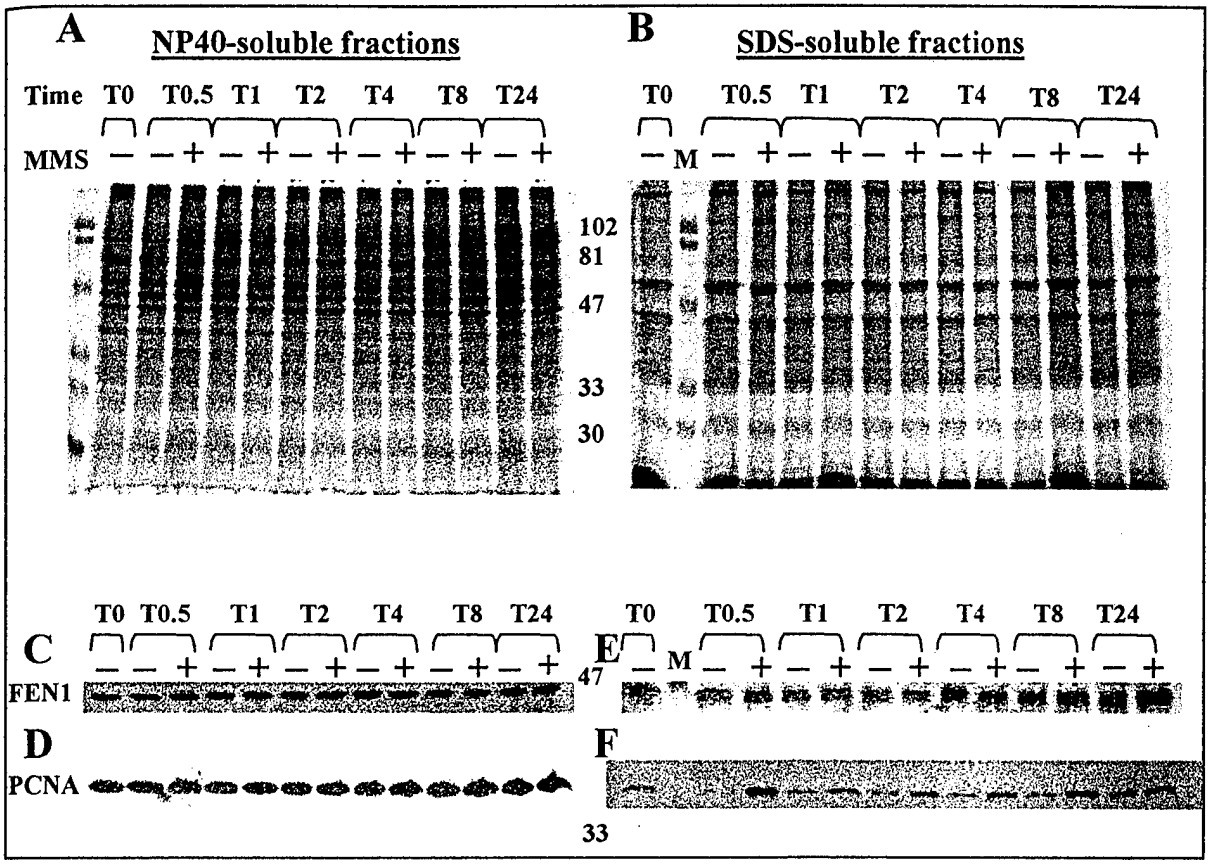

Figure 5-4. Levels of NP40 and SDS-soluble FEN1 and PCNA protein detected on western blots with protein extracted from human MRC5-SV cells treated for one hour with 1 mM MMS. MRC5-SV cells were treated for one hour with 1 mM MMS (in DMSO) and untreated and MMS-treated cells were harvested at 0, 0.5, 1, 2, 4, 8, and 24 hours. NP40-soluble and SDS-soluble protein was extracted, separated by 12% SDS-PAGE, and Coomassie-stained **(A)** and **(B)** or western blotted and probed with anti-Xenopus FEN1 polyclonal antibody (diluted to 1:2000) **(C)** and **(E)**, then anti-PCNA monoclonal antibody PC10 (1:1000) **(D)** and **(F)**. Molecular weight markers sizes (in kDa) are depicted in the centre of the figures. No differences were noted in the levels of soluble FEN1 or PCNA protein between untreated and MMS-treated MRC5-SV cells, nor were any significant changes detected in the levels of insoluble (SDS-extracted) FEN1 protein. In contrast, higher levels of insoluble PCNA protein were detected in virtually all MMS-treated fractions, in comparison to controls treated with DMSO only.

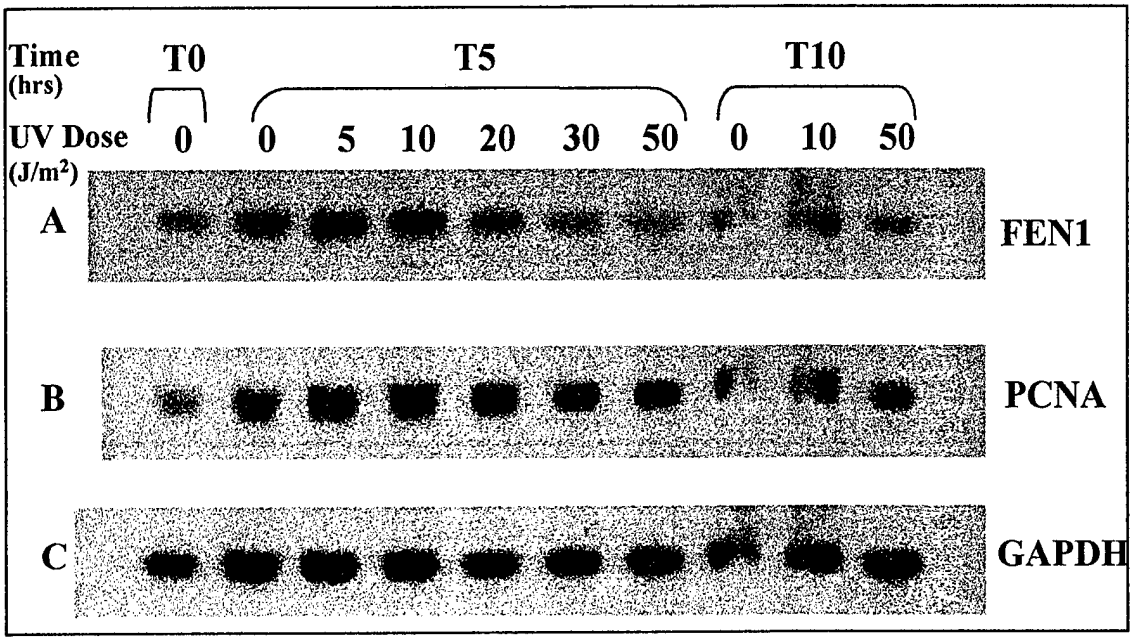

Figure 5-5. Northern blots of human MRC5-SV cells treated with various doses of UV irradiation detect FEN1, PCNA, and GAPDH mRNA. Human MRC5-SV cells were treated with varying doses (5-50 J/m^2) of UV irradiation and both untreated and UV-treated cells were harvested at 5 and 10 hours following treatment. Total RNA was extracted and approximately 15 μg of total RNA from each time-point were separated on a 1% formaldehyde-agarose denaturing gel, Northern blotted, and probed with α-[^{32}P] dATP-labeled human **(A)** FEN1, **(B)** PCNA, and the control **(C)** GAPDH cDNA. The labels above each lane indicate the time of cell harvest after UV irradiation (0, 5, or 10 hours), and the UV dose used (in J/m^2). It appears that both FEN1 and PCNA mRNA levels are slightly increased at non-lethal doses (5 & 10 J/m^2), but decreased at higher doses (20, 30, 50 J/m^2) 5 hours following UV irradiation. Analysis at 10 hours was inconclusive due to unclear RNA bands in the T0-NT and T10-10 J/m^2 fractions, probably due to a bubble in the gel.

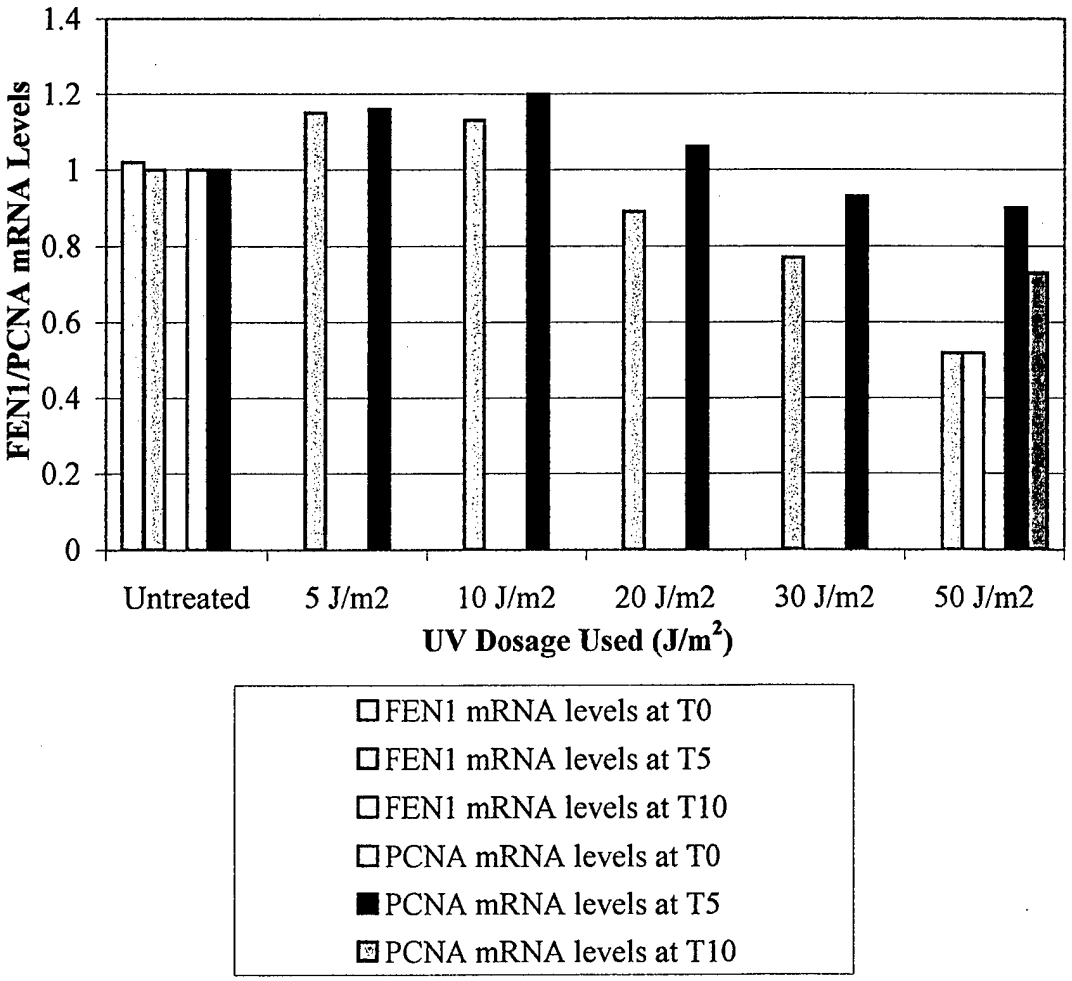

Figure 5-6. Normalized FEN1 and PCNA mRNA levels in human MRC5-SV cells in response to various doses (5-50 J/m^2) of UV irradiation. Autoradiograph films from Northern probes depicted in Figures 5-5A, B, and C were subjected to densitometry measurements on a BioRad GS-670 Imaging Densitometer and FEN1 and PCNA mRNA levels were normalized to account for loading variations detected by the GAPDH cDNA control. The results of this dosage-response experiment show that FEN1 and PCNA mRNA levels appear to slightly increase at 5 and 10 J/m^2, but increasingly decline at higher UV doses (20, 30, and 50 J/m^2, respectively) at 5 hours following UV irradiation. FEN1 and PCNA mRNA levels at 50 J/m^2 remained well below untreated control levels at 10 hours post-UV treatment. mRNA values at 10 hours post-treatment in untreated and 10 J/m^2-treated were omitted due to a bubble in the RNA gel. The X-axis shows UV dosage levels (in J/m^2) and the Y-axis refers to relative FEN1 and PCNA mRNA expression levels (in arbitrary units).

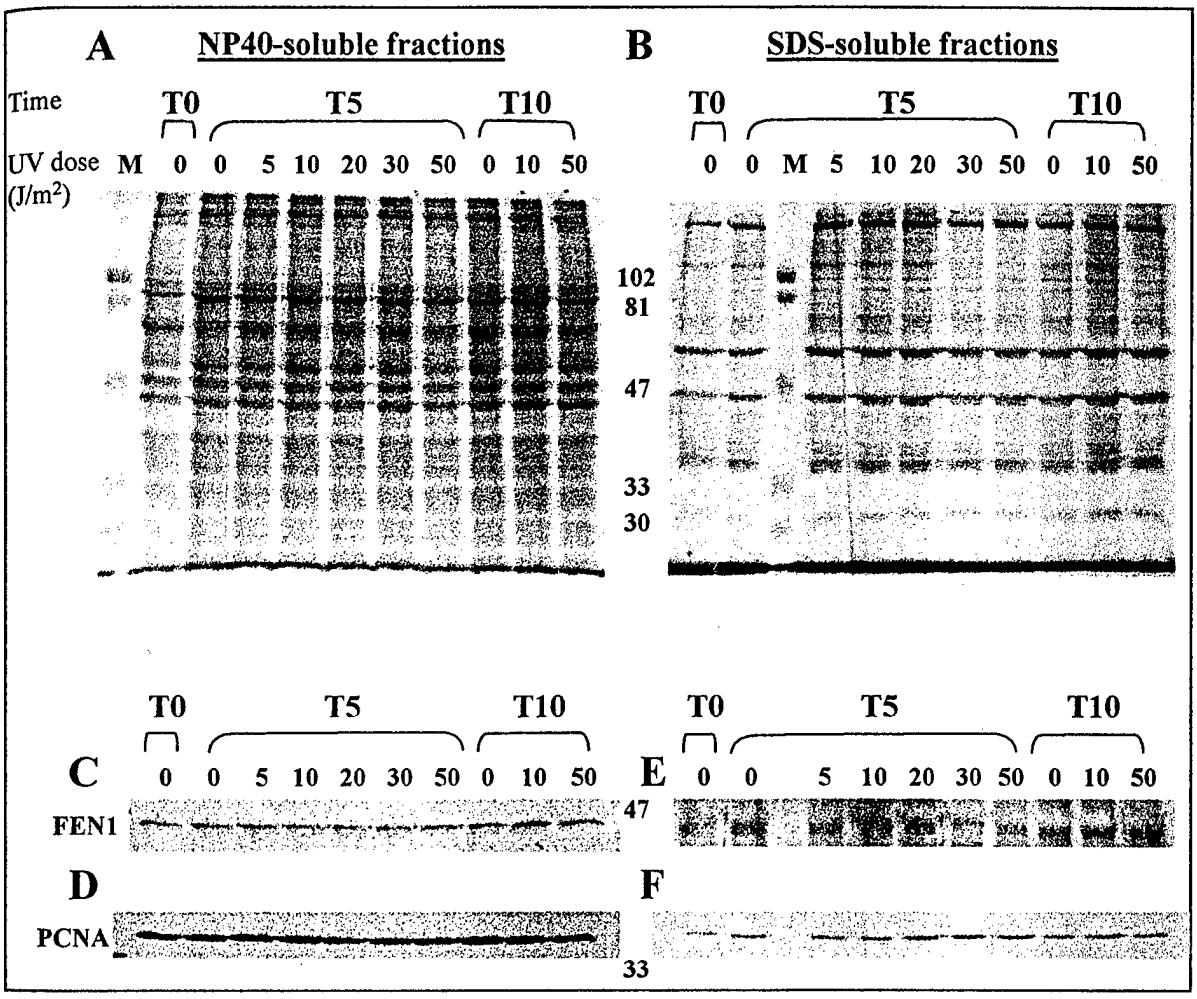

Figure 5-7. Levels of NP40 and SDS-soluble FEN1 and PCNA protein detected on western blots with protein extracted from human MRC5-SV cells treated with various doses (5-50 J/m^2) of UV irradiation. MRC5-SV cells were treated with various doses of UV irradiation (5-50 J/m^2). Untreated and UV-treated cells were harvested at 0, 5, and 10 hours following treatment. NP4- and SDS-soluble protein was extracted, separated by 10% SDS-PAGE, and Coomassie-stained **(A)**, **(B)** or western blotted and probed with anti-Xenopus FEN1 polyclonal antibody (diluted to 1:2000) **(C)** and **(E)** then anti-PCNA monoclonal antibody PC10 (1:1000) **(D)** and **(F)**. Molecular weight marker (M) sizes (in kDa) are indicated in the centre of the figure.

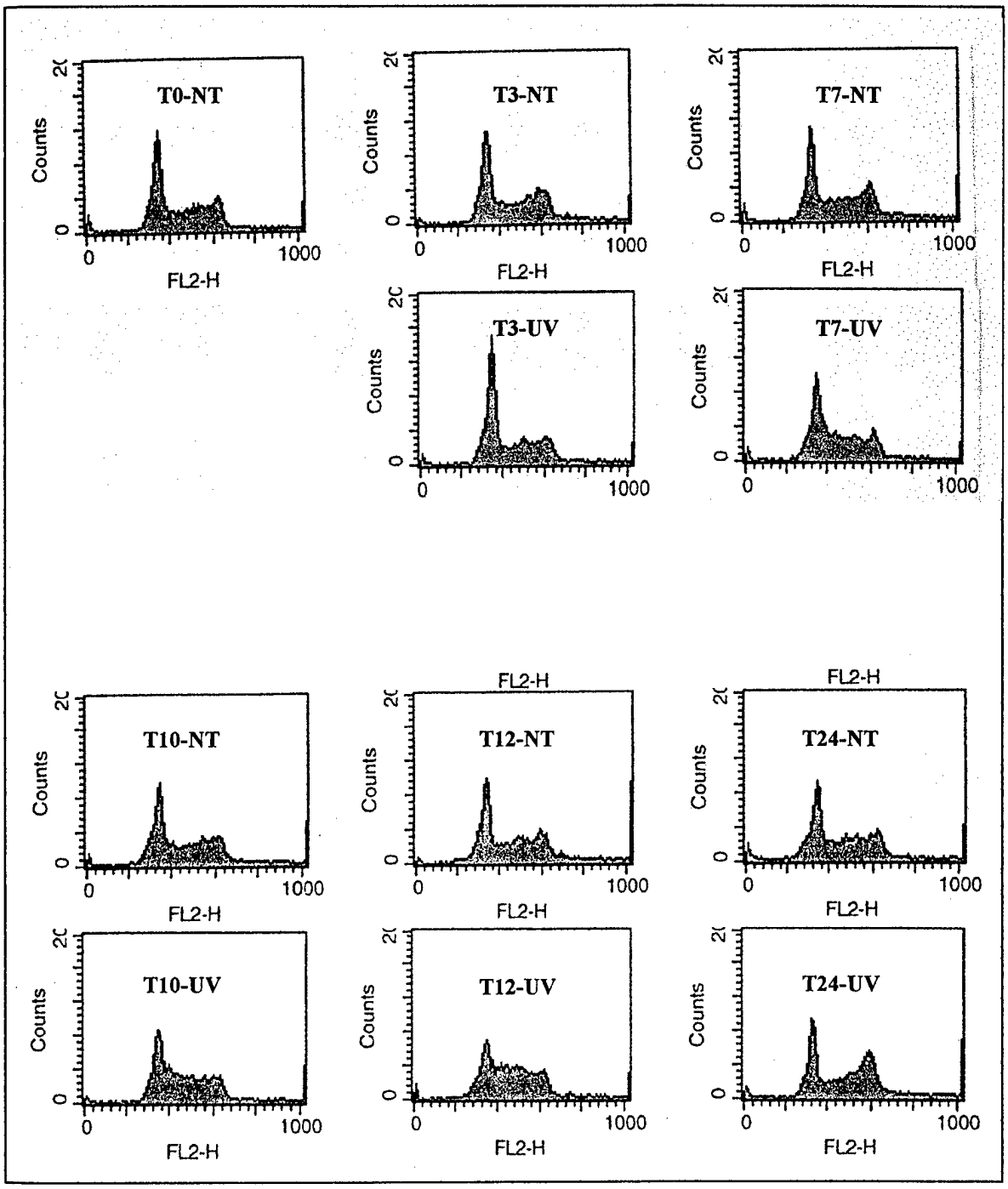

Figure 5-8. FACS analysis of human MRC5-SV cells treated with 10 J/m^2 UV irradiation. Human MRC5-SV cells were treated with 10 J/m2 UV irradiation and harvested at 0, 3, 7, 10, 12, and 24 hours following treatment, along with non-irradiated controls. All cells were methanol-fixed, stained with 25 μg/ml propidium iodide (PI), and analyzed by Cell Quest software (Becton-Dickenson). Labels on the individual FACS profiles above indicate time of harvest following UV treatment (T0-non treated), and whether the cells graphically depicted were UV-treated (UV) or untreated (NT). The X-axis indicates relative fluorescence, measuring PI staining (DNA content), and the Y-axis indicates cell numbers.

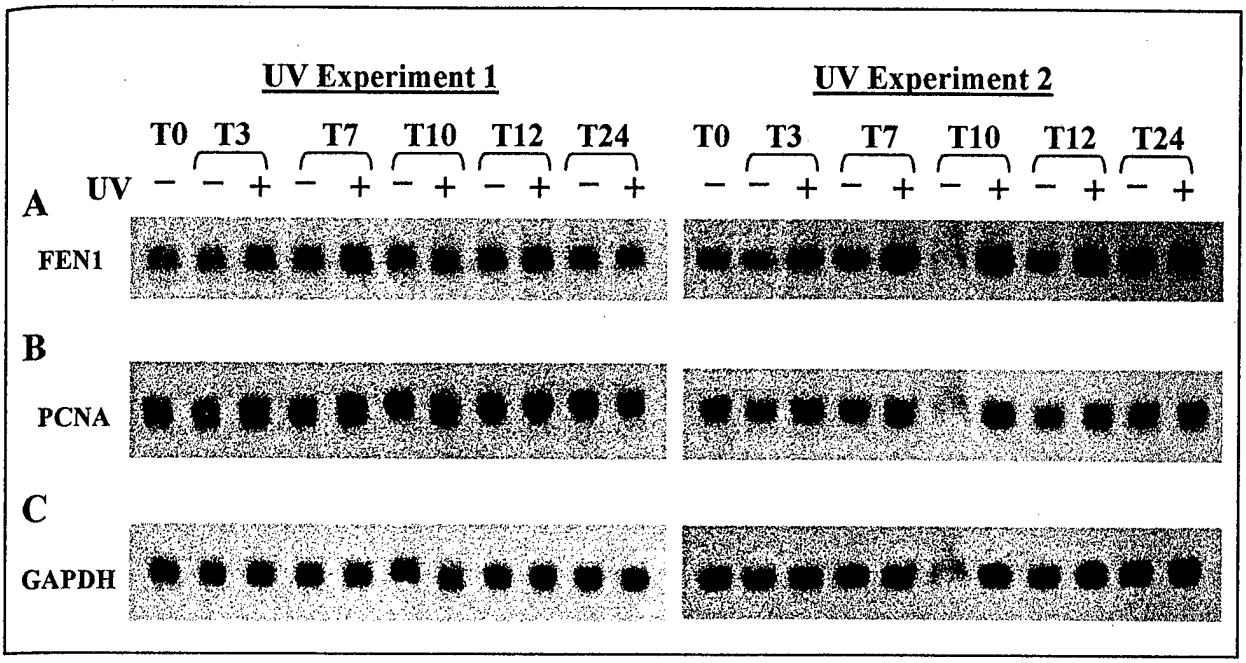

Figure 5-9. Northern blots of human MRC5-SV cells treated with 10 J/m^2 UV irradiation. Both 10 J/m^2 UV-treated and non-treated MRC5-SV cells from two independent experiments were harvested at the times indicated, total RNA was extracted, separated on a 1% denaturing gel, and transferred to a nylon membrane. Membranes were subsequently probed with α-[^{32}P] dATP-labeled **(A)** FEN1, **(B)** PCNA, and the control **(C)** GAPDH cDNA. Individual lanes are labeled to indicate the time (in hours) of harvest following UV-irradiation, and whether RNA was extracted from non-treated (-) or UV-treated (+) cells. The lack of distinct bands in T10 (-) of experiment 2 are thought to be the result of RNA degradation in that sample.

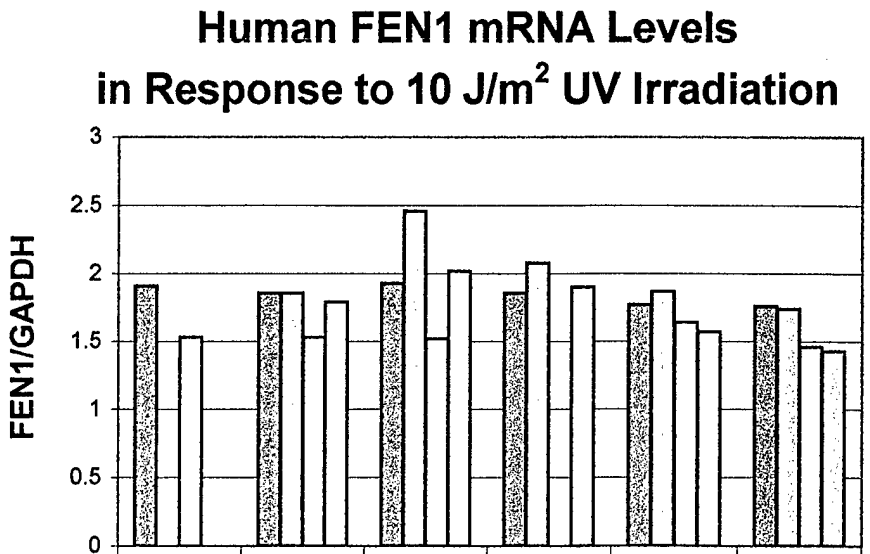

	0	3	7	10	12	24
Exp 1 - untreated	1.91	1.86	1.93	1.86	1.77	1.76
Exp 1 - UV treated		1.86	2.46	2.08	1.87	1.74
Exp 2 - untreated	1.53	1.53	1.52		1.64	1.46
Exp 2 - UV treated		1.79	2.02	1.9	1.57	1.43

Harvest Times (in hours) following UV Irradiation

Figure 5-10A. Normalized FEN1 mRNA levels in human MRC5-SV cells in response to 10 J/m^2 UV irradiation. Autoradiograph films from Northern probes depicted in Figures 5-9A & C were subjected to densitometry measurements on a BioRad GS-670 Imaging Densitometer and FEN1 mRNA levels were normalized to account for loading variations detected by the GAPDH cDNA control probe. The results from the two experiments show that FEN1 mRNA levels (in red and light blue) dramatically increase 7 hours following UV treatment and gradually decrease to untreated control levels (in purple and yellow) by 12 hours and remain at untreated levels 24 hours post-treatment. Non-treated controls (in purple and yellow) show little variation in FEN1 mRNA expression levels over the 24 hours analysed here. The numbers in the table below the graph are the normalized values of FEN1 mRNA expression levels obtained from densitometry measurements. The value for T10-untreated in experiment 2 is omitted due to RNA degradation that prevented densitometry measurements. The X-axis shows non-linear harvest times (in hours) following UV treatment and the Y-axis depicts relative FEN1 mRNA expression levels (in arbitrary units).

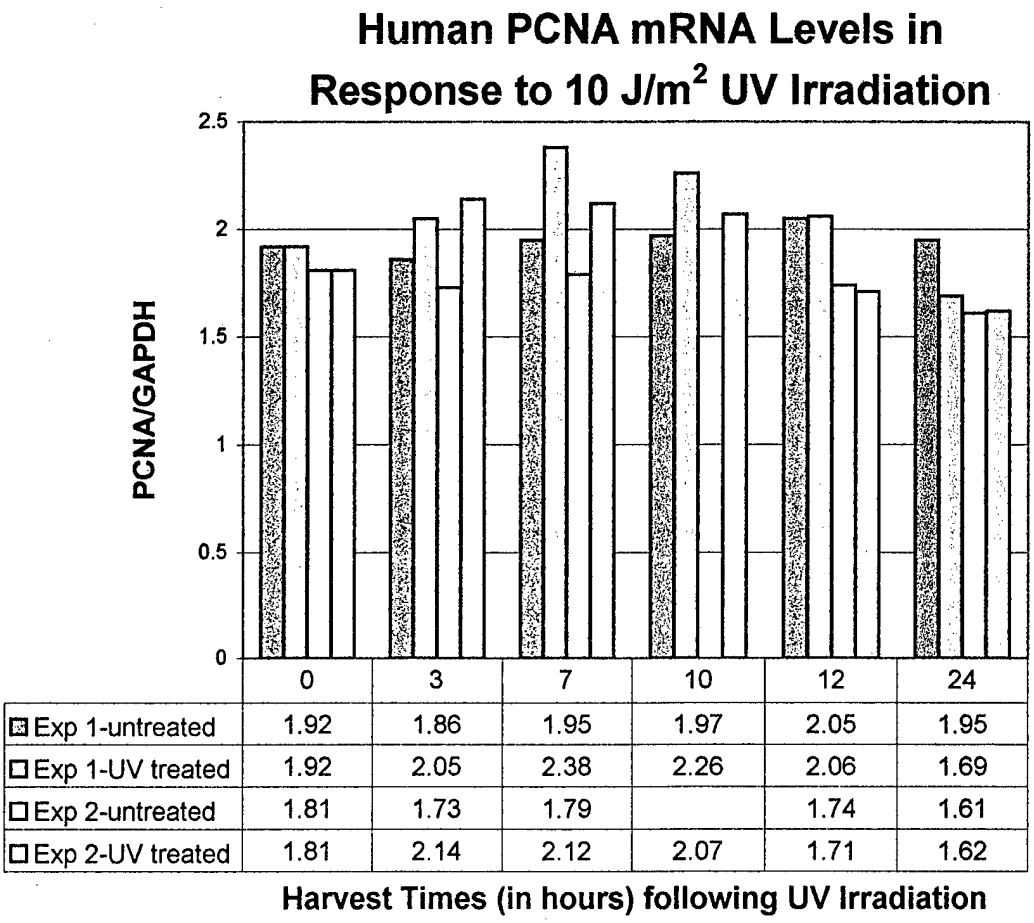

Figure 5-10B: Normalized PCNA mRNA levels in MRC5-SV cells in response to 10 J/m^2 UV irradiation. Autoradiograph films from Northern probes depicted in Figures 5-9B & C were subjected to densitometry measurements on a BioRad GS-670 Imaging Densitometer and PCNA mRNA levels were normalized to account for loading variations detected by the GAPDH cDNA control probe. The results from two independent experiments show that PCNA mRNA levels (in red and light blue) are increased by 3 hours, peak around 7 hours, and subsequently decrease to untreated control levels (in purple and yellow) by 24 hours in response to 10 J/m2 UV irradiation. Non-treated controls (in purple and yellow) show little variation in PCNA mRNA expression levels over the 24 hours analysed here. The numbers in the table below the graph are the normalized values of PCNA mRNA expression levels obtained from densitometry measurements. The value for T10-untreated in experiment 2 is omitted due to RNA degradation that prevented densitometry measurements. The X-axis shows harvest times (in hours) following UV treatment and the Y-axis depicts relative PCNA mRNA expression levels (in arbitrary units).

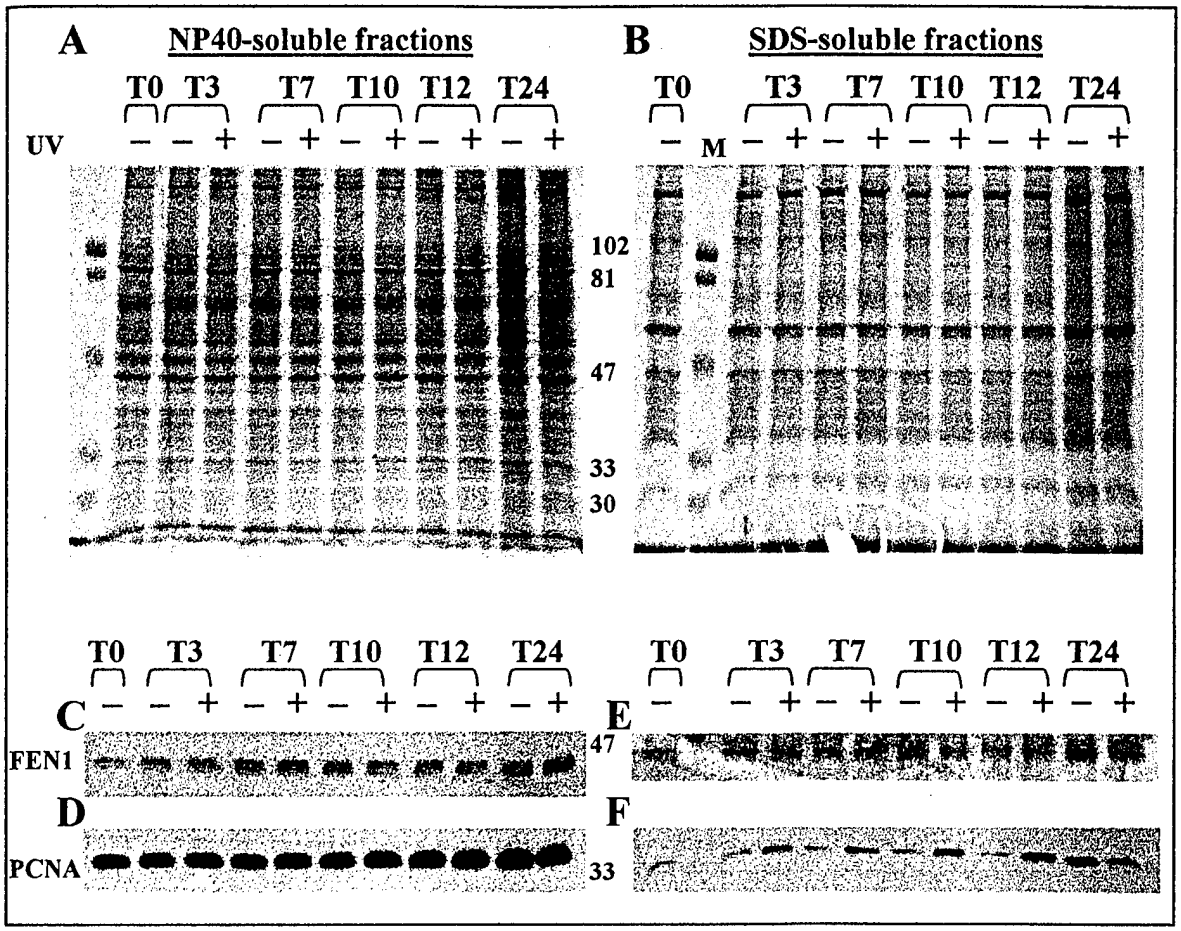

Figure 5-11. Levels of NP40 and SDS-soluble FEN1 and PCNA protein detected on western blots with protein extracted from human MRC5-SV cells treated with 10 J/m^2 UV irradiation. MRC5-SV cells were treated with 10 J/m^2 UV irradiation, UV-treated (+) and non-treated (-) cells were harvested, NP40-soluble and SDS-soluble protein extracted, separated by 10% SDS-PAGE, and Coomassie-stained **(A)**, **(B)** or western blotted, and probed with anti-Xenopus FEN1 polyclonal antibody (1:2000) **(C)** and **(E)**, then anti-PCNA monoclonal antibody PC10 (1:1000) **(D)** and **(F)**. Molecular weight markers (in kDa) are indicated in the centre of the figures (M).

CHAPTER SIX: ANALYSIS OF THE HUMAN *FEN1* GENE AND PROMOTER REGION

6-1: Introduction

In the preceding chapters of this thesis, I have shown that the human *FEN1* gene may be expressed in a cell cycle-regulated manner since FEN1 mRNA levels increase as cells approach S phase. A logical extension of this analysis is to examine the genomic *FEN1* coding sequence and promoter region, and eventually identify DNA sequences essential for cell cycle-regulation of expression. Until recently, only the cDNA sequence was available and it has been extensively examined (Robins *et al.*, 1994; Harrington & Lieber, 1994, 1995; Shen *et al.*, 1996, 1997, 1998) in regard to functional and putative interactive domains in the encoded protein sequence. Now that the genomic sequence, that encompasses the human *FEN1* gene, has been released as part of the Human Genome Project (Lamerdin *et al.*, unpublished, 1998), the promoter region and regulation of FEN1 gene expression can be analyzed. In this chapter, I examine expression of human FEN1 mRNA transcripts in various human tissues and several different human cell lines. I then use computer programs optimized for DNA sequence analysis to propose putative regulatory elements and transcriptional start sites for human *FEN1*. Due to time constraints, a more detailed analysis of the human *FEN1* promoter and putative regulatory sequences was not possible here. Instead, the purpose of this analysis is to provide a starting point for future research that will examine human *FEN1* gene regulation during the cell cycle and in response to DNA damage.

6-2: Results

6-2.1: Examination of human FEN1 mRNA levels in multiple human tissues

Having previously shown (Chapter 4) that human FEN1 mRNA is elevated in proliferating cells as they approach S phase, I asked here whether human FEN1 mRNA expression varied in different human tissues with varying proliferative and metabolic rates. Specifically, I wanted to examine FEN1 mRNA expression in various cell types to see if there is any distinctive tissue-specific pattern of expression, and to compare its expression with other well-characterized human genes, such as *PCNA*.

Approximately 2μg of polyA+ mRNA from each of 12 different human tissue types were separated by denaturing gel electrophoresis and transferred to nylon membrane (Multiple Choice™, Origene Technologies, Inc.). The 12 different tissue types examined include brain, heart, kidney, spleen, liver, colon, lung, small intestine, muscle, stomach, testis, and placenta. In addition, Northern blots also contained RNA size markers (RNA Millenium markers, Ambion), that were run in parallel with the samples, and are indicated on the membranes.

Northern blots were initially probed with [α-^{32}P] dATP-labeled human FEN1 cDNA (See Methods & Materials). As can be seen in Figure 6-1A, FEN1 mRNA expression was not detectable in all human tissue types. The highest level of detected FEN1 mRNA was noted in the small intestine, with lesser amounts detected in testis, lung, and muscle, respectively. Very long exposure times (10 days) detected extremely low levels of expression in the brain, heart, placenta, and possibly colon (data not shown), but no expression was detected in the kidney, spleen, liver, and stomach. Although it appears in Figure 6-1 that considerable FEN1 mRNA was detected in

placenta tissue, the majority of that signal can be attributed to background, and not actual mRNA. It should also be noted that the size of FEN1 transcripts detected here were approximately 2.2-2.3 kb, in comparison to the RNA size markers on the blots. This agrees with previous estimates (Chapters 4 and 5) of human FEN1 transcript size, in comparison to other known (eg. 18S rRNA, PCNA, GAPDH) mRNA sizes.

Figure 6-1 showing Multiple choice blots probed w/ FEN1, PCNA, GAPDH, Actin

Because I have demonstrated that human FEN1 mRNA expression appears to mirror PCNA mRNA expression patterns in synchronized HeLa and MRC5 cells (Chapter 4), I next compared FEN1 and PCNA mRNA expression on these same blots. After briefly stripping of other cDNA probes, the membranes were pre-hybridized and re-probed with [α-^{32}P] dATP-labeled human PCNA cDNA (See Methods and Materials). As can be seen in Figure 6-1B, human PCNA mRNA expression is similar to FEN1 mRNA expression levels in the various tissues. The highest level of expression was noted in the small intestine, with lesser amounts detected in testis, lung, and muscle, respectively. Very long exposure times revealed extremely low levels of expression in the placenta, brain, heart, and colon; but unlike FEN1, after long exposure times very low levels of PCNA mRNA expression were also detected in kidney, spleen, and liver (data not shown). In addition, and similar to FEN1, no PCNA expression was noted in stomach tissue. The putative PCNA mRNA band in Figure 6-1 is thought to be non-specific background probe not efficiently removed during the wash steps.

In general, it can be stated that where the highest levels of FEN1 and PCNA expression levels in the various tissues were detected (small intestine, lung, testis, and muscle), FEN1 and PCNA mRNA expression levels appeared quite similar. It should also be noted that PCNA expression may be slightly more ubiquitous than FEN1. This may reflect PCNA's well-documented role in several DNA damage repair mechanisms (Shivji *et al.*, 1992; Frosina *et al.*, 1996; Umar *et al.*, 1996) that have not yet been demonstrated for FEN1. However, the apparent similarities of FEN1 and PCNA expression patterns observed here may be simply indicative of the proliferative state of the cells in tissues examined.

To control for variation in mRNA loading on the tissue blots, membranes were also probed with [α-^{32}P] dATP-labeled human GAPDH (Figure 6-1C) and [^{32}P] dATP-labeled β-actin (Figure 6-1D) cDNA control probes. Interestingly, GAPDH expression was detected in all tissue types, but to varying degrees. Highest GAPDH expression was detected in muscle, followed by small intestine, testis, heart, brain, lung, liver, and colon. Lower levels of expression were noted in placenta, spleen, kidney, and stomach. Because of the essential role of GAPDH protein in cellular metabolism (Alberts *et al.*, 1994), the differences in expression level may simply reflect the metabolic state of cells in the various tissues examined. Although GAPDH may serve as a proper cell cycle-independent control for total RNA expression level estimation when examining samples from the same cell line, it appears that it may not be a valid control when comparing different cell types with varying metabolic rates.

Surprisingly, the β-actin cDNA control probe (Figure 6-1D) also revealed significant differences in actin mRNA detected in the various tissues. This was

unexpected, in that actin expression is thought not to be directly dependent on the metabolic or proliferative state of cells and is ubiquitously expressed in most cell types previously examined. In addition, the actin probe detected two different mRNA species among the various tissues. The expected 2.2-2.3 kb β-actin mRNA transcript was detected in all tissue types examined, but an additional 1.7-1.8 kb transcript was also detected in heart, colon, lung, small intestine, and muscle. The smaller (1.7-1.8 kb) transcript is most probably the result of non-specific cDNA probe hybridization to α-actin, since α-actin is the predominant species of actin found in muscle cells, and it shares considerable sequence identity with β-actin (Alberts *et al.*, 1994). Overall, assuming that the total level of actin mRNA expression indicates relative mRNA loading, it appears that the highest amounts of polyA+ mRNA were contained in muscle, small intestine, lung, heart, spleen, placenta, colon, testis, stomach, liver, brain, and kidney, respectively.

Because it appears that unequal amounts of polyA+ mRNA from the various types of human tissue were loaded, a direct comparison of human FEN1 mRNA expression levels in the different tissues would be inconclusive. Instead, a comparison between FEN1 and PCNA mRNA expression levels (Figures 6-1A & B) suggests that the two genes may be expressed similarly within the 12 different human tissues examined here, although PCNA mRNA expression appears slightly more ubiquitous. Additionally, the low levels, or absence of, FEN1 mRNA expression in certain types of human tissue (eg. spleen, stomach, and kidney) may simply reflect low concentrations of total mRNA present in those samples, and not reflect tissue-specific differences in the expression levels of those genes.

6-2.2: Comparison of Human *FEN1* cDNA and Genomic DNA Sequences

After analyzing human *FEN1* expression in various human tissues, I next wanted to examine the human *FEN1* cDNA and genomic DNA sequences. The human FEN1 cDNA sequence was originally obtained through RT-PCR amplification of HeLa cell polyA$^+$ RNA using primers derived from conserved regions of the *FEN1* homologue, *S. pombe rad2* gene (Murray *et al.*, 1994). It was subsequently cloned again during screening of a human leukemic T-cell cDNA phage library (Hiraoka *et al.*, 1995). Only one cDNA sequence (Murray *et al.*, 1994) contains sequence information 5' and 3' to the consensus coding region. Early analysis of HeLa cell mRNA described "moderate expression" of human FEN1 mRNA with a single transcript size of approximately 2.0 kb detected by FEN1 cDNA probes of Northern blots (Murray *et al.*, 1994). However, since that publication, there has been no further information concerning human FEN1 mRNA expression, nor have any analyses of genomic DNA promoter and coding regions been published.

In 1998, as part of the human genome project (Joint Genome Institute, Lawrence Livermore National Laboratory, USA), the genomic DNA sequence of clone CIT-HSP-311e8 from chromosome 11 was made available (Lamerdin *et al.*, accession number AC004770, unpublished, 1998). This 185 kb sequence contained the genomic DNA sequence of human *FEN1*. In addition, it verified previous results (Hiraoka *et al.*, 1995) which localised the human *FEN1* gene to chromosome 11q12 using fluorescent in situ hybridization (FISH).

Figure 6-2A/B/C/D showing genomic and cDNA sequences

Figure 6-2A shows the original human FEN1 cDNA sequence published by Murray *et al.* (1994) and Figure 6-2B depicts the genomic DNA sequence from chromosome 11 that was recently made available (Lamerdin *et al.*, unpublished). Interestingly, in comparing the genomic and cDNA sequences, it becomes evident that the human *FEN1* gene contains no introns. Although not unprecedented, coding genes containing no introns are not common in higher eukaryotes (Singer and Berg, 1991). The predicted 1140 base pair (bp) coding sequence from genomic DNA is identical to the cDNA sequence reported previously (Murray *et al.*, 1994; Hiraoka *et al.*, 1995). In addition, although the 3' untranslated region (UTR) shows only three minor discrepancies between the cDNA and genomic DNA sequences (highlighted in Figures 6-2A, B), there are significant differences in the 5' UTRs reported (Figures 6-2C, 6-2D). Only the 23 bases immediately 5' to the translational start site (ATG) are identical between the cDNA (Figure 6-2C) and genomic (Figure 6-2D) sequences. Upstream (5') of those 23 bases, there are no similarities between the two sequences. This suggests that one of these sequences is in error.

Because the original cDNA sequence (Murray *et al.*, 1994) was obtained by using FEN1 cDNA, derived from RT-PCR of HeLa cell polyA+ mRNA to probe a pDR2 human cDNA library, it is quite possible that sequences 5' to the coding region have been lost or modified during library construction and amplification. However, it is unclear as to why the 3' UTR sequences are nearly identical and the 5' sequences so dissimilar. In addition, Murray *et al.* (1994) suggested that their entire published cDNA sequence was

accurate, based on a single class of 2.0 kb mRNA transcripts detected using human FEN1 cDNA probes on Northern blots of total human RNA. However, my results suggest that human FEN1 mRNA transcripts are larger than 2.0 kb.

During this work, I have investigated FEN1 mRNA expression in HeLa, primary MRC-5, SV40-transformed MRC5 cells, and mRNA derived from multiple human tissues in order to investigate the size and expression patterns of human FEN1 mRNA under different cell cycle (Chapter 4) and repair (Chapter 5) conditions, and in different human tissues (Figure 6-1). In the study of human *FEN1* expression during DNA replication (Chapter 4) and repair (Chapter 5), 28S and 18S ribosomal RNA bands were used as relative size markers. Although it is difficult to ascertain exact transcript size based on a comparison with either the rRNA bands or the other mRNA bands examined (PCNA, GAPDH), it appeared that human FEN1 mRNA transcripts may be larger than the 2.0 kb originally estimated (Murray *et al.*, 1994). Multiple human tissue blots (Multiple Choice™, Origene Technologies, Inc.) are supplied with RNA markers (RNA Millenium markers, Ambion) shown to be accurate indicators of transcript size (Ambion , 1998). When Northern blots from multiple human tissues were probed with [α-^{32}P] dATP-labeled human FEN1 cDNA (Figure 6-1A), it appeared that human FEN1 transcripts were approximately 2.2-2.3 kb, based on a comparison with the RNA size markers. This single transcript size is similar in the various tissues where FEN1 expression was detected, indicating that FEN1 is most probably not alternatively spliced in the different cell types examined, nor are poly-adenylation sequence lengths significantly different. These results suggest that human FEN1 mRNA transcripts may be approximately 2.2-2.3 kb in length.

6-2.3: Prediction of Human *FEN1* Promoter Regions

To further investigate the disparity between reported (Murray *et al.*, 1994) and observed (Figure 6-1A) human FEN1 mRNA transcript length, I next examined the genomic *FEN1* sequence to identify putative transcriptional start sites (TSS). Promoter Prediction by Neural Network (NNPP: Reese, 1994, Reese & Eeckman, 1995; Reese *et al.*, 1996) is a method that can identify putative eukaryotic promoters and transcriptional start sites in genomic DNA sequences. Based on a careful 4-fold cross-validation test on 429 eukaryotic RNA Polymerase II (RNA Pol II) promoters (Bucher & Trifonov, 1986; Bucher, 1989) from the Eukaryotic Promoter Database (EPD, version 50) and on 305 unrelated genes where the false positive rate was less than 1%, 1300 bases 5' to the translational start site of the human *FEN1* genomic sequence were input and analyzed.

Table 6-1 putative Transcriptional Start Sites from NNPP

Three different putative 51-bp transcriptional start sites were identified (Table 6-1) by NNPP. Referring to Table 6-1, the first predicted transcriptional start site is located approximately 950 bp prior to the translational start codon (ATG) and would result in a mRNA transcript size of approximately 2.85 kb. The second predicted transcriptional start site is located approximately 700 bp prior to the translational start site, and would result in a 2.6 kb mRNA transcript size. Both these putative TSS would result in human FEN1 mRNA transcripts significantly larger than observed previously (2.0 kb, Murray *et al.*, 1994), and in current investigations (Chapter 4, 5, Figure 6-1A). Interestingly, using

the third NNPP-predicted transcriptional start site [-306 nt to the ATG start codon (+1)], and assuming that transcription terminates approximately 30-40 nucleotides downstream of the poly-adenylation signal (AAUAAA) (Birnstiel *et al.*, 1985) in the human FEN1 3' UTR (seen in both cDNA and genomic sequences, Figures 6-2A & B), the predicted human FEN1 mRNA transcript size is approximately 2.2 kb. This size is in agreement with human FEN1 transcript sizes observed here (Figure 6-1A), but only slightly larger than the 2.0 kb transcript estimated by Murray *et al.* (1994). Based on these observations, I propose that human FEN1 mRNA transcripts are approximately 2.2 kb. However, further studies, such as RT-PCR of extracted human mRNA using primers 5' and 3' of the proposed TSS, are necessary to validate the proposed human FEN1 transcriptional start site and mRNA transcript size.

6-2.4: Analysis of the Human *FEN1* Putative Promoter Region

Now that the human *FEN1* genomic sequence is available (Lemardin *et al.*, 1998, unpublished), I wanted to briefly examine the promoter region and identify putative sequences that may regulate its expression. Because FEN1 mRNA expression exhibited numerous similarities to PCNA mRNA expression in synchronized cell populations in response to serum stimulation (MRC-5), and during cell cycle progression from early G_1 towards S phase (HeLa, MRC-5; Chapter 4, Figures 4-2, 4-11), putative FEN1 regulatory elements were identified (Table 6-2) that display sequence similarities to published *PCNA* promoter sequences. In addition, the computer program, PROMOTER SCAN (Prestridge, Advanced Biosciences Computing Center, University of Minnesota), was also used to predict putative RNA Pol II promoter sequences contained in the region

approximately 1.3 kb upstream (5') of the human *FEN1* gene. This program was developed to recognize a high percentage of RNA Pol II promoter sequences, while allowing only a low rate (less than 1%) of false positives. Although neither conclusive nor comprehensive, the algorithm used by this program utilizes more than 2000 individual binding sites that have been described (Ghosh, 1993) and obtained from the eukaryotic promoter and GenBank sequence databases to identify putative promoter sequences using transcription factor binding sites. Table 6-2 summarizes the results of the human *FEN1* promoter analysis using this program, as well as comparisons to published *PCNA* promoter sequences, with the genomic DNA sequence 5' (proximal) to the human *FEN1* gene.

Table 6-2 showing results of promoter study

It should be noted that this analysis assumes that the genomic sequence used here is absolutely correct and without error. It is quite possible that minor sequence variations or errors are contained in the genomic sequence, possibly due to PCR amplification and/or sequencing analysis ambiguities. For that reason, some degenerative sequences are included among the putative regulatory sequences outlined in Table 6-2.

Table 6-2 shows that the human *FEN1* gene possesses several putative regulatory elements also contained in the *PCNA* gene. The presence of putative CAAT boxes, SP1, cAMP-response elements (CREs), AP1, AP2, AP3, and AP4 sites, some of which have been shown to regulate PCNA mRNA expression in response to mitogenic stimulation (reviewed by Baserga, 1991), suggests that human *FEN1* may possibly be regulated by

similar mechanisms. In contrast, although *PCNA* lacks a canonical TATA box (Travili *et al.*, 1989), six different putative *FEN1* TATA elements were identified (Table 6-2). Interestingly, the putative TATA element at –297 was also identified and used by the NNNP promoter prediction (Reese, 1994) to predict the proposed TSS for human *FEN1* (Table 6-1).

Further comparisons between the FEN1 and PCNA promoter sequences suggest that there are likely to be additional differences between human FEN1 and PCNA transcriptional regulation. Firstly, although the human *FEN1* gene contains no introns, the *PCNA* gene contains negative regulatory elements in intron 1 (Alder *et al.*, 1992) and intron 4 (Ottavio *et al.*, 1990). Secondly, the *PCNA* promoter contains a p53 consensus binding site (El-Deiry *et al.*, 1992) that leads to transcriptional activation of PCNA mRNA expression by low levels of wild-type p53 protein (Shivakumar *et al.*, 1995). Analysis of the 1300 bases 5' to the human *FEN1* ORF shows no putative p53 binding sites. It is possible that p53 activation of *PCNA* expression leads to PCNA protein's participation in various DNA repair mechanisms (Shivji *et al.*, 1992; Frosina *et al.*, 1996; Umar *et al.*, 1996).

Although this brief analysis highlights major similarities and differences between the human *FEN1* and *PCNA* promoter sequences, further studies are necessary to test these observations. Transfections of human cell lines with reporter constructs, containing various regions of the human *FEN1* 5' UTR, may help elucidate genomic sequences critical to regulated *FEN1* gene expression, as well as determine if FEN1's mRNA expression pattern is regulated similarly to PCNA. Lastly, extensive sequencing of

genomic DNA proximal to the human FEN1 gene will be necessary to both validate the original genomic sequence and further examine putative regulatory elements.

6-3: Conclusions

A role for human FEN1 protein has been proposed in DNA replication (Ishimi *et al.*, 1988; Goulian *et al.*, 1990; Turchi and Bambara, 1993; Waga *et al., 1994)* and DNA repair (Matsumoto *et al.*, 1994, 1998; Frosina *et al.*, 1996; Klungland and Lindahl, 1997). I have demonstrated that human FEN1 mRNA levels increase as HeLa cells progress from early G_1 towards S phase of the cell cycle (Chapter 4, Section 4-2.3) and when MRC-5 cells are serum-stimulated to proliferate (Chapter 4, Section 4-2.9). Additionally, results in Chapter 5 suggest that FEN1 mRNA levels decrease when asynchronous human MRC5-SV culture cells experience DNA damage caused by UV light or alkylating agents that results in cell cycle arrest. Because similar mRNA expression patterns were observed when PCNA mRNA levels were analyzed in parallel (Chapters 4,5), it is possible that human *FEN1* and *PCNA* gene expression may be regulated by similar mechanisms. Based on that premise, I examined FEN1 and PCNA mRNA levels in various human tissues. It appeared that FEN1 and PCNA mRNA levels were similar among the various tissues studied (Figures 6-1A, 6-1B), although PCNA mRNA may be slightly more ubiquitously expressed. Additionally, a comparison of the human *FEN1* and *PCNA* promoter regions (Table 6-2) revealed numerous similarities between the sequences. It is possible that transcriptional regulatory elements (TREs) in the *PCNA* promoter and similar putative elements in the *FEN1* promoter are controlled by the same

cell cycle-dependent mechanisms. Further studies are necessary to examine the actual *FEN1* TREs that govern its expression during the cell cycle.

A comparison of the human *FEN1* genomic sequence (Figure 6-2B, Lamerdin *et al.*, 1998) with the cDNA sequence (Figure 6-2A, Murray *et al.*, 1994) revealed that the human FEN1 gene contains no introns. Additionally, although the coding sequences are identical and only three minor discrepancies exist between the 3' UTR of genomic and cDNA sequences, significant differences are noted in the 5' UTRs (compare Figures 6-2C, 6-2D). This suggested that one of the 5' UTR sequences were in error, and I propose that it is the cDNA 5' UTR sequence (Murray *et al.*, 1994) that is incorrect.

This proposal is based on several observations. Firstly, the human *FEN1* cDNA sequence was obtained by RT-PCR of HeLa cell polyA+ mRNA to probe a pDR2 human cDNA library. It is quite possible that sequences 5' to the coding region were lost or modified during library construction or amplification. Secondly, the cDNA sequence was postulated to be correct based on approximately 2.0 kb FEN1 mRNA transcripts observed on Northern blots of total human RNA. Studies of human FEN1 mRNA levels in synchronized HeLa and MRC-5 cells (Chapter 4), and using 28S and 18S rRNA bands as relative size markers suggested that human FEN1 mRNA transcripts were slightly larger than 2.0 kb. Further investigations of FEN1 mRNA levels in different human tissues, using RNA markers run in parallel, shows that FEN1 mRNA transcripts are approximately 2.2-2.3 kb in size (Figure 6-1A). Lastly, analysis of 1300 bases from the genomic DNA sequence, 5' to the FEN1 coding region, by NNPP (Reese, 1994; Reese & Eeckman, 1995; Reese *et al.*, 1996) identifies three putative transcriptional start sites (TSS) for human *FEN1* (Table 6-1). Although two of the putative FEN1 TSS would

result in transcripts much larger than previously observed (Chapter 4,5; Murray *et al.*, 1994), the third NNPP-predicted TSS at -306 would result in human *FEN1* transcript sizes of approximately 2.2-2.3 kb. This is in agreement to what I observed here (Figure 6-1A, Chapter 4,5) and slightly larger than proposed originally by Murray *et al.* (1994).

In the future it will be interesting to see if transcriptional regulation of *FEN1* is similar to *PCNA*. Extensive sequencing of the human *FEN1* 5' UTR region and subsequent examination of putative TREs using reporter constructs will be necessary to test the observations reported here. It is thought that this initial analysis of the *FEN1* promoter region may be of use in future research into the regulation of the human *FEN1* gene.

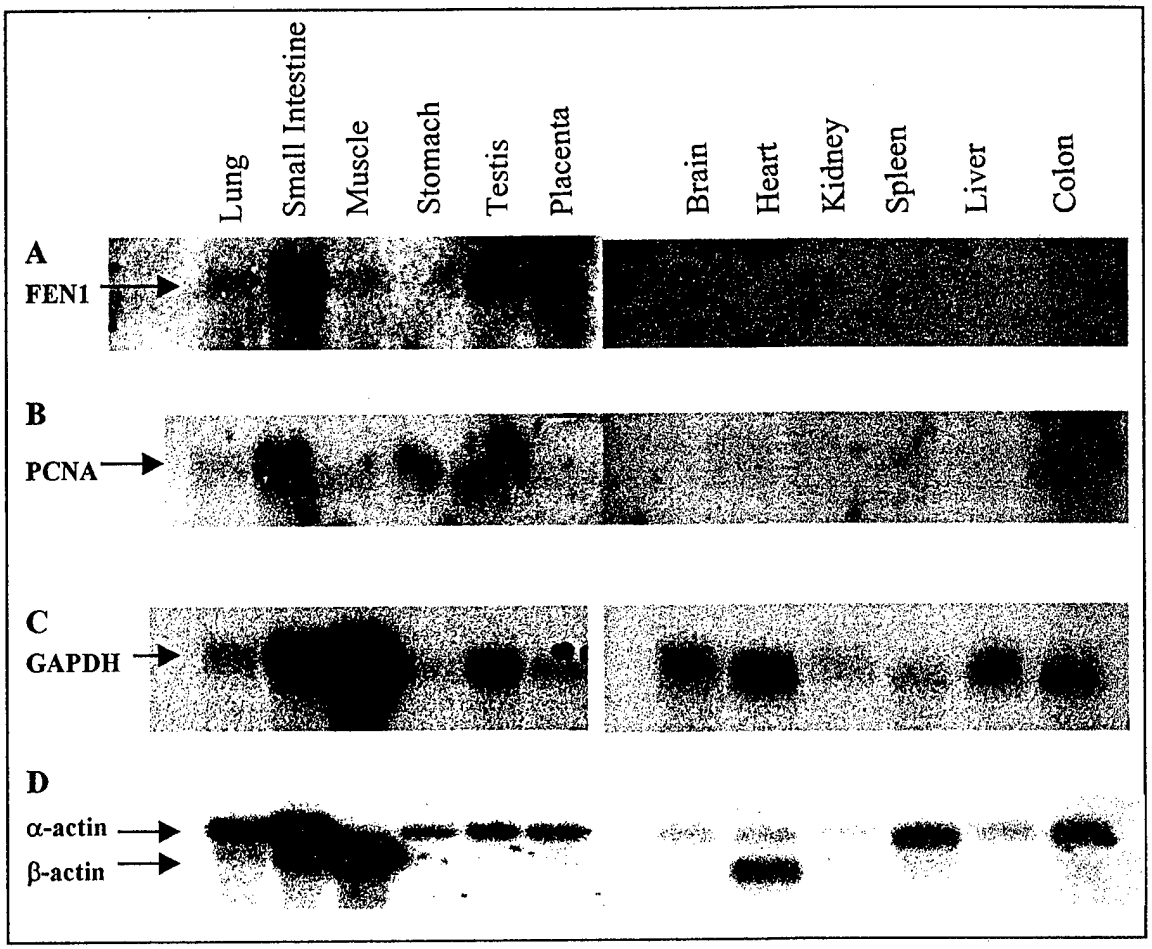

Figure 6-1. FEN1 and PCNA mRNA levels in 12 different human tissues. Approximately 2 μg of polyA+ mRNA from 12 different human tissues were separated by denaturing gel electrophoresis, transferred to nylon membranes (Multiple Choice™, Origene Technologies), and probed with α-[^{32}P] dATP-labeled **(A)** FEN1, **(B)** PCNA, **(C)** GAPDH, or **(D)** β-actin cDNA. The approximate sizes of mRNA transcripts detected were FEN1: 2.2-2.3 kb, PCNA: 1.6 kb, GAPDH: 1.4 kb, β-actin: 2.2-2.3 kb. The β-actin probe also detected α-actin (1.7-1.8 kb) in most tissues examined. The results suggest that human FEN1 and PCNA mRNA levels are similar in different human tissues.

```
ATGGGAATTCAAGGCCTGGCCAAACTAATTGCTGATGTGGCCCCCAGTGCCATCCGGGAG    60
M  G  I  Q  G  L  A  K  L  I  A  D  V  A  P  S  A  I  R  E
AATGACATCAAGAGCTACTTTGGCCGTAAGGTGGCCATTGATGCCTCTATGAGCATTTAT   120
N  D  I  K  S  Y  F  G  R  K  V  A  I  D  A  S  M  S  I  Y
CAGTTCCTGATTGCTGTTCGCCAGGGTGGGGATGTGCTGCAGAATGAGGAGGGTGAGACC   180
Q  F  L  I  A  V  R  Q  G  G  D  V  L  Q  N  E  E  G  E  T
ACCAGCCACCTGATGGGCATGTTCTACCGCACCATTCGCATGATGGAGAACGGCATCAAG   240
T  S  H  L  M  G  M  F  Y  R  T  I  R  M  M  E  N  G  I  K
CCCGTGTATGTCTTTGATGGCAAGCCGCCACAGCTCAAGTCAGGCGAGCTGGCCAAACGC   300
P  V  Y  V  F  D  G  K  P  P  Q  L  K  S  G  E  L  A  K  R
AGTGAGCGGCGGGCTGAGGCAGAGAAGCAGCTGCAGCAGGCTCAGGCTGCTGGGGCCGAG   360
S  E  R  R  A  E  A  E  K  Q  L  Q  Q  A  Q  A  A  G  A  E
CAGGAGGTGGAAAAATTCACTAAGCGGCTGGTGAAGGTCACTAAGCAGCACAATGATGAG   420
Q  E  V  E  K  F  T  K  R  L  V  K  V  T  K  Q  H  N  D  E
TGCAAACATCTGCTGAGCCTCATGGGCATCCCTTATCTTGATGCACCCAGTGAGGCAGAG   480
C  K  H  L  L  S  L  M  G  I  P  Y  L  D  A  P  S  E  A  E
GCCAGCTGTGCTGCCCTGGTGAAGGCTGGCAAAGTCTATGCTGCGGCTACCGAGGACATG   540
A  S  C  A  A  L  V  K  A  G  K  V  Y  A  A  A  T  E  D  M
GACTGCCTCACCTTCGGCAGCCCTGTGCTAATGCGACACCTGACTGCCAGTGAAGCCAAA   600
D  C  L  T  F  G  S  P  V  L  M  R  H  L  T  A  S  E  A  K
AAGCTGCCAATCCAGGAATTCCACCTGAGCCGGATTCTGCAGGAGCTGGGCCTGAACCAG   660
K  L  P  I  Q  E  F  H  L  S  R  I  L  Q  E  L  G  L  N  Q
GAACAGTTTGTGGATCTGTGCATCCTGCTAGGCAGTGACTACTGTGAGAGTATCCGGGGT   720
E  Q  F  V  D  L  C  I  L  L  G  S  D  Y  C  E  S  I  R  G
ATTGGGCCCAAGCGGGCTGTGGACCTCATCCAGAAGCACAAGAGCATCGAGGAGATCGTG   780
I  G  P  K  R  A  V  D  L  I  Q  K  H  K  S  I  E  E  I  V
CGGCGACTTGACCCCAACAAGTACCCTGTGCCAGAAAATTGGCTCCACAAGGAGGCTCAC   840
R  R  L  D  P  N  K  Y  P  V  P  E  N  W  L  H  K  E  A  H
CAGCTCTTCTTGGAACCTGAGGTGCTGGACCCAGAGTCTGTGGAGCTGAAGTGGAGCGAG   900
Q  L  F  L  E  P  E  V  L  D  P  E  S  V  E  L  K  W  S  E
CCAAATGAAGAAGAGCTGATCAAGTTCATGTGTGGTGAAAAGCAGTTCTCTGAGGAGCGA   960
P  N  E  E  E  L  I  K  F  M  C  G  E  K  Q  F  S  E  E  R
ATCCGCAGTGGGGTCAAGAGGCTGAGTAAGAGCCGCCAAGGCAGCACCCAGGGCCGCCTG  1020
I  R  S  G  V  K  R  L  S  K  S  R  Q  G  S  T  Q  G  R  L
GATGATTTCTTCAAGGTGACCGGCTCACTCTCTTCAGCTAAGCGCAAGGAGCCAGAACCC  1080
D  D  F  F  K  V  T  G  S  L  S  S  A  K  R  K  E  P  E  P
AAGGGATCCACTAAGAAGAAGGCAAAGACTGGGGCAGCAGGGAAGTTTAAAAGGGGAAAA  1140
K  G  S  T  K  K  K  A  K  T  G  A  A  G  K  F  K  R  G  K
TAA
*
```

Figure 6-2A. The human *FEN1* coding region. The human *FEN1* coding regions from the cDNA sequence (Murray *et al.*, 1994) and the genomic DNA sequence (Lemardin *et al.*, 1998 unpublished) were compared and found to be identical. The predicted translation product is shown below the coding region in single-letter amino acid code. The * symbol depicts the termination codon.

```
ATGTGTTTCCCCATTATACCTCCTTCACCCCAGAATATTTGCCGTCTTGTACCCTTAAGA
ATGTGTTTCCCCATTATACCTCCTTCACCCCAGAATATTTGCCGTCTTGTACCCTTAAGA  1200
************************************************************

GCTACAGCTAGAGAAACCTTCACGGGGTGGAGAGGATTCTAAGGCTTTTCTAGCGTGACC
GCTACAGCTAGAGAAACCTTCACGGGGTGGAGAGGATTCTAAGGCTTTTCTAGCGTGACC  1260
************************************************************

CTTTTCAGTAGTGCTAGTCCCTTTTTTACTTGATCTTAATGGCAAGAAGGCCACAGAGGT
CTTTTCAGTAGTGCTAGTCCCTTTTTTACTTGATCTTAATGGCAAGAAGGCCACAGAGGT  1320
************************************************************

ACTTTTCCTTTTTTTAGCTCAGGAAAATATGTCAGGCTCAAACCACTTCTCAGGCAGTTT
ACTTTTCCTTTTTTTAGCTCAGGAAAATATGTCAGGCTCAAACCACTTCTCAGGCAGTTT  1380
************************************************************

AATGGACACTAAGTCCATTGTTACATGAAAGTGATAGATAGCAACAAGTTTTGGAGAAGA
AATGGACACTAAGTCCATTGTTACATGAAAGTGATAGATAGCAACAAGTTTTGGAGAAGA  1440
************************************************************

GAGAGGGAGATAAAAGGGGGAGACAAAAGATGTACAGAAATGATTTCCTGGCTGGCAACT
GAGAGGGAGATAAAAGGGGGAGACAAAAGATGTACAGAAATGATTTCCTGGCTGGCAACT  1500
************************************************************

GGTGGCCAGTGGGAGGTGATGGTGGACCTAGACTGTGCTTTTCTGTCTTGTTCAGCCTTG
GGTGGCCAGTGGGAGGTGATGGTGGACCTAGACTGTGCTTTTCTGTCTTGTTCAGCCTTG  1560
************************************************************

ACCCACCTTGAGAGAGAGCCACCAGGAAGGCGCATCT-AGCAG-TGGGAGGAACTACTGA
ACCCACCTTGAGAGAGAGCCACCAGGAAGGCGCATCTTAGCAGATGGGAGGAACTGCTGA  1620
************************************ ***** *********** ****

GAGAAGATGGGCAGAAAGCTGGAGCCCCTGGAGTTGGCTGTGTCTGTGTTTGTGACTGAT
GAGAAGATGGGCAGAAAGCTGGAGCCCCTGGAGTTGGCTGTGTCTGTGTTTGTGACTGAT  1680
************************************************************

TACTGGCTGTGTCTTGGGTGGGCAGAAACTCGAACTTGCTATGTAATTTGTGTCTAGTTA
TACTGGCTGTGTCTTGGGTGGGCAGAAACTCGAACTTGCTATGTAATTTGTGTCTAGTTA  1740
************************************************************

TTCAGAGGAGTAAGATGGTGATGTTCACCTGGCAATCAGCTGAGTTGAGACTTTGGAATA
TTCAGAGGAGTAAGATGGTGATGTTCACCTGGCAATCAGCTGAGTTGAGACTTTGGAATA  1800
************************************************************

AGACACTGGTTTTCATGCGCTGTTTTTGTTTTAAGTTATGAAGAAAAAAGTCAATAAAAT
AGACACTGGTTTTCATGCGCTGTTTTTGTTTTAAGTTATGAAGAAAAAAGTCAATAAAAT  1860
************************************************************

TCTAAAAGTAACC
TCTAAAAGTAACC                                                  1877
*************
```

Figure 6-2B. Human FEN1 cDNA and genomic DNA 3'UTR comparison. The human *FEN1* 3' UTR sequences derived from cDNA (Murray *et al.*, 1994) and genomic DNA (Lemardin *et al.*, 1998 unpublished) were compared and show only 3 minor discrepancies (indicated above). The top rows depict the cDNA sequence and the bottom rows depict the genomic DNA sequence. The numbers to the right indicate the sequence position in relation to the 'A' (+1) of the initiator codon (ATG). The sequence CAATAA in both genomic and cDNA sequences (nt 1855-1860) is the poly-adenylation signal.

C.

```
-367                                                          AGTCCTG
-360    CGATTTCGGTGTAGAGGAGCAGGGGCTGCGGGACCTGGTGTGGGTGGAGTGGGACAAGCG
-300    GTGGAGAAGGGTACGCCAGGGTCGCTGAGAGACTCTGTTCTCCCTGGAGGGACTGGTTGC
-240    CATGAGAGCAGCCGTCTGAGGGGACGCAGCCTGCACTACGCGCCCCAAGAGGCTGTGCGT
-180    GGCGAGCAGGTCACGTGACGGGAGCGCGGGCTTTGGAAGGCGGCTGAACGTCAGGCCACC
-120    CGCCGCTAAGCTGAGAAGGGAGAGCGAGCTTAGGACCGCCTGCCCGGGGCAACCCCGAAC
-60     CAAGCTTTAGCCGCCGAGGCCGCGTGTCCCAAAGGCCAGTCATCCCTCCTCTGTGTTGCC
```

D.

```
-1320   CCTGGAACTCCTGGGCTCATGTGATCCTCCCACCACGGCCTCCCAAAGTGCTGGGATTAC
-1260   TGCCCAGAGCCTCTGTGCCTGGCCCCAGTAGAATATTTCTTGGAGTATTGGACACATACC
-1200   AACAGTGGGCACAAGATGAGTTTTTTATTTTTTTGAGACGGAGTCTCACTCTCTTGCTAG
-1140   GCTGGAGTGCAGCGGCACAATCTCGGCTCACTGCATTCTCTGCCTCCTGGGTTCAAGCGA
-1080   TTCTCCTGCCTCAGCCTCCCGAGTAGCTGGGATTACAGGTGCACACCACCACACCCAGCT
-1020   AATTTTTTTTTTTTTTGTATTTTTAGTAGAGACAGGGTTTCACCGTGTTGGCCAGGATGG
-960    CAAGATGATTTTAAATTGCACCCCCTAAAAATCCTTTTTAATAGTTATACATTTAATACA
-900    TATTAAAATATAACTAATAGAACACAAATATTATTGCTTATGAGTTTTCCAGTTTAGTTT
-840    TTTAAAAAAAATTCTAAGTGAATGAAAGTACGGGTTTTAGTTGGAAGTAGCAAAAATCTG
-780    GAGGGTGATTTGGGAAACACTGCTATCTGGGAAACACTGAACTCTGAAGTGCAATACTCT
-720    TTTGAGCCCAGTGACTACAGCATGCCAGACCCCTAAATCAGGACCTGGGGAGGAGCCATG
-660    GAGTTAACATTTCAGACTGAGTGGTGGCGAGAAAACGCAAAGGGAAAGACTTGAAACTCT
-600    AGCAACATTATAATAAAAGTAGAAACTCTTATGTGCTGAGGCGATGATGAAGAGAGTTTA
-540    GAGAAGCTTGTGAGAAAGCCACATCACCTCCATTCAGATATGTTTGCAATCCTTTTTCAA
-480    GGCTGCCTTATTAGTCAGGGTTCTCCAGAGACTCAAAACAAATCAGATCTGTTTGTTTAG
-420    CTGGTGTATTTGCCTGTCTTTCAGGTCTGCCATTATGGTCCCTGGACTCCTCAAGCCAGG
-360    CCAAGCATCCTGGCCTTCTGTGGTCCTTGATGGAGACCTATGTTGCAGGTTTTTTTTGTG
-300    TAATAAATAATGCTGCTACCTTAGAATATCAACAGTATCTTATTTCTCTAAGCACGTGGT
-240    TCAATTTCTGGTACTCGTTGAGCCTTACTATTGAGTAAATTCTCCTGCTAGACTGAGTTT
-180    TTTGAGAATGGGGACCTTGTTCATCTTTTTATCTTTAGCAGTGCTGACATGGTGTCCTTT
-120    TTGTTGTGTGGAATTTAGTTGAAGGCATGAAGTTGGTGAGATAACACCAGTTATAACCTT
-60     TCTCCTTTCCTCCGTCTCTGACTTGCCTTTCTTTTTTAGTCATCCCTCCTCTGTGTTGCC
```

Figure 6-2 (C, D). Comparison of *FEN1* cDNA and genomic 5' UTR sequences. 1320 bases from the genomic human *FEN1* sequence, upstream (5') of the translational (ATG) start site (+1), were compared to the cDNA sequence. **(C)** The 5' UTR of the human *FEN1* gene obtained from probes of a human pDR2-cDNA library (Murray *et al.*, 1994). **(D)** The sequence of the 5' UTR of the human *FEN1* gene was obtained from genomic DNA as part of the Human Genome sequencing project (Lamerdin *et al.*, 1998 unpublished). Only the 23 bases immediately 5' to the translational start site were identical between the two sequences (shown in **bold**). Prior (5') to that sequence, there are no significant identities or similarities between the cDNA and genomic 5' UTRs of human *FEN1*. Although the coding regions are identical between the two sequences, and there are only three minor differences in the 3' UTR comparison, the extensive differences in the 5' UTR suggests that the 5' UTR cDNA sequence may be incorrect.

Table 6-1. Putative Transcriptional Start Sites within the human *FEN1* 5' UTR. 1323 bases of genomic DNA sequence 5' to the human FEN1 initiator codon (ATG), were analyzed by Promoter Prediction by Neural Network (NNPP). The output of promoter predictions by NNPP is a list of the 51-base eukaryotic sequences containing the predicted transcription start site (TSS) of regions that the algorithm judges most likely to be promoters. Nucleotides (nts) are numbered, taking A of the initiator codon ATG as +1. The predicted TSS are indicated in **bold**.

Predicted Promoters:

	START	END	Putative TSS and flanking sequence
1.)	-959	-909	caagatgattttaaattgcacccccctaaaaatccttttta**A**tagttatac
2.)	-698	-648	atgccagacccctaaatcaggacctggggaggagccatgg**A**gttaacatt
3.)	-306	-256	ttttgtgtaataaataatgctgctaccttagaatatcaac**A**gtatcttat

Site	Consensus Sequence	*FEN1* Sequence	Location	*PCNA* Sequence
TATA box	TATA(A/T)A(A/T)	**TAAAAAT**	-934 -928	none
		TATTAAA	-900 -894	
		TATTATT	-871 -865	
		TAAAAAA	-838 -832	
		TATAATA	-591 -585	
		TAAATAA	-297 -291	
CAAT box	CCAAT	**CCATT**	-510 -506	**CCAAT**
		GCAAT	-494 -490	
		CAAAT	-442 -438	
		CCATT	-391 -387	
		CCAAG	-360 -356	
		CCTAT	-324 -320	
		TCAAT	-239 -235	
		CCAGT	-74 -70	
Sp1 site	(G/T)GGGCGG (GGC/AAT)	**GGGGAGG** **AGC**	-674 -665	**GGGGCGGGCC** **AGGGCGGGGC**
CRE	(T/G)(T/A)CGTCA	**ACATCA**	-520 -515	**ACGTCG**
		TCCTCA	-373 –368	**TCGTCA**
		TCCTCA	-370 -375	
		TCGTAA	-287 -292	
		TCGTGA	-135 -140	
AP-1	TGACTCA	**TGACTACA**	-708 -701	**TGACTA**
		AGACTGA	-647 -640	
		GGACTCA	-377 -370	
		AGACTGA	-191 -184	
AP-2	TGGGGA	**TGGGGA**	-172 -167	none
AP-3	TGTGG(AAA/TTT)G TGTG	**TGTGAGAAAG** **TGTGGAATT**	-532-523 -113 -105	**TGTGGAGAT**
AP-4	CAGCTGTGG	**GAGCGGTGG**	-630 -638	**CATATGTGG** **CAGCTGCTG**

Table 6-2. Analysis of putative human *FEN1* transcriptional response elements (TREs). 1323 bases 5' to the human FEN1 initiator codon (ATG) from the genomic DNA sequence were analyzed by PROMOTER SCAN (Prestridge, Advanced Biosciences Computing Center, University of Minnesota). Sequences obtained by that programme, as well as other putative human *FEN1* TREs that display sequence similarities to published *PCNA* TREs are depicted. Homology between the consensus sequence and similar sequences in the human *FEN1* gene are indicated in **bold**. Location of putative FEN1 sequences are in relation to the initiator codon ATG (+1). References to PCNA sequences are from Travali *et al.*, 1989.

CHAPTER SEVEN: CONCLUSIONS

The aims of this thesis were to examine human FEN1 expression and solubility patterns throughout the cell cycle, on re-entry into the cycle following quiescence, and in response to DNA damage. I also wanted to test whether human FEN1 and PCNA proteins might functionally interact in whole cells by examining solubility and localization of both proteins in asynchronous, synchronized, and damaged cells. To address these questions, I have purified human FEN1 protein, screened antibodies suitable for use in subsequent stages of the project, determined the subcellular localization of human FEN1 and PCNA proteins, analyzed expression of FEN1 and PCNA at the mRNA and protein level, and compared their solubility patterns throughout the cell cycle and in response to DNA damage. Finally, I have identified putative transcriptional control elements that might regulate *FEN1* gene expression in response to cell cycle-dependent or DNA repair-dependent mechanisms.

7-1 Summary

7-1.1 Novel Antibodies to FEN1 Protein

During the course of this project we have developed two novel antibodies to FEN1 protein: anti-Xenopus FEN1 (J.L.-Li *et al.*, manuscript submitted) and anti-peptide FEN1 polyclonal antibodies (see Chapter 3). I extensively tested both antibodies and showed that they recognize recombinant and endogenous human FEN1 protein on western blots. Side-by-side comparisons of the two antibodies demonstrated that anti-Xenopus FEN1 antibody provided the strongest detection signal; consequently, anti-Xenopus FEN1 antibodies were used for the remainder of the project.

7-1.2 Human FEN1 Appears to be a Nuclear Protein

Transient transfection of asynchronous HeLa cells with GFP-FEN1 plasmid cDNA, and fluorescence microscopic analysis of cells expressing GFP-FEN1 protein showed that GFP-FEN1 (GFP-wt FEN1) protein localizes to the nucleus (Chapter 3, Figure 3-12). This result agrees with FEN1's putative role in DNA replication (Ishimi *et al.*, 1988; Goulian *et al.*, 1990; Turchi and Bambara, 1993; Waga *et al.*, 1994), and its consensus nuclear localization signal (Murray *et al.*, 1994). Additionally, a mutant GFP-FEN1 protein (GFP-ΔFEN1), which lacks a 23 amino acid domain (amino acids 225-247) near the C-terminus that is present in wild-type FEN1 protein, also localized to the nucleus (Figure 3-12), suggesting that amino acids 225-247 are not required for nuclear localization. Because FEN1 and PCNA proteins have been shown to interact *in vitro* (Li *et al.*, 1995; Chen *et al.*, 1996; Warbrick *et al.*, 1997), and are suspected to interact in an S phase-specific manner *in vivo* (Warbrick *et al.*, 1997), I also analyzed the subcellular localization of PCNA protein in GFP-wt FEN1 transfected HeLa cells that were fixed *in situ* with methanol-acetone (50:50). Previous studies (Celis and Celis, 1985; Bravo and MacDonald-Bravo, 1987) had demonstrated that nuclear PCNA protein exhibits a punctate nuclear staining pattern in S phase cells fixed with organic solvents. Immunofluorescence microscopic examination of GFP-FEN1 transfected HeLa cells stained with the anti-PCNA antibody PC10 (Waseem and Lane, 1990) showed a number of cell nuclei that were positive for PCNA protein (Figure 3-13C). Surprisingly, further analysis of those same cells revealed that GFP-FEN1 protein was present not only in cell nuclei where PCNA protein was detected, but also in nuclei where little or no PCNA protein was observed (Figure 3-13). This suggests that a proportion of FEN1 protein may be methanol-insoluble in non-S phase, as well as S phase cells.

7-1.3 FEN1 mRNA/Protein Levels Increase in a Cell Cycle-Dependent Manner

It has been previously demonstrated that numerous factors involved either directly or indirectly with nuclear DNA replication show increased mRNA and protein expression during cell cycle progression from early G_1 towards S phase, and following transition from the quiescent to proliferative state (reviewed in Chapter 4). I have demonstrated here that human FEN1 mRNA and protein levels also increase as synchronized HeLa cells progress from early G_1 towards S phase of the cell cycle (Chapter 4, Figures 4-2, 4-5), and when primary MRC-5 cells exit the quiescent state and progress towards S phase (Chapter 4, Figures 4-11, 4-12), supporting a role for FEN1 in S phase. This observed increase in human FEN1 protein is thought to be regulated at the transcriptional level, based on increased mRNA levels and the existence of several putative cell cycle-dependent regulatory elements in the human FEN1 promoter; however, further regulation at the translational or post-translational level has not been ruled out.

7-1.4 FEN1 and PCNA Protein are not Co-Extracted by DNase I Treatment

Because FEN1 and PCNA are reported to associate with one another, and with DNA, in an S phase-specific manner (see Section 7-1.2), I expected FEN1 and PCNA proteins to have similar solubility patterns in synchronized cell populations. While substantial levels of DNase I-extracted PCNA protein were observed in S phase cells, very little FEN1 protein was detected in those same extracts (Chapter 4, Figures 4-7, 4-13). This suggests that the FEN1-PCNA protein interaction may be very transient, strongly supporting earlier observations (Warbrick *et al.*, 1997), and that PCNA may serve only to increase FEN1 residence time at the site of cleavage or it may stabilize FEN1 activity at physiological salt concentrations (Li *et al.*, 1995; Wu *et al.*, 1996;

Lieber, 1997). Additionally, it may also suggest that a decrease in FEN1 solubility may not be a requirement for its role in DNA replication.

7-1.5 Insoluble FEN1 Protein was Present throughout the Cell Cycle

Following extraction of soluble and DNA-associated protein from synchronized cell populations, substantial levels of insoluble FEN1 protein were still observed in G1 through to S phase cells (Chapter 4, Figures 4-8, 4-13). Unlike PCNA protein, which exhibits an S phase-specific pattern of insolubility (see Chapter 4, Section 4-1), this result suggests that a proportion of FEN1 protein remains insoluble throughout the cell cycle. This result also agrees with my observations of GFP-FEN1 protein in HeLa cell nuclei where no PCNA protein was detected (see 7-1.2).

7-1.6 Human FEN1 Expression and Solubility Patterns are not Significantly Altered in Response to DNA Damage

A role for human FEN1 in BER, and possibly other types of DNA repair mechanisms have been strongly suggested (reviewed in Chapter 5). When human MRC5-SV cells were treated with the alkylating agent MMS, both FEN1 and PCNA mRNA levels steadily decreased for up to 4 hours following treatment, and then increased to, or above, untreated control levels within 24 hours post-treatment (Figure 5-3). Increases in both FEN1 and PCNA mRNA levels 4-8 hours following treatment can be largely attributed to cell-cycle-dependent induction of those genes, since FACS analysis (Chapter 5, Figure 5-1) shows near synchronous entry into S phase 8 hours following MMS treatment. This suggests that neither *FEN1*, nor *PCNA*, are transcriptionally induced in response to alkylation damage. Additionally, because most BER mechanisms are completed within 60 minutes following DNA damage

(Fortini *et al.*, 1998), it is unlikely that increased FEN1 and PCNA mRNA levels observed here were part of a DNA damage response.

In contrast to mRNA levels, no changes in either FEN1 protein levels or solubility patterns were detected over the 24 hours following MMS treatment (Chapter 5, Figure 5-4). Although no increase in PCNA protein levels also was observed, PCNA protein did show a dramatic solubility decrease within 30 minutes of MMS treatment, and elevated levels of insoluble PCNA were observed for up to 24 hours post-treatment (Figure 5-4). Even though this decrease in PCNA protein solubility further supports a role for PCNA in BER *in vivo*, the lack of a solubility change for FEN1 protein does not imply that it does not participate in BER mechanisms. Instead, it may suggest that a role for FEN1 protein in BER is not dependent on a concomitant change in its solubility.

When human MRC5-SV cells were treated with 10 J/m^2 UV irradiation, FEN1 and PCNA mRNA levels increased within 3-7 hours following treatment (Figure 5-10). However, FACS analysis (Figure 5-8) suggest that the observed increases may have been the result of cell cycle-dependent transcriptional induction of *FEN1* and *PCNA*, although some form of transcriptional induction by DNA repair mechanisms has not been ruled out. No changes in either FEN1 protein levels or solubility were observed as a result of 10 J/m^2 UV irradiation of MRC5-SV cells. Similarly, no increase in PCNA protein levels were detected, however a significant decrease in PCNA solubility was noted within 3 hours, and continued for up to 12 hours post-treatment (Figure 5-11). This further supports a role for PCNA protein in NER mechanisms (Shivji *et al.*, 1992; reviewed in Chapter 5). The lack of FEN1 solubility changes in response to UV irradiation may indicate that either FEN1 does not

participate during NER *in vivo*, or that changes in FEN1 solubility or protein levels are not necessary for a functional role in NER.

7-1.7 The Human *FEN1* Gene Contains Numerous Putative TREs that may Regulate its Expression

Similar patterns of human FEN1 and PCNA mRNA levels were observed in both synchronized (Chapter 4) and DNA damaged cells (Chapter 5). Similarities in mRNA levels suggests that both genes may be similarly controlled at the transcriptional level. Now that the human *FEN1* genomic DNA sequence is available (Lamerdin et al., 1998 unpublished), I examined sequences upstream of the *FEN1* translational start site, and propose a putative transcriptional start site (TSS) (-306, Table 6-1) and several putative transcriptional regulatory elements (TREs) that may regulate *FEN1* expression by either cell cycle-dependent or DNA damage-dependent mechanisms (Chapter 6, Table 6-2). Additionally, based on my proposed TSS for *FEN1* at -306, and analysis of FEN1 mRNA derived from different human cell lines (Chapters 4, 5) and tissues (Chapter 6, Figure 6-1), I propose that FEN1 transcripts are 2.2-2.3 kb in size, which is slightly larger than the 2.0 kb previously reported (Murray et al., 1994).

7-2 Implications for FEN1's Role in DNA Replication and Repair

The results in this thesis lend strong support to a role for human FEN1 in nuclear DNA replication. The observation that human FEN1 mRNA and protein levels increase from early G_1 through to S phase, and peak coincident with the onset of S phase (Chapter 4), parallels similar mRNA and protein increases observed for numerous other factors involved in nuclear DNA replication (reviewed in Chapter 4).

Additionally, the observation that GFP-FEN1 protein localizes in HeLa cell nuclei (Chapter 3, Figures 3-12, 3-13) suggests that endogenous FEN1 protein also localizes and functions in the nucleus, further supporting a role for FEN1 during nuclear DNA replication *in vivo*.

Because PCNA has been shown to bind and stimulate FEN1 enzyme activity *in vitro* (Li *et al.*, 1995; Wu *et al.*, 1996; Chen *et al.*, 1996; Warbrick *et al.*, 1997), and because PCNA protein solubility has been shown to decrease in an S phase-specific manner *in vivo* (Madsen and Celis, 1985; Bravo and MacDonald-Bravo, 1985, 1987; Chapter 4), I expected to see a similar decrease in FEN1 protein solubility in S phase cells. However, this was not observed since significant levels of PCNA were extracted by DNase I treatment of S phase cells (Chapter 4, Figures 4-7, 4-13), but very little (Figure 4-7), or no (Figure 4-13) FEN1 protein were detected in those same extracts. This suggests that either the FEN1-PCNA interaction was disrupted during protein extraction, or more probably, that a stable FEN1-PCNA protein interaction does not exist *in vivo*.

PCNA's toroidal structure (Krishna *et al.*, 1994) and function during DNA replication (Bravo and MacDonald-Bravo, 1987) justify its decrease in solubility during S phase; however, the same cannot be said for FEN1 protein. Although the crystal structure of *P. furiosus* FEN1 (Figure 1-10, Hosfield *et al.*, 1998) shows that the enzyme has an arch structure that can encircle ssDNA, previous studies have shown that the movement of FEN1 is bi-directional and it can slide off ssDNA flap structures (Murante *et al.*, 1995). Hosfield *et al.* (1998) suggest that FEN1 slides down 5' flap structures, and when the H3TH domain contacts and binds duplex DNA at the flap junction, the helical arch encircling the ssDNA flap clamps down, bringing the flap junction into the active site of the FEN1 enzyme, and DNA/RNA cleavage

occurs. This implies that FEN1's association with DNA is very transient, and the only mechanism which could explain a replication-dependent decrease in FEN1 protein solubility would be a stable protein-protein interaction involving FEN1 and another S phase-insoluble factor such as PCNA. My results suggest that the FEN1-PCNA interaction is very transient. This is supported by the observation by Jonsson *et al.* (1998) that FEN1 can actually inhibit DNA synthesis by DNA Pol δ/PCNA *in vitro*, possibly by competing for PCNA binding with Pol δ. A further observation that PCNA stabilizes FEN1 activity at physiological salt concentrations (Li *et al.*, 1995; Wu *et al.*, 1996), leads me to propose the following mechanism for FEN1 activity during DNA replication:

As the PCNA-Pol δ (or Pol ε) replicative complex synthesizes DNA from an upstream primer, it eventually comes into contact with a downstream primer. It is possible that processive DNA replication from the upstream primer results in displacement of the downstream primer from its template (Siegal *et al.*, 1992), which now becomes a suitable substrate for both FEN1 (reviewed in Chapter 1) and RNase H1 (Murante *et al.*, 1998). RNase H1 either endo- or exonucleolytically cleaves the majority of the RNA primer, leaving 1 ribonucleotide (reviewed by Bambara *et al.*, 1997). Downstream strand displacement may result in a slowing/stalling of the replication complex, causing Pol δ/ε to dissociate. This dissociation now exposes the FEN1 binding site on PCNA (Jonsson *et al.*, 1998), and as FEN1 slides down the ssDNA flap structure, it transiently binds PCNA. Further binding of duplex DNA at the flap junction by the FEN1 H3TH domain (Hosfield et al., 1998) results in eventual flap cleavage. Cleavage may stimulate FEN1's dissociation from PCNA, allowing both enzymes to be recycled.

This proposed model may explain the very low levels of DNase I-extracted FEN1 protein I observed in S phase cell fractions. It is also consistent with a role for FEN1 protein in the removal of primers in both leading and lagging strand synthesis, and possibly in DNA repair mechanisms.

My investigation of FEN1 expression and protein solubility changes in response to MMS or UV treatment revealed that FEN1 is probably not transcriptionally induced as a result of alkylation damage or UV irradiation. This is not surprising in that most DNA repair genes, excluding important signalling molecules such as p53, are constitutively expressed and not induced as a result of DNA damage (Hoeijmakers, 1993). The lack of a solubility decrease of FEN1 protein in response to alkylation or UV-induced DNA damage does not imply that FEN1 does not participate in BER and NER mechanisms, respectively. FEN1 solubility does not appear to change during DNA replication, and a role for FEN1 in nuclear DNA replication is strongly suggested (Ishimi *et al.*, 1988; Waga *et al.*, 1994; this thesis). Although a role for FEN1 during long-patch BER has been suggested based on its ability to excise certain lesions not amenable to the predominant short-patch BER mechanism *in vitro* (Klungland and Lindahl, 1997; Kim *et al.*, 1998), an additional role for FEN1 in other repair processes is conceivable based on my proposed model. Following excision of DNA damage by either mismatch repair (MMR) or NER mechanisms, subsequent DNA synthesis is necessary for completion of repair. If processive DNA synthesis during repair results in strand displacement and flap formation, FEN1 may be required to resolve that intermediate DNA structure. Yeast FEN1 mutants are implicated in defective cellular responses to UV irradiation (Murray et al., 1994; Reagan et al., 1995) and alkylation damage (Reagan et al., 1995; Sommers et al., 1995), and show instability of simple repetitive DNA sequences

(Johnson et al., 1995). A role for FEN1 in the resolution of DNA intermediate structures resulting from DNA synthesis during repair, may explain those observed deficiencies in yFEN1 mutants.

It has been proposed that the FEN1 and $p21^{CIP1/WAF1}$ proteins may compete for PCNA binding, and that this may serve as a replication-repair switch (Warbrick *et al.*, 1997; Cox, 1997). In the future, that model may be tested by co-immunoprecipitation assays of cell extracts from synchronized cells that were subjected to DNA damage. Specifically, one could compare the levels of $p21^{CIP1/WAF1}$ and FEN1 protein in complex with PCNA in S phase cell populations, with and without DNA damage. Even though I detected very low levels of DNase I-extracted FEN1 protein in synchronized HeLa cells, immunoprecipitation of FEN1 protein from whole cell extracts would serve to increase the concentration of FEN1 protein, and levels should then be sufficient to allow an analysis of the proposed replication-repair switch model. However, such studies await the development of high-affinity, high-specificity antibodies capable of immunoprecipitating native and complexed FEN1 protein. Our lab is currently pursuing this goal (see Section 7-4).

7-3 Implications for the Regulation of FEN1 Activity

Unlike insoluble PCNA protein, which is readily extracted from S phase or DNA-damaged cells by DNase I digestion of dsDNA, a proportion of insoluble FEN1 protein remains in cells following DNase I treatment (Chapter 4). Further evidence that a population of insoluble FEN1 protein persists throughout the cell cycle was demonstrated when methanol-fixed GFP-FEN1-transfected HeLa cells showed GFP-FEN1 protein nuclear localization in cells where no PCNA protein was detected (Chapter 3, Figure 3-13). These results suggest that a proportion of insoluble FEN1

protein remains in the nucleus throughout the cell cycle. What is the purpose of insoluble nuclear FEN1 protein if it is not associated with DNA?

Analysis of insoluble protein extracted from synchronized HeLa cells showed that the levels of insoluble FEN1 (SDS-extracted) protein may actually decrease from early G_1 towards late S phase (Chapter 4, Figure 4-8). Although still tentative, this result suggests that an increase in FEN1 solubility may precede its activity in DNA replication and repair. Unregulated access to DNA by nucleases such as FEN1 could lead to disastrous consequences in terms of genomic integrity. Keeping nucleases sequestered within insoluble components in the nucleus, and regulating their release or activation, may be a way in which cells co-ordinate and control nuclease activity. It is possible that insoluble FEN1 protein sequestered within the nucleus may be actively recruited during DNA replication or repair by post-transcriptional modifications of FEN1 itself, or of other nuclear factors that regulate the solubility of FEN1 protein. Although I observed an S phase-dependent increase in FEN1 mRNA levels (Chapter 4), suggesting transcriptional control of FEN1 protein levels, it is possible that FEN1 protein also may be regulated post-transcriptionally, and cell cycle-dependent transcriptional induction may serve to simply re-establish minimum insoluble FEN1 protein levels.

These possibilities can be investigated in the future with pulse-chase ^{35}S-methionine labelling of nascent proteins in synchronized cell populations. By exposing synchronized cells to a brief radiolabel pulse, and subsequently following the sub-nuclear distribution of labelled FEN1 during the cell cycle, it may be possible to see any subtle changes in FEN1 protein solubility. Specifically, it may provide a way of determining if newly translated FEN1 protein becomes part of the insoluble FEN1 pool, and if insoluble FEN1 protein is released during S phase to function

during DNA replication. A similar study could be easily adapted to examine FEN1 solubility in response to various types of DNA damage.

In addition to determining whether insoluble FEN1 protein becomes soluble in a DNA replication or DNA repair-dependent manner, it would also be interesting to discover where insoluble FEN1 protein is bound, and what signals its release. Because insoluble protein extraction typically involves protein denaturation that disrupts most protein-protein interactions, an alternative method such as phage display mapping may be necessary to identify peptide motifs that bind purified native FEN1 protein. Determination of motifs capable of binding FEN1, and subsequent database searches, may identify other nuclear proteins that might bind and sequester FEN1. Further *in vitro* studies with purified proteins or whole cell extracts would then be necessary to verify putative protein-protein interactions suggested by phage display and database searches. Once putative interacting proteins are determined, an examination of factors that may regulate their association, such as phosphoylation or ADP-ribosylation, might help elucidate FEN1 regulatory mechanisms.

7-4 Future Directions

To further study FEN1's role and regulation during the cell cycle and in response to DNA damage, high affinity antibodies are essential. We are currently in the process of preparing recombinant human FEN1 protein to use as immunogen in chickens. Due to our previous difficulties in FEN1 antibody production in mice and rabbits, it is thought that chickens may provide a viable alternative, in that their self-tolerance profile to highly conserved proteins is different to that in mammals (Harlow and Lane, 1988), so chickens may show a strong immune response against human FEN1. Antibodies could be used for immunofluorescence microscopy or immuno-

precipitation of FEN1 protein complexes throughout the cell cycle, or in response to DNA damage, to determine if FEN1 forms protein complexes in a cell cycle or DNA repair-dependent manner. Additionally, establishing stable GFP-FEN1 transfected human cells, that are subsequently synchronized or subjected to DNA damage, should allow further elucidation of FEN1 protein's subcellular distribution throughout the cell cycle and in DNA repair. Lastly, establishment of human cell lines, stably transfected with an inducible GFP-FEN1 gene, may provide an alternative way for determining whether FEN1 expression is absolutely required for either DNA replication or repair *ex vivo*, and by inference, *in vivo*.

REFERENCES

Ambion International Catalogue 1999 (Witney, UK: Ambion Biotechnologies, Ltd).

Aboussekhra, A., Biggerstaff, M., Shivji, M. K., Vilpo, J. A., Moncollin, V., Podust, V. N., Protic, M., Hubscher, U., Egly, J. M., and Wood, R. D. (1995). Mammalian DNA nucleotide excision repair reconstituted with purified protein components. Cell *80*, 859-68.

Aboussekhra, A., and Wood, R. D. (1995). Detection of nucleotide excision repair incisions in human fibroblasts by immunostaining for PCNA. Exp-Cell-Res *221*, 326-32.

Alberts, B., Bray, D., Lewis, J., Raff, M., Roberts, K., and Watson, J. (1995). Molecular Biology of the Cell (New York, USA: Garland Publishing Inc.).

Alder, H., Yoshinouchi, M., Prystowsky, M. B., Appasamy, P., and Baserga, R. (1992). A conserved region in intron 1 negatively regulates the expression of the PCNA gene. Nucl. Acids Res. *20*, 1769-1775.

Almendral, J. M., Huebsch, D., Blundell, P. A., Macdonald-Bravo, H., and Bravo, R. (1987). Cloning and sequencing of the human nuclear protein cyclin: homology with DNA-binding proteins. PNAS *84*, 1575-1579.

Andrejco, M., Kalab, M., Oulton, A., Kolar, Z., Lichnovsky, V., Kod'ousek, R., and Vojtesek, B. (1996). Immunoreactivity of new antibodies anti-p53 and anti-MDM-2 in paraffin embedded tissue samples. Acta Univ Palacki Olomuc Fac Med *140*, 63-7.

Bambara, R. A., Murante, R. S., and Henricksen, L. A. (1997). Enzymes and reactions at the eukaryotic DNA replication fork. J-Biol-Chem *272*, 4647-50.

Bardwell, L., Cooper, A. J., and Friedberg, E. C. (1992). Stable and specific association between the yeast recombination and DNA repair proteins RAD1 and RAD10 in vitro [published erratum appears in Mol Cell Biol 1992 Sep;12(9):4249]. Mol Cell Biol *12*, 3041-9.

Barnes, C. J., Wahl, A. F., Shen, B., Park, M. S., and Bambara, R. A. (1996). Mechanism of tracking and cleavage of adduct-damaged DNA substrates by the mammalian 5'- to 3'-exonuclease/endonuclease RAD2 homologue 1 or flap endonuclease 1. J-Biol-Chem *271*, 29624-31.

Baserga, R. (1991). Growth regulation of the PCNA gene. J. Cell Sci. *98*, 433-436.

Bers, G., and Garfin, D. (1985). Protein and nucleic acid blotting and immunobiochemical detection. BioTechniques *3*, 276-288.

Birnstiel, M. L., Busslinger, M., and Strub, K. (1985). Transcription termination and 3' processing: The end is in sight. Cell *41*, 349.

Biswas, E. E., Zhu, F. X., and Biswas, S. B. (1997). Stimulation of RTH1 nuclease of the yeast Saccharomyces cerevisiae by replication protein A. Biochemistry *36*, 5955-62.

Blackwell, J. R., and Horgan, R. (1991). A novel strategy for production of a highly expressed recombinant protein in an active form. FEBS-Lett *295*, 10-2.

Blow, J. J., and Laskey, R. A. (1986). Initiation of DNA replication in nuclei and purified DNA by a cell-free extract of Xenopus eggs. Cell *47*, 577-587.

Blow, J. J., and Laskey, R. A. (1988). A role for the nuclear envelope in controlling DNA replciation within the cell cycle. Nature *322*, 546-548.

Bohr, V. A. (1994). Gene-specific damage and repair of DNA adducts and cross-links. IARC Sci Publ *125*, 361-9.

Bork, P., Hofmann, K., Bucher, P., Neuwald, A. F., Altschul, S. F., and Koonin, E. V. (1997). A superfamily of conserved domains in DNA damage-responsive cell cycle checkpoint proteins. Faseb J *11*, 68-76.

Bravo, R., Frank, R., Blundell, P. A., and MacDonald-Bravo, H. (1987). Cyclin/PCNA is the auxiliary protein of DNA polymerase delta. Nature *326*, 515-517.

Bravo, R., and MacDonald-Bravo, H. (1985). Changes in the nuclear distribution of cyclin (PCNA) but not its synthesis depend on DNA replication. EMBO J. *4*, 655-661.

Bravo, R., and MacDonald-Bravo, H. (1987). Existence of two populations of cyclin/Proliferating Cell Nuclear Antigen during the cell cycle: association with DNA replication sites. J. Cell Biol. *105*, 1549-1554.

Bucher, P. (1989). Weight matrix description of four eukaryotic RNA polymerase II promoter elements from 502 unrelated promoter sequences. J. Mol. Biol. *212*, 563-578.

Bucher, P., and Trifonov, E. N. (1986). Compilation and analysis of eukaryotic Pol II promoter sequences. Nucl. Acids Res. *14*, 10009-10026.

Buchkovich, K., Dyson, N., Whyte, P., and Harlow, E. (1990). Cellular proteins that are targets for transformation by DNA tumour viruses. Ciba Found Symp *150*, 262-71.

Budd, M. E., and Campbell, J. L. (1997). A yeast replicative helicase, Dna2 helicase, interacts with yeast FEN-1 nuclease in carrying out its essential function. Mol-Cell-Biol *17*, 2136-42.

Burgers, P. M., and Yoder, B. L. (1993). ATP-independent loading of the proliferating cell nuclear antigen requires DNA ends. J-Biol-Chem *268*, 19923-6.

Celis, J. E., and Celis, A. (1985). Individual nuclei in polykaryons can control cyclin distribution and DNA synthesis. EMBO J. *4*, 1187-1192.

Celis, J. E., and Madsen, P. (1986). Increased nuclear cyclin/PCNA antigen staining of non S-phase transformed human amnion cells engaged in nucleotide excision repair. FEBS Lett. *209*, 277-283.

Ceska, T. A., Sayers, J. R., Stier, G., and Suck, D. (1996). A helical arch allowing single-stranded DNA to thread through T5 5'-exonuclease. Nature *382*, 90-3.

Chalfie, M., Tu, Y., Euskirchen, G., Ward, W. W., and Prasher, D. C. (1994). Green fluorescent protein as a marker for gene expression. Science *263*, 802-5.

Chan, F. K., Zhang, J., Cheng, L., Shapiro, D. N., and Winoto, A. (1995). Identification of human and mouse p19, a novel CDK4 and CDK6 inhibitor with homology to p16ink4. Mol Cell Biol *15*, 2682-8.

Chen, J., Chen, S., Saha, P., and Dutta, A. (1996). $p21^{Cip1/Waf1}$ disrupts the recruitment of human Fen1 by proliferating-cell nuclear antigen into the DNA replciation complex. Proc. Natl. Acad. Sci. USA *93*, 11597-11602.

Chu, G. (1997). Double strand break repair. J Biol Chem *272*, 24097-100.

Coverley, D., Kenny, M. K., Munn, M., Rupp, W. D., Lane, D. P., and Wood, R. D. (1991). Requirement for the replication protein SSB in human DNA excision repair. Nature *349*, 538-41.

Cox, L. S. (1997). Who binds wins: PCNA rings out the cell cycle changes. Trends in Cell Biol. *7*, 493-498.

DeMott, M. S., Zigman, S., and Bambara, R. A. (1998). Replication protein A stimulates long patch DNA base excision repair. J-Biol-Chem *273*, 27492-8.

Dianov, G., Price, A., and Lindahl, T. (1992). Generation of single-nucleotide repair patches following excision of uracil residues from DNA. Mol-Cell-Biol *12*, 1605-12.

Dimri, G. P., Lee, X., Basile, G., Acosta, M., Scott, G., Roskelley, C., Medrano, E. E., Linskens, M., Rubelj, I., Pereira Smith, O., and et al. (1995). A biomarker that identifies senescent human cells in culture and in aging skin in vivo. Proc-Natl-Acad-Sci-U-S-A *92*, 9363-7.

El-Deiry, W. S., Kern, S. E., Pietenpol, J. A., Kinzler, K. W., and Vogelstein, B. (1992). Definition of a consensus binding site for p53. Nature Genetics *1*, 45-49.

El-Deiry, W. S., Tokino, T., Velculescu, V. E., Levy, D. B., Parsons, R., Trent, J. M., Lin, D., Mercer, W. E., Kinzler, K. W., and Vogelstein, B. (1993). WAF-1, a potential mediator of p53 tumour suppression. Cell *75*, 817-825.

Elledge, S. J. (1996). Cell cycle checkpoints: preventing an identity crisis. Science *274*, 1664-72.

Evans, E., Fellows, J., Coffer, A., and Wood, R. D. (1997). Open complex formation around a lesion during nucleotide excision repair provides a structure for cleavage by human XPG protein. EMBO-J *16*, 625-38.

Evans, T., Rosenthal, E., Youngbloom, J., Distel, D., and Hunt, T. (1983). Cyclin: a protein specified by maternal mRNA in sea urchin eggs that is destroyed at each cleavage division. Cell *33*, 389-396.

Ewen, M. E., Sluss, H. K., Sherr, C. J., Matsushime, H., Kato, J., and Livingston, D. M. (1993). Functional interactions of the retinoblastoma protein with mammalian D-type cyclins. Cell *73*, 487-97.

Ey, P. L., Prause, S., and Jenkin, C. R. (1978). Effects of MMS on Human Cells. Immunochemistry *15*, 429-436.

Fornace Jr, A. J., Nebert, D. W., Hollander, M. C., Luethy, J. D., Papathanasiou, M., Fargnoll, J., and Holbrook, N. J. (1989). Mammalian Genes Coordinately Regulated by Growth Arrest Signals and DNA-Damaging Agents. Mol. Cell. Biol. *9*, 4196-4203.

Fortini, P., Pascucci, B., Parlanti, E., Sobol, R. W., Wilson, S. H., and Dogliotti, E. (1998). Different DNA polymerases are involved in the short- and long-patch base excision repair in mammalian cells. Biochemistry *37*, 3575-80.

Friedberg, E. C., Walker, G. C., and Siede, W. (1995). DNA Repair and Mutagenesis (Washington, D.C.: ASM Press).

Frosina, G., Fortini, P., Rossi, O., Carrozzino, F., Raspaglio, G., Cox, L. S., Lane, D. P., Abbondandalo, A., and Dogliotti, E. (1996). Two pathways for base excision repair in mammalian cells. J. Biol. Chem. *271*, 9573-9578.

Furnari, B., Rhind, N., and Russell, P. (1997). Cdc25 mitotic inducer targeted by chk1 DNA damage checkpoint kinase. Science *277*, 1495-7.

Futreal, P. A., Soderkvist, P., Marks, J. R., Iglehart, J. D., Cochran, C., Barrett, J. C., and Wiseman, R. W. (1992). Detection of frequent allelic loss on proximal chromosome 17q in sporadic breast carcinoma using microsatellite length polymorphisms. Cancer Res *52*, 2624-7.

Ghosh, D. (1993). Status of the transcription factors database (TFD). Nucl. Acids Res. *21*, 3117-3118.

Goulian, M., Richards, S. H., Heard, C. J., and Bigsby, B. M. (1990). Discontinuous DNA synthesis by purified mammalian proteins [published erratum appears in J Biol Chem 1990 Dec 25;265(36):22569]. J-Biol-Chem *265*, 18461-71.

Grosch, S., Fritz, G., and Kaina, B. (1998). REF-1 is induced in mammalian cells by oxidative stress. Canc. Res. *58*, 4410-4416.

Gu, Y., Turck, C. W., and Morgan, D. O. (1993). Inhibition of Cdk2 activity in vivo by an associated 20K regulatory subunit. Nature *366*, 707-710.

Guan, K. L., Jenkins, C. W., Li, Y., Nichols, M. A., Wu, X., O'Keefe, C. L., Matera, A. G., and Xiong, Y. (1994). Growth suppression by p18, a p16INK4/MTS1- and p14INK4B/MTS2-related CDK6 inhibitor, correlates with wild-type pRb function. Genes-Dev *8*, 2939-52.

Gurdon, J. B. (1967). On the Origin and Persistence of a Cytoplasmic State Inducing Nuclear DNA Synthesis in Frogs' Eggs. Proc. Natl. Acad. Sci., USA *58*, 545-552.

Hall, M., and Peters, G. (1996). Genetic alterations of cyclins, cyclin-dependent kinases, and Cdk inhibitors in human cancer. Adv Cancer Res *68*, 67-108.

Hall, P. A., Mckee, P. H., Menage, H. d. P., Dover, P., and Lane, D. P. (1993). High levels of p53 protein in UV-irradiated normal human skin. Oncogene *8*, 203-207.

Hannon, G. J., and Beach, D. (1994). p15INK4B is a potential effector of TGF-beta-induced cell cycle arrest. Nature *371*, 257-61.

Harland, R. M., and Laskey, R. A. (1980). Regulated replication of DNA microinjected into eggs of Xenopus laevis. Cell *21*, 761-71.

Harlow, E., and Lane, D. P. (1988). Antibodies, A Laboratory Manual (New York, USA: Cold Spring Harbor Press).

Harper, J. W., Adami, G. R., Wei, N., Keyomarsi, K., and Elledge, S. J. (1993). The p21 Cdk-interacting protein Cip1 is a potent inhibitor of G1 cyclin-dependent kinases. Cell *75*, 805-816.

Harper, J. W., Elledge, S. J., Keyomarsi, K., Dynlacht, B., Tsai, L. H., Zhang, P., Dobrowolski, S., Bai, C., Connell Crowley, L., Swindell, E., and et al. (1995). Inhibition of cyclin-dependent kinases by p21. Mol-Biol-Cell *6*, 387-400.

Harrington, J. J., and Leiber, M. R. (1995). DNA structural elements required for FEN-1 binding. J. Biol. Chem. *270*, 4503-4508.

Harrington, J. J., and Lieber, M. R. (1994a). The characterisation of a mammalian DNA structure-specific endonuclease. EMBO J. *13*, 1235-1246.

Harrington, J. J., and Lieber, M. R. (1994b). Functional domains within FEN-1 and RAD2 define a family of structure-specific endonucleases: implications for nucleotide excision repair. Genes Dev. *8*, 1344-1355.

Hartwell, L. H., Culotti, J., and Reid, B. (1970). Genetic control of the cell-division cycle in yeast. I. Detection of mutants. Proc Natl Acad Sci U S A *66*, 352-9.

Hartwell, L. H., and Weinert, T. A. (1989). Checkpoints: controls that ensure the order of cell cycle events. Science *246*, 629-34.

Hiraoka, L. R., Harrington, J. J., Gerhard, D. S., Lieber, M. R., and Hsieh, C. L. (1995). Sequence of human FEN-1, a structure-specific endonuclease, and chromosomal localization of the gene (FEN1) in mouse and human. Genomics *25*, 220-5.

Hoeijmakers, J. H. (1993). Nucleotide excision repair. II: From yeast to mammals. Trends-Genet *9*, 211-7.

Hollander, M. C., Alamo, I., Jackman, J., Wang, M. G., McBride, O. W., and Fornace, A. J., Jr. (1993). Analysis of the mammalian gadd45 gene and its response to DNA damage. J Biol Chem *268*, 24385-93.

Hosfield, D. J., Frank, G., Weng, Y., Tainer, J. A., and Shen, B. (1998). Newly discovered archaebacterial flap endonucleases show a structure-specific mechanism for DNA substrate binding and catalysis resembling human flap endonuclease-1. J Biol Chem *273*, 27154-61.

Hosfield, D. J., Mol, C. D., Shen, B., and Tainer, J. A. (1998). Structure of the DNA repair and replication endonuclease and exonuclease FEN-1: coupling DNA and PCNA binding to FEN-1 activity. Cell *95*, 135-46.

Hozak, P., Hassan, A. B., Jackson, D. A., and Cook, P. R. (1993). Visualization of replication factories attached to a nucleoskeleton. Cell *73*, 361-373.

Huang, L., Rumbaugh, J. A., Murante, R. S., Lin, R. J., Rust, L., and Bambara, R. A. (1996). Role of calf RTH-1 nuclease in removal of 5'-ribonucleotides during Okazaki fragment processing. Biochemistry *35*, 9266-77.

Hunter, T., and Pines, J. (1994). Cyclins and cancer. II: Cyclin D and CDK inhibitors come of age. Cell *79*, 573-82.

Hutchinson, C., and Glover, D. M. (1995). Cell Cycle Control (New York, USA: Oxford University Press).

Hwang, K. Y., Baek, K., Kim, H. Y., and Cho, Y. (1998). The crystal structure of flap endonuclease-1 from Methanococcus jannaschii. Nat Struct Biol *5*, 707-13.

Inouye, S., and Tsuji, F. I. (1994). Aequorea green fluorescent protein. Expression of the gene and fluorescence characteristics of the recombinant protein. FEBS-Lett *341*, 277-80.

Irniger, S., Piatti, S., Michaelis, C., and Nasmyth, K. (1995). Genes involved in sister chromatid separation are needed for B-type cyclin proteolysis in budding yeast. Cell *81*, 269-277.

Ishimi, Y., Claude, A., Bullock, P., and Hurwitz, J. (1988). Complete enzymatic synthesis of DNA containing the SV40 origin of replication. J-Biol-Chem *263*, 19723-33.

Jacobs, J. P., Jones, C. M., and Baille, J. P. (1970). Characteristics of a human diploid cell designated MRC-5. Nature *227*, 168-70.

Jeffrey, P. D., Russo, A. A., Polyak, K., Gibbs, E., Hurwitz, J., Massague, J., and Pavletich, N. P. (1995). Mechanism of CDK activation revealed by the structure of a cyclinA-CDK2 complex. Nature *376*, 313-20.

Johnson, R. E., Kovvali, G. K., Prakash, L., and Prakash, S. (1995). Requirement of the yeast RTH1 5' to 3' exonuclease for the stability of simple repetitive DNA. Science *269*, 238-40.

Jonsson, Z. O., Hindges, R., and Hubscher, U. (1998). Regulation of DNA replication and repair proteins through interaction with the front side of proliferating cell nuclear antigen. EMBO J *17*, 2412-25.

Kastan, M. B., Zhan, Q., El-Deriy, W. S., Carrier, F., Jacks, T., Walsh, W. V., Plunkett, B. S., Vogelstein, B., and Fornace Jnr., A. J. (1992). A mammalian cell cycle checkpoint pathway utilizing p53 and GADD45 is defective in Ataxia-Telengiectasia. Cell *71*, 587-597.

Kim, K., Biade, S., and Matsumoto, Y. (1998). Involvement of flap endonuclease 1 in base excision DNA repair. J Biol Chem *273*, 8842-8.

King, R. W., Deshaies, R. J., Peters, J. M., and Kirschner, M. W. (1996). How proteolysis drives the cell cycle. Science *274*, 1652-9.

King, R. W., Peters, J. M., Tugendreich, S., Rolfe, M., Hieter, P., and Kirschner, M. W. (1995). A 20S complex containing CDC27 and CDC16 catalyzes the mitosis-specific conjugation of ubiquitin to cyclin B. Cell *81*, 279-88.

Kitazono, A., and Matsumoto, T. (1998). "Isogaba Maware": quality control of genome DNA by checkpoints. Bioessays *20*, 391-9.

Klungland, A., and Lindahl, T. (1997). Second pathway for completion of human DNA base excision-repair: reconstitution with purified proteins and requirement for DNase IV (FEN1). EMBO-J *16*, 3341-8.

Knudson, A. G. (1993). Antioncogenes and human cancer. Proc Natl Acad Sci U S A *90*, 10914-21.

Kohler, G., and Milstein, C. (1975). Continuous cultures of fused cells secreting antibody of predefined specificity. Nature *256*, 495-7.

Kokoska, R. J., Stefanovic, L., Tran, H. T., Resnick, M. A., Gordenin, D. A., and Petes, T. D. (1998). Destabilization of yeast micro- and minisatellite DNA sequences by

mutations affecting a nuclease involved in Okazaki fragment processing (rad27) and DNA polymerase delta (pol3-t). Mol-Cell-Biol *18*, 2779-88.

Koonin, E. V., Altschul, S. F., and Bork, P. (1996). BRCA1 protein products ... Functional motifs... Nat Genet *13*, 266-8.

Krishna, T. S., Fenyo, D., Kong, X. P., Gary, S., Chait, B. T., Burgers, P., and Kuriyan, J. (1994). Crystallization of proliferating cell nuclear antigen (PCNA) from Saccharomyces cerevisiae. J-Mol-Biol *241*, 265-8.

Krude, T., Jackman, M., Pines, J., and Laskey, R. A. (1997). Cyclin/Cdk-dependent initiation of DNA replication in a human cell-free system. Cell *88*, 109-19.

Kubota, Y., Nash, R. A., Klungland, A., Schar, P., Barnes, D. E., and Lindahl, T. (1996). Reconstitution of DNA base excision-repair with purified human proteins: interaction between DNA polymerase beta and the XRCC1 protein. EMBO-J *15*, 6662-70.

Lahue, E. E., Smith, A. V., and Orr Weaver, T. L. (1991). A novel cyclin gene from Drosophila complements CLN function in yeast. Genes Dev *5*, 2166-75.

Lane, D. P. (1992). p53, guardian of the genome. Nature *358*, 15-16.

Lane, D. P., and Crawford, L. V. (1979). T antigen is bound to a host protein in SV40-transformed cells. Nature *278*, 261-3.

Lavin, M. F., and Shiloh, Y. (1997). The genetic defect in ataxia-telangiectasia. Annu Rev Immunol *15*, 177-202.

Lee, S. H., Pan, Z. Q., Kwong, A. D., Burgers, P. M., and Hurwitz, J. (1991). Synthesis of DNA by DNA polymerase epsilon in vitro. J-Biol-Chem *266*, 22707-17.

Lees, E. (1995). Cyclin dependent kinase regulation. Curr Opin Cell Biol *7*, 773-80.

Leonhardt, H., and Cardoso, M. C. (1995). Targeting and association of proteins with functional domains in the nucleus: the insoluble solution. Int Rev Cytol, 303-35.

Li, J. J., and Kelly, T. J. (1984). Simian virus 40 DNA replication in vitro. Proc. Natl. Acad. Sci. USA *81*, 6973-6977.

Li, R., Hannon, G. J., Beach, D., and Stillman, B. (1996). Subcellular distribution of p21 and PCNA in normal and repair-deficient cells following DNA damage. Curr-Biol *6*, 189-99.

Li, R., Waga, S., Hannon, G. J., Beach, D., and Stillman, B. (1994). Differential effects by the p21 CDK inhibitor on PCNA-dependent DNA replication and repair. Nature *371*, 534-537.

Li, X., Li, J., Harrington, J., Lieber, M. R., and Burgers, P. M. (1995). Lagging strand synthesis at the eukaryotic replication fork involves binding and stimulation of FEN-1 by proliferating cell nuclear antigen. J. Biol. Chem. *270*, 22109-22112.

Lieber, M. R. (1997). The FEN-1 family of structure-specific nucleases in eukaryotic DNA replication, recombination and repair. Bioessays *19*, 233-40.

Lindahl, T. (1971). The action pattern of mammalian deoxyribonuclease IV. Eur J Biochem *18*, 415-21.

Lindahl, T., Gally, J. A., and Edelman, G. M. (1969). Deoxyribonuclease IV: a new exonuclease from mammalian tissues. Proc Natl Acad Sci U S A *62*, 597-603.

Lindahl, T., Karran, P., and Wood, R. D. (1997). DNA excision repair pathways. Curr-Opin-Genet-Dev *7*, 158-69.

Linzer, D. I., and Levine, A. J. (1979). Characterization of a 54K dalton cellular SV40 tumor antigen present in SV40-transformed cells and uninfected embryonal carcinoma cells. Cell *17*, 43-52.

Lohka, M. J., and Masui, Y. (1983). Formation in vitro of sperm pronuclei and mitotic chromosomes induced by amphibian ooplasmic components. Science *220*, 719-21.

Madsen, P., and Celis, J. E. (1985). S-phase patterns of cyclin (PCNA) antigen staining resemble topographical patterns of DNA synthesis. A role for cyclin in DNA replication? FEBS-Lett *193*, 5-11.

Maga, G., Mossi, R., Fischer, R., Berchtold, M. W., and Hubscher, U. (1997). Phosphorylation of the PCNA binding domain of the large subunit of replication factor

C by Ca2+/calmodulin-dependent protein kinase II inhibits DNA synthesis. Biochemistry *36*, 5300-10.

Masui, Y., and Markert, C. L. (1971). Cytoplasmic control of nuclear behavior during meiotic maturation of frog oocytes. J Exp Zool *177*, 129-45.

Matsumoto, K., Moriuchi, T., Koji, T., and Nakane, P. K. (1987). Molecular cloning of cDNA coding for rat proliferating cell nuclear antigen. EMBO J. *6*, 637-642.

Matsumoto, Y., Kim, K., and Bogenhagen, D. F. (1994). Proliferating cell nuclear antigen-dependent abasic site repair in Xenopus laevis oocytes: an alternative pathway of base excision DNA repair. Mol-Cell-Biol *14*, 6187-97.

Mcknight, S. L., Lane, M. D., and Gluecksohn-Waelsch, S. (1989). Genes and Dev. *3*, 2021-2024.

Meyerson, M., and Harlow, E. (1994). Identification of G1 kinase activity for cdk6, a novel cyclin D partner. Mol Cell Biol *14*, 2077-86.

Midgley, C. A., Fisher, C. J., Bartek, J., Vojtesek, B., Lane, D. P., and Barnes, D. M. (1992). Analysis of p53 expression in human tumours: an antibody raised against human p3 expressed in Escerichia coli. J. Cell Sci. *101*, 183-189.

Miura, M., Sasaki, T., and Takasaki, Y. (1996). Characterisation of X-ray-induced immunostaining of proliferating cell nuclear antigen in human diploid fibroblasts. Radiat. Res. *145*, 75-80.

Modrich, P. (1997). Strand-specific mismatch repair in mammalian cells. J Biol Chem *272*, 24727-30.

Moggs, J. G., Yarema, K. J., Essigmann, J. M., and Wood, R. D. (1996). Analysis of incision sites produced by human cell extracts and purified proteins during nucleotide excision repair of a 1,3-intrastrand d(GpTpG)-cisplatin adduct. J-Biol-Chem *271*, 7177-86.

Montecucco, A., Savini, E., Weighardt, F., Rossi, R., Ciarrocchi, G., Villa, A., and Biamonti, G. (1995). The N-terminal domain of human ligase 1 contains the nuclear localisation signal and directs the enzyme to sites of DNA replication. EMBO J. *14*, 5379-5386.

Morin, J. G., and Hastings, J. W. (1971). Energy transfer in a bioluminescent system. J-Cell-Physiol *77*, 313-8.

Morris, G. F., Bischoff, J. R., and Mathews, M. B. (1996). Transcriptional activation of the human proliferating-cell nuclear antigen promoter by p53. Proc Natl Acad Sci U S A *93*, 895-9.

Morris, G. F., and Mathews, M. B. (1990). Analysis of the proliferating cell nuclear antigen promoter and its response to adenovirus early region 1. J Biol Chem *265*, 16116-25.

Morris, G. F., and Mathews, M. B. (1989). Regulation of proliferating cell nuclear antigen during the cell cycle. J Biol Chem *264*, 13856-64.

Mu, D., Hsu, D. S., and Sancar, A. (1996). Reaction mechanism of human DNA repair excision nuclease. J-Biol-Chem *271*, 8285-94.

Mueser, T. C., Nossal, N. G., and Hyde, C. C. (1996). Structure of bacteriophage T4 RNase H, a 5' to 3' RNA-DNA and DNA-DNA exonuclease with sequence similarity to the RAD2 family of eukaryotic proteins. Cell *85*, 1101-12.

Murante, R. S., Henricksen, L. A., and Bambara, R. A. (1998). Junction ribonuclease: an activity in Okazaki fragment processing. Proc Natl Acad Sci U S A *95*, 2244-9.

Murante, R. S., Huang, L., Turchi, J. J., and Bambara, R. A. (1994). The calf 5'- to 3'-exonuclease is also an endonuclease with both activities dependent on primers annealed upstream of the point of cleavage. J-Biol-Chem *269*, 1191-6.

Murante, R. S., Rust, L., and Bambara, R. A. (1995). Calf 5' to 3' exo/endonuclease must slide from a 5' end of the substrate to perform structure-specific cleavage. J-Biol-Chem *270*, 30377-83.

Murray, J. M., Tarassoli, M., al-Harithy, R., Sheldrick, K. S., Lehman, A. R., Carr, A. M., and Watts, F. Z. (1994). Structural and functional conservation of the human homologue of the Schizosaccharomyces pombe rad2 gene, which is required for chromosome segregation and recovery from DNA damage. Mol. Cell Biol. *14*, 4878-4888.

Nasmyth, K. (1996). Viewpoint: putting the cell cycle in order. Science *274*, 1643-5.

Nealon, K., Nicholl, I. D., and Kenny, M. K. (1996). Characterization of the DNA polymerase requirement of human base excision repair. Nucleic-Acids-Res *24*, 3763-70.

Nethanel, T., Zlotkin, T., and Kaufmann, G. (1992). Assembly of simian virus 40 Okazaki pieces from DNA primers is reversibly arrested by ATP depletion. J-Virol *66*, 6634-40.

Newport, J. W., and Kirschner, M. W. (1984). Regulation of the cell cycle during early Xenopus development. Cell *37*, 731-42.

Nichols, A. F., and Sancar, A. (1992). Purification of PCNA as a nucleotide excision repair protein [corrected and republished with original paging, article originally printed in Nucleic Acids Res 1992 May 25;20(10):2441-6]. Nucleic-Acids-Res *20*, 2441-6.

Nigg, E. A. (1995). Cyclin-dependent protein kinases: key regulators of the eukaryotic cell cycle. Bioessays *17*, 471-80.

Nurse, P., and Bissett, Y. (1981). Gene required in G1 for commitment to cell cycle and in G2 for control of mitosis in fission yeast. Nature *292*, 558-60.

Nurse, P., Thuriaux, P., and Nasmyth, K. (1976). Genetic control of the cell division cycle in the fission yeast Schizosaccharomyces pombe. Mol Gen Genet *146*, 167-78.

Ottavio, L., Chang, C.-D., Rizzo, M.-G., Travali, S., Casadevall, C., and Baserga, R. (1990). Importance of introns in the growth regulation of the mRNA levels of the proliferating cell nuclear antigen gene. Mol. Cell. Biol. *10*, 303-309.

Pagano, M., Tam, S. W., Theodoras, A. M., Beer Romero, P., Del Sal, G., Chau, V., Yew, P. R., Draetta, G. F., and Rolfe, M. (1995). Role of the ubiquitin-proteasome pathway in regulating abundance of the cyclin-dependent kinase inhibitor p27. Science *269*, 682-5.

Patel, G., and Jones, N. C. (1990). Activation in vitro of RNA polymerase II and III directed transcription by baculovirus produced E1A protein. Nucleic-Acids-Res *18*, 2909-15.

Paulovich, A. G., and Hartwell, L. H. (1995). A checkpoint regulates the rate of progression through S phase in S. cerevisiae in response to DNA damage. Cell *82*, 841-7.

Peng, C. Y., Graves, P. R., Thoma, R. S., Wu, Z., Shaw, A. S., and Piwnica Worms, H. (1997). Mitotic and G2 checkpoint control: regulation of 14-3-3 protein binding by phosphorylation of Cdc25C on serine-216. Science *277*, 1501-5.

Pines, J. (1995). Cyclins and cyclin-dependent kinases: a biochemical view. Biochem J *308*, 697-711.

Pines, J. (1995). GFP in mammalian cells. Trends Genet *11*, 326-7.

Podust, V. N., Tiwari, N., Stephan, S., and Fanning, E. (1998). Replication factor C disengages from proliferating cell nuclear antigen (PCNA) upon sliding clamp formation, and PCNA itself tethers DNA polymerase delta to DNA. J Biol Chem *273*, 31992-9.

Polyak, K., Lee, M. H., Erdjument, B. H., Koff, A., Roberts, J. M., Tempst, P., and Massague, J. (1994). Cloning of p27Kip1, a cyclin-dependent kinase inhibitor and a potential mediator of extracellular antimitogenic signals. Cell *78*, 59-66.

Prelich, G., Kostura, M., Marshak, D. R., Mathews, M. B., and Stillman, B. (1987). The cell-cycle regulated proliferating cell nuclear antigen is required for SV40 DNA replication in vitro. Nature *326*, 471-475.

Prestridge, D. (1991). SIGNAL SCAN: A computer program that scans DNA sequences for eukaryotic transcriptional elements. CABIOS *7*, 203-206.

Prosperi, E., Stivala, L. A., Sala, E., Scovassi, A. I., and Bianchi, L. (1993). Proliferating cell nuclear antigen complex formation induced by ultraviolet irradiation in human quiescent fibroblasts as detected by immunostaining and flow cytometry. Exp-Cell-Res *205*, 320-5.

Ramana, C. V., Boldogh, I., Izumi, T., and Mitra, S. (1998). Activation of apurinic/apyrimidinic endonuclease in human cells by reactive oxygen species and its correlation with their adaptive response to genotoxicity of free radicals. Proc-Natl-Acad-Sci-U-S-A *95*, 5061-6.

Rao, P. N., and Johnson, R. T. (1970). Mammalian cell fusion studies on the regulation of DNA synthesis and mitosis. Nature *225*, 159-164.

Reagan, M. S., Pittenger, C., Siede, W., and Friedberg, E. C. (1995). Characterisation of a mutant strain of Saccharomyces cerevisiae with a deletion of the RAD27 gene, a structural homolog of the RAD2 nucleotide excision repair gene. J. Bact. *177*, 364-371.

Reese, M. G. (1994). Diploma Thesis. German Cancer Research Center *Heidelberg, Germany*.

Reese, M. G., and Eeckman, F. H. (1995). Novel Neural Network Algorithms for Improved Eukaryotic Promoter and Splice Site Recognition. The Seventh Annual International Genome Sequencing and Analysis Conference *Hilton Head, S.C., USA*.

Reese, M. G., Harris, N. L., and Eeckman, F. H. (1996). Large Scale sequencing Specific Neural Networks for Promoter and Splice Site Recognition. Biocomputing: Proceedings of the 1996 Pacific Symposium *World Scientific Publishing, Co. Singapore*.

Rickwood, D. (1989). Centrifugation, A Practical Approach, Volume 2nd Edition (Oxford, UK: IRL Press).

Robins, P., Pappin, D. J., Wood, R. D., and Lindahl, T. (1994). Structural and functional homology between mammalian DNase IV and the 5'-nuclease domain of Escherichia coli DNA polymerase I. J. Biol. Chem. *269*, 28535-28538.

Romanowski, P., Madine, M. A., Rowles, A., Blow, J. J., and Laskey, R. A. (1996). The Xenopus origin recognition complex is essential for DNA replication and MCM binding to chromatin. Curr-Biol *6*, 1416-25.

Roos, G., Landberg, G., Huff, J. P., Houghten, R., Takasaki, Y., and Tan, E. M. (1993). Analysis of the epitopes of proliferating cell nuclear antigen recognized by monoclonal antibodies. Lab. Invest. *68*, 204-210.

Russo, A. A., Jeffrey, P. D., Patten, A. K., Massague, J., and Pavletich, N. P. (1996). Crystal structure of the p27Kip1 cyclin-dependent-kinase inhibitor bound to the cyclin A-Cdk2 complex. Nature *382*, 325-31.

Sambrook, J., Fritsch, E. F., and Maniatis, T. (1989). Molecular Cloning. A laboratory manual., Second Edition: Cold Spring Harbor Laboratory Press).

Sanchez, Y., Wong, C., Thoma, R. S., Richman, R., Wu, Z., Piwnica Worms, H., and Elledge, S. J. (1997). Conservation of the Chk1 checkpoint pathway in mammals: linkage of DNA damage to Cdk regulation through Cdc25. Science *277*, 1497-501.

Savio, M., Stivala, L. A., Bianchi, L., Vannini, V., and Prosperi, E. (1998). Involvement of the proliferating cell nuclear antigen (PCNA) in DNA repair induced by alkylating agents and oxidative damage in human fibroblasts. Carcinogenesis *19*, 591-6.

Savitsky, K., Sfez, S., Tagle, D. A., Ziv, Y., Sartiel, A., Collins, F. S., Shiloh, Y., and Rotman, G. (1995). The complete sequence of the coding region of the ATM gene reveals similarity to cell cycle regulators in different species. Human Mol. Genet. *4*, 2025-2032.

Schlosser, C. A., Steglich, C., deWet, J. R., and Scheffler, I. E. (1981). Cell cycle-dependent regulation of thymidine kinase activity introduced into mouse LMTK- cells by DNA and chromatin-mediated gene transfer. Proc Natl Acad Sci U S A *78*, 1119-23.

Schweitzer, J. K., and Livingston, D. M. (1998). Expansions of CAG repeat tracts are frequent in a yeast mutant defective in Okazaki fragment maturation. Hum-Mol-Genet *7*, 69-74.

Serrano, M., Hannon, G., and Beach, D. (1993). A new regulatory motif in cell-cycle control causing specific inhibition of cyclin D/cdk4. Nature *366*, 704-707.

Shen, B., Nolan, J. P., Sklar, L. A., and Park, M. S. (1996). Essential amino acids for substrate binding and catalysis of human flap endonuclease 1. J. Biol. Chem. *271*, 9173-9176.

Shen, B., Nolan, J. P., Sklar, L. A., and Park, M. S. (1997). Functional analysis of point mutations in human flap endonuclease-1 active site. Nucleic-Acids-Res *25*, 3332-8.

Shen, B., Qiu, J., Hosfield, D., and Tainer, J. A. (1998). Flap endonuclease homologs in archaebacteria exist as independent proteins. Trends Biochem Sci *23*, 171-3.

Sherr, C. J. (1994). G1 phase progression: cycling on cue. Cell *79*, 551-5.

Sherr, C. J., and Roberts, J. M. (1995). Inhibitors of mammalian G1 cyclin-dependent kinases. Genes-Dev *9*, 1149-63.

Shivakumar, C. V., Brown, D. R., Deb, S., and Deb, S. P. (1995). Wild-type human p53 transactivates the humna proliferating cell nuclear antigen promoter. Mol. Cell. Biol. *15*, 6785-6793.

Shivji, M. K. K., Kenny, M. K., and Wood, R. D. (1992). Proliferating cell nuclear antigen is required for DNA excision repair. Cell *69*, 367-374.

Siede, W., Friedberg, A. S., and Friedberg, E. C. (1993). RAD9-dependent G1 arrest defines a second checkpoint for damaged DNA in the cell cycle of Saccharomyces cerevisiae. Proc Natl Acad Sci U S A *90*, 7985-9.

Siegal, G., Turchii, J. J., Myers, T. W., and Bambara, R. A. (1992). A 5' to 3' exonuclease functionally interacts with calf polymerase ε. Proc. Natl. Acad. Sci. *89*, 9377-9381.

Sijbers, A. M., de Laat, W. L., Ariza, R. R., Biggerstaff, M., Wei, Y. F., Moggs, J. G., Carter, K. C., Shell, B. K., Evans, E., de Jong, M. C., Rademakers, S., de Rooij, J., Jaspers, N. G., Hoeijmakers, J. H., and Wood, R. D. (1996). Xeroderma pigmentosum group F caused by a defect in a structure-specific DNA repair endonuclease. Cell *86*, 811-22.

Sikora, E., Kaminska, B., Radziszewska, E., and Kaczmarek, L. (1992). Loss of transcription factor AP-1 DNA binding activity during lymphocyte aging in vivo. FEBS-Lett *312*, 179-82.

Simbulan Rosenthal, C. M., Rosenthal, D. S., Hilz, H., Hickey, R., Malkas, L., Applegren, N., Wu, Y., Bers, G., and Smulson, M. E. (1996). The expression of poly(ADP-ribose) polymerase during differentiation-linked DNA replication reveals that

it is a component of the multiprotein DNA replication complex. Biochemistry *35*, 11622-33.

Singer, M., and Berg, P. (1991). Genes and Genomes: A Changing Perspective (Oxford, UK: University Science Books).

Sommers, C. H., Miller, E. J., Dujon, B., Prakash, S., and Prakash, L. (1995). Conditional lethality of null mutations in RTH1 that encodes the yeast counterpart of a mammalian 5'- to 3'-exonuclease required for lagging strand DNA synthesis in reconstituted systems. J-Biol-Chem *270*, 4193-6.

Stillman, B. W., and Gluzman, Y. (1985). Replication and supercoiling of simian virus 40 DNA in cell extracts of human cells. Mol. Cell. Biol. *5*, 2051-2060.

Stucki, M., Pascucci, B., Parlanti, E., Fortini, P., Wilson, S. H., Hubscher, U., and Dogliotti, E. (1998). Mammalian base excision repair by DNA polymerases delta and epsilon. Oncogene *17*, 835-43.

Th'ng, J. P., Wright, P. S., Hamaguchi, J., Lee, M. G., Norbury, C. J., Nurse, P., and Bradbury, E. M. (1990). The FT210 cell line is a mouse G2 phase mutant with a temperature-sensitive CDC2 gene product. Cell *63*, 313-24.

Thommes, P., Reiter, T., and Knippers, R. (1986). Synthesis of DNA polymerase alpha analyzed by immunoprecipitation from synchronously proliferating cells. Biochemistry *25*, 1308-14.

Tishkoff, D. X., Filosi, N., Gaida, G. M., and Kolodner, R. D. (1997). A novel mutation avoidance mechanism dependent on S. cerevisiae RAD27 is distinct from DNA mismatch repair. Cell *88*, 253-63.

Tokino, T., Thiagalingam, S., el Deiry, W. S., Waldman, T., Kinzler, K. W., and Vogelstein, B. (1994). p53 tagged sites from human genomic DNA. Hum-Mol-Genet *3*, 1537-42.

Toschi, L., and Bravo, R. (1988). Changes in cyclin/proliferating cell nuclear antigen distribution during DNA repair synthesis. J. Cell Biol. *107*, 1623-1628.

Travali, S., Ku, D. H., Rizzo, M. G., Ottavio, L., Baserga, R., and Calabretta, B. (1989). Structure of the gene for the human proliferating cell ncuelar antigen. J. Biol. Chem. *264*, 7466-7472.

Tricoli, J. V., Sahai, B. M., McCormick, P. J., Jarlinski, S. J., Bertram, J. S., and Kowalski, D. (1985). DNA topoisomerase I and II activities during cell proliferation and the cell cycle in cultured mouse embryo fibroblast (C3H 10T1/2) cells. Exp Cell Res *158*, 1-14.

Tseng, B. Y., and Goulian, M. (1977). Initiator RNA of discontinuous DNA synthesis in human lymphocytes. Cell *12*, 483-9.

Tsurimoto, T., and Stillman, B. (1989). Multiple replication factors augment DNA synthesis by the two eukaryotic DNA polymerases, alpha and delta. EMBO. J. *8*, 3883-3889.

Turchi, J. J., and Bambara, R. A. (1993). Completion of mammalian lagging strand DNA replication using purified proteins. J-Biol-Chem *268*, 15136-41.

Turchi, J. J., Huang, L., Murante, R. S., Kim, Y., and Bambara, R. A. (1994). Enzymatic completion of mammalian lagging-strand DNA replication. Proc-Natl-Acad-Sci-U-S-A *91*, 9803-7.

Turchii, J. J., and Bambara, R. A. (1993). Completion of mammlian lagging strand DNA replciation using purified proteins. J. Biol. Chem. *268*, 15136-15141.

Umar, A., Buermeyer, A. B., Simon, J. A., Thomas, D. C., Clark, A. B., Liskay, R. M., and A., K. T. (1996). Requirement for PCNA in DNA mismatch repair at a step preceding DNA synthesis. Cell *87*, 65-73.

Umar, A., and Kunkel, T. A. (1996). DNA-replication fidelity, mismatch repair and genome instability in cancer cells. Eur-J-Biochem *238*, 297-307

Vialard, J. E., Gilbert, C. S., Green, C. M., and Lowndes, N. F. (1998). The budding yeast Rad9 checkpoint protein is subjected to Mec1/Tel1-dependent hyperphosphorylation and interacts with Rad53 after DNA damage. EMBO J *17*, 5679-88.

Waga, S., and Stillman, B. (1994). Anatomy of a DNA replication fork revealed by reconstitution of SV40 DNA replication in vitro. Nature *369*, 207-12.

Wang, J. Y. (1998). Cellular responses to DNA damage [published erratum appears in Curr Opin Cell Biol 1998 Jun;10(3):416]. Curr Opin Cell Biol *10*, 240-7.

Warbrick, E., Lane, D. P., Glover, D. M., and Cox, L. S. (1997). Homologous regions of Fen1 and $p21^{Cip1}$ compete for binding to the same site on PCNA: a potential mechanism to co-ordinate DNA replication and repair. Oncogene *14*, 2313-2321.

Warbrick, E., Lane, D. P., Glover, D. M., and Cox, L. S. (1995). A small peptide inhibitor of DNA replication defines the site of interaction between the cyclin-kinase inhibitor p21WAF1 and proliferating cell nuclear antigen. Current Biology *5*, 275-282.

Waseem, N. H., and Lane, D. P. (1990). Monoclonal antibody analysis of the proliferating cell nuclear antigen (PCNA). Structural conservation and the detection of a nucleolar form. J. Cell Sci. *96*, 121-129.

Weeda, G., Hoeijmakers, J. H., and Bootsma, D. (1993). Genes controlling nucleotide excision repair in eukaryotic cells. Bioessays *15*, 249-58.

Weinberg, D. H., Collins, K. L., Simancek, P., Russo, A., Wold, M. S., Virshup, D. M., and Kelly, T. J. (1990). Reconstitution of simian virus 40 DNA replication with purified proteins. Proc Natl Acad Sci U S A *87*, 8692-6.

Weinert, T. A., and Hartwell, L. H. (1988). The RAD9 gene controls the cell cycle response to DNA damage in Saccharomyces cerevisiae. Science *241*, 317-22.

Weinert, T. A., Kiser, G. L., and Hartwell, L. H. (1994). Mitotic checkpoint genes in budding yeast and the dependence of mitosis on DNA replication and repair. Genes Dev *8*, 652-65.

Westphal, C. H. (1997). Cell-cycle signaling: Atm displays its many talents. Curr-Biol *7*, R789-92.

Westphal, C. H., Schmaltz, C., Rowan, S., Elson, A., Fisher, D. E., and Leder, P. (1997). Genetic interactions between atm and p53 influence cellular proliferation and irradiation-induced cell cycle checkpoints. Cancer Res *57*, 1664-7.

Wobbe, C. R., Dean, F., Weissbach, L., and Hurwitz, J. (1985). In vitro replication of duplex circular DNA containing the simian virus 40 DNA origin site. Proc. Natl. Acad. Sci. *82*, 5710-5714.

Wold, M. S., Li, J. J., and Kelly, T. J. (1987). Initiation of simian virus 40 DNA replication in vitro: large-tumor-antigen- and origin-dependent unwinding of the template. Proc Natl Acad Sci U S A *84*, 3643-7.

Wood, R. D. (1996). DNA repair in eukaryotes. Annu Rev Biochem *65*, 135-67.

Wood, R. D. (1997). Nucleotide excision repair in mammalian cells. J-Biol-Chem *272*, 23465-8.

Wu, X., Li, J., Li, X., Hseih, C.-L., Burgers, P. M. J., and Lieber, M. R. (1996). Processing of branched DNA intermediates by a complex of human Fen-1 and PCNA. Nucl. Acids Res. *24*, 2036-2043.

Wu, X., Wilson, T. E., and Lieber, M. R. (1999). A role for FEN-1 in nonhomologous DNA end-joining: The order of strand annealing and nucleolytic processing events. Proc. Natl. Acad. Sci., USA *96*, 1303-1308.

Wuarin, J., and Nurse, P. (1996). Regulating S phase: CDKs, licensing and proteolysis. Cell *85*, 785-7.

Xu, J., and Morris, G. F. (1999). p53-mediated regulation of proliferating cell nuclear antigen expression in cells exposed to ionizing radiation. Mol Cell Biol *19*, 12-20.

Xu, Y., and Baltimore, D. (1996). Dual roles of ATM in the cellular response to radiation and in cell growth control. Genes-Dev *10*, 2401-10.

Zeng, X. R., Jiang, Y., Zhang, S. J., Hao, H., and Lee, M. Y. (1994). DNA polymerase delta is involved in the cellular response to UV damage in human cells. J-Biol-Chem *269*, 13748-51.

Zhang, H., Xiong, Y., and Beach, D. (1993). Proliferating cell nuclear antigen and p21 are components of multiple cell cycle kinase complexes. Mol. Biol. of the Cell *4*, 897-906.